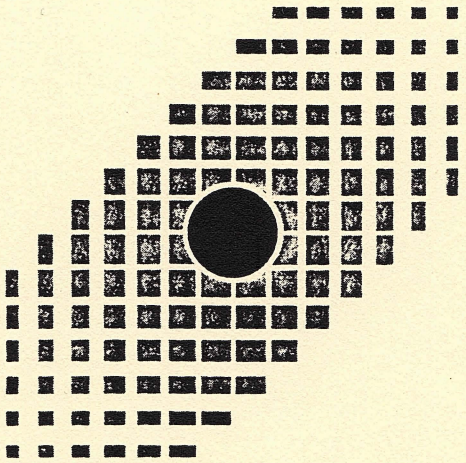
SCHOOL OF ENGINEERING
DUKE UNIVERSITY
DURHAM, NC 27706

CENTER FOR SOLID-STATE POWER CONDITIONING AND CONTROL



Modeling Multiwinding Transformers for High-Frequency Applications

Part II: Literature Review

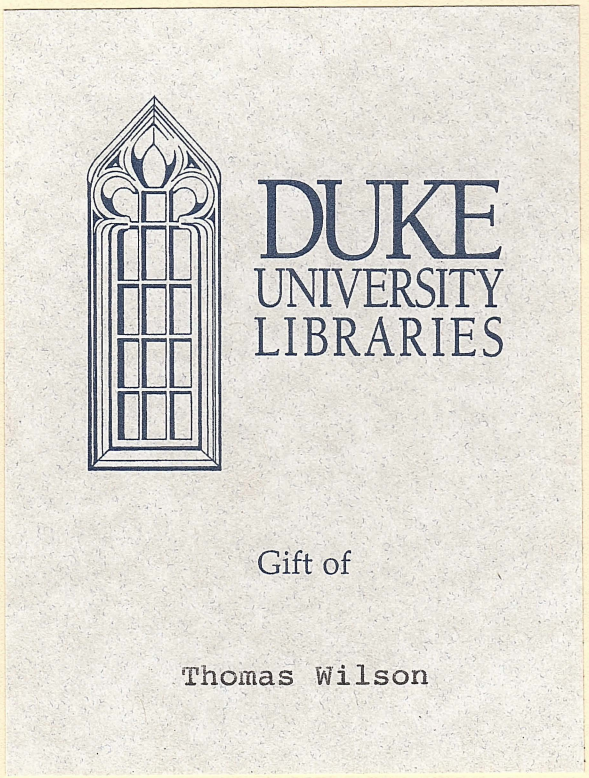
Van A. Niemela, Glenn R. Skutt, Audrey M. Urling
Thomas G. Wilson, Ronald C. Wong

Prepared for Digital Equipment Corporation
Maynard, Massachusetts

October 6, 1989

Vesic
621.314
M689
1989
pt. 2

Modeling multiwinding transformers
for high-frequency applications



Contents

Glossary of Symbols v

1 Introduction 1
- 1.1 OVERVIEW OF PART II . . . 1
  - 1.1.1 Chapter Summaries . . . 2
  - 1.1.2 Initial Comparisons of the Reviewed Articles . . . 5
- 1.2 CONVENTIONS . . . 8
  - 1.2.1 Notational Conventions . . . 8
  - 1.2.2 Chapter Format and Content . . . 10
- 1.3 OTHER GENERAL COMMENTS . . . 12

2 Dowell 15
- 2.1 OVERVIEW . . . 15
- 2.2 APPLICABILITY . . . 19
  - 2.2.1 Conditions . . . 19
  - 2.2.2 Assumptions . . . 20
- 2.3 MAJOR RESULTS . . . 20
  - 2.3.1 Current Density . . . 20
  - 2.3.2 Leakage Inductance . . . 24
  - 2.3.3 Optimum Winding Arrangement . . . 28
  - 2.3.4 AC Winding Resistance . . . 28
- 2.4 CLARIFICATIONS . . . 28
- 2.5 EXTENSION BY OTHERS . . . 31

3 Venkatraman 33
- 3.1 OVERVIEW . . . 33
- 3.2 MAJOR RESULTS . . . 36
- 3.3 CLARIFICATIONS . . . 39
  - 3.3.1 Winding Portions . . . 39
  - 3.3.2 Equivalent-Foil Thickness . . . 40
  - 3.3.3 Horizontal Axis of the Plots . . . 42
- 3.4 EXPERIMENTAL VERIFICATION . . . 42

3.5 LITZ WIRE 43
3.6 EVALUATION OF THE APPROACH 43

4 Carsten **45**
4.1 SUMMARY 45
4.2 SOURCES OF CONFUSION IN CARSTEN'S PAPER 49
4.3 TYPICAL RESULTS 52
4.4 NOTABLE EQUATIONS 55
4.4.1 Equations Found in Carsten's Appendix 55
4.4.2 K_r for Triangular Wave with DC Offset 57

5 Jongsma: Minimum-Loss Transformer Windings for Ultrasonic Frequencies **63**
5.1 SUMMARY AND CRITIQUE 63
5.1.1 Part 1 – Background and Theory 66
5.1.2 Part 2 – Design Methods and Aids 67
5.2 SIGNIFICANT EQUATIONS 68
5.2.1 Calculation and use of F_R 68
5.2.2 Improper Normalization 72
5.2.3 Comparison of Jongsma's and Carsten's Methods 73
5.3 TYPICAL RESULTS 74

6 Jongsma: High-Frequency Ferrite Power Transformer and Choke Design **77**
6.1 SUMMARY AND CRITIQUE 77
6.2 TERMINOLOGY USED 82
6.3 THE EFFECTIVE FREQUENCY 82
6.4 SIGNIFICANT FIGURES 84

7 Perry **89**
7.1 SUMMARY 89
7.2 GEOMETRY 92
7.3 GENERAL COMMENTS ON PERRY'S ANALYSIS 94
7.4 IMPORTANT RESULTS 95
7.4.1 Normalized Power Dissipation 95
7.4.2 Minimum Loss Design 98
7.5 STRENGTH AND WEAKNESSES 98
7.6 NOTABLE EQUATIONS 100
7.6.1 Current Density 100
7.6.2 Power Dissipation per Square Meter 102
7.6.3 Reference Values 104
7.7 CONCLUSION 105

8 Vandelac & Ziogas **107**
8.1 OVERVIEW 107
8.2 LAYER-BASED APPROACH 111
8.2.1 Comparison to Perry's Analysis 112
8.2.2 Plot of Normalized Power Dissipation 112
8.2.3 Optimum Layer Height and Arrangement 116
8.2.4 Losses in Electrostatic Shields 117
8.2.5 Other Winding Geometries 120
8.3 FIELD HARMONIC ANALYSIS 122
8.3.1 Method 122
8.3.2 Applications 131
8.3.3 Limitations 133

9 Rosa **135**
9.1 OVERVIEW 135
9.2 SUMMARY 138
9.3 CRITIQUE 141
9.4 NOTABLE EQUATIONS 143

10 Transformer Equivalent Circuits **145**
10.1 INTRODUCTION 145
10.2 M.I.T. 150
10.3 STARR 152
10.4 BLUME 153

11 Conclusion **155**

Appendix

Characterizing High-Frequency Effects in Transformer Windings—A Guide to Several Significant Articles **A–1**

Bibliography **1001**

This page has been left blank intentionally.

Glossary of Symbols

The common set of symbols used throughout this report is listed in this glossary, which is essentially the same as the glossary found in Part I. Appearing with each symbol is its name and the page number where it is defined, discussed, or first used.

Some of these symbols appear in the text of the two parts of the report in several different forms, e.g., in boldface or italic type, in upper or lower case, with or without an underline, or possibly subscripted in different ways. The form of a symbol usually conveys additional meaning beyond the basic meaning given in the table below. This additional meaning is explained in Section 1.3 of Part I or in the text where a particular form is used. As an additional aid to understanding some of the more complicated notation, examples of the different forms used with vector phasors and ratios of phasors are reviewed below.

Vector phasors such as $\underline{\mathbf{B}}$, $\underline{\mathbf{D}}$, $\underline{\mathbf{E}}$, $\underline{\mathbf{H}}$, and $\underline{\mathbf{J}}$ are directed quantities which vary in space and time as described in Section 1.3 of Part I. The notational conventions associated with vector phasors are shown below for the symbol $\underline{\mathbf{E}}$, defined in the table of symbols as "electric field intensity." In Section 1.3 of Part I, several different forms of this symbol are described with reference to a three-dimensional space. To understand the notation, it is helpful to keep in mind that boldface type signifies a vector with three spatial components, and an underline means "complex."

- $\underline{\mathbf{E}}$ electric-field-intensity vector phasor consisting of a phasor (complex number) in each of the three spatial coordinate directions
- $\underline{E}_y$ (complex number) phasor that is the y-directed component of the electric-field-intensity vector phasor
- $\mathbf{E}$ electric-field-intensity vector at some instant in time, consisting of three time-varying quantities, one in each of the spatial coordinate directions
- E_y (real number) y-directed component of the electric-field-intensity vector at some instant in time
- $|\underline{E}_y(x)|$ (real number) rms magnitude of the phasor that is the y-directed component of the electric-field-intensity vector phasor, as a function of x

- $\mathrm{Re}(\underline{E}_y)$ (real number) real part of the phasor that is the y-directed component of the electric-field-intensity vector phasor

Another set of notational conventions applies to ratios of phasors such as the impedance $\underline{Z}$ and the admittance $\underline{Y}$. For example, $\underline{Z}$ appears in Chapter 7 of Part I in several forms:

- $[\underline{Z}]$ complex impedance matrix
- $\underline{Z}_{34}$ complex impedance of element in 3rd row 4th column of $[\underline{Z}]$
- $[\underline{Z}']$ "referred" form of $[\underline{Z}]$
- $[\underline{Z}_r]$ "reduced" complex impedance matrix obtained from $[\underline{Z}']$
- $\underline{Z}_{r,23}$ complex impedance element of the matrix $[\underline{Z}_r]$. The element is a linear combination of short-circuit impedances involving windings 3 and 4.
- $\underline{Z}_{(34)}$ complex short-circuit impedance between windings 3 and 4
- $\underline{z}_{34}$ complex impedance element in a circuit. This symbol is not actually found in the report, but its inverse, the complex admittance element $\underline{y}_{34}$, does appear.

The table of symbols is alphabetized as follows. The relative order of two symbols is determined by the first pair of non-matching characters in the two symbols being compared. The order of the symbols is the same as the order of the two characters in an outline with the following hierarchy of headings:

1. **Alphabet:** Arabic, Greek, numerals, other characters
2. **Case:** upper, lower
3. **Style:** bold, italic, special, Roman
4. **Letter:** No next character, meaning the end of a symbol, comes before additional characters.

To form the outline, the four items in the third level "**Style:**" appear as subheadings for each of the items in the next higher level "**Case:**", and so on. According to this outline, the italicized upper-case W comes before the upper-case special character (subscript) $_W$, which comes before the lower-case w. Greek letters follow all Arabic letters.

If a particular symbol is not found in the table, its root and subscript are probably listed separately. The page numbers refer to Part I of this report unless preceded by a letter which refers to a page number in one of the appendices of Part I, or a "II" which refers to a page number in Part II of the report. SI units are used throughout.

Glossary of Symbols

Symbol	*Meaning*	*Part I Page*
A	cross-sectional area	19
AWG	American Wire Gauge	156
$\hat{\mathbf{a}}_x, \hat{\mathbf{a}}_y, \hat{\mathbf{a}}_z$	unit vectors in the reference directions x, y, and z	9
$\mathbf{B}$	magnetic flux density, a vector	A-1
$_{BASE}$	(subscript) basis value for normalizing a variable	9
b	breadth	36
b_{cu}	breadth of each conductor in a winding layer	15
b_{max}	maximum breadth available in which to place a winding	15
b_w	breadth of a winding layer	15
b_{win}	breadth of the core window; $b_{win} \geq b_{max} \geq b_w$	15
$_{bob}$	(subscript) "bobbin"	156
$_C$	(subscript) "cross-section"	31
$_c$	(subscript) "critical"	89
c.m.	units of circular mils; 1 c.m. $= 5.067 \times 10^{-10}$ m^2	156
$_{cu}$	(subscript) copper, or more generally, the conductor	15
$\mathbf{D}$	electric flux density, a vector	A-1
$_d$	(subscript) "dissipated"	56
d_{cu}	diameter of the conductor alone in a round wire	16
d_o	outside diameter of a wire, including insulation	16
$\underline{\mathbf{E}}$	electric field intensity, a vector phasor	58
$_E$	(subscript) "eddy-current"	45
	(subscript) "excited-winding"	137
e	constant, 2.71828	8
F_1, F_2	dimensionless functions of Δ, where $\Delta = h_{cu}/\delta$	118
F_3, F_4	dimensionless functions of Δ, where $\Delta = h_{cu}/\delta$	123
f	frequency	72
$\underline{\mathcal{F}}$	magnetomotive force, a vector phasor	136
g_a	"additional" interlayer gap, a length used to correct the calculations	159
g_{inters}	gap between surfaces of conducting layers of adjacent winding	159
g_{intras}	gap between surfaces of conducting layers within a winding	159

(continued)

Glossary of Symbols (continued)

Symbol	*Meaning*	*Part I Page*
g_n	gap height between winding layers n and $n+1$	147
$_{gn}$	(subscript) "in interlayer gap number n"	136
$\underline{\mathbf{H}}$	magnetic field intensity, a vector phasor	53
$\mathcal{H}_{jk}$	gain of the voltage source in secondary j that is controlled by the current in secondary k	226
$H_{(jk)}$	magnetic field intensity in the z-direction with winding j excited and winding k short-circuited	133
$H_{(jk)(lm)}$	product of $H_{(jk)}$ and $H_{(lm)}$	232
HF	"high-frequency"	179
h_{cu}	height of copper in a layer of foil, strip, or equivalent rectangular conductors	15
h_t	height of insulating tape	156
I	a constant value of current, rms unless indicated otherwise by a subscript	8
$\underline{I}$	complex current phasor	8
[I]	identity matrix	216
I_j	integral expression j	G-2
$\underline{I}_m$	magnetizing current phasor	131
Im	"imaginary" operator to signify "imaginary part of ..."	67
i	instantaneous current	8
$\underline{\mathbf{J}}$	current density, a vector phasor	60
j	$\sqrt{-1}$	8
	winding number	129
	row index of a matrix	191
(jk)	(subscript) refers to a short-circuit test where winding j is excited and winding k is short-circuited	129
K	total number of windings in a transformer	190
K_T	temperature coefficient of resistivity; $K_T = 3.93 \times 10^{-11}$ Ω-m/°C for annealed copper wire [14, p. E-88]	156
k	winding number	129
	column index of a matrix	191
$\underline{k}$	complex wave number	58

(continued)

Glossary of Symbols (continued)

Symbol	*Meaning*	*Part I Page*
L	inductance	130
LF	"low-frequency"	179
$L_{(jk)}$	short-circuit inductance at winding j with winding k short-circuited	149
$L_{\ell n}$	leakage inductance associated with winding n	130
L_m	magnetizing inductance	130
ℓ	length	19
l	loop	34
ℓ_{gn}	"length of turn" for the interlayer gap number n	147
ℓ_m	magnetic path length	II–24
ℓ_T	length of turn in a winding layer	16
ℓ	(subscript) "layer"	16
	(subscript) "leakage"	130
M	mutual inductance	191
N	number of winding layers in a transformer	140
N_c	number of current-carrying conductors in a winding layer; $N_c = n_s N_\ell$	16
N_j	number of turns in winding j	26
N_ℓ	number of turns in one winding layer	16
$-N$	(subscript) "normalized"	9
n	number of turns per meter across the breadth of a winding	37
	layer or interlayer-gap number, counted from the innermost outward	112
n_s	number of electrically-paralleled conductors with the same height coordinate	16
n	(subscript) layer number	112
OC	(subscript) "open-circuit"	130
P	power	139
$< P_D >$	average power dissipated in all the windings of a transformer	139
$P_{R(jk)}$	power dissipated in a resistance $R_{(jk)}$	139
P_n	total power dissipated in winding layer n	112

(continued)

Glossary of Symbols (continued)

Symbol	*Meaning*	*Part I Page*
$\mathcal{P}$	permeance	II–141
p_d	power dissipated per unit volume (power density)	56
$< Q_H >$	average magnetic energy storage per square meter in the y-z plane	123
$< Q_J >$	average power dissipated per square meter of current sheet in the y-z plane	119
$< Q'_H >$	normalized average magnetic energy storage in a layer, a dimensionless function of α, β, and Δ	123
$< Q'_J >$	normalized average power dissipation in a layer, a dimensionless function of α, β, and Δ	119
R	resistance	19
	radius	31
R_c	core loss resistance	130
$R_{(jk)}$	short-circuit resistance at winding j with winding k short-circuited	149
R_{wn}	resistance of winding n	130
$_R$	(subscript) "ring"	31
$\mathcal{R}$	reluctance	24
Re	"real" operator to signify "real part of ..."	8
r	"radius" direction in a cylindrical coordinate system where a point is specified as (r, ϕ, z); distance in the radius direction	34
$_r$	(subscript) "reduced"	200
S	surface	34
S_ℓ	center-to-center distance between two adjacent layers of the same winding section	18
$S_{\ell s}$	center-to-center distance between two adjacent layers of different winding sections	18
S_s	center-to-center distance between two adjacent sections of the same winding	18
$_s$	(subscript) "secondary"	226
$_{SC}$	(subscript) "short-circuit"	8
$_{s,j}$	(subscript) "secondary j"	226

(continued)

Glossary of Symbols (continued)

Symbol	*Meaning*	*Part I Page*
T	period of a waveform	113
	temperature	II–30
T_S	switching period	II–51
TEM	"transverse electromagnetic"	105
$_T$	(subscript) "total"	144
^{T}	(superscript) transpose of a matrix or vector	200
t	time	7
$_(t)$	"time" as an independent variable; indicates that the preceding quantity is instantaneous or time-varying	7
$[\underline{V}_{d4}]$	vector of differential voltages $\underline{V}_{j4}$, all referenced to terminal 4	200
$\underline{V}$	complex voltage phasor	8
$\underline{V}_{jk}$	differential-voltage phasor between terminals j and k	199
V_n	volume of winding layer n	113
v	instantaneous voltage	177
	distance from $\chi = h_{cu}$, in the negative χ direction, in units of skin depth; $v = (h_{cu} - \chi)/\delta$; $v = w - \Delta$	E-3
W	energy	112
w	distance measured along the χ-axis in units of skin depth δ; $w = \chi/\delta$	117
$< W_g >$	time-average magnetic energy stored in all the interlayer gaps of a transformer	144
$W_{L(jk)}$	magnetic energy stored in an inductance $L_{(jk)}$	144
$< W_\ell >$	time-average magnetic energy stored in all the winding layers of a transformer	144
W_n	magnetic energy stored in winding layer n	112
$< W_T >$	total time-average magnetic energy stored in a transformer	144
w_m	magnetic energy stored per unit volume (energy density)	56
X_{bob}	height of the center leg of the bobbin	156
x, y, z	the three axes in a right-handed Cartesian coordinate system which correspond to the dimensions of *height*, *depth*, and *breadth* respectively; distance in the corresponding reference direction; as subscripts, a quantity in the designated direction	55

(continued)

Glossary of Symbols (continued)

Symbol	*Meaning*	*Part I Page*
χ	(actually the Greek letter chi) variable denoting a position across the finite dimension of an infinite current sheet	66
$\underline{Y}$	admittance	190
Y_{bob}	depth of the center leg of the bobbin	156
$\underline{Y}_{jk}$	admittance $\underline{I}_k/\underline{V}_j$ of a transformer with all windings short-circuited except the excited winding j	192
Y_o	distance across the windings in the y direction	158
y_j	expression j	F-1
$\underline{y}_{jk}$	admittance element between terminals j and k of the admittance-link equivalent circuit	205
$\underline{Z}$	impedance	8
$\underline{Z}_{(jk)}$	short-circuit impedance with winding j excited and winding k short-circuit	149
$[\underline{Z}_S]$	coupled-secondaries equivalent-circuit impedance matrix	228
z_n	(subscript) component in z-direction in layer n	136
α	real part of the boundary-condition ratio $\underline{\Gamma}$	67
β	imaginary part of the boundary-condition ratio $\underline{\Gamma}$	67
$\underline{\Gamma}$	boundary-condition ratio; $\underline{\Gamma} = \alpha + j\beta$	67
Δ	height of a winding layer in skin depths; $\Delta = h_{cu}/\delta$	117
δ	skin depth; $\delta = \sqrt{2/\omega\mu\sigma}$	59
ε	variable which is either 1 or 0 depending upon the magnetic-field-intensity boundary conditions	68
ϵ	permittivity	58
ϵ_r	relative permittivity; $\epsilon_r = \epsilon/\epsilon_0$	A-2
ϵ_0	permittivity of free space, 8.854×10^{-12} [F/m]	58
η	layer porosity; $\eta = N_c b_{cu}/b_{win}$	22
θ	phase angle	8
Λ	flux linkage	II–141
λ	wavelength	D-8
μ	permeability	23
μ_r	relative permeability; $\mu_r = \mu/\mu_0$	A-2
μ_0	permeability of free space, $4\pi \times 10^{-7}$ [H/m]	23

(continued)

Glossary of Symbols (continued)

Symbol	*Meaning*	*Part I Page*
ν	volume; $d\nu$ is a differential volume element	112
π	constant, 3.14159	72
ρ	resistivity in general, which could be the actual resistivity of a material or an "effective" resistivity; $\rho = 1/\sigma$	
	charge density	A-1
ρ_{cu}	resistivity of copper; for annealed copper wire: 1.7241×10^{-8} Ω-m at 20°C with temperature coefficient 3.93×10^{-11} Ω-m/°C [13, p. E-88]; $\rho_{cu} = 1.8813 \times 10^{-8}$ Ω-m at 60°C	164
σ	conductivity in general, which could be the actual conductivity of a material or an "effective" conductivity	19
σ_{cu}	conductivity of copper; $\sigma_{cu} = 1/\rho_{cu} = 5.315 \times 10^7$ S/m at 60°C	164
σ_{eff}	effective conductivity; replaces the σ in the equations of Part I when calculating for equivalent-foil windings; $\sigma_{eff} = \eta\sigma_{cu}$	126
$\underline{\Phi}$	flux phasor	II–30
ϕ	instantaneous magnetic flux	24
	the angle dimension in a cylindrical coordinate system where a point is specified as (r, ϕ, z)	53
χ	variable denoting a position across the finite dimension of an infinite current sheet	66
ω	angular frequency of a periodic waveform	8
$'$	prime, the identifier for a circuit-element value which has been multiplied by a transformer turns ratio to reflect it from its original-winding location to a location in another winding circuit	195
*	(superscript) "star," meaning the complex conjugate of the preceding quantity	116
$< _ >$	angle brackets, denoting the time average of the enclosed quantity	8
$\tilde{}$	block-partitioned matrix	216
	complex quantity	D-3

This page has been left blank intentionally.

Chapter 1

Introduction

1.1 OVERVIEW OF PART II

In Part I of this report, we present an analytical approach to the problem of characterizing a multiwinding transformer used under high-frequency excitation conditions. The analysis in Part I is based on a set of approximations and assumptions that allow us to evaluate the fields in the transformer using a general boundary-value problem in a single dimension. We use the approximate distribution of the magnetic field intensity in and around the windings of the transformer to calculate values of resistance and inductance which can be used to model the terminal characteristics of a multiwinding transformer based upon the geometry of the device and the excitation conditions in the various windings.

Part I of this report is meant as a detailed and comprehensible development of the field-analysis approach to calculating high-frequency transformer characteristics. It is built upon basic concepts of transformer modeling as well as on ideas presented in recent articles that address the specific topics of eddy-current losses and high-frequency leakage inductances in the windings of transformers. In this second part, Part II of the report, we review eight articles which address issues related to the design of transformers for high-frequency applications. Of particular interest in what follows are the specific application of different analysis procedures by the different authors to the design of transformers, and the relationships between the ideas in the various papers reviewed and the ideas presented in Part I.

The discussion that follows in Part II is structured as a set of loosely related evaluations of certain significant articles which have been examined in some detail. In reviewing each particular article, we do not emphasize equally all aspects of the material covered by the authors; rather we focus on what in that article we believe is likely to provide the most insight to the designer of high-frequency transformers. We emphasize the main points of the analysis in each paper and discuss the significance and shortcomings of the various assumptions that the author of the paper makes in presenting the analysis. We attempt to clarify, and in some cases correct, the most important results given by each

of the authors. We seek further to provide the reader with a clear understanding of the interrelations between the various papers.

1.1.1 Chapter Summaries

Table 1.1 lists the titles and the authors of the articles that are considered in this document. Although the earliest work in this table was published by Dowell over twenty years ago, more than half of the papers reported on were published in the last five years.

In Chapter 2 of Part II, we give an in depth review of the article by P.L. Dowell which is the earliest and most often cited work of the eight papers. Dowell is the first of the authors to present formulas for computing the ac resistance and ac leakage inductance of transformers based only on the winding layout, the core geometry and the current-excitation conditions. Dowell's work was intended specifically to optimize the design of communications transformers operated under sinusoidal-excitation conditions. His analysis is somewhat limited by his use of winding portions as the unit of analysis and by his consideration of only what he calls "optimum" winding arrangements. Nonetheless, the main ideas that he develops are important keys to understanding the design-optimization algorithms presented in later papers.

Dowell's paper is based solely on sinusoidal-current-excitation conditions in a transformer. In Chapter 3, we review the work by P.S. Venkatraman that extends Dowell's results to nonsinusoidal excitation conditions. Venkatraman applies Fourier decomposition techniques to selected nonsinusoidal waveforms and then uses Dowell's resistance formulas at each of the Fourier-component frequencies to calculate the total effect of the nonsinusoidal currents. Venkatraman's paper is important not only because the analysis is for nonsinusoidal excitations but also because it is the only one of the selected papers that presents experimental verification of some of the theoretical formulations.

In Chapter 4, we look at a paper by Bruce Carsten that builds further on the work presented by Dowell and Venkatraman. Carsten presents plots of the copper losses in the windings of a transformer for specific nonsinusoidal current waveforms commonly encountered in power converters. From these preplotted design charts, Carsten determines the conductor size that will produce the lowest power dissipation in a given transformer winding structure. The virtue of Carsten's design charts is that they represent normalized loss data and are plotted for a normalized winding-conductor size. Because of this, a single set of charts serves equally well for any combination of conductor size and excitation frequency for a given winding-current waveform.

We discuss two articles by J. Jongsma in Chapters 5 and 6. In Chapter 5 we review Jongsma's article "Minimum-Loss Transformer Windings for Ultrasonic Frequencies" which comprises bibliographic references [4] and [5] since it was published in two parts. In Chapter 6 we review "High-Frequency Ferrite Power Transformer and Choke Design; Part 3: Transformer Winding Design" which is reference [6]. Jongsma, like Carsten and Venkatraman, bases his analysis primarily on the ideas presented by Dowell, however, he make several assumptions which permit a simplification of Dowell's results. Jongsma then develops a design algorithm that can be used to choose the conductor

Table 1.1: List of Paper Titles and Authors

Dowell, P.L.	[1] "Effects of Eddy Currents in Transformer Windings," *Proceedings of the IEE*, Vol. 113, No. 8, August 1966, pp. 1387–1394.
Venkatraman, P.S.	[2] "Winding Eddy Current Losses in Switch Mode Power Transformers Due to Rectangular Wave Currents," *Proceedings of Powercon 11*, Power Concepts Inc., Ventura Ca., 1984, Section A-1, pp. 1–11.
Carsten, Bruce	[3] "High Frequency Conductor Losses in Switchmode Magnetics," *High-Frequency Power Converter Conference*, May 1986, pp. 155–176.
Jongsma, J.	"Minimum-Loss Transformer Windings for Ultrasonic Frequencies," *Phillips Electronics Application Bulletin*, Phillips, The Netherlands, 1978. [4] "Part 1: Background and Theory," E.A.B. 35, No. 3, pp. 146–163, [5] "Part 2: Design Methods and Aids," E.A.B. 35, No. 4, pp. 211–226.
	[6] "High-Frequency Ferrite Power Transformer and Choke Design; Part 3: Transformer Winding Design," *Philips Electronic Components and Materials Technical Publication 207*, Phillips, The Netherlands, 1986.
Perry, M.P.	[7] "Multiple Layer Series Connected Winding Design for Minimum Losses," *IEEE Transactions on Power Apparatus and Systems*, Vol. PAS-98, No. 1 Jan./Feb. 1979, pp. 116–123.
Vandelac, J.P., and Ziogas, P.	[8] "A Novel Approach for Minimizing High Frequency Transformer Copper Losses," *IEEE Power Electronics Specialists Conference Record*, 1987, pp. 355–367.
Rosa, John	[9] "Calculation of Flux Linkages in Multiwinding Transformers," *IEEE Power Electronics Specialists Conference Record*, 1986, pp. 639–644.

size which gives the best (i.e., lowest copper loss) transformer performance for a given device. Jongsma's articles are of considerable length, and they present a fairly thorough discussion of the practical considerations that the transformer designer must address in order to apply Dowell's analysis to any actual transformer design problem.

The paper by M.P. Perry discussed in Chapter 7 examines the eddy-current losses that occur in a series-connected infinite solenoid. Perry develops expressions for the power dissipated in a unit length of such a solenoid based solely on the sinusoidal currents in the winding layers of the solenoid. The general current-sheet analysis presented by Perry is the foundation for the field solution presented in Part I of this report, and Perry's paper is unlike those by Venkatraman, Carsten and Jongsma in that it does not cite or rely on the work by Dowell. As we show in the discussion of Dowell's results in Chapter 2, the current-sheet approach is more general than, but consistent with, the analysis presented by Dowell.

J.P. Vandelac and P. Ziogas's paper that we review in Chapter 8 brings together the key aspects of the analysis trail started by Dowell and the general field analysis presented by Perry to produce the most general transformer analysis method of those presented in the articles under review. Vandelac and Ziogas rely most heavily on Perry's work, but they also incorporate the Fourier decomposition techniques presented by Venkatraman. In the article, Vandelac and Ziogas introduce an approach for analyzing the power dissipation characteristics of transformers used in flyback converters or other such circuits where the transformer must drive switching secondary loads.

The next chapter of Part II of the report discusses a paper by John Rosa. This paper addresses only low-frequency transformer inductances; it is included here primarily because it presents a method for creating an equivalent-circuit model for a multiwinding transformer. The circuit proposed in Rosa's article is discussed in Chapter 8 of Part I of this report where it is modified to produce the $(K-1)$-port coupled secondaries equivalent circuit. In Chapter 9 of Part II below, we summarize Rosa's main ideas and explain some of the terminology from his paper.

Chapter 7 in Part I of this report presents the admittance-link equivalent circuit, a potentially useful model for high-frequency multiwinding transformers. In that chapter, the admittance-link model is developed and it is shown how the link admittances can be determined from the short-circuit impedances of the transformer. Although the computer-based calculation of the short-circuit impedances necessary to determine these link admittances is new, the admittance-link model itself dates back to the early part of this century. Three sources of information on this equivalent circuit which were used as background material for Chapter 7 of Part I are the subjects of Chapter 10 here. Chapter 10 serves primarily to translate the terminology adopted by the various authors into a set consistent with that adopted in Part I, and to indicate the relative merits of each author's discussion; it is not intended as a stand-alone explanation of the admittance-link model.

The literature review presented in Chapters 2 through 9 was summarized in a paper presented at the *1989 Applied Power Electronics Conference* in Baltimore, Maryland. A

reprint of this paper is included as Appendix A. This appendix is provided as an concise introduction to various issues discussed in Chapters 2 through 9. In addition, it serves as a supplement to those chapters since it directly addresses specific issues, such as the use of Litz wire, and examines the various authors' approaches to each issue, rather than focusing on only one author at a time as this report does.

1.1.2 Initial Comparisons of the Reviewed Articles

Figure 1.1 presents a quick overview of the trail of analysis that exists between the papers in this literature review. A primary contribution of each author and the relationships between the papers under review are indicated in the figure. The different analysis techniques that flow from the original work of Dowell and Perry are represented by separate paths. Also shown is how the ideas of the various authors converge in the work by Vandelac and Ziogas. The arrows leading away from the boxes for the papers by Dowell, Perry, Venkatraman, and Carsten are labeled with the coefficient developed in each paper that is most significant to later work. The four coefficients are as follows:

F_R = the ratio of the ac to dc winding resistances of a winding portion under sinusoidal excitation. (Dowell [1])

F_H = the ratio of transformer winding losses for a trapezoidal current waveform to the losses for sine-wave excitation. (Venkatraman [2])

K_R = the ratio of the effective resistance of a winding for a particular nonsinusoidal current to the dc resistance when the winding conductor is one skin depth in height at the fundamental (i.e., switching) frequency. (Carsten [3])

Q = the amount of power dissipated per unit area of a winding layer in an infinite solenoid, based on its thickness and the frequency and magnitudes of the sinusoidally varying magnetic fields at the boundaries of the layer. (Perry [7])

The flowchart also shows that the paper by Rosa is rather unrelated to the main concepts discussed in the other articles reviewed here.

Table 1.2 summarizes some of the technical issues presented in the various articles. The topics listed in this table are not specifically discussed in this introduction and we make no attempt here to expand on the significance of the descriptors used in Table 1.2; rather, the reader is encouraged to use this table as a reference and guidepost in comparing the articles discussed in Chapters 2 through 9. In Table 1.2, we place a check mark under the name of a particular author if the topic on the left of the table is addressed in that author's paper. A check mark does not convey any information about how thorough a treatment the author gives to the topic, but only that the topic is at least mentioned in the paper. The reader should notice also that the first column under the heading *Authors* is labeled *Part I*; this column indicates the issues that are addressed in Part I of this report. In Chapters 2 through 9, we often discuss what relationship, if any, the ideas in a particular paper have to the ideas developed in Part I, but we do not give a

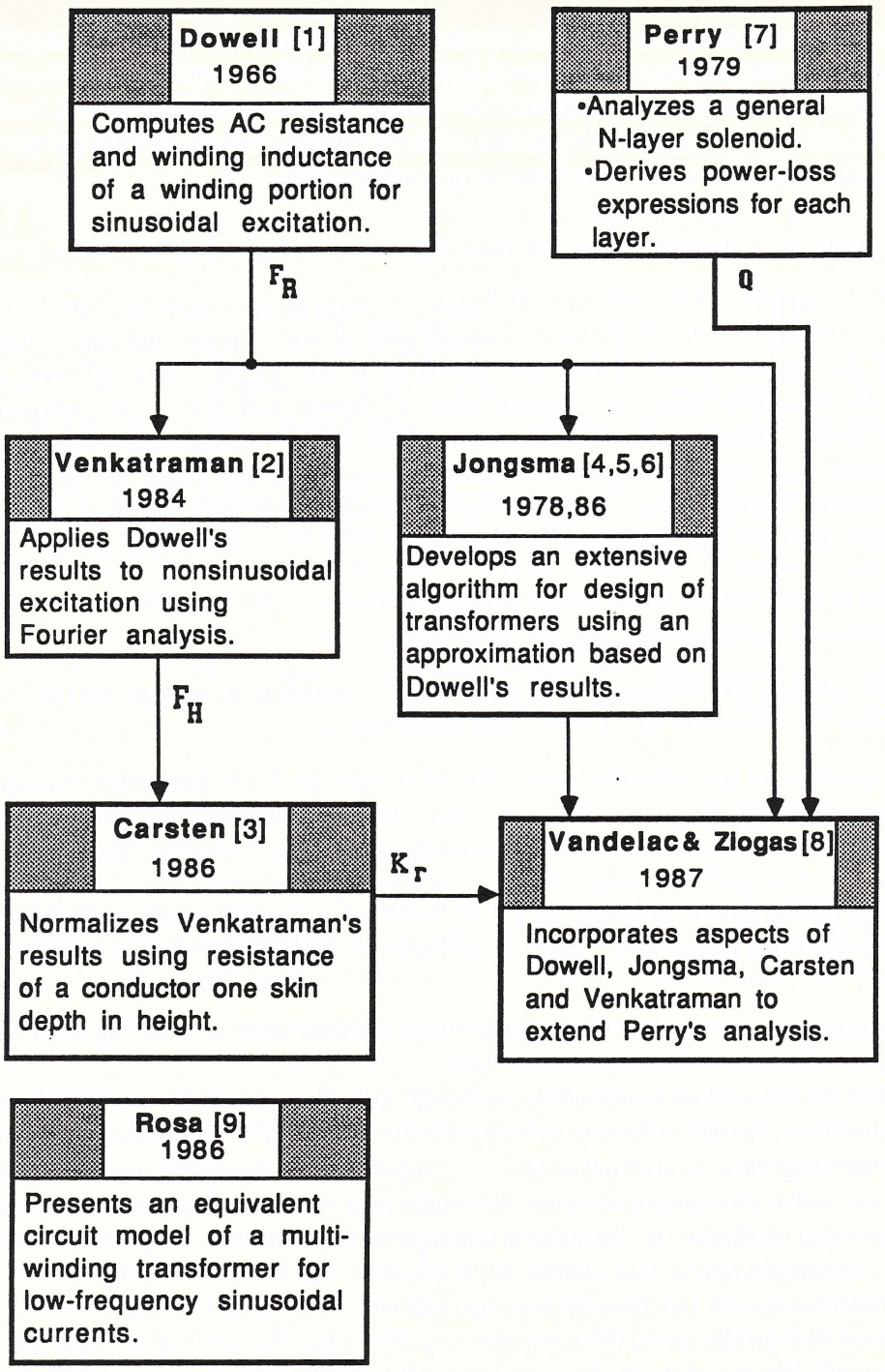


Figure 1.1: Literature flowchart representing a primary contribution of each author, and the progression of analysis between papers.

Table 1.2: Matrix of Topics Discussed in the Literature

Feature	*Authors*							
	Part I	*Dowell* [1]	*Venka-traman* [2]	*Carsten* [3]	*Jongsma* [4,5,6]	*Perry* [7]	*Vandelac & Ziogas* [8]	*Rosa* [9]
sinusoidal analysis	√	√	√	√	√	√	√	√
nonsinusoidal analysis			√	√	√		√	
switching secondary currents							√	
neglects magnetizing current	√	√	√	√	√		√	√
formulas for power dissipated in a layer	√					√	√	
formulas for power dissipated in a winding	√		√	√			√	
formulas for resistance of a winding		√	√	√	√			
formulas for inductance of a winding		√	√					
considers ac resistance	√	√	√	√	√			
considers ac inductance	√	√	√					
considers only low-frequency inductance								√
discusses minimum-loss windings				√	√	√	√	
algorithms for design of minimum-loss transformers					√			
based on Dowell's paper		√	√	√	√			
based on Perry's paper	√					√	√	
uses normalized wire size	√	√	√	√	√	√	√	
presents graphical design charts		√	√	√	√	√	√	
presents experimental data	√		√					
considers loss in electrostatic shields	√			√	√		√	
uses field-intensity diagrams	√	√	√		√		√	√
multiwinding equivalent circuits	√							√
discusses Litz wire			√	√	√			
shell windings	√	√	√	√	√	√	√	√
stacked-disk windings							√	√
cylindrical-coordinate solution						√		

detailed explanation or description of the contents of Part I. The reader should refer to the text of Part I for the development of the relevant topics.

1.2 CONVENTIONS

1.2.1 Notational Conventions

In Chapters 2 through 9, we discuss the eight papers listed in Table 1.1. Since we are examining in these chapters the work of several different authors, there are certain notational differences and/or conflicts that the reader should be clear about at the outset. We are particularly interested in resolving differences that exist between the terminology used in Part I of this report and that used in the articles we are reviewing. On the second page of each of Chapters 2 through 9, we provide a table of important terminology used by each author. The terminology listed in each of these tables is intended to translate from each authors's different symbols and terminology to that used in Part I. The Glossary of Symbols which follows the Table of Contents contains a complete set of terminology adopted for the two parts of this report. Notational conventions adopted for the report are discussed in Section 1.3 of Part I, however, we reiterate that SI units are used throughout this report.

There are some terminology conventions that concern many if not most of the articles discussed in Part II. These can be broken into three areas: equation references, representation of sinusoidally varying quantities, and the designation of effective conductivity for the wire in a particular winding of a transformer. We discuss each of these areas below.

1.2.1.1 References to Equations and Figures of Part I

When we have occasion in the following chapters to refer to equations, figures, and sections of Part I of this report, we always include an explicit reference in the text that indicates that the item of interest is found in the detailed analysis of Part I. The reader should assume that unless such a reference is given, then the equation number, section number, or figure number refers to the numbering of the current document, i.e., Part II of this report. In addition, any references to equations, etc., of a particular paper will be explicitly identified.

1.2.1.2 Sinusoidally Varying Quantities

In Part I of this report, we often denote a quantity that varies sinusoidally in time using phasor notation which we indicate by underlining the symbol for the quantity in question. For example, we designate a sinusoidally varying current $i(t) = \sqrt{2}I\sin(\omega t+\theta)$ as a phasor $\underline{I} = I\angle\theta$. The reader should review Section 1.3 of Part I for a discussion of the phasor conventions adopted for the report. What we need to point out here is that: (1) some of the papers we review in the following chapters are not clear in indicating

when a given quantity is in fact sinusoidally varying with time, and (2) some authors use the peak value of the sinusoidal quantity as the magnitude of the phasor, whereas, we use the rms value as the phasor magnitude. This latter discrepancy means that some of the results given in the different papers may appear in a slightly different form from the results given in Part I when in fact they represent the exact same quantity. We indicate in the different chapters which convention the particular author uses in that paper.

1.2.1.3 Effective Conductivity

The formulas for power dissipation and energy storage presented in Chapter 4 of Part I of this report are derived for a current sheet that is infinite in two dimensions, has a finite height (or thickness), and has a conductivity σ. This formulation is general and places no restrictions on the value of σ; if the geometry of the conductors in a given transformer matches that of the current sheet in the theoretical development, then σ in the mathematical development is the same as σ_{cu}, the conductivity of the actual winding material. When an actual winding layer that is made up of real conductors is modeled by a *porous* foil conductor as described in Section 2.2 of Part I, then the conductivity σ in the mathematical results represents the effective conductivity σ_{eff} of this model current sheet. This notation is adopted in Section 4.6 of Part I and is used in the equations for short-circuit resistance and inductance derived in Chapter 5 of Part I.

We state in Section 2.2.1 of Part I that we can compensate for the changes introduced in the geometric modeling process by introducing the layer porosity η as a factor that multiplies the conductivity of the winding wires. We find in reviewing the papers in the literature that this η term is usually included as an integral part of the stated results. To avoid confusion on this point, we wish to emphasize that in Part II the symbol σ_{eff} is employed to stand for the effective conductivity of the *porous* layer as is done in Section 4.6 and Chapter 5 of Part I. The effective conductivity is given by (4.127) of Part I

$$\sigma_{eff} = \eta \sigma_{cu} \tag{1.1}$$

where σ_{cu} represents the actual conductivity of the material—here assumed to be copper—in the windings of the transformer. The reader should be aware of the drawbacks associated with the use of layer porosity η. These are discussed in Section 2.2.2 of Part I. The reader should be aware as well that the various authors reviewed here use σ to represent the conductivity of the winding-conductor material itself, i.e. what we call σ_{cu}.

All terms that are derived with the conductivity as a parameter are also affected by our use of an effective conductivity. Among such derived quantities are the complex wave number and the skin depth. However, we do not make a distinction between the derived quantities that result from the use of different expressions for conductivity; for example, we do not adopt an effective complex wave number $\underline{k}_{eff}$ that results from evaluating the expression $\underline{k} = \sqrt{j\omega\mu\sigma_{eff}}$. Unless otherwise stated, it is assumed that the complex wave

number is expressed by (4.128) of Part I

$$\underline{k} \approx \sqrt{j\omega\mu_0\sigma_{eff}} \tag{1.2}$$

and that the skin depth is expressed by (4.129) of Part I

$$\delta = \sqrt{\frac{2}{\omega\mu_0\sigma_{eff}}} \tag{1.3}$$

1.2.2 Chapter Format and Content

In addition to the terminology conventions discussed above, several other conventions have been adopted with regard to the format and content of Chapters 2 through 9. Although not essential to the understanding of the chapters, an awareness of these conventions should facilitate the location of information within each chapter and the comparison of information between chapters.

For the most part, the format and content vary among Chapters 2 through 9, but certain conventions were adopted where conformity was deemed useful. The second page of each chapter was reserved for a symbol table comparing the nomenclature adopted in Part I with that adopted by the author of the paper under review. The format adopted for these tables is described in the next two paragraphs. In addition to introducing the table, the initial section of each chapter serves as an overview or summary of the paper and of the author's methods. Highlighted in this overview is the author's approach to several issues that we designated as being of interest to designers of multiwinding transformers for converter applications. These key issues are enumerated at the end of Section 1.2.2. Within the body of each chapter, important equations and representative figures from the paper under review are given to help illustrate the discussion of the author's methods. No convention for the placement of these equations and figures within the chapters was adopted by the authors of this report. Unless otherwise noted, equations are given using the symbols of Part I wherever applicable. Figures from the papers are presented with their original labels, and, where applicable, with boxed labels which represent the translations of the original labels into the symbols of Part I.

Each of the chapters contains a table which compares the symbols and definitions adopted by the author of the paper under review to those adopted in the Glossary of Symbols. These tables do not serve as complete recapitulations of the symbols employed in the paper under review or in the Glossary. Rather, they present only those symbols and definitions for which a conflict exists between the paper and the Glossary of Symbols, and those symbols that are needed for the discussion within the chapter. Symbols listed in the table are given alphabetically as described in the introduction to the Glossary.

Table 1.3 shows a sample of one of these tables. As we can see, each table is composed of three columns. The left-hand column is labeled with the name of the author, in this case Dowell, and contains the symbols used in the paper under review. The center column is labeled *Duke* and contains the symbols adopted in the Glossary of Symbols.

Table 1.3: Comparison of Symbols and Definitions

Dowell	*Duke*	*Meaning* Dl: Dowell, Du: Duke
a	b_{cu}	breadth of copper in equivalent rectangular conductors
J	$J_y(x,t)$	instantaneous, y-directed current density as a function of x
	$\underline{J}_y(x)$	phasor of y-directed current density, a function of x
ℓ_T	ℓ_T	Dl: mean length-of-turn in a winding portion Du: length-of-turn in a winding layer
m	—	number of whole layers in a winding portion
Z_W	$\underline{Z}_W{}^{\dagger}$	impedance of a winding portion
δ	—	insulation thickness
—	δ	skin depth

† Used only in this chapter.

The right-hand column of the table contains the definitions for the symbols listed in the first two columns. If different symbols are used in the paper and the Glossary to represent the same quantity, then the symbols are listed and defined in a single table entry. The first entry in Table 1.3 which defines the symbols a and b_{cu} represents such a case. When a symbol in one system, such as Dowell's symbol J in Table 1.3, corresponds to more than one symbol in the other system, such as Duke's symbols $J_y(x,t)$ and $\underline{J}_y(x)$, then the table entry contains all of the corresponding symbols with their definitions. When symbols in the two systems represent essentially the same quantity but there is some noteworthy difference in the definitions, or the same quantity is called by different names, the symbols are given in the same entry but with both definitions. These definitions are differentiated by one or two letter codes representing the author's name and the word "Duke". An example is given in Table 1.3 by the entry for ℓ_T. A "—" in either symbol column means that there is no symbol in that system which corresponds to the symbol in the other system being defined by that table entry. This is demonstrated by the entry for m in Table 1.3. When it is necessary within a chapter to use a symbol which is not adopted by the Glossary of Symbols or by the author of the paper under review, the symbol is denoted in the table by a dagger (†) as is the symbol $\underline{Z}_W{}^{\dagger}$ of Table 1.3. When the two systems of symbols employ the same symbol for different quantities, then two separate entries are given in the table. This is represented in Table 1.3 by the entries for δ.

In the introductory section of each chapter, the following questions are answered:

1. What is the principal concern of the paper?

2. What device does the author analyze? This includes information on whether the author addresses two-winding or multiwinding transformers, shell or stacked-disk windings, and the like.

3. Does the author discuss the variation of both winding losses and energy storage which are usually modeled with an equivalent R and L, or is the discussion limited to only resistive winding losses?

4. How does the author represent complex quantities such as field intensity and current density? Is phasor notation employed, or are real-valued instantaneous or rms values used instead?

5. Does the method provide for the eddy-current losses due to shields and open-circuited windings located in regions of nonzero magnetic field intensity?

6. Is the presented method restricted to sinusoidal excitation, or is it applicable to nonsinusoidal excitation also?

7. Does the author present any experimental verification of his methods?

1.3 OTHER GENERAL COMMENTS

There are a few general comments and guidelines that are useful to reinforce at this point. First, it is assumed in what follows that the reader is acquainted with the concepts presented in Part I of this report. We also assume that the reviewed articles are available for the reader to consult as necessary, however, we do not assume that the reader is familiar with them.

The discussion of Part I is aimed at developing an equivalent-circuit representation for multiwinding transformers based on an analytical approximation of the fields inside the device. We believe that such an equivalent circuit may prove useful in simulating the behavior of a given transformer in different power-converter circuits, and it is with this goal in mind that we develop the results given in Part I. The equivalent circuit determination is simply one particular application of the general field solution that we develop in Part I. This general field solution is heavily based on the concepts given in the articles discussed in the following chapters. The papers from the literature that we discuss here, however, are not concerned for the most part with developing a transformer equivalent circuit, therefore, they do not apply the field solution in quite the same way; the emphasis in most of the papers lies in choosing the winding layout and conductor size that results in the minimum amount of power dissipation in the device. A quick look through the many algorithms and design charts that the different authors present is likely to be somewhat confusing, but the reader is reminded that the basic ideas behind almost all of these results are the same as those given in Part I of this report.

While the analytical basis for the papers in the literature and in the discussion of Part I are very closely related, we should remember that this common base is only an

approximation to the actual field distribution that exists in and around the windings of an actual transformer. We can expect that the many assumptions used to derive analytical field solutions will in fact be unacceptably inaccurate in some applications. There is not a great deal of experimental verification for any of the results presented in the various papers—including the results given in Part I of this report—so it is rather difficult to know exactly what applications will benefit from design formulas based on a general analytical solution.

An alternative method for determining the loss and energy-storage characteristics of a transformer operating under high-frequency sinusoidal conditions that does not rely on many of the simplifying assumptions made in developing analytical solutions is to use a numerical-analysis tool to calculate the field distribution directly. One such numerical tool utilizes a finite element analysis technique to calculate the magnetic field distribution at a suitable number of points in the structure of a given magnetic device. Such analysis tools that can solve for the eddy-current losses in conductors in a reasonable amount of time on standard laboratory computers are beginning to come into more common usage, but they have not yet been applied extensively to the type of problems discussed in the present report.

At Duke, we have carried out some rudimentary magnetostatic finite-element evaluations of the type of transformers discussed in this report. The results of these investigations have added to our qualitative "feel" for the distribution of magnetic energy in such devices, but have yielded little usable data due to the restriction to magnetostatic analyses. We have not, therefore, been able to quantify the significance of any differences between analytic and numeric field solutions. Numerical analysis of the high-frequency characteristics of magnetic devices has the considerable advantage that it is not based on the type of approximations used in the analytical development discussed in this report, but at present the numerical techniques are not currently in wide use and their utility is not certain.

This page has been left blank intentionally.

Chapter 2

Dowell

P. L. Dowell, "Effects of Eddy Currents in Transformer Windings," *Proceedings of the IEE*, Vol. 113, No. 8, August 1966, pp. 1387–1394.

2.1 OVERVIEW

This frequently-cited paper lays the foundation for much of the current literature on high-frequency effects in transformers. For a two-winding transformer under sinusoidal excitation, Dowell shows how to calculate the ac winding resistance and ac leakage inductance associated with each winding from the geometry of the transformer. Other authors, including Venkatraman and Carsten, apply Dowell's approach to nonsinusoidal excitation by summing results for sinusoidal components in the Fourier-series decomposition of a nonsinusoidal waveform.

To illustrate the relationship between Dowell's work, that of other authors, and Part I of this report, this summary is presented in terms of the common set of symbols found in the Glossary of Symbols, with Dowell's original symbols translated according to Table 2.1. In the paper, Dowell makes no distinction between instantaneous variables and phasor variables. Certain equations such as the second one following his (1) clearly contain instantaneous variables, others such as his (25) clearly contain phasors, while still others are correct for either instantaneous or phasor variables. To avoid confusion, phasor variables are always underlined in this chapter.

Dowell's equations were checked by rederiving them, except those for a half-layer of conductors. As for experimental verification, Dowell only mentions that he obtained good agreement between calculated and measured values of leakage inductance and resistance in tests performed on a transformer with single-layer windings over the frequency range of dc to 10 MHz. No details are given.

Table 2.1: Comparison of Symbols and Definitions

Dowell	*Duke*	*Meaning* Dl: Dowell, Du: Duke
a	b_{cu}	breadth of copper in equivalent rectangular conductors
b	b_{win}	breadth of the core window; Dowell's equations imply $b_{win} = b_{max} = b_w$ (defined in the Glossary of Symbols)
D	—	unnamed variable of convenience; $D = 2\underline{k}h_{cu} \tanh \frac{\underline{k}h_{cu}}{2}$
F_L	—	ac-to-dc inductance ratio for a winding portion
F_R	—	ac-to-dc resistance ratio for a winding portion
g	g_{inters}	height of an intersection gap
H	$H_z(x,t)$	instantaneous, z-directed magnetic field-intensity as a function of x
	$\underline{H}_z(x)$	phasor of z-directed magnetic field-intensity, a function of x
h	h_{cu}	height of copper in an equivalent square conductor
I	$i(t)$	total, instantaneous winding current
	$\underline{I}$	phasor of winding current
J	$J_y(x,t)$	instantaneous, y-directed current density as a function of x
	$\underline{J}_y(x)$	phasor of y-directed current density, a function of x
—	K_T	temperature coefficient of resistivity
L_g	—	leakage inductance due to the flux cutting a gap between winding portions
—	$L_{\ell n}$	leakage inductance associated with winding n
L_U	—	leakage inductance due to the flux cutting all of the interlayer gaps within a winding portion
L_{w0}	—	dc leakage inductance due to the flux cutting all conductors of a winding portion
—	ℓ_g	"length-of-turn" for a gap between winding layers
ℓ_T	ℓ_T	Dl: mean length-of-turn in a winding portion Du: length-of-turn in a winding layer
M	—	unnamed variable of convenience; $M = \underline{k}h_{cu} \coth \underline{k}h_{cu}$
m	—	number of whole layers in a winding portion

(continued)

Table 2.1: Comparison of Symbols and Definitions (continued)

Dowell	*Duke*	*Meaning* Dl: Dowell, Du: Duke
—	N_c	number of current-carrying conductors in a winding layer
N_ℓ	N_ℓ	number of turns in a winding layer; each turn contains one or more electrically-paralleled conductors
N_p	—	number of turns in a winding portion
p	—	positive integer, the layer count from a position of zero mmf
R_{w0}	—	dc resistance of a winding portion
u	g_{intras}	Dl: height of an interlayer gap within a winding portion Du: height of the gap between adjacent equivalent-foil layers of the same winding
x	x	height coordinate of a winding layer as shown in Figure 2.2
Z_W	$\underline{Z}_W$ †	impedance of a winding portion
α	$\underline{k}$	complex wave number for a good conductor; $\underline{k} = \sqrt{j\omega\mu_0(\eta\sigma_{cu})}$
—	α	real part of the boundary-condition ratio; $\underline{\Gamma} = \alpha + j\beta = \underline{H}_z(\chi = 0)/\underline{H}_z(\chi = h_{cu})$
δ	—	insulation thickness
—	δ	skin depth
—	Δ	conductor height normalized to skin depth; $\Delta = h_{cu}/\delta$
η	η	layer porosity; $\eta = N_c b_{cu}/b_{win}$
θ	T	temperature in degrees C
μ_0	μ_0	permeability of free space
ρ	ρ_{cu}	resistivity of copper
σ	σ_{cu}	conductivity of copper
$\eta\sigma$	σ_{eff}	effective conductivity; $\sigma_{eff} = \eta\sigma_{cu}$
ϕ	$\phi(t)$	instantaneous magnetic flux
	$\underline{\Phi}$	phasor of magnetic flux
ω	ω	angular frequency of a periodic waveform

† Used only in this chapter.

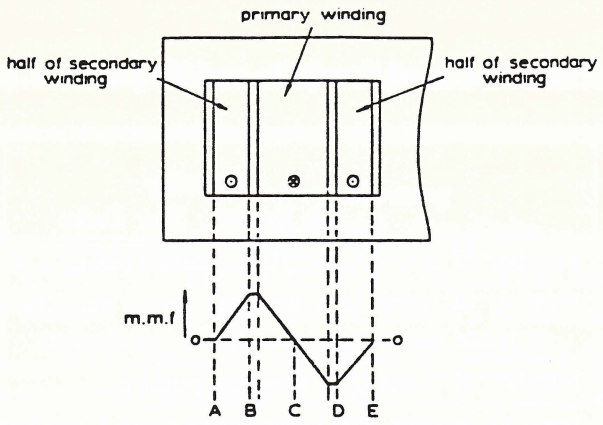


Figure 2.1: Dowell's Figure 4, which shows a winding arrangement with four portions.

The following definition is central to the form Dowell chooses for his results:

winding portion: A part of a transformer winding which, when examining the low-frequency magnetic-field-intensity profile, or mmf diagram, extends radially in either direction from a position of zero field intensity to the first positive or negative peak of field intensity. Figure 2.1 illustrates a winding arrangement with four portions.

Leakage inductance and winding resistance are calculated for one portion at a time, then summed over each winding or the whole transformer.

This approach is valid for two-winding transformers, but it is unsuitable for analyzing transformers with three or more windings. Associating the stored and dissipated energy in the winding space with particular windings is not straightforward in multiple-output-winding transformers, although it is for the two-winding case. Also, the positions of zero-crossings in the magnetic-field-intensity profile move as the relative loads on such transformers change. The zero-crossings may occur at any position across the height of a winding layer, but Dowell's equations apply only for two positions, namely, between two layers of conductors and exactly at the center of a layer. Another deficiency of Dowell's approach is that there is no way to analyze a transformer with an electrostatic shield embedded in its windings.

A more general, layer-based approach is adopted in Part I, based primarily on the work of Perry and Vandelac and Ziogas, described in Chapters 7 and 8. The equations in Part I give the same answers as Dowell's equations for the types of problems he considers, but the layer-based approach applies equally well to transformers with any number of windings, and to transformers with shields or open-circuit windings.

Section 2.2 details the conditions necessary to apply Dowell's results, as well as the assumptions underlying his analysis. Although Dowell's approach is not adopted in Part I, his major results are reported in Section 2.3, expressed in terms of the common

set of symbols adopted for this study. Finally, Section 2.4 contains clarifications and additional information which is helpful in following the paper, and Section 2.5 mentions how other authors have extended Dowell's work.

2.2 APPLICABILITY

Because Dowell's results are commonly used by other authors, it is important to understand the limitations of his results. Section 2.2.1 describes the specific conditions analyzed by Dowell, and Section 2.2.2 explains the simplifying assumptions he makes to derive his results.

2.2.1 Conditions

Dowell's results apply only under the following conditions:

1. The transformer is restricted to two windings.

2. Voltages and currents in both windings are sinusoidal.

3. There are no conducting shields or open-circuit windings present in which eddy-current losses would occur.

4. The transformer is wound with circular conductors where each layer fills the breadth of the winding space. Dowell's results are easily extended to square, strip, and foil conductors, but not to twisted-wire bundles or Litz wire. The effect of a partial layer, one which spans substantially less than the core window breadth, is not considered.

5. Although Dowell addresses only single-conductor windings, his results apply to multi-conductor windings as well if the number of turns in a layer N_ℓ is used as defined in Table 2.1, the same way it is defined in Part I.

6. The positions of zero magnetic field intensity, or mmf, in the winding space occur only between two layers of conductors or at the center of a layer. Dowell derives results for these two cases only, arguing that the windings of a transformer should always be arranged in an "optimum" configuration which minimizes total leakage energy and has the effect of locating the zero-crossings in these two positions only. This is further discussed in Section 2.3.3. In contrast, it is reasonable to assume that sometimes other considerations may dictate selection of a "non-optimal" winding arrangement, considerations such as minimizing the number of layers in a winding, minimizing inter-winding capacitance, achieving a desired leakage inductance, meeting primary-to-secondary isolation requirements, or facilitating manufacturing.

2.2.2 Assumptions

Under the conditions above, the following assumptions are made to simplify the calculations:

1. The magnetic flux in the core window is parallel to the axis of the core. This follows from the assumption that the fields in a transformer are similar to those in concentric, infinite solenoids as discussed in Section 3.1 of Part I. Based on some modeling done at Duke using a two-dimensional magnetostatic finite-element-analysis program, it appears that this assumption is good if the transformer core is radially symmetric, like a pot core, and has high permeability.

   Dowell's results can also be applied to EE and other non-radially-symmetric cores, but it is unclear how much accuracy is lost in doing so. Some static finite-element analysis was performed for a cross-section of an EE-core transformer in which the windings are not enclosed in core material, and it showed that the leakage flux takes curved paths through the winding layers, which is contrary to the tangential-flux assumption. However, good agreement has been obtained between measured short-circuit impedances and values calculated using this assumption for EE-core as well as pot-core transformers. It should be noted that the actual conditions of interest involve time-varying fields rather than the static fields calculated by our finite-element analysis. Time-varying fields induce eddy currents which oppose the penetration of leakage flux into the conductors, creating flux patterns known to be somewhat different from those calculated.

2. A single mean length-of-turn ℓ_T applies to all layers within a winding portion.

2.3 MAJOR RESULTS

In Section 2.3.1, Dowell's equation for the profile of current density across a winding layer is proven equivalent to the corresponding equation derived in Part I. After this point in the analysis, Dowell derives loss and magnetic-energy-storage equations for winding portions, while in Part I, equations are derived for individual winding layers instead. Although Dowell's results for winding portions are not used in Part I, they are translated into the common set of symbols and included here for completeness. Section 2.3.2 shows how Dowell calculates a leakage inductance for each winding, Section 2.3.3 explains Dowell's concept of an "optimum" winding arrangement, and Section 2.3.4 gives Dowell's equations for calculating ac winding resistance.

2.3.1 Current Density

In the appendix of his paper, Dowell derives an expression for the one-dimensional variation of current density across a winding layer of a transformer, his (31).

$$J = \frac{N_\ell I \alpha}{\eta b}\left\{\frac{\cosh \alpha x}{\sinh \alpha h} - (p-1)\tanh\frac{\alpha h}{2}\cosh \alpha x + (p-1)\sinh \alpha x\right\} \qquad (2.1)$$

Although Dowell does not mention the words *phasor* or *vector* in his article, it is apparent from the context that J and I in (2.1) are phasors that represent sinusoidal time functions. This equation is quite different in appearance from the corresponding equation (4.39) derived in Part I, repeated here.

$$\underline{J}_y(x) = \frac{-\underline{k}}{\sinh \underline{k}h_{cu}} \left[\underline{H}_z(h_{cu}) \cosh \underline{k}x - \underline{H}_z(0) \cosh \underline{k}(x - h_{cu})\right] \tag{2.2}$$

The two equations, however, are shown below to be equivalent. A sample plot of the magnitude of this phasor current density across a winding layer for different sinusoidal excitation frequencies appears in Figure 4.3 of Part I.

Dowell defines α[1] as

$$\alpha = \sqrt{\frac{j\omega\mu_0\eta}{\rho}} = \sqrt{j\omega\mu_0(\eta\sigma)} \tag{2.3}$$

which is the same as our complex wave number $\underline{k}$ for a good conductor, given in (4.3) of Part I.

$$\underline{k} \approx \sqrt{j\omega\mu_0\sigma} \tag{2.4}$$

Although layer porosity η appears in (2.3) but is absent in (2.4), it is understood that the conductivity σ in (2.4) is equal to $(\eta\sigma_{cu})$ when calculating the current density in the equivalent copper-foil windings of the transformer model developed in Section 2.2.1 of Part I.

The following is a derivation which transforms (2.1) from Dowell's paper into our form of the equation, (2.2), showing that they are the same. Symbols in (2.1) are first replaced by equivalent symbols from the common set in the Glossary of Symbols according to the translation given in Table 2.1. For example, $\underline{k}$ is used in place of α, and J and I are written explicitly as phasors. The result is

$$\underline{J}_y(x) = \frac{N_\ell \underline{I}\,\underline{k}}{\eta b_{win}} \left\{ \frac{\cosh \underline{k}x}{\sinh \underline{k}h_{cu}} - (p-1) \tanh \frac{\underline{k}h_{cu}}{2} \cosh \underline{k}x + (p-1) \sinh \underline{k}x \right\} \tag{2.5}$$

The half-angle relation

$$\tanh \frac{\underline{k}h_{cu}}{2} = \frac{\cosh \underline{k}h_{cu} - 1}{\sinh \underline{k}h_{cu}} \tag{2.6}$$

is used and $\sinh \underline{k}h_{cu}$ is moved outside the braces to produce

$$\underline{J}_y(x) = \frac{N_\ell \underline{I}\,\underline{k}}{\eta b_{win} \sinh \underline{k}h_{cu}} \left\{ \cosh \underline{k}x - (p-1)(\cosh \underline{k}h_{cu} - 1) \cosh \underline{k}x + (p-1) \sinh \underline{k}x \sinh \underline{k}h_{cu} \right\} \tag{2.7}$$

[1]The meaning of the symbol α here is completely different from its meaning in Part I of the report.

Rearrangement of terms gives

$$\underline{J}_y(x) = \frac{N_\ell \underline{I} \underline{k}}{\eta b_{win} \sinh \underline{k} h_{cu}} \Big\{ \cosh \underline{k}x + p \cosh \underline{k}x - \cosh \underline{k}x - (p-1)[\cosh \underline{k}x \cosh \underline{k}h_{cu} - \sinh \underline{k}x \sinh \underline{k}h_{cu}] \Big\} \tag{2.8}$$

The angle-difference relation

$$\cosh \underline{k}(x - h_{cu}) = \cosh \underline{k}x \cosh \underline{k}h_{cu} - \sinh \underline{k}x \sinh \underline{k}h_{cu} \tag{2.9}$$

is substituted and terms are canceled to yield

$$\underline{J}_y(x) = \frac{N_\ell \underline{I}\, \underline{k}}{\eta b_{win} \sinh \underline{k} h_{cu}} \Big\{ p \cosh \underline{k}x - (p-1) \cosh \underline{k}(x - h_{cu}) \Big\} \tag{2.10}$$

For sinusoidally-varying currents and fields with no diffusion current present, Ampere's law may be written

$$\oint \underline{\mathbf{H}} \bullet \mathbf{dl} = \underline{I}_{\text{enclosed}} \tag{2.11}$$

where $\underline{\mathbf{H}}$ is the magnetic-field-intensity vector phasor introduced in Section 3.3.1 of Part I, **dl** is an incremental path-length vector, and $\underline{I}_{\text{enclosed}}$ is the phasor of net current enclosed by the integration path. As described in detail in Section 3.1.2 of Part I, Ampere's law may be applied to integration paths such as those shown in Figure 2.2 to give expressions for the magnetic field intensity on both sides of the p^{th} layer of a winding portion. Since the permeability of the magnetic material is assumed to be infinite, the magnetic field intensity $\underline{H}$ in the core material is zero and only the right-hand segment of the line integral is nonzero. When the enclosed current is in the positive-y direction, the magnetic field $H_z(x,t)$ is in the negative-z direction as pictured. Therefore Ampere's law is written with a negative sign as

$$\underline{H}_z(0) = \frac{-(p-1) N_\ell \underline{I}}{b_{win}} \tag{2.12}$$

for Path 1 and

$$\underline{H}_z(h_{cu}) = \frac{-p N_\ell \underline{I}}{b_{win}} \tag{2.13}$$

for Path 2 where $x = 0$ corresponds to the left edge of the p^{th} layer, $x = h_{cu}$ corresponds to the right edge, and all layers of the winding portion have N_ℓ turns.

Substituting (2.12) and (2.13) into (2.10) gives

$$\underline{J}_y(x) = \frac{-\underline{k}}{\eta \sinh \underline{k} h_{cu}} \Big\{ \underline{H}_z(h_{cu}) \cosh \underline{k}x - \underline{H}_z(0) \cosh \underline{k}(x - h_{cu}) \Big\} \tag{2.14}$$

The transformation of (2.1) into (2.2) to show their equivalence is now complete, except that the resulting equation (2.14) has an η in the denominator which does not appear in (2.2). This occurs because (2.14) gives the current density in the hypothetical square conductors which have the same cross-sectional area as the real copper wires, while (2.2) applies to the equivalent-foil layers obtained by *stretching* the square conductors as described in Section 2.2.1 of Part I. The current density in the square conductors is higher by the factor $(1/\eta)$ as expected.

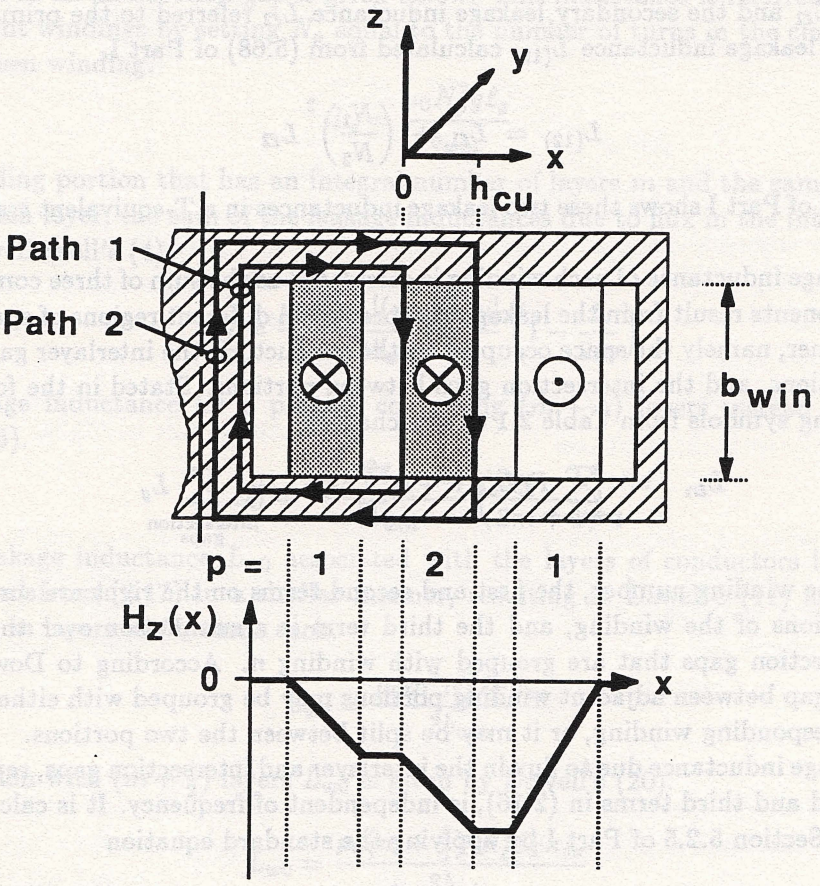


Figure 2.2: The right-hand side of a two-winding, EE-core transformer, and the low-frequency magnetic-field-intensity profile which results from current flowing into the plane of the figure in the inner winding and in the opposite direction in the outer winding.

2.3.2 Leakage Inductance

For the special case of a transformer with only two windings, which is the only case considered by Dowell, the magnetic energy stored in each region of space inside the transformer can be associated with one or the other of the windings, thus allowing a leakage inductance to be calculated for each winding. The sum of the primary leakage inductance $L_{\ell 1}$ and the secondary leakage inductance $L_{\ell 2}$ referred to the primary is the short-circuit leakage inductance $L_{(12)}$ calculated from (5.68) of Part I.

$$L_{(12)} = L_{\ell 1} + \left(\frac{N_1}{N_2}\right)^2 L_{\ell 2} \tag{2.15}$$

Figure 5.1(c) of Part I shows these two leakage inductances in a T-equivalent transformer model.

The leakage inductance of each winding is calculated as the sum of three components. These components result from the leakage flux present in different regions of space inside the transformer, namely the space occupied by the conductors, the interlayer gaps within winding portions, and the intersection gaps between portions. Stated in the form of an equation using symbols from Table 2.1 of this chapter

$$L_{\ell n} = \sum_{\text{portions}} F_L L_{w0} + \sum_{\text{portions}} L_U + \sum_{\substack{\text{intersection} \\ \text{gaps}}} L_g \tag{2.16}$$

where n is the winding number, the first and second terms on the right are summations over all portions of the winding, and the third term is a summation over those parts of the intersection gaps that are grouped with winding n. According to Dowell, each intersection gap between adjacent winding portions may be grouped with either portion and the corresponding winding, or it may be split between the two portions.

The leakage inductance due to flux in the interlayer and intersection gaps, represented by the second and third terms in (2.16), is independent of frequency. It is calculated as discussed in Section 5.2.5 of Part I by applying the standard equation

$$L = \frac{\mu N^2 A}{\ell_m} \tag{2.17}$$

to a cylindrical shell that approximates the volume of the gap, where

L = inductance
μ = permeability of the region
N = number of turns of current-carrying conductor which generate the flux in the region
A = cross-sectional area normal to the magnetic flux
ℓ_m = magnetic path length

The part of the magnetic path inside the core is neglected because the permeability

of the core material is assumed to be very high, causing almost all of the drop in mmf to appear across the winding space. This phenomenon follows from the discussion of the relationship between a transformer and an infinite solenoid in Section 3.1 of Part I.

In terms of the geometry variables introduced in Chapter 2 of Part I and listed in Table 2.1 of this chapter, Dowell's resulting Equation (3) for the leakage inductance L_g due to flux in an intersection gap is given below. This inductance is referred to either of the adjacent windings by setting N_p equal to the number of turns in the closest portion of the chosen winding.

$$L_g = \frac{\mu_0 N_p^2 g \ell_g}{b_{win}} \tag{2.18}$$

For a winding portion that has an integral number of layers m and the same number of turns in each layer, the sum of the leakage inductances due to flux in the interlayer gaps is given by Dowell's (4).

$$L_U = \frac{\mu_0 N_p^2 \ell_g [(m-1)u]}{3 b_{win}} \left(1 - \frac{1}{2m}\right) \tag{2.19}$$

This leakage inductance for a portion containing $(m + \frac{1}{2})$ layers instead is given by Dowell's (5).

$$L_U = \frac{\mu_0 N_p^2 \ell_g (mu)}{3 b_{win}} \left(\frac{2m-1}{2m+1}\right) \tag{2.20}$$

The dc leakage inductance L_{w0} associated with the layers of conductors in a portion is calculated from (2.17) in a similar manner, resulting in Dowell's (11) for a portion containing m layers of N_ℓ turns each.

$$L_{w0} = \frac{\mu_0 m^3 N_\ell^2 \ell_T h_{cu}}{3 b_{win}} \tag{2.21}$$

For a portion with $(m + \frac{1}{2})$ layers L_{w0} is given by Dowell's (20).

$$L_{w0} = \frac{\mu_0 (m+\frac{1}{2})^3 N_\ell^2 \ell_T h_{cu}}{3 b_{win}} \tag{2.22}$$

The first term in (2.16), which represents the ac leakage inductance due to flux in the conductors, is calculated from the imaginary part of a complex winding-portion impedance $\underline{Z}_W$.

$$\underline{Z}_W = F_R R_{w0} + j\omega F_L L_{w0} \tag{2.23}$$

The real part of $\underline{Z}_W$ gives the ac resistance of the conductors in a winding portion. An expression for $\underline{Z}_W$ is derived in the appendix of Dowell's paper from

$$\underline{Z}_W = \frac{\underline{V}}{\underline{I}} \tag{2.24}$$

where $\underline{I}$ is the phasor of winding current, and $\underline{V}$ is the phasor of voltage across a winding portion which is the sum of two components. One is a resistive voltage drop calculated

from the current density given by (2.14), and the other is a voltage induced by the flux linking the winding layers of the portion. These components of voltage each vary across the height of a layer of conductors, but their sum, the total voltage across that layer of the winding, is constant across the height of the conductors. The resulting equation is Dowell's (8)

$$\underline{Z_W} = \frac{\rho_{cu}\ell_T N_\ell^2}{\eta b_{win} h_{cu}} \left\{ mM + \frac{m(m^2-1)D}{3} \right\} \tag{2.25}$$

where

$$M = \underline{k}h_{cu} \coth \underline{k}h_{cu} \tag{2.26}$$

$$D = 2\underline{k}h_{cu} \tanh \frac{\underline{k}h_{cu}}{2} \tag{2.27}$$

M and D are complex quantities used by Dowell for convenience in several equations, and are essentially just renamed parts of (2.14) with $x = h_{cu}$. This can be seen by first writing the equivalent equation (2.5) with $x = h_{cu}$ and regrouping terms.

$$\underline{J_y}(h_{cu}) = \frac{N_\ell I \underline{k}}{\eta b_{win}} \left\{ \frac{\cosh \underline{k}h_{cu}}{\sinh \underline{k}h_{cu}} + (p-1)[\sinh \underline{k}h_{cu} - \tanh \frac{\underline{k}h_{cu}}{2} \cosh \underline{k}h_{cu}] \right\} \tag{2.28}$$

Applying the hyperbolic identities

$$\tanh \frac{x}{2} = \frac{\cosh x - 1}{\sinh x} \tag{2.29}$$

$$\cosh^2 x = \sinh^2 x + 1 \tag{2.30}$$

to the expression in brackets

$$\sinh \underline{k}h_{cu} - \tanh \frac{\underline{k}h_{cu}}{2} \cosh \underline{k}h_{cu}$$

$$= \sinh \underline{k}h_{cu} - \left(\frac{\cosh \underline{k}h_{cu} - 1}{\sinh \underline{k}h_{cu}} \right) \cosh \underline{k}h_{cu} \tag{2.31}$$

$$= \frac{(\sinh^2 \underline{k}h_{cu} - \cosh^2 \underline{k}h_{cu}) + \cosh \underline{k}h_{cu}}{\sinh \underline{k}h_{cu}} \tag{2.32}$$

$$= \tanh \frac{\underline{k}h_{cu}}{2} \tag{2.33}$$

Substituting this into (2.28) gives

$$\underline{J_y}(h_{cu}) = \frac{N_\ell I \underline{k}}{\eta b_{win}} \left\{ \coth \underline{k}h_{cu} + (p-1) \tanh \frac{\underline{k}h_{cu}}{2} \right\} \tag{2.34}$$

Regrouping terms, Dowell's (6) is obtained.

$$\underline{J_y}(h_{cu}) = \frac{N_\ell \underline{I}}{\eta b_{win} h_{cu}} \left\{ (\underline{k}h_{cu} \coth \underline{k}h_{cu}) + \frac{(p-1)}{2} (2\underline{k}h_{cu} \tanh \frac{\underline{k}h_{cu}}{2}) \right\} \tag{2.35}$$

$$= \frac{N_\ell \underline{I}}{\eta b_{win} h_{cu}} \left\{ M + \frac{(p-1)}{2} D \right\} \tag{2.36}$$

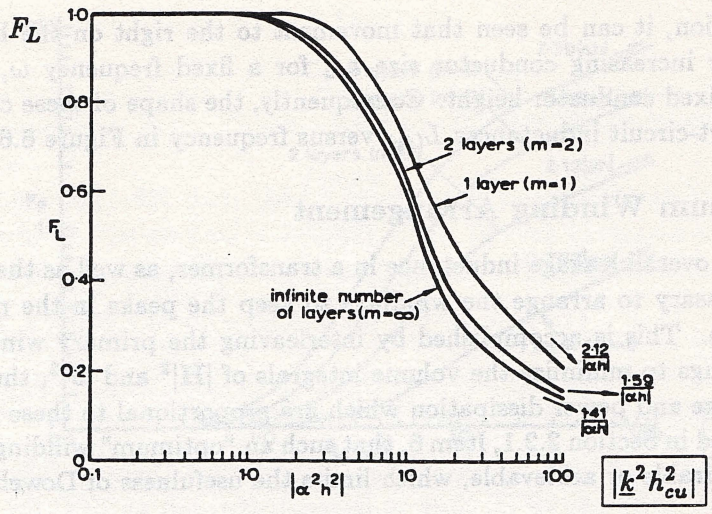


Figure 2.3: Dowell's Figure 10, which for integral numbers of layers shows curves of F_L versus $|\underline{k}^2 h_{cu}^2|$ which is proportional to the square of the conductor height in skin-depth thicknesses.

Curves of the ac-to-dc inductance ratio F_L may be precalculated for different numbers of layers in a winding portion using an expression obtained by combining (2.25), (2.23), and (2.21) or (2.22). With a double prime ($''$) signifying the imaginary portion of M or D, the result is Dowell's (13) for an integral number of layers in the winding portion.

$$F_L = \frac{3M'' + (m^2 - 1)D''}{m^2 |\underline{k}^2 h_{cu}^2|} \tag{2.37}$$

Figure 2.3 shows the result graphed as a function of $|\underline{k}^2 h_{cu}^2|$ in our symbols. As $|\underline{k}^2 h_{cu}^2|$ becomes large, each curve asymptotically approaches the simple function shown at the right side of the figure.

The definition of $\underline{k}$ for a good conductor and the definition of skin depth δ applied to a conducting layer of porosity η

$$\underline{k} = \sqrt{j\omega\mu_0(\eta\sigma_{cu})} \tag{2.38}$$

$$\delta = \sqrt{\frac{2}{\omega\mu_0(\eta\sigma_{cu})}} \tag{2.39}$$

may be used to write an expression for the abscissa of Dowell's plots in terms of Δ, the conductor height normalized to skin depth.

$$|\underline{k}^2 h_{cu}^2| = (\omega\mu_0\eta\sigma_{cu}) h_{cu}^2 = 2\left(\frac{h_{cu}}{\delta}\right)^2 = 2\Delta^2 \tag{2.40}$$

From this equation, it can be seen that movement to the right on the horizontal axis represents either increasing conductor size h_{cu} for a fixed frequency ω, or increasing frequency for a fixed conductor height. Consequently, the shape of these curves matches those of the short-circuit inductances $L_{(jk)}$ versus frequency in Figure 6.6 of Part I.

2.3.3 Optimum Winding Arrangement

To minimize the overall leakage inductance in a transformer, as well as the eddy-current losses, it is necessary to arrange the windings to keep the peaks in the mmf profile as small as possible. This is accomplished by interleaving the primary winding with the secondary windings to minimize the volume integrals of $|\mathbf{H}|^2$ and $|\mathbf{J}|^2$, thus minimizing the energy storage and power dissipation which are proportional to these integrals.

It is mentioned in Section 2.2.1, Item 6, that such an "optimum" winding arrangement is not always desirable or achievable, which limits the usefulness of Dowell's results.

2.3.4 AC Winding Resistance

The ac winding resistance is obtained as a sum of the real parts of (2.23) for all portions of the winding. The dc resistance of each portion R_{w0} is calculated from the standard equation

$$R = \frac{l}{\sigma A} \tag{2.41}$$

where l is the length of the conductor, σ is its conductivity, and A is the cross-sectional area. The result is Dowell's equation following (8).

$$R_{w0} = \frac{m\rho_{cu}N_\ell^2\ell_T}{\eta b_{win}h_{cu}} \tag{2.42}$$

As was done for F_L, the ac-to-dc resistance ratio F_R may be precalculated using an expression obtained from (2.42), (2.25), and (2.23). For a winding portion with an integral number of layers, where a prime ($'$) signifies the real part of M or D, the result is Dowell's (10).

$$F_R = M' + \frac{(m^2-1)D'}{3} \tag{2.43}$$

A sample plot is shown in Fig 2.4.

The shape of these curves is seen to be the same as those for the short-circuit resistance $R_{(jk)}$ versus frequency in Figure 6.5 of Part I. Equations for the asymptotes approached as $|\underline{k}^2h_{cu}^2|$ becomes large appear near the right end of each curve in the figure.

2.4 CLARIFICATIONS

The following additional information is provided as an aid to understanding Dowell's article.

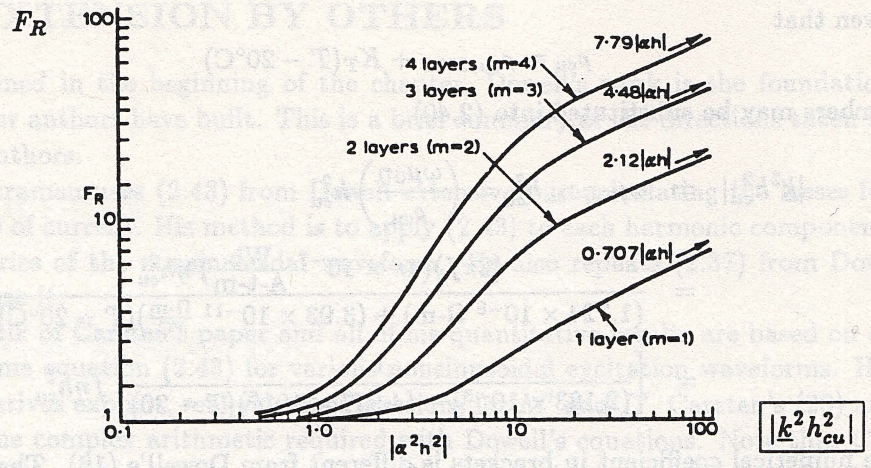


Figure 2.4: Dowell's Figure 8, which shows curves of F_R versus $|\underline{k}^2 h_{cu}^2|$ for integral numbers of layers.

Sum of powers. An identity from combinatorics is needed to obtain Dowell's (2).

$$\sum_{p=1}^{m} p^2 = \frac{m(m+1)(2m+1)}{6} \tag{2.44}$$

In addition, the following is used to obtain the second equation after (36).

$$\sum_{p=1}^{m} p = \frac{m(m+1)}{2} \tag{2.45}$$

Numerical coefficient error. A correction to Dowell's (16), the numerical coefficient in $|\underline{k}^2 h_{cu}^2|$, is justified as follows:

For annealed copper wire, resistivity at 20°C and its temperature coefficient K_T are given by [13, p. E-88].

$$\begin{aligned} \rho_{cu,\,20°C} &= 1.7241\ \mu\Omega\text{-cm}\left(\frac{10^{-6}\ \Omega}{\mu\Omega}\right)\left(\frac{1\ \text{m}}{100\ \text{cm}}\right) \\ &= 1.7241 \times 10^{-8}\ \Omega\text{-m} \end{aligned} \tag{2.46}$$

$$\begin{aligned} K_T &= 0.00393\ \frac{\mu\Omega\text{-cm}}{°\text{C}}\left(\frac{10^{-6}\ \Omega}{\mu\Omega}\right)\left(\frac{1\ \text{m}}{100\ \text{cm}}\right) \\ &= 3.93 \times 10^{-11}\ \frac{\Omega\text{-m}}{°\text{C}} \end{aligned} \tag{2.47}$$

Given that

$$\rho_{cu} = \rho_{cu,\,20°C} + K_T(T - 20°C) \tag{2.48}$$

numbers may be substituted into (2.40).

$$|\underline{k}^2 h_{cu}^2| = \omega\mu_0\eta\sigma_{cu}h_{cu}^2 = \left(\frac{\omega\mu_0\eta}{\rho_{cu}}\right)h_{cu}^2 \tag{2.49}$$

$$= \frac{(2\pi f)(4\pi \times 10^{-7}\,\frac{\text{Wb}}{\text{A-t-m}})\,\eta h_{cu}^2}{(1.724 \times 10^{-8}\ \Omega\text{-m}) + (3.93 \times 10^{-11}\,\frac{\Omega\text{-m}}{°\text{C}})(T - 20°\text{C})} \tag{2.50}$$

$$= \left[\frac{1}{(2.183 \times 10^{-3}) + (4.977 \times 10^{-6})(T - 20)}\right] f\eta h_{cu}^2 \tag{2.51}$$

The numerical coefficient in brackets is different from Dowell's (16). The value of the coefficient is 458 at 20°C, close to Dowell's 464, but at 70°C the correct value is 411, not 500 as reported in the paper. The origin of even the form of Dowell's (16) is not understood.

Phasor notation is implied but not explicit in the appendix of Dowell's paper. To match his analysis, the magnitude of a phasor is taken to be the *peak* value of the corresponding sinusoidal waveform in the discussion below. This is different from the convention adopted in Part I where the magnitude of a phasor is the *rms* value of the sinusoid.

The equations in the paragraph following Dowell's (24) may be written more clearly as follows: The instantaneous waveform of flux is defined

$$[\phi_b + \phi_c](t) = |[\underline{\Phi_b + \Phi_c}]|\cos\omega t \tag{2.52}$$

for the zero-angle flux phasor $[\underline{\Phi_b + \Phi_c}] = |[\underline{\Phi_b + \Phi_c}]|\angle 0°$. Choosing the reference-voltage polarity and flux direction according to Lenz's law, Faraday's law gives

$$v_\ell(t) = N_\ell \frac{d[\phi_b + \phi_c](t)}{dt} \tag{2.53}$$

$$= N_\ell\,|[\underline{\Phi_b + \Phi_c}]|\,\omega(-\sin\omega t) \tag{2.54}$$

$$= N_\ell\,|[\underline{\Phi_b + \Phi_c}]|\,\omega\cos(\omega t + \frac{\pi}{2}) \tag{2.55}$$

This has the form

$$v_\ell(t) = |\underline{V_\ell}|\cos(\omega t + \angle\underline{V_\ell}) \tag{2.56}$$

for the voltage phasor

$$\underline{V_\ell} = N_\ell|[\underline{\Phi_b + \Phi_c}]|\omega\angle 90° = j\omega[\underline{\Phi_b + \Phi_c}]N_\ell \tag{2.57}$$

which leads the flux phasor by 90°.

2.5 EXTENSION BY OTHERS

As mentioned in the beginning of the chapter, Dowell's work is the foundation upon which other authors have built. This is a brief summary of the directions taken by some of those authors.

Venkatraman uses (2.43) from Dowell extensively in calculating the losses for pulse waveforms of current. His method is to apply (2.43) to each harmonic component in the Fourier series of the nonsinusoidal waveform. He also repeats (2.37) from Dowell but does not use it.

The bulk of Carsten's paper and all of his quantitative results are based on evaluating the same equation (2.43) for various nonsinusoidal excitation waveforms. However, Carsten derives explicit, real-valued expressions for M' and D', Carsten's (20) and (21), to avoid the complex arithmetic required with Dowell's equations. Note that Carsten's (20) and (21) contain errors; the correct forms are given as (4.10) and (4.11) in this document.

In the first of the three Jongsma articles considered [4], the author combines both of Dowell's results for F_R, (2.43) and Dowell's (17), producing an equation that gives F_R for winding portions with either an integral number of layers or a half-layer of conductors. For the rest of Jongsma's analysis in [4] and [5], he uses an approximation to this equation which was originally proposed by Snelling [14]. In the third article by Jongsma [6], Dowell's results for F_R are used directly.

Whereas all of the authors mentioned above use Dowell's concept of a winding portion, Vandelac and Ziogas do not. They derive an equivalent form of (2.1), a result more fundamental than (2.43); then they diverge from Dowell's approach by using a winding layer as the fundamental unit of analysis rather than the winding portion.

This page has been left blank intentionally.

Chapter 3

Venkatraman

P. S. Venkatraman, "Winding Eddy Current Losses in Switch Mode Power Transformers due to Rectangular Wave Currents," *Proceedings of Powercon 11*, 1984, Section A-1, pp. 1-11.

3.1 OVERVIEW

Given Dowell's method for calculating the copper losses and effective winding resistances of two-winding transformers under sinusoidal excitation [1], Venkatraman uses Fourier analysis to extend those results to the nonsinusoidal excitation commonly found in switch-mode power converters. Specifically, he considers unipolar pulse-current excitation having a rectangular or trapezoidal waveform.

Under conditions of nonsinusoidal excitation, the effective winding resistances are shown to vary greatly with the duty ratio and the rise and fall times of the exciting-current waveform, as well as with the frequency of excitation and the winding geometry. Venkatraman introduces the quantity F_H, the ratio of rectangular-wave losses to sine-wave losses, which may be precalculated and used in conjunction with Dowell's ac-to-dc resistance ratio F_R to compute easily the effective winding resistances for nonsinusoidal excitation. Experimental data are provided that validate the approach.

To illustrate the relationship between Venkatraman's work, that of other authors, and Part I of this report, this chapter is presented in terms of the common set of symbols found in the Glossary of Symbols, with Venkatraman's original symbols translated according to Table 3.1.

Because Venkatraman uses Dowell's results directly, most of Dowell's restrictions and assumptions apply, listed in Section 2.2. Most importantly, only two-winding transformers with no conducting shields or open-circuit windings are considered; and only Dowell's "optimal" winding arrangements, defined in Item 6 of Section 2.2.1, can be analyzed with the existing equations. While Dowell discusses windings of only single round conductors, Venkatraman demonstrates that both his and Dowell'a analyses apply to windings of multiple, electrically-paralleled round conductors as well as strip conductors and foil.

Table 3.1: Comparison of Symbols and Definitions

Venki	*Duke*	*Meaning*
A	Δ	height of a winding layer in skin depths; $\Delta = h_{cu}/\delta$
—	A	area
a	b_{cu}	breadth of a rectangular conductor
b	b_{win}	core-window breadth; Venkatraman's equations imply $b_{win} = b_{max} = b_w$ (defined in the Glossary of Symbols)
D	—	duty ratio
d	d_{cu}	diameter of the copper in a round wire
f	f	frequency of excitation
F_H	—	ratio of rectangular-wave to sine-wave losses
F_L	—	ac-to-dc inductance ratio for a winding portion (from Dowell)
F_R	—	ac-to-dc resistance ratio for a winding portion (from Dowell)
h	h_{cu}	height of a rectangular conductor, excluding insulation
I	$I_{W,MAX}$	maximum value of the winding current
I_{eff}	I_W	rms value of the winding current
I_n	$\frac{I_{n,PEAK}}{\sqrt{2}}$	rms value of the n^{th} harmonic of the winding current
M	$K^\dagger$	number of layers in a winding portion, Dowell's m
(MLT)	$\langle \ell_T \rangle$	mean length-of-turn in a winding portion
N	—	number of turns in a winding portion, Dowell's N_p
—	N_c	number of current-carrying conductors in a winding layer
n	—	harmonic number, with "1" designating the fundamental frequency

(continued)

† Has this meaning only in this chapter.

Table 3.1: Comparison of Symbols and Definitions (continued)

Venki	*Duke*	*Meaning* V: Venkatraman, D: Duke
P	—	$\underline{k}h_{cu} \coth \underline{k}h_{cu}$, equal to Dowell's M
—	$_{Pk}$ †	(subscript) winding portion number k
Q	—	$2\underline{k}h_{cu} \tanh \frac{\underline{k}h_{cu}}{2}$, equal to Dowell's D
R_{DC}	$R_{W,DC}$	dc resistance of a winding, Dowell's R_{w0}
R_n	$F_{R,n}R_{W,DC}$	ac resistance of a winding portion at the n^{th} harmonic frequency
T	T	period of a waveform
T_0	—	time that a waveform is at its peak value
T_1	—	rise or fall time of a waveform
—	$_{Ven}$ †	(subscript) "Venkatraman"
—	$_{W}$ †	(subscript) "winding"
α	$\underline{k}$	complex wave number; $\underline{k} = \sqrt{j\omega\mu_0(\eta\sigma_{cu})}$
δ	δ	skin depth; $\delta = \sqrt{2/\omega\mu_0(\eta\sigma_{cu})}$
η	η	V: layer space factor D: layer porosity; $\eta = N_c\, b_{cu}/b_{win}$
μ_0	μ_0	permeability of free space, $4\pi \times 10^{-7}$ H/m
ρ	ρ_{cu}	resistivity of copper, 1.8813×10^{-8} Ω-m at 60°C
—	σ_{cu}	conductivity of copper, 5.315×10^{7} S/m at 60°C
ω	ω	angular frequency of a periodic waveform

† Used only in this chapter.

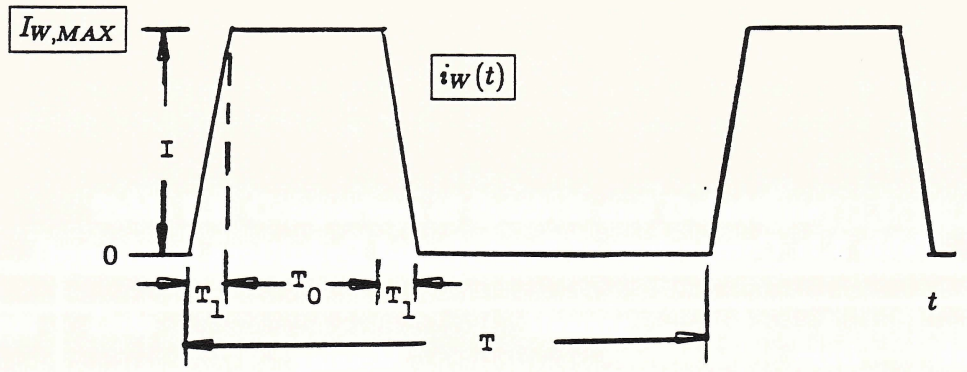


Figure 3.1: Venkatraman's Figure 10, the trapezoidal exciting-current waveform which is analyzed. The Duke symbols in boxes have been added to be consistent with the symbols used throughout the report.

For Litz wire, Venkatraman shows that the calculated F_H is accurate, but F_R calculated by Dowell's method is not.

The paper is easy to follow, and it makes clear whether variables represent instantaneous, peak, or rms quantities. Phasor math is unnecessary because most of the equations contain only non-time-varying quantities.

In the next section, the major equations describing Venkatraman's results are rewritten in terms of the common set of symbols. Section 3.3 contains additional information helpful to understanding the paper, Section 3.4 takes a critical look at the experiments performed, and Section 3.5 reviews the significant findings about Litz wire. Finally, Section 3.6 contains concluding remarks about the usefulness of this approach relative to the other approaches encountered.

3.2 MAJOR RESULTS

The trapezoidal waveform of exciting current in Figure 3.1 is assumed for this analysis. Venkatraman loosely refers to this as a "rectangular" waveform with finite rise and fall times, assumed to be equal and each designated T_1. In this section, a true rectangular waveform with $T_1 = 0$ is treated as a special case of the trapezoidal waveform pictured.

The subscript "w", meaning "winding," is used to distinguish our rms winding current I_W from Venkatraman's I which is not used in this report. Instead of I, $I_{W,MAX}$ is used for the maximum instantaneous value of $i_W(t)$ as labeled in Figure 3.1. The current waveform has a duty ratio defined $D = (T_0 + T_1)/T$, and its average value is denoted $\langle I_W \rangle$ in the equations below.

The Fourier cosine series for the waveform of Figure 3.1 is

$$i_W(t) = \langle I_W \rangle + \sum_{n=1}^{\infty} I_{n,PEAK} \cos n\omega t \qquad (3.1)$$

with coefficients given by Venkatraman's (7) and (8) as

$$I_{n,PEAK} = \frac{2I_{W,MAX}}{\pi n}\left(\sin\frac{\pi n(T_1+T_0)}{T}\right)\left[\frac{\sin\frac{\pi nT_1}{T}}{\frac{\pi nT_1}{T}}\right] \tag{3.2}$$

$$\langle I_W\rangle = \frac{I_{W,MAX}(T_0+T_1)}{T} \tag{3.3}$$

It is important to distinguish between $I_{n,PEAK}$, the amplitude of the n^{th} harmonic of $i_W(t)$, and $I_{W,MAX}$, the maximum instantaneous value of that current. The value of $I_{W,MAX}$ may be chosen arbitrarily for this calculation because it has no effect on the final result, the apparent winding resistances. As T_1 approaches zero, the condition for a true rectangular waveform, that part of (3.2) in brackets [ ] approaches one. This limiting case of (3.2), and the corresponding form of (3.3), are substituted into (3.1) to give an equation equivalent to Venkatraman's (5) for rectangular-wave excitation.

$$i_W(t) = \frac{I_{W,MAX}T_0}{T} + \sum_{n=1}^{\infty}\frac{2I_{W,MAX}}{\pi n}\sin\frac{\pi nT_0}{T}\cos n\omega t \tag{3.4}$$

Dowell spends most of the paper discussing this degenerate case of zero transition time because it produces the highest F_H of any transition time T_1.

The part of (3.2) in brackets [ ] approaches one in the limit as T_1 approaches zero, giving the result for a true rectangular waveform, Venkatraman's (5). He spends most of his time discussing this degenerate case because it gives the highest F_H as the transition time T_1 is varied.

There is an implicit assumption in Venkatraman's equations that *every winding is composed of only one winding portion*, defined in Section 2.1. This is the case for most of the two-winding transformers he considers, but *not* for those with split windings. For windings with more than one portion, some of the following equations must be modified as shown in Section 3.3.1.

Based on Dowell's work, the ac resistance of a single-portion transformer winding can be expressed

$$R_{W,AC} = F_R R_{W,DC} \tag{3.5}$$

where F_R is given by (2.43) and the dc winding resistance $R_{W,DC}$ is given by (2.42), labeled R_{w0} by Dowell. Once this ac resistance is known, the average power dissipated in the winding is given by

$$\langle P_W\rangle = I_W^2 R_{W,AC} = \frac{I_{W,PEAK}^2}{2}F_R\,R_{W,DC} \tag{3.6}$$

For nonsinusoidal excitation, the power dissipation may be calculated separately for the dc component and each of the harmonics of the current waveform, then summed to give the average power dissipated in the winding. With

$$\langle P_W\rangle = I_{W,DC}^2 R_{W,DC} \tag{3.7}$$

giving the average power for a dc current flowing in the winding, the summation which gives the total power dissipation in a winding for an exciting current described by the Fourier series (3.1) is

$$\langle P_W \rangle = \left(\langle I_W \rangle^2 + \sum_{n=1}^{\infty} \frac{I_{n,PEAK}^2}{2} F_{R,n} \right) R_{W,DC} \tag{3.8}$$

The quantity $F_{R,n}$ is just F_R at the frequency of the n^{th} harmonic. The number of terms which must be calculated to obtain an accurate result is not specified, but Carsten implies that it may be over a hundred [3].

From this total power dissipation, the effective winding resistance can easily be calculated. It is the resistance that would dissipate the power calculated above while carrying the exciting current $i_W(t)$.

$$R_{W,EFF} = \frac{\langle P_W \rangle}{I_W^2} \tag{3.9}$$

The subscript "*EFF*" is used here instead of "*AC*" to indicate that the resistance is derived from a nonsinusoidal excitation waveform.

While the effective winding resistance $R_{W,EFF}$ is the desired result, insight may be gained by examining plots of the ratio of rectangular-wave to sine-wave losses,

$$F_H = \frac{\langle P_W \rangle}{(F_R R_{W,DC}) I_W^2} \tag{3.10}$$

where F_R is computed at the fundamental frequency. For a particular ratio of transition time T_1 to duty cycle T, and a particular number of layers in the winding, a family of F_H curves for different duty ratios may be calculated and graphed versus normalized wire size. Families for two different values of T_1/T are plotted in Figure 3.2. The curves are made frequency-independent by plotting conductor size normalized to skin depth along the horizontal axis, defined as

$$\Delta = \frac{h_{cu}}{\delta} \tag{3.11}$$

for a foil winding. The quantity h_{cu} is the thickness of the foil, and $\delta = \sqrt{2/\omega\mu_0\eta\sigma_{cu}}$ is the skin depth. For round conductors, Venkatraman gives the equivalent foil thickness as $h_{cu} = 0.8\, d_{cu}$, discussed further in Section 3.3.2.

If many transformer designs are to be evaluated, time may be saved by precalculating curves such as those in Figure 3.2. Then the ac winding resistance for different designs may be quickly determined using

$$R_{W,EFF} = F_H F_R R_{W,DC} \tag{3.12}$$

which involves no long summations. The easiest way to calculate Dowell's F_R, avoiding complex arithmetic, is by using (2.43) in conjunction with (4.10) and (4.11), the corrected versions of two of Carsten's equations. Precalculating F_R is not as advantageous as precalculating F_H because the equations used to obtain F_R do not contain a long, time-consuming summation as does (3.8).

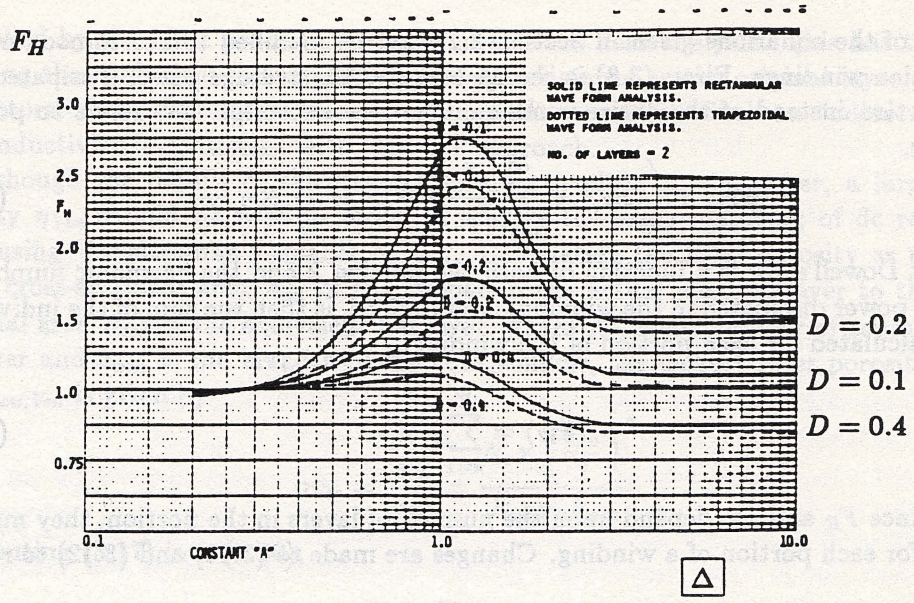


Figure 3.2: Venkatraman's Figure 11, curves of the ratio F_H of rectangular-wave to sine-wave losses versus normalized wire size Δ for a two-layer winding. Curves for three different duty ratios D are plotted with $T_1/T = 0$ (solid) and $T_1/T = 0.06$ (dashed).

3.3 CLARIFICATIONS

The first two sections below explain items which may be unclear after reading the paper, namely how F_H is calculated for windings of more that one portion and how the expression for the "equivalent-foil thickness" for round wires is derived. The third section below gives the relationship between the horizontal axes of Dowell's F_R plots and those of Venkatraman's F_H.

3.3.1 Winding Portions

With Dowell's equations, dissipated-power calculations are performed for one winding portion at a time, defined in Section 2.1, then the results for all portions in one winding are summed. Confusion may arise in Venkatraman's paper because this fact is not made clear.

It is not stated in much of the discussion just what part of the transformer is the object of the calculations being performed. An entire winding is mentioned at least once, which is a correct unit of analysis for most of Venkatraman's test transformers, but *not* for those with multiple-portion windings. Different values of F_H and F_R may be required for the different portions of a split winding.

Some of the equations given in Section 3.2 must be modified to accommodate multiple-portion windings. First, (3.8) is changed to give the average power dissipated in a single portion instead of the entire winding. The new subscript "Pk" refers to portion number k.

$$\langle P_{Pk} \rangle = \left(\langle I_W \rangle^2 + \sum_{n=1}^{\infty} \frac{I_{n,PEAK}^2}{2} F_{R,Pk,n} \right) R_{Pk,DC} \tag{3.13}$$

Note that Dowell's F_R is a function of both the portion k and the harmonic number n. The total power dissipated in the winding, used in (3.9), is then the sum of the individual powers calculated for each portion of the winding.

$$\langle P_W \rangle = \sum_{k=1}^{K} \langle P_{Pk} \rangle \tag{3.14}$$

Finally, since F_R and F_H depend upon the number of layers in the portion, they may be different for each portion of a winding. Changes are made to (3.10) and (3.12) to reflect this.

$$F_{H,Pk} = \frac{\langle P_{Pk} \rangle}{(F_{R,Pk} R_{Pk,DC}) I_W^2} \tag{3.15}$$

$$R_{W,EFF} = \sum_{k=1}^{K} F_{H,Pk} F_{R,Pk} R_{Pk,DC} \tag{3.16}$$

As before, the factor $F_{R,Pk}$ is calculated at the fundamental frequency.

3.3.2 Equivalent-Foil Thickness

For a layer of round conductors, the thickness of an equivalent layer of foil is given in the paper as

$$h_{cu,Ven} = 0.8\, d_{cu} \tag{3.17}$$

which, according to Venkatraman, is an empirical fit to measured data. The new symbol $h_{cu,Ven}$ is used because this value is smaller than the h_{cu} for round conductors proposed by Dowell and adopted in Part I. Dowell defines h_{cu} as the height of a square conductor with the same cross-sectional area as copper in the round wire, expressed mathematically in (2.3) of Part I as

$$h_{cu} = \sqrt{\pi \left(\frac{d_{cu}}{2} \right)^2} = \frac{\sqrt{\pi}}{2} d_{cu} = 0.886\, d_{cu} \tag{3.18}$$

The ratio of the two is

$$\frac{h_{cu,Ven}}{h_{cu}} = \frac{2(0.8\, d_{cu})}{d_{cu}\sqrt{\pi}} = 0.903 \tag{3.19}$$

In Section 2.2.1 of Part I, where an equivalent-foil layer is derived for an actual layer of round conductors, it is shown that the conductivity of the copper conductors should be

multiplied by the layer porosity η everywhere in the field analysis. This has the effect of giving the equivalent-foil layer the same dc resistance as the original layer of round conductors, if the conductors were all connected in parallel. Such an "adjustment" of the conductivity is consistent with Dowell's approach.

Although the details of calculating F_R are not given in the paper, a larger layer porosity η_{Ven} should be used in order to achieve the same matching of dc resistance when using Venkatraman's smaller $h_{cu,Ven}$. Calculating the layer porosity as the ratio of the cross-sectional area A_{cu} of the copper in the actual winding layer to the cross-sectional area A_{foil} of the equivalent foil layer, where N_c is the number of conductors in the layer and b_{win} is the breadth of the core window, the correct layer porosity to use with $h_{cu,Ven}$ is given by

$$\eta_{Ven} = \frac{A_{cu}}{A_{foil}} = \frac{N_c \pi \left(\frac{d_{cu}}{2}\right)^2}{h_{cu,Ven} b_{win}} \tag{3.20}$$

Substituting (3.17) into (3.20),

$$\eta_{Ven} = \frac{N_c \pi d_{cu}^2}{4(0.8\, d_{cu}) b_{win}} = 0.982 \frac{N_c\, d_{cu}}{b_{win}} \tag{3.21}$$

For comparison, the layer porosity used by Dowell and adopted in Part I, given as (2.4) in Part I, is

$$\eta = \frac{A_{cu}}{A_{foil}} = \frac{N_c \pi \left(\frac{d_{cu}}{2}\right)^2}{h_{cu} b_{win}} = \frac{N_c\, h_{cu}^2}{h_{cu} b_{win}} = \frac{N_c\, h_{cu}}{b_{win}} \tag{3.22}$$

The ratio of the two layer porosities, making use of (3.18), is

$$\frac{\eta_{Ven}}{\eta} = 0.982 \frac{N_c\, d_{cu}}{b_{win}} \left(\frac{b_{win}}{N_c\, h_{cu}}\right) = 0.982 \frac{d_{cu}}{h_{cu}} = \frac{0.982\, d_{cu}}{(0.886\, d_{cu})} = 1.11 \tag{3.23}$$

which is the inverse of (3.19).

Using $h_{cu,Ven}$ instead of h_{cu}, with either η_{Ven} or η, gives different results for F_R and the quantities derived from it, including $\langle P_W \rangle$ and $R_{W,EFF}$. The effect of Venkatrman's approximations can be seen by examining Dowell's F_R plots, like the one in Fig. 2.4, and comparing abscissas calculated with the different values of h_{cu} and η. Using $h_{cu,Ven}$ instead of h_{cu} and η_{Ven} instead of η, (2.40) gives

$$|\underline{k}^2 h_{cu}^2|_{Ven1} = (\omega \mu_0 \eta_{Ven} \sigma_{cu}) h_{cu,Ven}^2 = \omega \mu_0 (1.11\, \eta) \sigma_{cu} (0.903\, h_{cu})^2 = 0.903\, |\underline{k}^2 h_{cu}^2| \tag{3.24}$$

If, instead, $h_{cu,Ven}$ and η are used,

$$|\underline{k}^2 h_{cu}^2|_{Ven2} = (\omega \mu_0 \eta \sigma_{cu}) h_{cu,Ven}^2 = \omega \mu_0 \eta \sigma_{cu} (0.903\, h_{cu})^2 = 0.815\, |\underline{k}^2 h_{cu}^2| \tag{3.25}$$

Either way, the resulting value of F_R could be somewhat different from the value Dowell would calculate for the same geometry.

3.3.3 Horizontal Axis of the Plots

The plots of F_R and F_L versus A that appear in the paper, where Venkatraman's A is equal to Duke's Δ, have exactly the same shape as Dowell's own plots of the same quantities with $|\underline{k}^2 h_{cu}^2|$ on the horizontal axis, shown in Figures 2.4 and 2.3. Equation (2.40) gives the relationship between the two abscissas.

$$|\underline{k}^2 h_{cu}^2| = 2\left(\frac{h_{cu}}{\delta}\right)^2 = 2\Delta^2 \tag{3.26}$$

Because a logarithmic scale is used on the horizontal axis by both authors, the plots are equivalent and the axis may be labeled with either quantity.

It is useful to remember that at a fixed frequency, one moves to the right on these plots as wire size increases, and for a fixed wire size, one moves to the right as frequency increases.

3.4 EXPERIMENTAL VERIFICATION

Venkatraman is to be highly commended for including in his paper experimental verification of results, an element which is absent from most of the other papers considered in this report. Furthermore, an important conclusion not mentioned in the paper can be drawn from those results. That is, the approach taken by both Dowell and Venkatraman works very well for EE cores, where it is not intuitively clear that a one-dimensional analysis of the fields present in the winding space is adequate. Recall that a key assumption in this entire report is that the magnetic flux in the winding space is parallel to the center leg of the core, an assumption expected to be good for pot cores but initially questioned for EE cores.

In Venkatraman's tests, the transformers are excited with sinusoidal, then rectangular-wave currents of the same rms value. Using the fact that power dissipation in the windings is proportional to the difference between the average winding temperature and the ambient temperature, the ratio of rectangular-wave to sine-wave losses is determined from measured temperatures. While the results are good, one should keep in mind the limits of the tests performed. Specifically, the tests are conducted using frequencies from 20 to 40 kHz, round wire sizes from AWG #15 to AWG #21, duty ratios from 0.13 to 0.50, two sizes of ferrite EE cores, and Δ values from 1.00 to 2.02, a rather limited range on the abscissa of Figure 3.2.[1] To illustrate Venkatraman's calculations, the low end of this range is calculated below using (3.17), (3.20), the definition of skin depth, and (3.11). The object of the calculation is a winding layer with 12 turns of two #21 wires, for which $d_{cu} = 0.723$ mm and $\sigma_{cu} = 5.315 \times 10^7$ S/m at 60°C, wound on a core with

[1] These Δ values correspond to Venkatraman's Figures 13 and 12, respectively.

window breadth $b_{win} = 30.2$ mm, excited at a frequency of 25 kHz.[2]

$$h_{cu,Ven} = 0.8\, d_{cu} = 0.8(0.723 \times 10^{-3}\ \text{m}) = 5.78 \times 10^{-4}\ \text{m} \tag{3.27}$$

$$\eta_{Ven} = 0.982 \frac{N_c\, d_{cu}}{b_{win}} = 0.982 \frac{24(0.723 \times 10^{-3}\ \text{m})}{30.2 \times 10^{-3}\ \text{m}} = 0.564 \tag{3.28}$$

$$\delta_{Ven} = \sqrt{2/\omega\mu_0\eta_{Ven}\sigma_{cu}} \tag{3.29}$$

$$= \sqrt{2/2\pi(25{,}000\ \text{Hz})(4\pi \times 10^{-7}\ \text{H/m})(0.564)(5.315 \times 10^{7}\ \text{S/m})} \tag{3.30}$$

$$= 5.81 \times 10^{-4}\ \text{m} \tag{3.31}$$

$$\Delta = \frac{h_{cu,Ven}}{\delta_{Ven}} = \frac{5.78 \times 10^{-4}\ \text{m}}{5.81 \times 10^{-4}\ \text{m}} = 0.995 \tag{3.32}$$

Tests are also reported on transformers with Litz-wire windings as discussed in the next section, and on an unidentified foil-winding transformer which is only briefly mentioned.

3.5 LITZ WIRE

Three of the test transformers are wound with Litz wire of size 20/#30 or 50/#34, where the first part of that designation is the number of strands and the second is the AWG size of each strand. Venkatraman says that for the one case examined, Dowell's F_R grossly underestimates the ac winding resistance of the Litz-wire. However, he provides experimental results demonstrating that the F_H calculated from *measured* ac winding resistances is accurate. In Venkatraman's Figure 15, which displays those results, it is not apparent that the "calculated" curve of F_H versus duty cycle is actually calculated from *measured* ac winding-resistance data, unlike any of the other similar curves, but this fact is mentioned in the text.

A significant conclusion drawn from another test is that Litz wire is not as effective in reducing losses for rectangular waveforms as it is for sinusoidal waveforms. It is noted that the moderate gain in efficiency with Litz wire may not offset its higher cost.

3.6 EVALUATION OF THE APPROACH

For our purposes, the most important contributions of the paper are its experimental verification of Dowell's results and its demonstration that the Fourier series is a valid tool for extending sinusoidal results to conditions of nonsinusoidal excitation. Venkatraman's results represent a sound and significant extension of the work performed by Dowell;

[2]Diameter d_{cu} is the Brown & Sharpe standard from p. F-112 of [13], which is equivalent to "American Wire Gauge" according to p. F-114. Window breadth b_{win} is for core number 50-0874 on p. 17 of Stackpole Bulletin 59-107.

however, Carsten has subsequently presented essentially the same results in a more convenient form [3]. In a nutshell, Carsten groups F_H, F_R, and the size-dependence of $R_{W,DC}$ into a single term, his K_r. Therefore, only one precalculated factor changes when comparing conductors of different sizes, instead of the three factors which change in Venkatraman's equations. Carsten's paper is the subject of Chapter 4.

Because this report focuses on transformers with more than two windings, Venkatraman's results cannot be used directly. Section 2.1 contains a more complete discussion of the reasons. Instead, the more general approach of Part I involves a layer-by-layer calculation of stored and dissipated energy, with no reference to winding portions. Although only sinusoidal excitation is considered there, it is worth noting that Vandelac and Ziogas use Venkatraman's Fourier-based approach to analyze nonsinusoidal excitations, but they do it in a manner consistent with the layer-by-layer analysis of Part I [8]. Vandelac and Ziogas's paper is the topic of Chapter 8 of Part II of this report.

Chapter 4

Carsten

Carsten, Bruce,"High Frequency Conductor Losses in Switchmode Magnetics," *High-Frequency Power Converter Conference Proceedings*, May 1986, pp. 155–176.

4.1 SUMMARY

This paper focuses on the calculation and minimization of losses due to the skin and proximity effects in transformer windings carrying arbitrary current waveforms. This analysis is based upon the work done by Dowell [1] and Venkatraman [2], and is similar to Venkatraman's analysis in that it extends Dowell's work to determining the effective winding resistance for nonsinusoidal waveforms of current. This is done by determining the harmonic content of the waveform and repeatedly applying Dowell's results, given below in (4.5), to determine the winding resistance at each harmonic. Although Carsten briefly discusses the reduction of leakage inductance with increasing frequency, he dismisses this as a minor effect and analyzes only the case of resistive loss.

The effective winding resistance, which accounts for power losses due to the waveform harmonics, is used in the paper to calculate what Carsten calls K_r, the normalized effective resistance factor. K_r is defined as the ratio of the effective resistance of the winding to the dc resistance when the conductor is one skin depth in height at the fundamental frequency of the winding-current waveform. Graphs are presented which display calculated values of K_r for several frequently encountered nonsinusoidal current waveforms. These graphs are used to determine the optimum winding height for minimum losses, and the variation of K_r with parameter variations such as waveform rise and fall time and number of winding layers. We have not verified any of Carsten's numerical results, and so can say nothing about their validity.

Table 4.1 gives a comparison of the nomenclature used by Carsten and that which is adopted in the general *Glossary of Symbols*. Most of the terminology needed to read Carsten's paper is defined therein or in Dowell's paper. Table 4.1 presents those terms and symbols which are needed to understand Sections 4.3 and 4.4, or which are inconsistent with the derivations in Part I of this report, or whose definitions as presented

Table 4.1 Comparison of Symbols and Definitions

Carsten	*Duke*	*Meaning* C: Carsten; D: Duke
—	$_{ac}$†	(subscript) denotes variables associated with ac waveforms which *contain no dc offset*
—	b_{win}	breadth of the core window
D	—	duty cycle
		$2\underline{k}h_{cu}\tanh(\underline{k}h_{cu}/2)$ — from Dowell
D'	—	the real part of $D = 2\underline{k}h_{cu}\tanh(\underline{k}h_{cu}/2)$
—	$_{dc}$†	(subscript) denotes variables associated with ac waveforms which *contain a dc offset*
F_r	—	ratio of ac winding resistance to dc winding resistance
F_{rn}	—	F_r at harmonic frequency n for $n \geq 1$
h	h_{cu}	conductor height or conductor thickness
I_{ac}	$I^{\dagger}_{ac\text{-}pp}$	Peak-to-peak ac winding current
I_{dc}	—	dc component of an ac winding current waveform with dc offset
I_n	—	*rms value* of winding current at harmonic frequency n
I_{rms}	—	total rms current in the winding
$K_r = R_{we}/R_{w\star}$	—	normalized effective resistance factor
—	ℓ_T	length of turn in a winding layer
m	—	number of layers in a winding (an integer)
M	—	$\underline{k}h_{cu}\coth\underline{k}h_{cu}$ — from Dowell
M'	—	the real part of $M = \underline{k}h_{cu}\coth\underline{k}h_{cu}$
—	N_ℓ	number of turns in one winding layer
n	—	integer subscript to denote harmonic of fundamental frequency. $n = 0$ at dc; $n = 1$ at fundamental

(Continued on next page)

Table 4.1 Comparison of Symbols and Definitions, cont.

Carsten	*Duke*	*Meaning* C: Carsten; D: Duke
P_{loss}	—	total power loss in winding with nonsinusoidal currents
p	—	index to distinguish layers of a winding
—	$_{pp}$†	(subscript) denotes peak-to-peak values
R_{we}	—	effective winding resistance
R_{wn}	—	winding resistance at harmonic frequency n for $n \geq 0$ (From Dowell: $R_{w0} = (mN_\ell^2 \ell_T) \,/\, (\eta \sigma_{cu} b_{win} h_{cu})$)
$R_{w\star} = R_{w0}\vert_{h=\delta}$	—	dc resistance of winding when conductor height is one skin depth at fundamental frequency
T	T_S	period of current waveform
T_F, T_f	—	fall time of current relative to the period
T_R, T_r	—	rise time of current relative to the period
$X = h/\delta$	$\Delta = h_{cu}/\delta$	C: Conductor height normalized to skin depth D: Height of a layer in skin depths
$\alpha = \sqrt{\frac{j\omega\mu_0\eta}{\rho}}$	$\underline{k} = \sqrt{j\omega\mu_0\sigma_{eff}}$	Complex wave number; the extra η in Carsten's definition of α is consistent because Duke uses $(\eta\sigma_{cu})$ for the effective conductivity σ_{eff} when modeling a winding layer
$\delta = \sqrt{\frac{2\rho}{\omega\mu_0}}$	$\delta = \sqrt{\frac{2}{\omega\mu_0\sigma_{eff}}}$	Skin depth
η	η	C: horizontal porosity, assumed to be unity; D: layer porosity

† denotes symbols not included in the *Glossary of Symbols*

by Carsten require clarification. Where definitions for the same quantity differ, the definition from Carsten's paper is preceded by a "C: " and the definition from Part I of this report is preceded by a "D: ."

Although Carsten builds upon Dowell's work, he differs somewhat from Dowell in terminology. Dowell's equations are all derived for winding portions and a portion may or may not contain a half layer. Carsten uses Dowell's equations for portions with an integral number of layers only (no half layers), but in general he refers to such a group of layers as a *winding* instead of as a *portion*.

Carsten identifies and briefly discusses the influence of certain key parameters on the total winding loss. These parameters which he terms "loss mechanisms" and "sources of loss" are:

- End Effects
- Core Gap Effects
- Extraneous Conductor Effects
- Skin Effects
- Proximity Effects

As presented by Carsten, the last two items are limited to the current-carrying windings which are being analyzed, so losses in open-circuited windings or conductive shields are not included. Further, Carsten's equations, which are derived from Dowell's analysis, accommodate losses due only to these last two "mechanisms," i.e., losses in current-carrying windings.

The paper focuses on other topics of interest. A comparison is made of the predicted losses in transformers conducting square-wave currents versus those conducting unipolar-pulse currents. The use of Litz wire to reduce losses is discussed by Carsten. By breaking a layer of regular conductors into several layers of conductors of less height (Carsten call this vertical sectionalizing), he argues that under certain conditions Litz wire can actually increase winding loss over a solid conductor for nonsinusoidal currents.[1] The appendix to the paper contains a comprehensible derivation of the expressions for the real parts of Dowell's complex variables M and D. Unfortunately, during the course of this derivation, Carsten picks up an erroneous 'j' within his expressions. This derivation and the contained error are discussed more in Section 4.4.1 below.

The paper has several shortcomings, many of which are enumerated in Section 4.2. Since he begins with Dowell's results, many of the assumptions behind Dowell's work are not clearly specified in Carsten's paper. Although the text of the paper does not clearly state what device is being analyzed, Dowell assumes transformers of only two

[1] Jongsma discusses Litz wire in [6], but instead claims that it reduces winding losses. In [2], Venkatraman shows that losses in Litz wire are much higher for nonsinusoidal currents than for the sinusoidal case and so has a reduced benefit over solid wire which may justify using solid wire for reduced cost.

shell windings, therefore, it would appear that Carsten assumes them also. Carsten presents no experimental data to verify the results of his calculations.

Normalizing the effective resistance of the windings to the dc resistance of a conductor one skin depth in height is an important contribution, since it removes from the resultant data the conductor-height dependence of the dc resistance. Another strength of the paper is that values of the normalized effective resistance factor K_r can be precalculated, represented graphically or tabularly, and then used to calculate easily the effective winding resistance for any size of conductor. Graphs such as those presented in the paper can be used to determine what design conditions will minimize winding losses. However, unless you are interested in parametric studies such as those presented in the paper, in minimum-loss designs, or in doing a large number of related calculations, direct evaluation of the total power loss using equations (4.12) and (4.13) of Section 4.4.1 would probably involve less work. This is because calculation of K_r can involve determining $I_n^2 F_{rn}$ at 500 or more of the waveform's harmonics.

4.2 SOURCES OF CONFUSION IN CARSTEN'S PAPER

Although Carsten's paper is instructive, it contains some errors, assumptions and incomplete explanations that hamper the reader's understanding. One such source of confusion is the erroneous 'j' which Carsten includes in several of his expressions. This error is mentioned in Section 4.1 and is discussed at length in Section 4.4.1. Other difficulties with the paper are given in this subsection.

1. Because he begins with Dowell's results, Carsten's method contains the same conditions and assumptions as does Dowell's but Carsten does not explicitly tell the reader what these are. The conditions and assumptions behind Dowell's analysis are enumerated in Section 2.2 of Part II of this report. One of these conditions, which the reader should remember, is that only optimum winding arrangements are analyzed. Optimum winding arrangements are discussed in Item 6 of Section 2.2.1 and in Section 2.3.3. Another of these conditions is that losses in conductive shields and open-circuited windings are not modeled.[2]

2. The terminology Carsten uses to describe the "loss mechanisms" and "sources of loss" is vague and can be misleading. All the mechanisms listed in Section 4.1 are descriptions of the same phenomenon—high-frequency eddy-current losses. Yet, as Carsten points out in his discussion of these "mechanisms," some parts of the total loss, such as a current-carrying wire's self-induced eddy-current losses (termed skin effects) and eddy-current loss induced in the current-carrying wire by other nearby wires (termed proximity effects) are relatively easy to analyze using Dowell's

[2]To model the losses in open-circuited windings and conductive shields, the methods presented in Part I of this report should be followed.

results, whereas the influence on total loss due to such things as non-axial fields produced by a gap in the core are harder to quantify since no analysis tool like Dowell's results exists.

3. For most of his analysis Carsten assumes a layer porosity of $\eta = 1$, thereby constraining his analysis to foil windings which fill the available core window breadth. Layer porosity is introduced and discussed in Section 2.2 of Part I of this report. Although it does affect Carsten's specific results, this assumption is not essential to the general methods that he presents. Other values of layer porosity can be accommodated by substituting (ρ_{cu}/η) for ρ in Carsten's equations (9) through (13).

4. Contained in the appendix to Carsten's paper are his equations (34) and (35) for determining the equivalent height of a layer of round wires. We are unable at this time to verify the derivation and use of these equations and so can say nothing about their validity. If the modeling approach presented in Section 2.2 of Part I of this report is followed, (34) and (35) are not needed.

5. Throughout his analysis Carsten normalizes conductor height to one skin depth. (See definition of X in Table 4.1). However, the novice reader of Carsten's paper may become confused as to when the fundamental frequency is to be used to calculate the skin depth for a normalization, and when the appropriate harmonic of the fundamental is to be used. When one uses (4.5), (4.10) and (4.11) and the definition of F_r to calculate the value of winding resistance at the n^{th} harmonic frequency, one uses the conductor height normalized to the skin depth at that harmonic. On the other hand, the various graphs in the paper which display K_r as a function of normalized conductor height use conductor height normalized to the skin depth *at the fundamental frequency*.

6. In the paper, Carsten does not actually define what he means by "duty cycle." Assuming that duty cycle is the ratio of ON time to switching period, it is not specifically stated in the text whether the rise and fall times are considered part of the ON time or not. Figure 4.1 shows a unipolar pulse of current with rise and fall times of T_R and T_F respectively. It is not clear from the paper whether Carsten considers duty cycle to be

$$D = \frac{T_3 - T_0}{T} \tag{4.1}$$

$$D = \frac{T_2 - T_1}{T} \tag{4.2}$$

or

$$D = \frac{T_2 - T_0}{T} \tag{4.3}$$

Equation (4.3) is the definition used by Venkatraman in [2]. Although this does not effect the validity of Carsten's general method, much of the paper is devoted

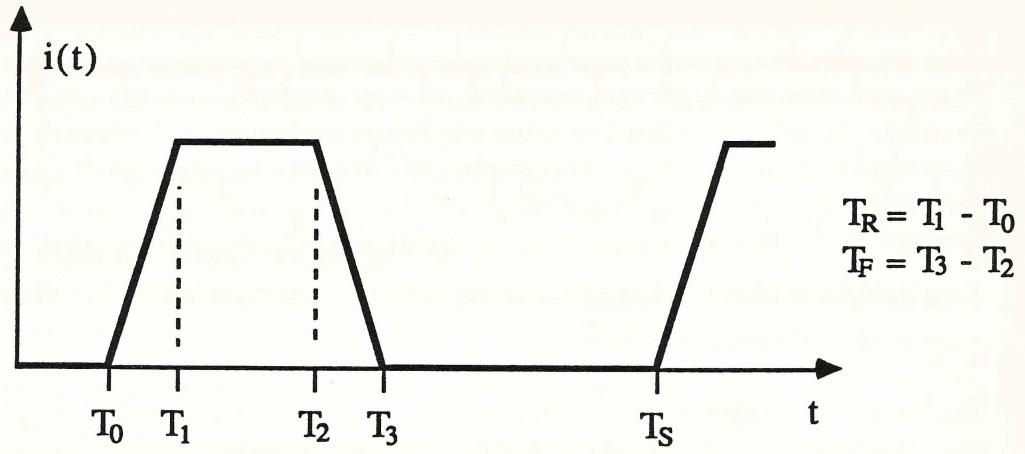


Figure 4.1: Unipolar pulse of current with rise and fall times of T_R and T_F respectively. Carsten is unclear on whether the rise and fall times are part of the ON time. This in turn effects the value of duty cycle.

to presenting design graphs plotted for specific waveforms with specified duty cycle and rise and fall times. If one is unsure as to what Carsten means by duty cycle, it compromises ones confidence in the graphs and ones ability to use them.

Several statements in Carsten's paper [3, page 158] lead us, however, to believe that he uses (4.1) rather than the definitions given in (4.2) and (4.3).

(a) He states that the rise and fall times of the waveform can be approximated by truncating the Fourier series once the correct 10% and 90% rise time is achieved.

(b) He states that this truncated series produces as good an approximation to the actual switchmode waveform as a trapezoidal approximation. Such an approximation is shown in Fig. 4.1. Although Carsten does not reference it, the trapezoidal approximation is employed by Venkatraman in [2].

(c) Carsten states that his approximation method simplifies the calculation of loss for several different rise times since the series can be halted at selected harmonics to determine the loss for different rise times. He provides the equation

$$\text{harmonic number} = \frac{T}{2T_R} - 1 \tag{4.4}$$

to determine where the series is to be truncated.

Thus it would appear that rather than using the Fourier coefficients for a trapezoidal waveform such as is Fig. 4.1, Carsten uses the coefficients for pulsed waveforms of duration $(T_3 - T_0)$ with zero rise and fall time, but halts the series once the desired 10% to 90% rise time is achieved.

7. Although the equations Carsten borrows from Dowell describe sinusoidally varying complex quantities, the term *phasor* is not mentioned in Carsten's paper. This is not a problem since in the initial steps of Carsten's derivation he finds the real parts of these complex quantities and uses the real-valued quantities for the rest of his calculations. Also, Carsten is not specific whether his harmonic winding currents I_n are phasors, rms values, or peak values. By context, the reader can determine that they must be rms values.

8. Carsten uses one symbol, D, to denote two very different quantities. As shown in Table 4.1, Carsten defines D as the duty cycle of the current waveform. Also, he uses the symbol D when repeating Dowell's results to describe the complex quantity given in (4.7) and in Table 4.1 as the second definition of D. When reading the paper, it is not difficult to determine from context which D Carsten is using.

4.3 TYPICAL RESULTS

As mentioned in Section 4.1, Carsten presents several graphs in his paper which display calculated values of K_r, the normalized effective resistance factor, for frequently encountered nonsinusoidal current waveforms. A typical example of these graphs is Fig. 1 of Carsten's paper which is reproduced here as Fig. 4.2. Here we see K_r plotted versus the normalized conductor height (h_{cu}/δ) for a pulsed current waveform of 50% duty cycle in an eight-layer winding. Curves in Fig. 4.2 are plotted for variation in the pulse rise and fall time of the current pulse. By looking at Fig. 4.2 we see that, as normalized conductor height increases, K_r initially decreases and then increases. Thus, according to Carsten, we can talk about an "optimum" conductor height as one which has the minimum amount of resistance and consequently the least loss for that waveform. The dashed line on Fig. 4.2 represents the optimum conductor heights, which initially decrease with a decrease in the rise and fall time but become constant for $T_R = T_F \leq 0.5\%$ of T_S.

Other representative graphs are presented in Figs. 4.3 and 4.4. Reproduced in these figures are Carsten's Figs. 3 and 4, respectively. Graphs similar to Figs. 4.2, 4.3 and 4.4 are presented in the paper for other conditions including square-wave currents and symmetrical triangular-wave currents.

In Fig. 4.3, we show mh_{cu}/δ, the product of optimum normalized conductor height and the number of layers, plotted versus the rise and fall time for a 50% duty cycle pulse of current. Separate curves are plotted for variation of the number of layers m in the winding. We can see that for waveforms with fast rise and fall times the optimum total winding thickness mh_{cu} is approximately constant around 2.17 skin depths [3, page 160].

In Fig. 4.4, the resistance factor at optimum is divided by the number of layers and plotted versus the waveform rise and fall times for a 50% duty cycle current pulse as a "convenient way to summarize loss data for optimum conditions."[3, page 161]

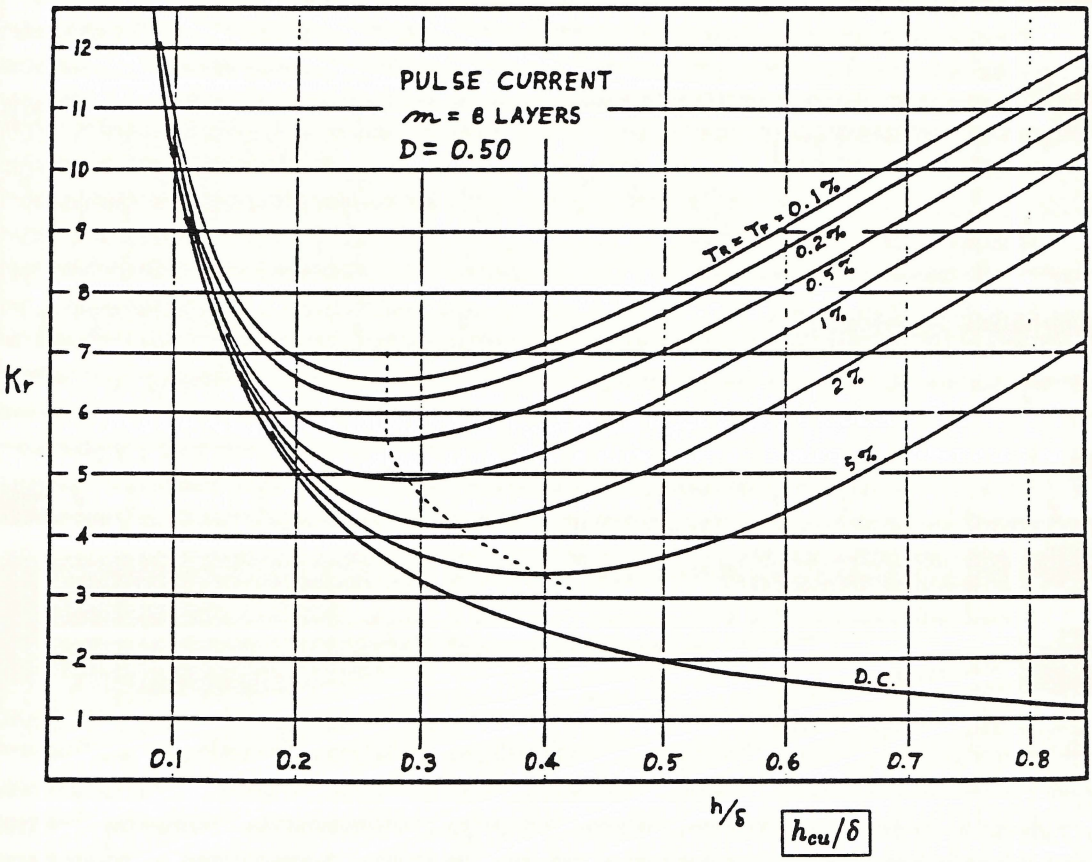


Figure 4.2: Carsten's Fig. 1 showing K_r vs. h_{cu}/δ with percentage rise and fall times T_R, T_F as parameters for a unipolar 50% duty cycle current pulse train in a winding with eight layers.

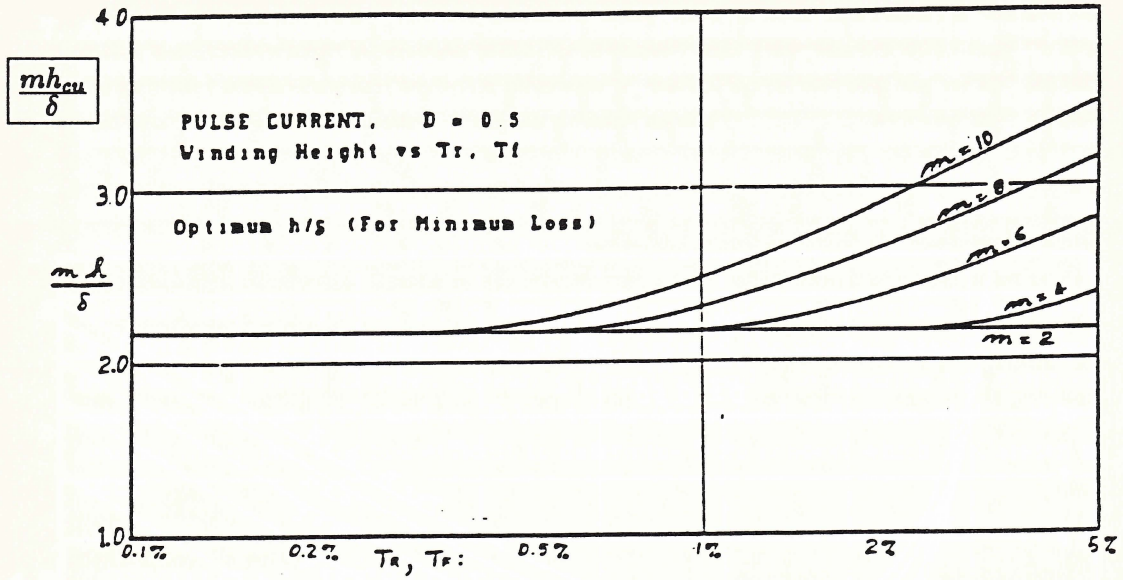


Figure 4.3: Carsten's Fig. 3 showing mh_{cu}/δ at optimum vs. T_R, T_F with m as parameter for pulsed current with a 50% duty cycle.

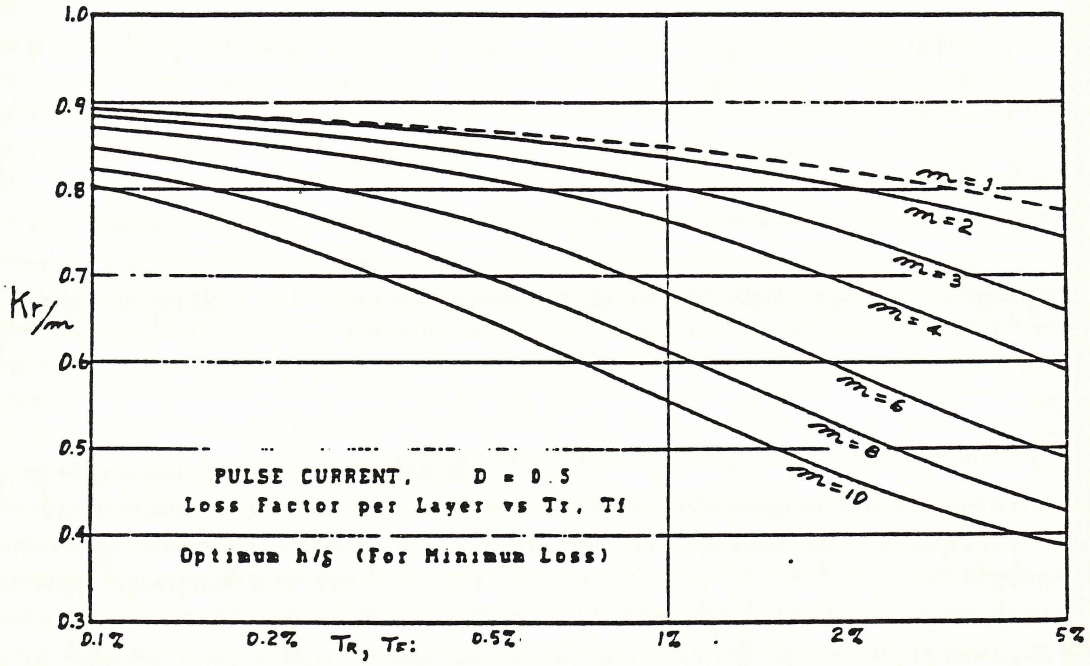


Figure 4.4: Carsten's Fig. 4 showing K_r/m at optimum h_{cu}/δ vs. T_R, T_F with m as parameter for pulsed current.

4.4 NOTABLE EQUATIONS

In this section, we examine several equations from Carsten's paper *using those symbols listed in Table 4.1 under the column titled Duke* where appropriate.

4.4.1 Equations Found in Carsten's Appendix

Beginning with Dowell's results, Carsten presents equations (2), (3) and (4), reproduced here as (4.5), (4.7) and (4.6), for windings of multiple layers when all layers are of the same thickness and no half layers are present.

$$F_r = M' + \frac{m^2 - 1}{3} D' \qquad \text{for } m \geq 1 \tag{4.5}$$

$$M = \underline{k} h_{cu} \coth \underline{k} h_{cu} \tag{4.6}$$

$$D = 2\underline{k} h_{cu} \tanh\left(\frac{\underline{k} h_{cu}}{2}\right) \tag{4.7}$$

where M' and D' are the real parts of M and D, respectively. Equation (4.7) describes Dowell's D, a complex quantity. This should not be confused with Carsten's other use of D to represent duty cycle. The complex quantities M and D are discussed in Section 2.3.2 of Part II of this report.

In the appendix of his paper, Carsten derives equations (20) and (21) which are presented here as they appear in his paper

$$D' = 2X\left(\frac{\sinh(X) - \sin(jX)}{\cosh(X) + \cos(jX)}\right) \tag{4.8}$$

$$M' = X\left(\frac{\sinh(2X) + \sin(2jX)}{\cosh(2X) - \cos(2jX)}\right) \tag{4.9}$$

Note that the j's contained in the sin and cos terms of equations (4.8) and (4.9) are errors and should be deleted. This is also true for Carsten's equations (16), (17), (18), and (19) which are not repeated here. Using the symbols derived in Part I of this report, the correct form of equations (4.8) and (4.9) is, respectively,

$$D' = 2\Delta\left(\frac{\sinh\Delta - \sin\Delta}{\cosh\Delta + \cos\Delta}\right) \tag{4.10}$$

$$M' = \Delta\left(\frac{\sinh 2\Delta + \sin 2\Delta}{\cosh 2\Delta - \cos 2\Delta}\right) \tag{4.11}$$

To calculate P_{loss} the total loss in a winding for nonsinusoidal current, Carsten presents equations (22) and (23) which represent the winding loss as the sum of the losses at each harmonic of the fundamental frequency. Carsten's equations (22) and (23) are, respectively,

$$P_{loss} = I_0^2 R_{w0} + I_1^2 R_{w1} + I_2^2 R_{w2} + \cdots + I_n^2 R_{wn} \tag{4.12}$$

$$P_{loss} = R_{w0}\left(I_0^2 + I_1^2 F_{r1} + I_2^2 F_{r2} + \cdots + I_n^2 F_{rn}\right) \tag{4.13}$$

where I_n, F_{rn} and R_{wn} are as defined in Table 4.1. By equating the total loss P_{loss} to the effective winding resistance R_{we} times the square of the total rms winding current I_{rms}^2, (4.13) leads to equation (26) for calculating R_{we}

$$R_{we} = \frac{R_{w0}(I_0^2 + I_1^2 F_{r1} + \cdots + I_n^2 F_{rn})}{I_{rms}^2} \tag{4.14}$$

where I_{rms}^2 is given in Carsten's equation (25) as

$$I_{rms}^2 = I_0^2 + I_1^2 + I_2^2 + \cdots + I_n^2 \tag{4.15}$$

By dividing both side of (4.14) by R_{w0} and Δ, we get

$$\frac{R_{we}}{R_{w0}\Delta} = \frac{I_0^2 + I_1^2 F_{r1} + \cdots + I_n^2 F_{rn}}{I_{rms}^2\,\Delta} \tag{4.16}$$

Using Carsten's definition for $R_{w\star}$

$$R_{w\star} = R_{w0}\,\Delta \tag{4.17}$$

and noting that

$$K_r = \frac{R_{we}}{R_{w\star}} \tag{4.18}$$

the equation for calculating K_r is derived from (4.16)

$$K_r = \frac{I_0^2 + I_1^2 F_{r1} + \cdots + I_n^2 F_{rn}}{I_{rms}^2\,\Delta} \tag{4.19}$$

Equations (4.17), (4.18) and (4.19) correspond to Carsten's (30), (28) and (32) respectively. Equation (4.19) is used to precalculate values of K_r from rms values of the harmonics in the current waveforms and the value of (4.5) evaluated using (4.10), (4.11) and the normalized conductor height at the corresponding harmonic frequency. The values of K_r so calculated can then be used to determine the effective resistance R_{we} using

$$R_{we} = K_r R_{w\star} = K_r\, R_{w0}|_{h_{cu}=\delta} \tag{4.20}$$

Carsten presents equation (33) which is reproduced here as (4.21)

$$F_r = M' + D'(p^2 - p) \tag{4.21}$$

which is used instead of (4.5), his equation (2), to calculate the ratio of ac to dc resistance for the pth layer in a winding when layer heights vary between layers of a winding. Carsten refers to this type of winding as "tapered". This equation can be derived from several equations presented on page 139 of Dowell's paper [1].

4.4.2 K_r for Triangular Wave with DC Offset

Another equation which is worth noting does not appear in the appendix to Carsten's paper. Rather, it appears in the body of Carsten's text without an equation number. This equation [3, page 164], given in Carsten's symbols,

$$K_r' = \frac{\frac{K_r}{12} + \frac{(I_{dc}/I_{ac})^2}{h/\delta}}{\frac{1}{12} + (I_{dc}/I_{ac})^2} \tag{4.22}$$

is used to calculate a "new loss factor with a DC component" for a triangular wave with a significant dc component. In this equation, K_r is the normalized effective resistance factor for the ac triangular waveform with zero dc offset, whereas K_r' is the same factor for the ac waveform plus dc offset. This equation assumes that the triangular waveform is of 50% duty cycle, or has equal rising and falling slopes, as is shown in Fig. 4.5. K_r for the triangular waveform without offset is shown in Fig. 4.6.

Adopting the symbols given as Duke's in Table 4.1, and using the subscript '*ac*' to denote quantities associated with the triangular wave *without* offset, the subscript '*dc*' to denote those associated with the waveform *with* offset, and the subscript '*pp*' to denote peak-to-peak values, we can write a more comprehensible version of equation (4.22).

$$K_{r\text{-}dc} = \frac{\frac{K_{r\text{-}ac}}{12} + \frac{(I_{dc}/I_{ac\text{-}pp})^2}{\Delta}}{\frac{1}{12} + (I_{dc}/I_{ac\text{-}pp})^2} \tag{4.23}$$

Hyphens have been used to append subscripts. At first glance (4.23) is not very enlightening, and is perhaps even perplexing. In order to assure the reader of the validity of this equation, we present a detailed derivation using the equations given in Section 4.4.1.

Before deriving equation (4.23), we must note two things. First, we know that since the two waveforms are identical except for the dc offset, then the harmonic content of the wavforms is the same. Thus, the coefficients $F_{r1}, F_{r2}, \ldots, F_{rn}$ are the same for the two waveforms, i.e.,

$$F_{rn\text{-}ac} = F_{rn\text{-}dc} = F_{rn} \qquad \text{for } n \geq 1 \tag{4.24}$$

Second, from Fourier analysis and (4.15) we know that the mean square value of a waveform is equal to the sum of the mean square values at the harmonics, i.e.,

$$I_{rms}^2 = I_0^2 + \sum_{n=1}^{\infty} I_n^2 \tag{4.25}$$

Using this information, we can now proceed with the derivation.

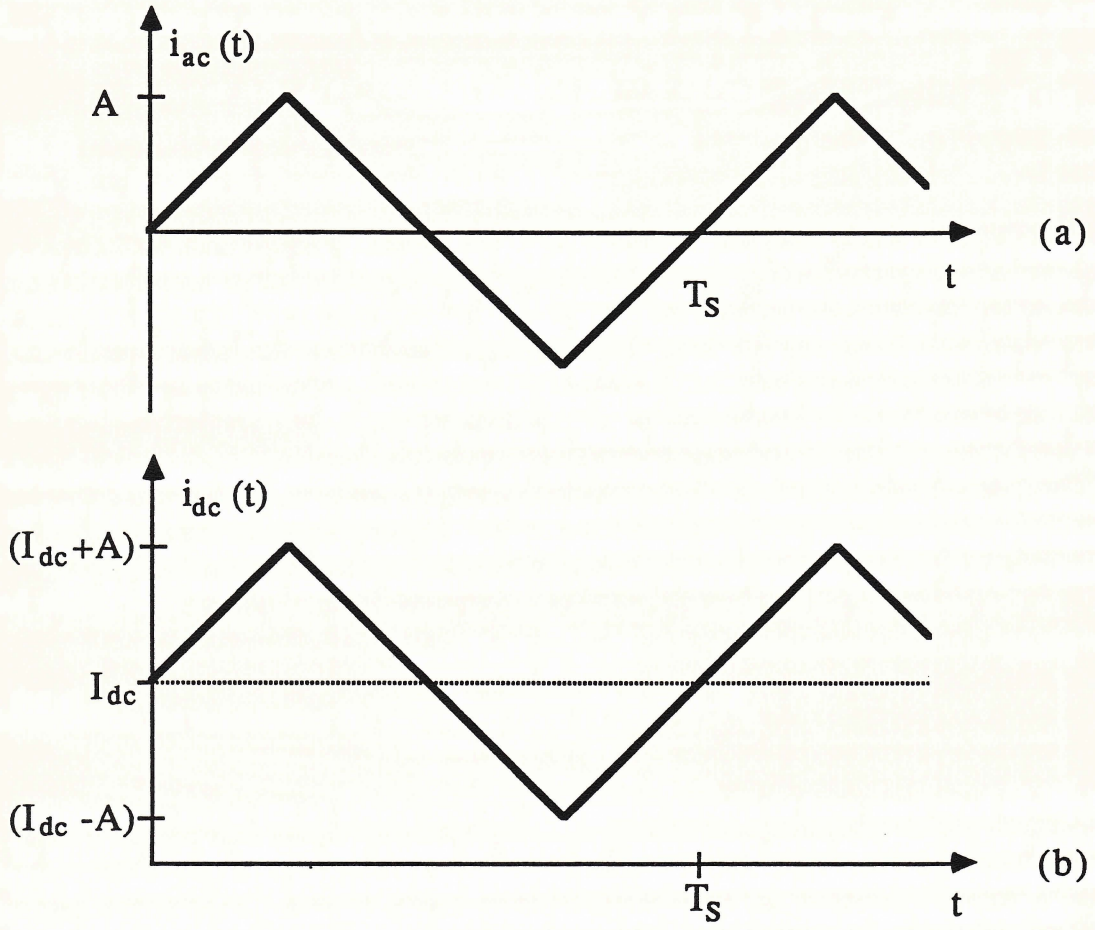


Figure 4.5: Triangular waveform of current with amplitude A and 50% duty cycle (a) with no dc offset, and (b) with dc offset I_{dc}.

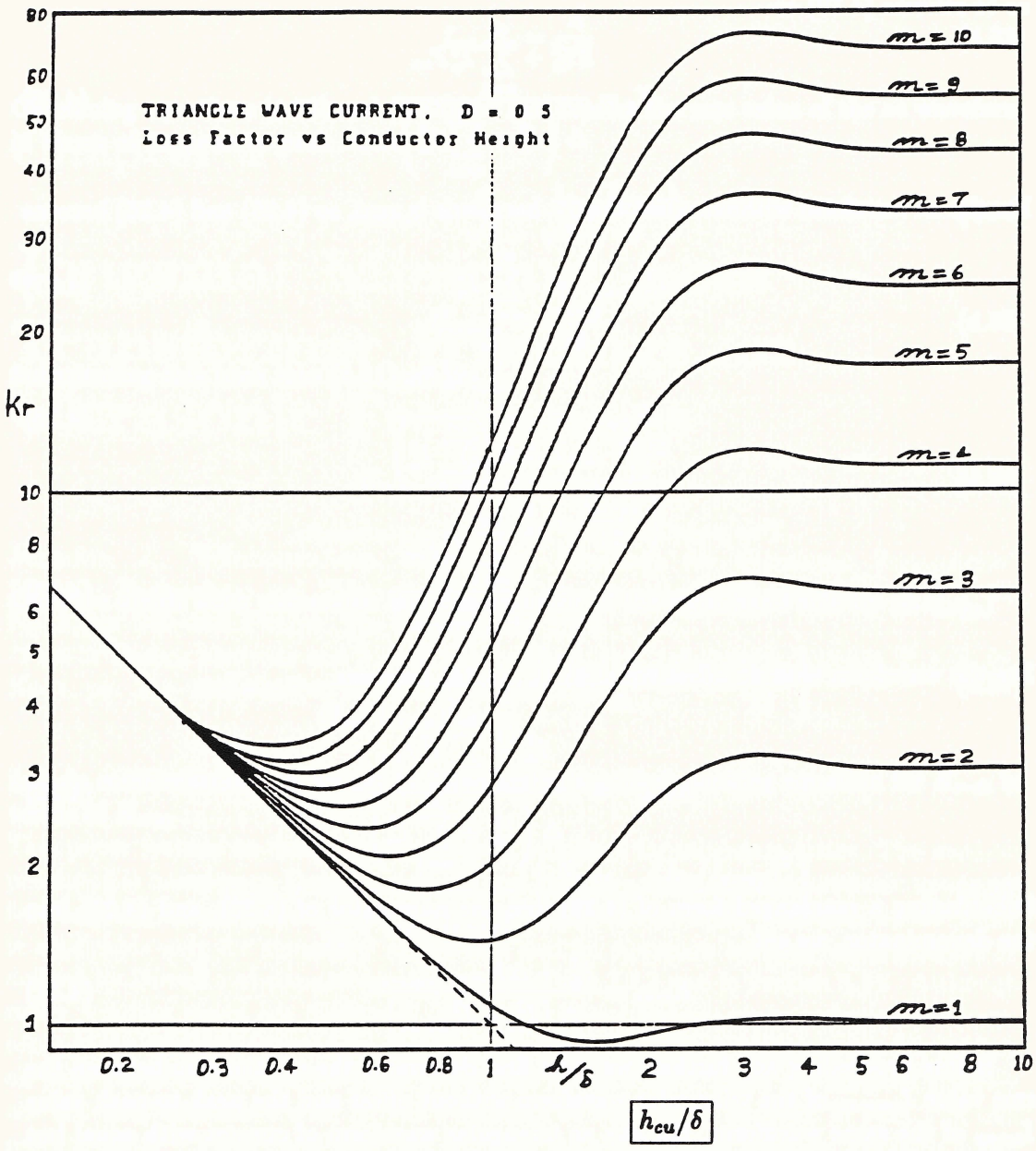


Figure 4.6: Carsten's Figure 7 showing K_r vs. h_{cu}/δ with the number of layers m as parameter for a triangular waveform of equal rise and fall times and no dc offset.

Staying for the moment with the general definition of K_r given in (4.19), (4.25) allows us to rewrite (4.19) as

$$K_r = \frac{I_0^2 + \sum_{n=1}^{\infty} I_n^2 F_{rn}}{\Delta\left(I_0^2 + \sum_{n=1}^{\infty} I_n^2\right)} \tag{4.26}$$

For the ac waveform without offset the 0^{th} harmonic is zero, so (4.25) and (4.26) become

$$I_{rms\text{-}ac}^2 = \sum_{n=1}^{\infty} I_n^2 \tag{4.27}$$

$$K_{r\text{-}ac} = \frac{\sum_{n=1}^{\infty} I_n^2 F_{rn}}{\Delta\left(\sum_{n=1}^{\infty} I_n^2\right)} \tag{4.28}$$

$$= \frac{\sum_{n=1}^{\infty} I_n^2 F_{rn}}{\Delta\left(I_{rms\text{-}ac}^2\right)} \tag{4.29}$$

For the waveform with dc offset equal to I_{dc}, (4.26) becomes

$$K_{r\text{-}dc} = \frac{I_{dc}^2 + \sum_{n=1}^{\infty} I_n^2 F_{rn}}{\Delta\left(I_{dc}^2 + \sum_{n=1}^{\infty} I_n^2\right)} \tag{4.30}$$

Substituting a rearranged form of (4.29) into the numerator of (4.30), and (4.27) into the denominator, we get

$$K_{r\text{-}dc} = \frac{I_{dc}^2 + \Delta K_{r\text{-}ac} I_{rms\text{-}ac}^2}{\Delta\left(I_{dc}^2 + I_{rms\text{-}ac}^2\right)} \tag{4.31}$$

Before proceeding any further, we must first determine the relationship between the rms value $I_{rms\text{-}ac}$ of the triangular waveform without offset and the peak-to-peak value $I_{ac\text{-}pp}$ of the same waveform. For any ac triangular waveform of current with equal but oppositely valued rising and falling slopes and arbitrary amplitude A and no dc offset such as is shown in Fig. 4.5(a), we know that the peak-to-peak value is

$$I_{ac\text{-}pp} = 2A \tag{4.32}$$

Also, by taking the function which describes the waveform $i(t)$, squaring it to get $i^2(t)$, determining the mean of the squared function $\langle i^2(t) \rangle$, and then taking the square root,

we find that the rms value of the waveform is

$$I_{rms\text{-}ac} = \frac{A}{\sqrt{3}} \tag{4.33}$$

Combining equations (4.32) and (4.33), we can express the rms value of the ac waveform in terms of its peak-to-peak value

$$I_{rms\text{-}ac} = \frac{A}{\sqrt{3}} = \frac{1}{\sqrt{3}}\left(\frac{I_{ac\text{-}pp}}{2}\right) \tag{4.34}$$

so

$$I^2_{rms\text{-}ac} = \frac{I^2_{ac\text{-}pp}}{12} \tag{4.35}$$

Substituting this back into (4.31) we get

$$K_{r\text{-}dc} = \frac{I^2_{dc} + \Delta K_{r\text{-}ac}\dfrac{I^2_{ac\text{-}pp}}{12}}{\Delta\left(I^2_{dc} + \dfrac{I^2_{ac\text{-}pp}}{12}\right)} \tag{4.36}$$

Once we divide both numerator and denominator of the right-hand side by $(\Delta I^2_{ac\text{-}pp})$

$$K_{r\text{-}dc} = \frac{1}{(I_{dc}/I_{ac\text{-}pp})^2 + \dfrac{1}{12}}\left\{\frac{(I_{dc}/I_{ac\text{-}pp})^2}{\Delta} + \frac{K_{r\text{-}ac}}{12}\right\} \tag{4.37}$$

and do some rearranging, we get (4.23), Carsten's unlikely looking equation for $K_{r\text{-}dc}$ in terms of $K_{r\text{-}ac}$

$$K_{r\text{-}dc} = \frac{1}{\dfrac{1}{12} + (I_{dc}/I_{ac\text{-}pp})^2}\left\{\frac{K_{r\text{-}ac}}{12} + \frac{(I_{dc}/I_{ac\text{-}pp})^2}{\Delta}\right\} \tag{4.23}$$

This page has been left blank intentionally.

Chapter 5

Jongsma: Minimum-Loss Transformer Windings for Ultrasonic Frequencies

Jongsma, J., "Minimum-Loss Transformer Windings for Ultrasonic Frequencies" "Part 1: Background and Theory," *Philips Electronic Application Bulletin*, E.A.B. 35, No. 3, pp. 146–163, Philips, The Netherlands, 1978.
"Part 2: Design Methods and Aids," *Philips Electronic Application Bulletin*, E.A.B. 35, No. 4, pp. 211–226, Philips, The Netherlands, 1978.

5.1 SUMMARY AND CRITIQUE

This paper focuses on designing transformer windings for minimum losses. The method presented is based upon Dowell's work [1] and gives the designer an algorithmic approach for designing minimum-loss transformer windings. The analysis presented in the paper is applicable only for sinusoidal excitations and for optimum winding arrangements as defined by Dowell and discussed in Item 6 of Section 2.2.1 and in Section 2.3.3. Although many winding types are discussed, Jongsma's paper focuses on round-wire windings. Most of the symbols adopted by Jongsma are clearly defined in his paper via his Table 1 on page 148 of Part 1 and his Table 1a on page 221 of Part 2. Since the adopted symbols are not fully consistent with Dowell's symbols or with those adopted in Part I of this report, Table 5.1 has been provided to show the relationship between Jongsma's and Duke's terminology. Where definitions differ, the definition related to Jongsma's paper is preceded by a "J: " and the definition related to Part I of this report is preceded by a "D: ." Additional symbols needed to understand the equations and figures presented in this chapter also are included in the table.

Part 1 of Jongsma's paper is primarily a theoretical development of various equations and design charts to help the designer determine the lowest-loss windings using design

Table 5.1 Comparison of Symbols and Definitions

Jongsma	*Duke*	*Meaning* *J: Jongsma; D: Duke*
—	A_{cu}	cross-sectional area of conductor
b	b_{cu}	J: breadth of (rectangular) conductor D: breadth of each conductor in a winding layer
b_m	b_{max}	maximum available winding breadth
b_w	b_w	breadth of a winding layer
D	—	D: $D = 2\Delta\,[(\sinh\Delta - \sin\Delta)\,/\,(\cosh\Delta + \cos\Delta)]$. Identical to Dowell's D', the real part of Dowell's D
d	d_{cu}	J: nominal wire diameter D: diameter of conductor without insulation
d_o	d_o	overall wire diameter including insulation
$d_o' = d_o/\Delta$	—	overall diameter normalized to skin depth
F_l	η	J: layer copper (space) factor D: layer porosity
F_R	—	ratio of ac resistance to dc resistance
f	f	J: operating frequency D: frequency
H	—	winding height including interleaving. Similar to build discussed in Section 2.1.3 of Part I of this report.
h	h_{cu}	J: effective conductor height (for solid, round wire $h = d\sqrt{\pi/4}$) D: height of copper in a layer of foil, strip or equivalent rectangular conductors.
$h' = h/\Delta$	$\Delta = h_{cu}/\delta$	J: effective conductor height normalized to skin depth D: height of winding layer in skin depths where σ_{cu} is use to determine δ as in (4.7) of Part I of this report.
h_s	h_{cu}	J: strip thickness D: see definition above — no differentiation between round-wire and strip windings
i	h_t	J: interleaving thickness between layers D: height of insulating tape
—	i	instantaneous current
id	—	(subscript) denotes variables which pertain to a winding which is ideal, i.e., not affected by height restrictions
—	ℓ	length

(Continued on next page)

Table 5.1 Comparison of Symbols and Definitions, cont.

Jongsma	*Duke*	*Meaning* *J: Jongsma; D: Duke*
l_{av}	ℓ_T	J: average turn length D: length of turn of a layer
M	—	D: $M = \Delta\,[(\sinh 2\Delta + \sin 2\Delta)\,/\,(\cosh 2\Delta - \cos 2\Delta)]$ Identical to Dowell's M', the real part of Dowell's M
$M_{0,5}$	—	D: $M_{0,5} = (\Delta/2)\,[(\sinh \Delta + \sin \Delta)\,/\,(\cosh \Delta - \cos \Delta)]$ Identical to Dowell's $M'_{1/2}$
m	—	integer truncation of p
N	—	number of turns in a winding or winding portion
—	N_c	number of current-carrying conductors in a winding layer
N_l	N_ℓ	number of turns in a winding layer
n_s	n_s	J: number of strands in a multiple wire D: number of electrically-paralleled conductors with the same height coordinate
P_w	$\langle P_D \rangle$	J: total winding loss in transformer (in split-and-sandwiched designs sometimes half total winding loss) D: average power dissipated in all the windings of a transformer
p	—	number of layers in a winding or winding portion
R_{ac}	—	ac resistance of winding
R_{dc}	—	dc resistance of winding
r_{ac}	—	ac resistance per unit length of conductor
s	—	$s = p - m$ (either 0 or 0.5)
$T = b_w/N$	—	breadth-to-turn ratio
—	T	temperature or the period of a waveform
$T' = T/\Delta$	—	normalized breadth-to-turn ratio
t	—	winding pitch
—	t	time
Δ	δ	J: penetration depth in *millimeters* D: skin depth in *meters*
$\varphi = \frac{h}{\Delta}\sqrt{F_l}$	$\Delta = \frac{h_{cu}}{\delta}$	J: normalized effective conductor height including the layer copper factor. D: height of winding layer in skin depth where $\sigma_{eff} = \eta\sigma_{cu}$ is used to determine δ as in (4.129) of Part I
—	ω	angular frequency of a periodic waveform
$'$	—	(superscript) denotes variables which are normalized

boundary conditions such as operating frequency and available winding breadth. How the design charts are used and an algorithm to design the lowest-loss combination of windings are the subjects of Part 2. The ability to design transformer windings using this paper is somewhat limited because the design charts that Jongsma presents have poor resolution and are frequency dependent. Calculation of data for frequencies not graphed is possible using equations detailed in Part 2. If a designer is primarily interested in minimum-loss designs, then this paper presents an easy-to-follow, almost mechanical method of achieving this. Before attempting to use the design rules presented by Jongsma however, the reader should recall the European use of commas where decimal points would be used in the United States. Also the reader should be warned that units are not clearly stated for many variables and that the equations presented are for winding portions as defined by Dowell and discussed in Section 2.1.

Because the analysis presented by Jongsma is based upon Dowell's work, it is limited to two-winding transformers and cannot be used to predict losses in shields or open-circuited windings. The primary concern of the paper is the algorithmic design of minimum-loss transformer windings, so the variation with frequency of the winding leakage inductance is not discussed, and only rms currents are used in the calculations. Jongsma presents no experimental data in the paper to verify his loss predictions.

5.1.1 Part 1 – Background and Theory

In Part 1 of the paper, Jongsma presents (1)

$$F_R = \frac{m[M + \{ps + (m^2 - 1)/3\}D] + sM_{0,5}}{p} \tag{5.1}$$

where $s = p - m$ and

$$M = \Delta \left(\frac{\sinh 2\Delta + \sin 2\Delta}{\cosh 2\Delta - \cos 2\Delta} \right) \tag{5.2}$$

$$M_{0,5} = \frac{\Delta}{2} \left(\frac{\sinh \Delta + \sin \Delta}{\cosh \Delta - \cos \Delta} \right) \tag{5.3}$$

$$D = 2\Delta \left(\frac{\sinh \Delta - \sin \Delta}{\cosh \Delta + \cos \Delta} \right) \tag{5.4}$$

which combines Dowell's two equations (10) and (17) for calculating F_R, the ratio of ac winding resistance to dc winding resistance for a winding portion with or without a half layer. Equations (5.2) through (5.4) are presented using the notation of Part I of this report where applicable, as is (5.5) below. Jongsma then presents (2)

$$F_R = 1 + \frac{5p^2 - 1}{45} (\Delta)^4 \tag{5.5}$$

which is an approximation to Dowell's results proposed by Snelling [14, page 323]. More is said about this approximation in Section 5.2. Jongsma uses (5.5) to derive several

equations and charts to determine the ideal (minimum-loss) ac resistance, and the corresponding wire diameter and winding height for several winding types and configurations. An example of such a chart is given in Fig. 5.3 of Section 5.3 below. Jongsma discusses the effects on the ideal resistance of boundary conditions such as conductor materials and breadth-to-turns ratio. He also addresses the merits and demerits of foil windings, multiple-strand windings and Litz wire.

The drawbacks of Part 1 of Jongsma's paper are legion. It is unclear which of Jongsma's numerous simplifying assumptions are used to generate each particular chart or equation. Also, the large number of assumptions and approximations does not inspire immediate confidence in the analysis. He normalizes several variables with respect to skin depth, and in one case normalizes a variable which "cannot properly be scaled" to skin depth [4, page 150], thus introducing inaccuracies. Still, Jongsma corroborates some of his results with those resulting from (5.1).

One apparent error in Jongsma's analysis relates to his approach to bifilar push-pull windings. Because of their push-pull nature, each wire carries current for only part of an operating cycle. Since his discussion on these windings is somewhat brief, it is hard to reconstruct precisely how he analyses them, yet, in his discussion he says that since the nonconducting wire does not contribute to the mmf, it can be ignored [4, page 158]. But, as can be inferred from Figs. 4.22 to 4.26 and (5.35) in Part I of this report, open-circuited conductors in high-field regions have substantial losses at high frequencies due to eddy currents. Thus their contribution to the overall losses in a transformer cannot be ignored. Bifilar push-pull windings are also discussed by Vandelac and Ziogas whose paper is reviewed in Chapter 8.

5.1.2 Part 2 – Design Methods and Aids

In Part 2 of Jongsma's paper, the methods for determining the ac resistance for various winding configurations developed in Part 1 are applied to a practical design algorithm. The algorithm consists of four major parts.

1. Determine the minimum possible ac resistance and the corresponding wire diameter and winding height for each power winding.

2. Compare the height needed for these minimum-loss windings with that which is available.

3. If there is insufficient height for the minimum-loss windings, find the lowest-loss combination of windings of less height (but more resistance) which fit in the available height.

4. Check that the winding losses are acceptable. If they are not, then make changes to the boundary conditions such as changing the conductor type, the winding configuration or core size.

Jongsma presents frequency-dependent charts of ac winding resistance versus breadth-to-turns ratio with the number of layers as the parameter. An example of such a chart is presented in Fig. 5.4 of Section 5.3 below. Jongsma demonstrates through examples the use of these charts and the determination of data for frequencies between those represented by the charts.

By making the charts in Part 2 of his paper frequency dependent, Jongsma eliminates the inaccuracy incurred in Part 1 by his improper normalization, however, a separate chart is needed for each operating frequency. The mechanical nature of the algorithm appears to make design easy and quick, but it tends to mask what assumptions have been used to generate the data in the charts. Although we have not verified the efficacy of Jongsma's methods, the charts and algorithm could prove a time saver, as long as the engineer does not blindly accept the data nor use them without discretion.

5.2 SIGNIFICANT EQUATIONS

A full recapitulation of all the equations presented by Jongsma would be excessively long for our interest here, however several equations from his paper are worth noting. Equations will be given *using the symbols derived in the Part I of this report wherever applicable.*

5.2.1 Calculation and use of F_R

Jongsma begins his development by presenting (1) — given as (5.1) in Section 5.1.1 and repeated here — which is a combination of Dowell's equations for calculating F_R for winding portions with or without a half layer

$$F_R = \frac{m[M + \{ps + (m^2 - 1)/3\}D] + sM_{0,5}}{p} \tag{5.1}$$

where $s = p - m$ and

$$M = \Delta\left(\frac{\sinh 2\Delta + \sin 2\Delta}{\cosh 2\Delta - \cos 2\Delta}\right) \tag{5.2}$$

$$M_{0,5} = \frac{\Delta}{2}\left(\frac{\sinh \Delta + \sin \Delta}{\cosh \Delta - \cos \Delta}\right) \tag{5.3}$$

$$D = 2\Delta\left(\frac{\sinh \Delta - \sin \Delta}{\cosh \Delta + \cos \Delta}\right) \tag{5.4}$$

Note that Dowell uses the symbols M', $M'_{1/2}$, and D' instead of Jongsma's M, $M_{0,5}$ and D, respectively, and that (5.2) and (5.4) are the same as (4.11) and (4.10) presented in the previous chapter on Carsten's paper [3]. If there are no half layers then $s = 0$ and (5.1) simplifies to

$$F_R = M + \frac{m^2 - 1}{3}D \tag{5.6}$$

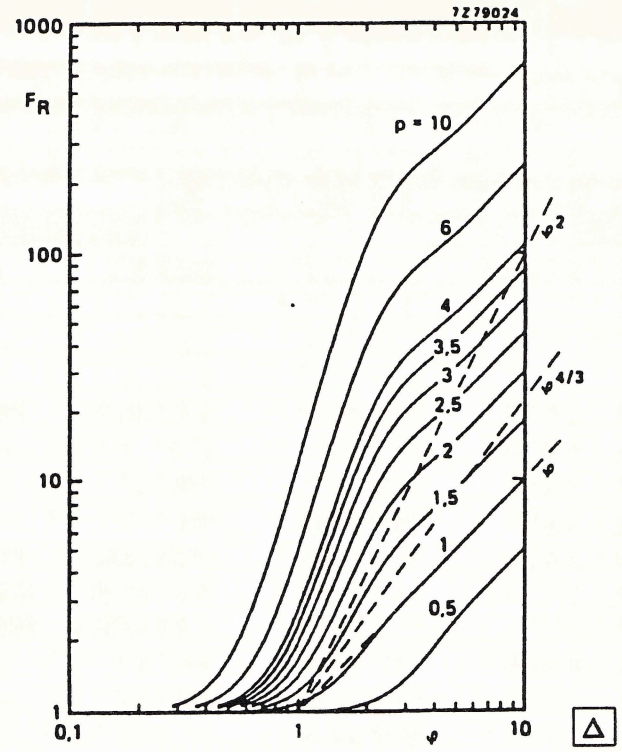


Figure 5.1: Figure 2 from Jongsma's paper. F_R calculated using (5.1) vs. Δ.

which is Dowell's (10) and Carsten's (2). If a half layer is present then $s = 0.5$ and $p = m + 0.5$ so (5.1) becomes

$$\begin{aligned} F_R &= \frac{m[M + \{(m+0.5)(0.5) + (m^2-1)/3\}D] + 0.5M_{0,5}}{m+0.5} \\ &= \frac{m[M + \{1.5m + m^2 - 0.25\}D/3] + 0.5M_{0,5}}{m+0.5} \\ &= \frac{12mM + m(4m^2+6m-1)D + 6M_{0,5}}{12m+6} \end{aligned} \tag{5.7}$$

which is Dowell's (17). Jongsma's Fig. 2 which shows F_R versus Δ (Jongsma's φ) generated using (5.1) is reproduced here as Fig. 5.1. The lines of $F_R = \Delta$, $F_R = \Delta^{4/3}$ and $F_R = \Delta^2$ are included by Jongsma as references to the slopes of the F_R curves.

The other significant equation presented by Jongsma is Snelling's approximation [14, page 323] to (5.1) which is presented as (5.5) in Section 5.1.1 and repeated here. Jongsma uses (5.5) to develop most of the other equations which are presented in the paper.

$$F_R = 1 + \frac{5p^2 - 1}{45}(\Delta)^4 \tag{5.5}$$

Jongsma writes that Snelling states that (5.5) is unreliable when p approaches unity [4, page 149]. Since Snelling proposes (5.5) in a discussion on close-packed multilayer

Table 5.2 Comparison of F_R Produced by Dowell's and Snelling's Equations

p	Δ	F_R using (5.1) [Dowell]	F_R using (5.5) [Snelling]	% Difference
0.5	0.1	1.0000	1.0000	-8.0×10^{-7}
	0.2	1.0000	1.0000	1.1×10^{-6}
	0.5	1.0003	1.0003	5.4×10^{-6}
	1.0	1.0055	1.0056	1.3×10^{-3}
	2.0	1.0856	1.0889	0.30
1.0	0.1	1.0000	1.0000	1.1×10^{-6}
	0.2	1.0001	1.0001	9.0×10^{-7}
	0.5	1.0055	1.0056	1.3×10^{-3}
	1.0	1.0856	1.0889	0.30
	1.5	1.3781	1.4500	5.2
	2.0	1.8978	2.4222	28
2	0.1	1.0000	1.0000	1.1×10^{-6}
	0.2	1.0007	1.0007	4.4×10^{-6}
	0.5	1.0263	1.0264	6.4×10^{-3}
	1.0	1.4060	1.4222	1.2
	1.5	2.7793	3.1375	13
	2.0	5.145	7.7556	51
3.0	0.1	1.0001	1.0001	1.1×10^{-6}
	0.2	1.0016	1.0016	1.0×10^{-5}
	0.5	1.0610	1.0611	1.4×10^{-2}
	1.0	1.9400	1.9778	1.9
	1.5	5.1147	5.9500	16
	2.0	10.561	16.644	58

windings, [14, pages 323,324] it would seem that he considers (5.5) to be reliable only for values of p greater than one. Still, we are unable to find a direct statement to that effect. After calculating F_R with both equations it appears that (5.5) is an accurate approximation to (5.1) for both $p \leq 1$ and $p > 1$, as long as one uses values of Δ less than about 2.0 [14, page 323]. These calculations are presented in Table 5.2. Jongsma also states that the approximation is inaccurate for $p = 1$ and $p = 0.5$ unless $F_R < 1.37$ where the error falls below 5% [5, page 217], which is verified by the data of Table 5.2. It is unclear from Snelling's discussion of (5.5) exactly what he means by the term "close-packed windings," however, Jongsma uses this term to describe windings where the winding pitch pT is nominally equal to the outer diameter of the wire d_o [4, page 150], i.e. where $d_o = b_{win}/N_c$.

Even though it fails as a general approximation to (5.1), (5.5) is quite useful for determining the wire diameter to produce the minimum value of ac resistance, which is the purpose of Jongsma's paper and of Section 9.5.3 of [14]. Beginning with Snelling's argument presented in Section 9.5.3 of [14], we recall (2.1) from Part I and write the dc resistance R_{dc} of a winding as

$$R_{dc} = \frac{\ell}{\sigma_{cu} A_{cu}} \tag{5.8}$$

where ℓ is the length of the conductor and A_{cu} is the cross sectional area of the conductor. If the winding has a total of N turns, each with a mean length of ℓ_T, and a cross-sectional area $A_{cu} = \pi d_{cu}^2/4$ for round wires and $A_{cu} = h_{cu}^2$ for the equivalent square wires, (5.8) becomes

$$R_{dc} = \frac{N\ell_T}{\sigma_{cu}\left(\pi d_{cu}^2/4\right)} = \frac{N\ell_T}{\sigma_{cu} h_{cu}^2} \tag{5.9}$$

By definition the ac resistance $R_{ac} = F_R R_{dc}$ so we can write

$$R_{ac} = F_R\left[\frac{N\ell_T}{\sigma_{cu} h_{cu}^2}\right] = \left(\frac{F_R N\ell_T}{\sigma_{cu}}\right)\left(\frac{1}{h_{cu}^2}\right) \tag{5.10}$$

From Table 5.1 we recall that $\Delta = h_{cu}/\delta$ so (5.10) becomes

$$R_{ac} = \left(\frac{F_R N\ell_T}{\sigma_{cu}}\right)\left(\frac{1}{\Delta^2\delta^2}\right) = \frac{N\ell_T}{\sigma_{cu}\delta^2}\left(\frac{F_R}{\Delta^2}\right) \tag{5.11}$$

where

$$\delta = \sqrt{\frac{2}{\omega\mu_0\sigma_{eff}}} = \sqrt{\frac{2}{\omega\mu_0\eta\sigma_{cu}}} \tag{5.12}$$

According to Jongsma, η is essentially constant for close-packed windings [4, page 148], so from (5.11) we can write that

$$R_{ac} \propto \frac{F_R}{\Delta^2} \tag{5.13}$$

at a specific operating frequency. Thus we can see that to minimize the ac resistance, one must minimize F_R/Δ^2. The ratio F_R/Δ^2 is plotted versus Δ for various values of p in Fig. 5.2. These curves are plotted using (5.1). Examining this figure we confirm Snelling's assertion that in the linear high-frequency region of Fig. 5.1 the ac resistance R_{ac} is minimized by using the largest conductor possible [14, page 323]. We see also that a local minimum in ac resistance is achieved for $p > 1$ in the region of $\Delta < 2$. Recalling from Table 5.2 that (5.5) was an adequate approximation of (5.1) for $\Delta < 2$, we see that either equation can be used in the region of the local minima of Fig. 5.2. Jongsma's analysis is based upon manipulating (5.5) to determine the wire diameters which correspond to these local minima since he considers the wire diameters needed to produce the minima at the right of Fig. 5.2 to be excessive.

Although we were unable to trace Jongsma's assertion that Snelling states that (5.5) becomes unreliable when p approaches unity [4, page 149], we *were* able to trace the other references that Jongsma makes to Snelling's book.

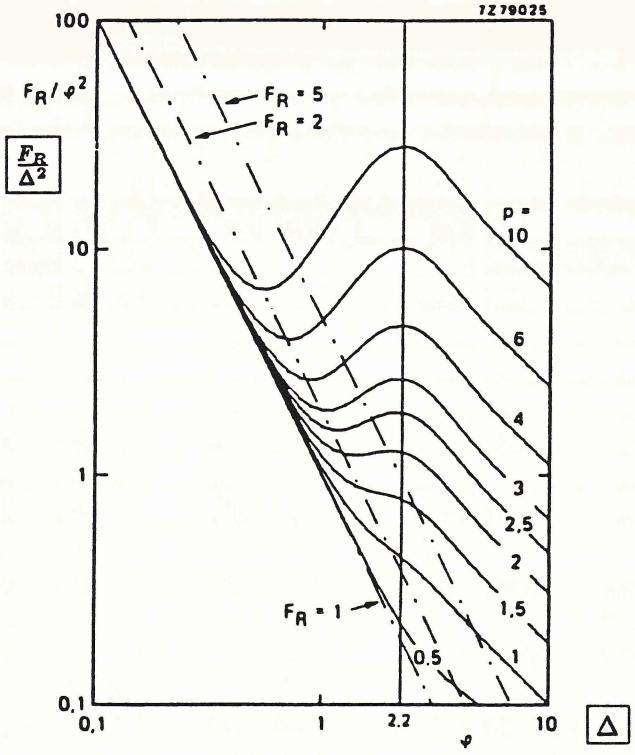


Figure 5.2: Figure 3 from Part 1 of Jongsma's paper. $F_R/(\Delta^2)$ versus Δ.

- "r_{ac}[1] must have a minimum in the lower curved region of the F_R versus [Δ] curves." Jongsma: page 148. Corresponds to Snelling: page 323.
- "incomplete layers invalidate the theory" (referring to Dowell's analysis) Jongsma: page 149. Corresponds to Snelling: page 322.
- "[Dowell's] theory becomes unreliable when [η] becomes too small." Jongsma: page 149. Corresponds to Snelling: page 323.

5.2.2 Improper Normalization

During the development presented in Part 1 of his paper, Jongsma normalizes several of his parameters by dividing by skin depth to eliminate a dependence on frequency. This is carried to an extreme when he normalizes the outer diameter of a conductor d_o to get the normalized outer diameter d_o'. He states that for "IEC grade 2 range of winding wire it can be shown empirically that $d_o = 1,229h^{0,93}$" [4, page 150]. In order to express d_o' as a function of the normalized effective conductor height h', a value of skin depth must be assumed, thus making d_o' dependent upon frequency. Using an assumed value of frequency, Jongsma then states that for "purposes of illustration it is satisfactory to use

[1] R_{ac} is the ac resistance of a winding whereas r_{ac} is the ac resistance per unit length

$d_o' = 1,31(h')^{0,93}$... in the frequency range 20 kHz to 50 kHz" [4, page 150]. By using a value of resistivity $\rho = 2.22 \times 10^{-8}$ [Ωm] given in Part 2 of Jongsma's paper, and keeping in mind that Jongsma expresses penetration depth in *millimeters*, we have verified that he assumes a value of 35 kHz and that the formula for d_o' introduces less than 2.5% error over the specified frequency range. This improperly normalized expression for d_o' is used to generate the data for close-packed windings represented in Figs. 4 and 5 and perhaps 7 in Part 1 of the paper. In Part 2, Jongsma avoids this improper normalization by making the design charts presented there frequency dependent.

5.2.3 Comparison of Jongsma's and Carsten's Methods

By ignoring the term $(N\ell_T/\sigma_{cu}\delta^2)$ in (5.11) and minimizing values of F_R/Δ^2, Jongsma essentially normalizes R_{ac} to the dc resistance of a conductor with a cross-sectional area of δ^2. The term $(N\ell_T/\sigma_{cu}\delta^2)$ results directly if the skin depth δ is substituted in (5.9) for the conductor copper height h_{cu}. This normalization is essentially the same as is proposed by Carsten in his paper [3], however, the resultant equations given by the two authors differ.

To minimize losses Jongsma examines the variations of F_R/Δ^2 versus Δ, whereas Carsten examines the variations of K_r versus Δ. The relationship between these two factors can be determined by first examining Carsten's (32) to calculate K_r for a non-sinusoidal waveform. This equation is given as (4.19) in the previous chapter and is repeated here[2]

$$K_r = \frac{I_0^2 + I_1^2 F_{r1} + \cdots + I_n^2 F_{rn}}{I_{rms}^2 \, \Delta} \tag{5.14}$$

If we assume sinusoidal current waveforms, the dc component I_0 and the harmonics of the fundamental, I_n for $n > 1$, are all equal to zero and (5.14) degenerates to

$$K_r = \frac{F_{r1}}{\Delta} \tag{5.15}$$

which is the same as F_R/Δ. So we see that to minimize losses, Jongsma examines F_R/Δ^2, whereas, Carsten examines (for sinusoids) F_R/Δ. Why the difference? It is believed by the author of the present chapter that this difference stems from different definitions for the cross-sectional area of conductor in a winding.

If instead of (5.9) we use Dowell's definition for the dc resistance of a winding portion without a half layer

$$R_{dc} = \frac{mN_\ell^2 \ell_T}{\eta \sigma_{cu} b_{win} h_{cu}} \tag{5.16}$$

then $R_{ac} = F_R R_{dc}$ becomes

$$R_{ac} = F_R \left[\frac{mN_\ell^2 \ell_T}{\eta \sigma_{cu} b_{win} h_{cu}} \right] = \left(\frac{F_R \, mN_\ell^2 \ell_T}{\eta \sigma_{cu} b_{win}} \right) \left(\frac{1}{h_{cu}} \right) \tag{5.17}$$

[2]The terms in the equation are given using Carsten's terminology summarized in Table 4.1.

Recalling that $\Delta = h_{cu}/\delta$, (5.17) can be rewritten

$$R_{ac} = \left(\frac{F_R\, m N_\ell^2 \ell_T}{\eta \sigma_{cu} b_{win}}\right)\left(\frac{1}{\Delta\delta}\right) = \frac{m N_\ell^2 \ell_T}{\eta \sigma_{cu} b_{win} \delta}\left(\frac{F_R}{\Delta}\right) \tag{5.18}$$

where δ is given by (5.12). If η is assumed to be essentially constant, then for a specific operating frequency

$$R_{ac} \propto \frac{F_R}{\Delta}$$

which agrees with Carsten's minimization of of $K_r = (F_R/\Delta)$ for sinusoidal current excitation. Thus we see that the difference between minimizing F_R/Δ^2 and F_R/Δ can be attributed to a difference between using a conductor cross-section of $A_{cu} = h_{cu}^2$ and a winding layer cross-section of $A = b_{win} h_{cu}$, in other words, the difference between using round-wire and foil conductors.

5.3 TYPICAL RESULTS

In order to understand the charts and figures which result from Jongsma's analysis, the reader should be acquainted with the details of that analysis. Since a full recapitulation of Jongsma's equations is impossible in the limited space of this chapter, we have not presented sufficient equations for the reader to understand the figures presented in this section. These figures are included to give the reader a general feel for what kinds of figures Jongsma presents. Figure 5.3 shows the characteristics of ideal simple and split windings of solid round wire. Part (a) shows the ideal normalized ac resistance $r'_{ac\,id}$ versus the normalized breadth-to-turns ratio T'; (b) shows the ideal normalized wire diameter d'_{id} versus T'; and (c) shows the ideal normalized winding height excluding insulation $H'_{e\,id}$ versus T'. Dotted lines apply to close-packed windings, full lines to spaced windings. Figure 5.4 is a reproduction of the first design chart presented in Part 2 of Jongsma's paper. This chart represents values of ac resistance r_{ac} versus breadth-to-turns ratio T for single-strand round wire windings and values of total ac resistance $(n_s r_{ac})$ versus breadth-to-turns ratio T/n_s for multiple-round-wire windings of n_s strands. Also shown are the nominal and outer diameters d_{cu} and d_o of various wire sizes.

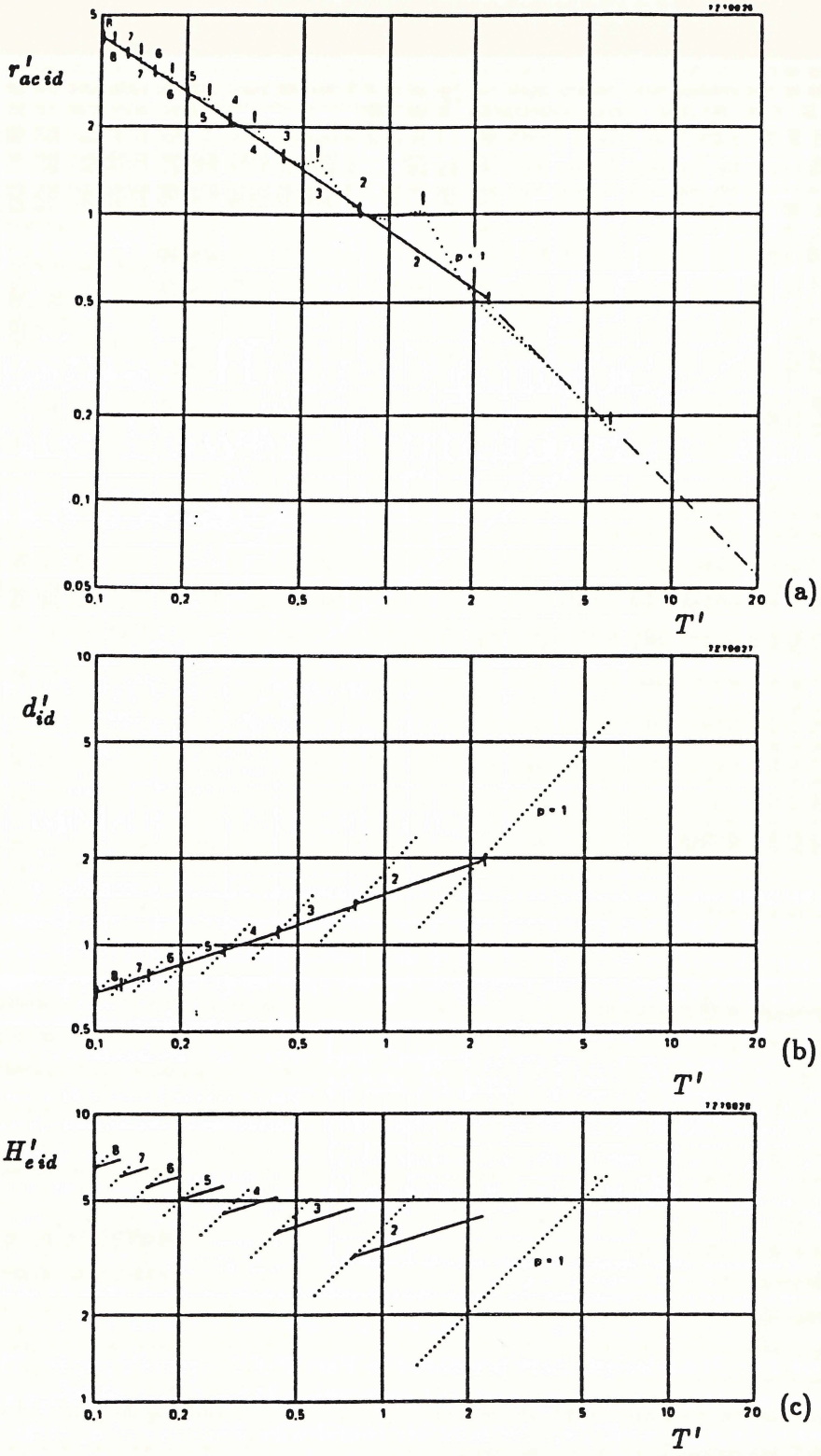


Figure 5.3: Figure 4 from Part 1 of Jongsma's paper. The characteristics of ideal simple and split windings of solid round wire. (a) $r'_{ac\,id}$ vs. T'; (b) d'_{id} vs. T'; (c) $H'_{e\,id}$ vs. T'. Dotted lines apply to close-packed windings, full lines to spaced windings.

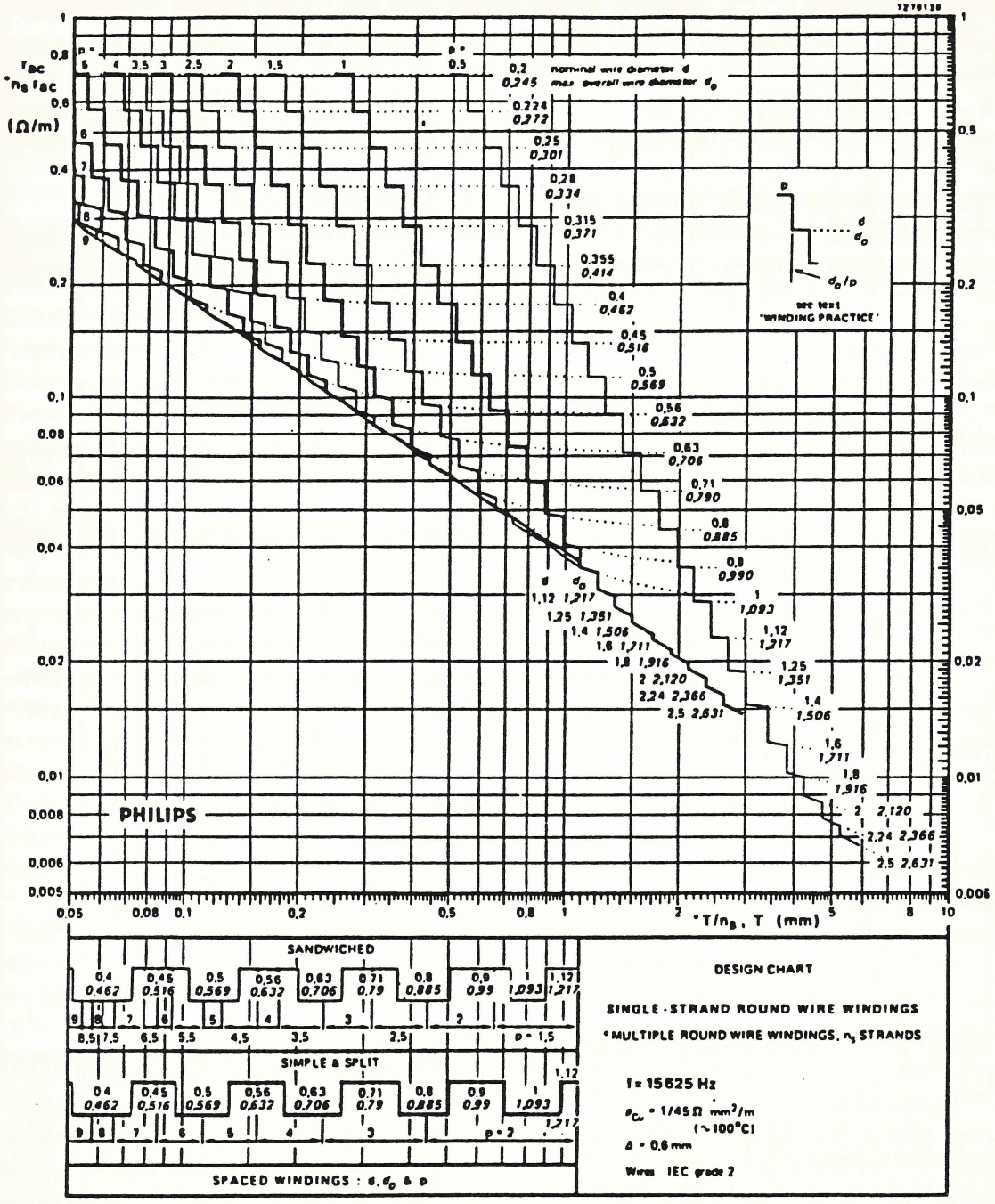


Figure 5.4: First design chart presented in Part 2 of Jongsma's paper. This chart represents values of r_{ac} vs. T for single-strand round wire windings and values of $(n_s r_{ac})$ vs. (T/n_s) for multiple round-wire windings of n_s strands.

Chapter 6

Jongsma: High-Frequency Ferrite Power Transformer and Choke Design

Jongsma, J., "High-Frequency Ferrite Power Transformer and Choke Design; Part 3: Transformer Winding Design," *Philips Electronic Components and Materials Technical Publication 207*, Philips, The Netherlands, 1986.

6.1 SUMMARY AND CRITIQUE

The paper by Jongsma that is reviewed in this chapter presents a detailed algorithm for the design of minimum-loss transformer windings including the design equations and tabular data needed for calculating power loss in a winding. The methods presented are loosely based on Dowell's work [1], but are far enough removed that an understanding of Dowell's work is not essential to the implementation of the design algorithm. Similarly, the methods presented in the paper have little relation to the discussion in Part I of the present report. However, to provide a context for discussing Jongsma's paper and comparing it to the work presented in Part I and to the other articles discussed in Part II, Table 6.1 has been provided. This table shows the relationship between Jongsma's nomenclature as used in the paper under review and that adopted in Part I of the present report.

Jongsma's primary interest is the design of minimum-loss transformers, so he focuses on calculating the resistive winding losses rather than on calculating leakage inductance. Most of his analysis assumes two-winding transformers, although he does discuss how to adapt the design algorithm to accommodate multiple-output transformers as well as push-pull transformers. He briefly discusses the resistive losses in shields and open-circuited windings, but does not incorporate these losses into his design algorithm. His algorithm is applicable to designing for sinusoidal or nonsinusoidal currents. The latter

Table 6.1 Comparison of Symbols and Definitions

Jongsma	*Duke*	*Meaning* J: Jongsma; D: Duke
—	A_{cu}	cross-sectional area of conductor
—	a_m, b_m †	Fourier coefficients at harmonic m
B_{CF}	b_{max}	J: coil former (or winding window) breadth D: maximum breadth available
b	b_{cu}	J: breadth of (rectangular) conductor D: breadth of each conductor in a winding layer
b_w	b_w	breadth of a winding layer
d	d_{cu}	diameter of copper in a round wire
F_ℓ	η	J: space (copper) factor in layer breadth D: layer porosity
F_R	—	ratio of ac resistance to dc resistance (at a specified frequency)
f	f	J: operating frequency D: frequency
f_e	—	effective frequency (discussed in Section 6.3)
H	—	height of a winding portion. Similar to build discussed in Section 2.1.3 of Part I of this report
h	h_{cu}	J: conductor height — round wire: $h = d\sqrt{\pi/4}$ — strip: h = strip thickness D: height of copper in a layer of foil, strip or equivalent rectangular conductors
I	I	J: rms value of winding current D: a constant value of current, rms unless indicated otherwise by a subscript
—	I_{rms} †	rms value of $i(t)$
$\dot{I}$	—	rms value of the first derivative of the current waveform
i	h_t	J: thickness of interleaving D: height of insulating tape
—	$i(t)$	instantaneous winding current
—	ℓ	length
ℓ_{av}	ℓ_T	J: average turn length D: length of turn of a layer
—	m †	subscript denoting the index number for harmonics of the waveform of current

(Continued on next page)

Table 6.1 Comparison of Symbols and Definitions, cont.

Jongsma	*Duke*	*Meaning* J: Jongsma; D: Duke
N	—	rounded number of turns in a winding portion
N_ℓ	N_ℓ	number of turns per layer
n	—	preliminary number of turns
—	n	layer or interlayer gap number or the number of turns per meter
n_s	n_s	J: number of strands in either bunched or multiple wire D: number of electrically-paralleled conductors with the same height coordinate
P_w	$\langle P_D \rangle$	J: dissipation in transformer winding at f_c for a given load condition D: average power dissipated in all the windings of a transformer
R_{ac}	—	ac resistance of winding
R_{dc}	—	dc resistance of winding
r	—	transformer turns ratio
—	r	"radius" direction in cylindrical coordinate system
r_{ac}	—	ac resistance of winding per unit length
r_{dc}	—	dc resistance of winding per unit length
$T = b_w/N$	—	winding breadth to turns ratio
—	T	temperature or the period of a waveform
t	—	winding pitch
—	t	time
Δ	δ	J: skin thickness *in millimeters* D: skin depth *in meters*. $\delta = \sqrt{(2/\omega\mu_0\sigma_{eff})}$
ϑ	$\underline{\Gamma}$	J: ratio of minimum to maximum leakage flux density over height of winding D: boundary condition ratio $\underline{\Gamma} = (\underline{H}_z(X=0)/\underline{H}_z(X=h_{cu})) = \alpha + j\beta$
$\varphi = \frac{h}{\Delta}\sqrt{F_\ell}$	$\Delta = \frac{h_{cu}}{\delta}$	J: effective conductor height D: height of layer in skin depths. The inclusion of $\sqrt{F_\ell}$ in Jongsma's definition is consistent since Duke uses $(\eta\sigma_{cu})$ for the effective conductivity σ_{eff} when modeling a winding layer
—	ω	angular frequency of a periodic waveform

† denotes symbols not included in the Glossary of Symbols

is accommodated by determining an effective sinusoidal frequency for the nonsinusoidal current. Although he talks in terms of sinusoids, Jongsma does not use the term phasor to describe sinusoidally varying quantities, and calculations are performed using only geometric factors, the rms current, the excitation frequency and the ratio of minimum to maximum leakage flux density for the winding. No evidence of experimental verification of the design algorithm appears in this paper.

The first third of the paper is primarily a verbal flow chart detailing the design algorithm with the appropriate equations and tables; the rest of the paper explains the theory behind the design equations and algorithm and some of the assumptions made.

Jongsma uses the adjectives *ideal*, *nonideal*, and *optimum* to mean very specific things when referring to transformer windings.

ideal windings are designed for the lowest possible loss regardless of available winding height. He uses this term to imply desirability but not necessarily feasibility [6, page 16].

nonideal windings are windings of less winding height and higher losses than *ideal* windings, but have the lowest loss possible for the winding height used.

optimum combination of *nonideal* windings is that combination of nonideal power windings which produces the lowest total loss while still fitting into the available height. This use of *optimum* should not be confused with Dowell's optimum winding arrangements which are discussed Item 6 of Section 2.2.1 and in Section 2.3.3.

The main steps in the design algorithm detailed in the first part of Jongsma's paper are as follows:

1. Collect what Jongsma calls the design boundary conditions. By this he means write down in a quantitative form all the conditions and requirements that the design must satisfy including such things as operating frequency, permissible winding loss, winding configuration, available winding height, etc.

2. Determine the ideal power windings, i.e., the lowest-loss windings regardless of winding height.

3. Compare the total height and power loss of the ideal windings to the maximum allowable height and winding loss, respectively. Depending upon the result go to Step 4, Step 5, or start over with a new design.

    - If the ideal windings fit into the available window height *and* satisfy the maximum winding-loss specification, proceed to Step 5.
    - If the ideal windings exceed the available height but are within the maximum-loss specification, go to Step 4.
    - If both criteria exceed specification, or if the ideal windings fit into the available window but are too lossy, the design process must be restarted with a change in the boundary conditions.

4. If there is insufficient height for the ideal windings, find the optimum (lowest-loss) combination of nonideal windings that fit in the available height.

5. Finalize the design. This includes checking the design calculations, determining the actual turn lengths and amounts of wire needed, estimating the temperature rise and producing the manufacturing specifications.

The steps of this algorithm are described in great detail with the appropriate design equations for different types of windings (wire, strip etc.) winding configurations (simple, split/sandwiched) and for single- or multi-layer windings. The description of the algorithm seems thorough and appears to be easy to follow and to implement although we have not verified this with an actual design.

The theoretical section which follows the design-algorithm section covers several topics of interest. First, there is a comprehensible discussion of high-frequency current redistribution and losses, and the importance of field-intensity diagrams[1]. Second, the theory behind the winding-optimization algorithm is discussed in detail starting with curves of F_R the ratio of ac resistance to dc resistance generated using Dowell's analysis; however, Dowell's equations are not actually reproduced in Jongsma's paper. Third, Jongsma discusses the variation of field-intensity (leakage-flux) diagrams during a switching cycle for transformers in power converters. The highly nonsinusoidal currents conducted by windings in these transformers is accommodated by the calculation of the effective frequency for each winding current. Last, Jongsma introduces the concept of an effective frequency f_e for the nonsinusoidal current carried by a transformer winding. According to Jongsma, use of f_e weights other frequency-dependent calculations toward the high-frequency harmonics of the fundamental frequency and away from the dc component of the current waveform. As discussed below in Section 6.3, the validity of Jongsma's effective frequency beyond weighting things toward the correct direction is disputable.

The theoretical section of Jongsma's paper also contains some instructive discussion on eddy-current losses in windings and shields that carry no net current. Unfortunately, the application of this information to the design of minimum-loss transformer windings is only sketched in the theoretical section, and totally ignored in the algorithmic section. Thus, the presented algorithm totally ignores the substantial losses produced in open-circuited conductors in regions of nonzero field intensity.

The paper has other shortcomings. In the initial, algorithmic part of the paper, many of the equations are presented with numeric values already incorporated for such things as the resistivity of copper, the permeability of free space, π and other parameters. In general, the full equations appear in the later theoretical section. Still, when one encounters one of these equations without any explanation, one's first reaction is an aggravated "where did that come from?" This can also lead to incorrect results if one is not careful. One example is the effective frequency f_e which is assumed throughout the paper to be in kilohertz but whose value when calculated by equation (6.1) is in hertz.

[1]Jongsma calls these leakage-flux diagrams. The use of field-intensity diagrams is discussed in detail in Part I of this report.

Equations throughout the text are presented with little explanation as to their origins, so it is difficult for the reader to independently verify the results. It is not very easy or particularly useful therefore, to attempt to translate Jongsma into terms more closely related to the results presented in Part I of this report.

6.2 TERMINOLOGY USED

Most of the terminology needed to read the paper is defined clearly therein. Terminology which is inconsistent with the derivations in Part I of the present report or which is needed for the discussion in this chapter is given in Table 6.1. Where definitions differ or where the notation used by Jongsma to represent a given parameter differs from that in the general Glossary of Symbols, the definition presented in Jongsma's paper is preceded by a "J: " and that used in the Glossary is preceded by a "D: ." If a symbol proposed by Jongsma does not correspond to or conflict with any of Duke's symbols and is needed for the discussion in this chapter, it is presented in Table 6.1 in the column entitled *Jongsma* but is not adopted as a Duke symbol. Additional symbols needed for this chapter that are not defined either by Jongsma or in Part I are listed under the column entitled *Duke* and are denoted by a †.

6.3 THE EFFECTIVE FREQUENCY

This particular paper contains a tremendous number of equations, most of which are relatively easy to understand, so a full recapitulation of all the contained equations would be excessively long. However, in this section we examine Jongsma's use of effective frequency f_e which is one particularly confusing and unclear concept in his paper.

Jongsma does not use the term *phasor* when referring to time varying quantities in his paper. Rather, his equations assume either a sinusoidal current at a specific frequency, or a nonsinusoidal current for which an effective sinusoidal frequency can be calculated. As is stated in Section 6.1, Jongsma introduces the concept of the effective frequency f_e to weight the design calculations toward the high-frequency harmonics of the current waveform fundamental frequency. The introduction of effective frequency is an attempt to accommodate the eddy-current losses due to the harmonics in a nonsinusoidal current without resorting to Fourier analysis. Neither the Duke research group nor Vandelac and Ziogas [8, pages 365,366] are convinced that this is a valid method, although it is an easy calculation and gives an easily used result.

According to Jongsma, the effective frequency f_e is calculated using the following equation which we present in his notation

$$f_e = \frac{1}{2\pi}\left(\frac{\dot{I}}{I}\right) \tag{6.1}$$

where I is the rms value of the winding current and $\dot{I}$ is the rms value of the first derivative of the current waveform. "This expression does not apply in the region... where the eddy-

current loss is proportional to... $\sqrt{f}$" [6, page 25]. This region where the equation is invalid corresponds to the region above approximately 100 kHz in Fig. 6.5 in Part I of this report. Since the result of (6.1) for an arbitrary current waveform is not obvious, let us determine f_e assuming first a sinusoidal current and second a nonsinusoidal current.

For a sinusoidal current

$$i(t) = \sqrt{2} I_{rms} \sin \omega t \tag{6.2}$$

we have a derivative with respect to time of

$$\frac{di(t)}{dt} = \omega \sqrt{2} I_{rms} \cos \omega t \tag{6.3}$$

Substituting (6.2) and (6.3) into (6.1) yields, for a sinusoidal current, an effective frequency equal to the operating frequency of the transformer, as is expected.

$$f_e = \frac{1}{2\pi} \left(\frac{\omega I_{rms}}{I_{rms}} \right) \tag{6.4}$$

If the current $i(t)$ is nonsinusoidal, it can be expressed in terms of a Fourier expansion

$$i(t) = a_0 + \sum_{m=1}^{\infty} \Big(a_m \cos(m\omega_0 t) + b_m \sin(m\omega_0 t) \Big) \tag{6.5}$$

where ω_0 is the fundamental frequency in radians, and a_m and b_m represent the Fourier coefficients. The rms value of the nonlinear current is then

$$I_{rms} = \left[a_0^2 + \sum_{m=1}^{\infty} \frac{1}{2} \left(a_m^2 + b_m^2 \right) \right]^{1/2} \tag{6.6}$$

The derivative with respect to time of (6.5) is

$$\frac{di(t)}{dt} = \sum_{m=1}^{\infty} \Big(-m\omega_0 a_m \sin(m\omega_0 t) + m\omega_0 b_m \cos(m\omega_0 t) \Big) \tag{6.7}$$

which has an rms value of

$$\dot{I}_{rms} = \left[\sum_{m=1}^{\infty} \frac{\omega_0^2 m^2}{2} \left(a_m^2 + b_m^2 \right) \right]^{1/2} \tag{6.8}$$

if we divide (6.8) by (6.6) we get

$$\begin{aligned} \frac{\dot{I}_{rms}}{I_{rms}} &= \frac{\left[\sum_{m=1}^{\infty} \frac{\omega_0^2 m^2}{2} \left(a_m^2 + b_m^2 \right) \right]^{1/2}}{\left[a_0^2 + \sum_{m=1}^{\infty} \frac{1}{2} \left(a_m^2 + b_m^2 \right) \right]^{1/2}} \\ &= \frac{\omega_0 \left[\sum_{m=1}^{\infty} \frac{m^2}{2} \left(a_m^2 + b_m^2 \right) \right]^{1/2}}{\left[a_0^2 + \sum_{m=1}^{\infty} \frac{1}{2} \left(a_m^2 + b_m^2 \right) \right]^{1/2}} \end{aligned} \tag{6.9}$$

Therefore, in terms of Fourier coefficients, Jongsma's effective frequency from (6.1) is equal to

$$f_e = f_0 \left\{ \frac{\left[\sum_{m=1}^{\infty} \frac{m^2}{2}\left(a_m^2 + b_m^2\right)\right]^{1/2}}{\left[a_0^2 + \sum_{m=1}^{\infty} \frac{1}{2}\left(a_m^2 + b_m^2\right)\right]^{1/2}} \right\} \tag{6.10}$$

where f_0 is the fundamental frequency. From examining (6.10), we see that the calculation produces a result with two significant factors. The first factor f_0 is simply the fundamental operating frequency of the nonsinusoidal current. The second factor — enclosed in braces — consists of a ratio where the denominator includes the rms values at all harmonics of the current, including dc; the numerator includes the rms values of the fundamental and the higher-frequency harmonics each scaled by the square of its harmonic number. Although we are unconvinced that f_e calculated by (6.1) will give the optimal (minimum-loss) results upon which Jongsma's design algorithm is based, it does appear that it *will* weight the operating frequency toward the high-frequency harmonics, and so accomplish Jongsma's goal concerning the effective frequency.

6.4 SIGNIFICANT FIGURES

In Jongsma's discussion of the theory behind the loss-minimization design algorithm, he presents several charts and figures. In this section we reproduce some of these figures and discuss how they are important to understanding Jongsma's paper and the larger problem of modeling high-frequency multiwinding transformers.

Jongsma's Fig. 10 is shown here as Fig. 6.1. Shown in Fig. 6.1 is the proximity effect in a winding of five layers for three different values for the dimensionless ratio of conductor height in skin depths. For this ratio, we use the symbol Δ as employed in Part I of this report instead of Jongsma's symbol φ. For the left portion of the figure, $\Delta = 0.59$ which represents a relatively thin wire. In the center portion of Fig.6.1, $\Delta = 2$ and on the right $\Delta = 8$. Since skin depth δ is inversely proportional to the square root of frequency, the increase of $\Delta = (h_{cu}/\delta)$ from left to right can represent an increase in conductor height at a set frequency, or an increase in frequency at a set conductor height. The current density distribution is plotted in Fig. 6.1(a) where the solid line represents amplitude, the dashed line the real part and the dotted line the imaginary part. Figure 6.1(b) shows the loss distribution which is proportional to the square of the current-density amplitude in each layer plotted with a solid line, the average loss in each layer plotted with a dashed line, and the average loss in the complete winding with a dotted line. The field-intensity diagrams[2] for the five-layer windings are shown in Fig. 6.1(c). Noting the substantial change in ordinate scales in parts (a) and (b) as Δ increases from 0.59 to 2 to 8, it is very clear that power losses increase with the

[2]Jongsma refers to these as leakage flux diagrams.

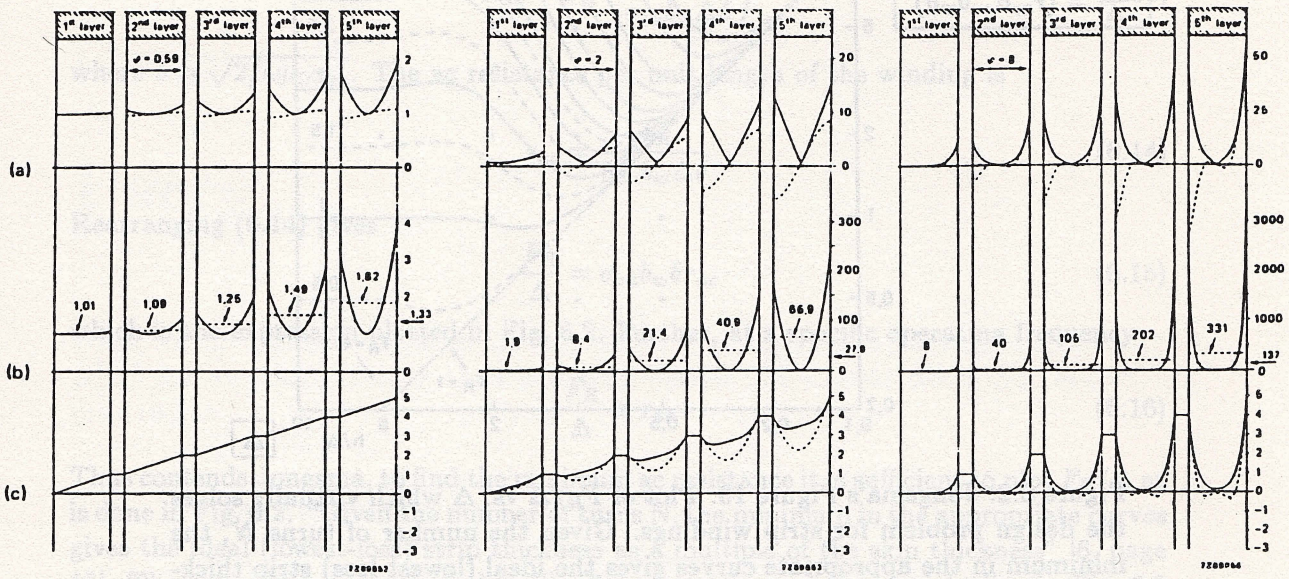


Figure 6.1: Jongsma's Figure 10. The proximity effect in a winding of 5 layers. Effective conductor heights are $\Delta = 0.59$ (left), $\Delta = 2$ (center) and $\Delta = 8$ (right). Sections through the ends of the layers of the winding are shown, hatched. The layers are of strip conductor but could also be N_ℓ turns of rectangular wire. The current density distribution is plotted in (a). The full line is the amplitude, the broken line the real part, and the dotted line the imaginary part. The losses are plotted in (b). The loss distribution (solid line) is proportional to the square of the current density amplitude. The broken line shows the average loss in each layer, and the dotted line the average loss in the complete winding. Since the scale calibration is multiples of the dc loss, the dotted line shows the value of F_R. (c) is the leakage flux diagram, obtained by integration of the current density. Scale divisions are layer current; line types are as in (a). {Jongsma's Caption.}

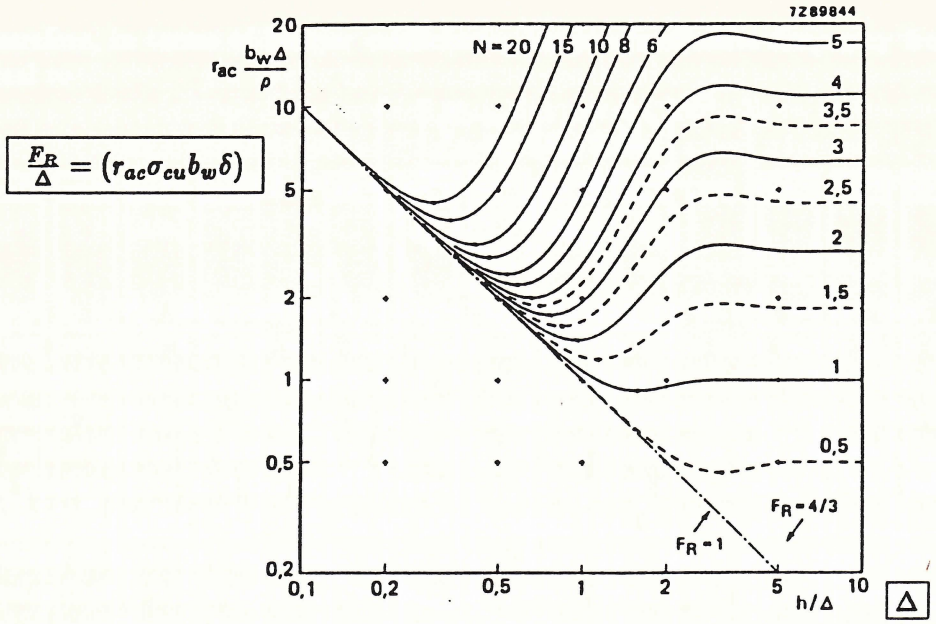


Figure 6.2: Jongsma's Figure 13. Plot of F_R/Δ vs. Δ which virtually solves the design problem for strip windings. Given the number of turns N, the minimum in the appropriate curves gives the ideal (lowest loss) strip thickness as a multiple of the skin thickness. The resistance per meter length of strip can also be determined. {Jongsma's caption.}

increased bunching of current that occurs as Δ increases. Since increasing Δ corresponds to an increase in frequency for a set conductor height, the solid-line amplitude curves of Fig. 6.1(a) represent the same phenomena as do the curves in Fig. 4.3 of Part I of this report. Likewise, the solid-line field-intensity diagrams of Fig. 6.1(c) correspond to the curves of Fig. 4.2 of Part I.

In Chapter 5 above, we discuss Jongsma's earlier work on loss minimization. In that chapter we present Fig. 5.2 and discuss Jongsma's use of (F_R/Δ^2) in the minimization of conductor loss for round-wire conductors. It would be well for the reader to review Sections 5.2.1 and 5.2.3 at this time. In the paper currently being discussed, Jongsma also includes his Fig. 13 given here as Fig. 6.2 which shows $(F_R/\Delta = (r_{ac}\sigma_{cu}b_w\delta))$ versus Δ for strip windings and discusses how this figure is used to minimize losses in strip windings. The value of F_R is calculated using Dowell's results.

For a strip winding, the dc resistance is equal to

$$R_{dc} = \frac{\ell}{\sigma_{cu}A_{cu}} = \frac{\ell}{\sigma_{cu}b_{cu}h_{cu}} \tag{6.11}$$

By definition, $R_{ac} = F_R R_{dc}$ so

$$R_{ac} = F_R\left(\frac{\ell}{\sigma_{cu}b_{cu}h_{cu}}\right) \tag{6.12}$$

From Table 6.1 we know that $\Delta = h_{cu}/\delta$ and that $\delta = \sqrt{2/\omega\mu_0\sigma_{eff}}$ where $\sigma_{eff} = \eta\sigma_{cu}$. Additionally, $\eta = 1$ and $b_{cu} = b_w$ for a strip conductor, so (6.12) can be written as

$$R_{ac} = F_R\left(\frac{\ell}{\sigma_{cu} b_w \Delta\delta}\right) \tag{6.13}$$

where $\delta = \sqrt{2/\omega\mu_0\sigma_{cu}}$. The ac resistance per unit length of the winding is

$$r_{ac} = \frac{F_R}{\sigma_{cu} b_w \Delta\delta} \tag{6.14}$$

Rearranging (6.14) gives

$$\frac{F_R}{\Delta} = \sigma_{cu} b_w \delta r_{ac} \tag{6.15}$$

which is the expression plotted in Fig. 6.2. Further, at a specific operating frequency

$$\frac{F_R}{\Delta} \propto r_{ac} \tag{6.16}$$

Thus contends Jongsma, to find the minimum ac resistance it is sufficient to plot F_R/Δ as is done in Fig. 6.2. "Given the number of turns N, the minimum in the appropriate curves gives the ideal (lowest-loss) strip thickness as a multiple of the skin thickness" [6, page 16]. The loss minima are marked in Fig. 6.2 with dots, and the straight line in Fig. 6.2 represents r_{dc} the dc resistance per unit length. Curves for $N = 0.5, 1.5, 2.5, 3.5$ represent sandwiched windings with $1, 3, 5, 7$ turns whose representation as winding portions results in portions containing half layers.

In Section 5.2.3, we recall that to minimize winding losses Carsten [3] examines curves of K_r, his proposed normalized effective resistance factor, plotted as functions of Δ. Also, we prove that this resistance factor degenerates to $K_r = F_R/\Delta$ for sinusoidal waveforms. Comparing this with the above discussion of Fig. 6.2, we see that for sinusoidal excitation and strip windings, Jongsma's and Carsten's loss-minimization schemes are identical.

This page has been left blank intentionally.

Chapter 7

Perry

Perry, M.P., "Multiple Layer Series Connected Winding Design for Minimum Losses," *IEEE Transactions on Power Apparatus and Systems*, Vol. PAS-98, No. 1, Jan/Feb 1979, pp. 116-123.

7.1 SUMMARY

In this paper, Perry solves for the current density function in the coils of a single-winding multilayer series-connected solenoid. His analysis is based on general field solutions for the distribution of current density in the layers of an infinitely long solenoid that carries a sinusoidally varying current. He presents this analysis in both rectangular and cylindrical coordinates, and he uses the results he obtains for the current density in the layers to calculate the power dissipation per unit length of the infinite solenoidal structure. Perry then examines these power dissipation calculations and determines the optimum thickness, i.e., that thickness which minimizes losses, for each of the layers of the multilayer structure. His dissipation calculations are written as functions of normalized layer thickness and are compared to an appropriate reference value.

Much of the terminology employed in Perry's paper was used later by Vandelac and Ziogas in their paper [8] and subsequently adopted by Duke for use in the derivations of Part I of this report. Table 7.1 lists the symbols associated with Perry's paper along with other symbols used in the review of this article. Table 7.1 also lists symbols used by Perry which are inconsistent with the common set in the general Glossary of Symbols. When different definitions exist for the same quantity, Perry's definition is preceded by "P: " and the definition from the Glossary of Symbols is preceded by "D: ". If Perry has a symbol for which there is no Duke equivalent, then we use Perry's symbol in this chapter. If Duke and Perry use different symbols to represent the same quantity, then the Duke symbol is used in this review. In Section 7.6, exceptions to this last convention are made so that some of Perry's equations can be reproduced exactly as they appear in his paper. These exceptions are clearly noted.

Perry is concerned with determining and minimizing resistive losses in a multilayer

Table 7.1 Comparison of Symbols and Definitions

Perry	*Duke*	*Meaning* P: Perry; D: Duke
B	B	magnetic flux density
c_0, c_1, c_2	—	coefficients of Bessel functions
d_n	—	distance from outside surface of coil to the inner surface of layer n
$F_1(\Delta_n)$	$F_1(\Delta)$	$(\sinh 2\Delta + \sin 2\Delta)/(\cosh 2\Delta - \cos 2\Delta)$
$F_2(\Delta_n)$	$F_2(\Delta)$	$(\sinh \Delta \cos \Delta + \cosh \Delta \sin \Delta)/(\cosh 2\Delta - \cos 2\Delta)$
—	$\underline{H}'(x)^\dagger$	field intensity phasor whose magnitude is the peak value of the sinusoid
I	$\underline{I}$	P: sinusoidal current in a conductor D: complex phasor of current in a conductor
$I' = \frac{mI}{\ell}$	—	current per unit length in a winding layer. Comparable to Duke's $(N_\ell \underline{I}_\ell / b_{win})$ except I' represents the peak value of sinusoidal current, and $\underline{I}_\ell$ is a phasor with magnitude equal to the rms value of current
i	—	general argument used in summations
—	i	instantaneous current
—	$\underline{J}'(y)^\dagger$	current density phasor whose magnitude is the peak value of the sinusoidal current density
$\hat{J}_n(y)$	$\underline{J}_y(x)$	P: phasor of current density in the n^{th} layer. Magnitude of phasor is the peak value of the sinusoidal current density. D: phasor representation of current density. Magnitude of phasor is the rms value of the sinusoidal current density
$\hat{J}_n^*(y)$	$\underline{J}_y^*(x)$	P: complex conjugate of current density in the n^{th} layer. D: Complex conjugate of $\underline{J}_y^*(x)$
$\mathrm{J}_p(\,)$	—	Bessel function of first kind of order p
$J_x(y,t)$	$J_y(x,t)$	sinusoidal current density as a function of time and position in the layer
j	j	$\sqrt{-1}$
$k = \frac{(-1+j)}{\delta}$	$\underline{k} = \frac{(1+j)}{\delta}$	complex wave number
ℓ	b_{win}	P: length of coil in the axial or z-direction D: breadth of core window. Equal to breadth of equivalent foils which model winding layers
m	N_ℓ	number of turns in one winding layer
N	N	P: total number of layers in a coil D: total number of layers in the winding space
n	n	(subscript) denotes the layer number P: $n = 1$ for outermost layer D: $n = 1$ for innermost layer

(Continued on next page)

Table 7.1 Comparison of Symbols and Definitions, cont.

Perry	*Duke*	*Meaning* P: Perry; D: Duke
p	—	(subscript) denotes order of Bessel function
$Q_{dc} = \frac{I'^2}{2\sigma\tau}$	—	power dissipated per square meter of a layer at dc
Q_N	—	total power dissipation in a coil of N layers
Q_n	$\langle Q_J \rangle$	power dissipation per unit area for n^{th} layer
Q_n/Q_{ref}	$\langle Q'_J \rangle$	normalized power dissipation in n^{th} layer
Q'_n	—	power dissipation per unit length of the n^{th} cylindrical layer
$Q_{ref} = \frac{I'^2}{2\sigma\delta}$	—	power in layer one when $\Delta \to \infty$
Re( )	Re( )	signifies "the real part" of a complex quantity
R_n	—	inner radius of the n^{th} cylindrical layer
r, ϕ, z	r, ϕ, z	cylindrical coordinate axes
x	—	general argument of a function
x, y, z	x, y, z	axes in a right-handed Cartesian coordinate system P: x corresponds to direction of current flow, y corresponds to layer thickness, and z corresponds to length D: x, y, z correspond to height, depth, and breadth
$Y_p( )$	—	Bessel function of second kind of order p
y	x	P: coordinate in the direction of layer thickness D: coordinate in the direction of layer height
$\alpha_n = R_n/R_{n-1}$	—	ratio of radii for n^{th} layer
—	α	real part of $\underline{\Gamma}$, the complex ratio of the phasor magnetic fields on the surfaces of a winding layer, where $\underline{\Gamma} = \alpha + j\beta$
—	β	imaginary part of $\underline{\Gamma}$ which is defined above
Δ, $\Delta_n = \frac{\tau}{\delta}$	$\Delta = \frac{h_{cu}}{\delta}$	P: normalized winding-layer thickness of the n^{th} layer D: normalized winding-layer height
Δ^c,Δ^c_n	—	"critical" normalized layer thickness of layer n that gives minimum power dissipation
$\delta = \sqrt{\frac{2}{\omega\mu\sigma}}$	$\delta = \sqrt{\frac{2}{\omega\mu\sigma_{eff}}}$	skin depth
σ	σ	conductivity
—	σ_{eff}	effective conductivity
τ, τ_n	h_{cu}	P: winding-layer thickness D: equivalent-conductor height
$\wedge$	$\underline{\ }$	P: a circumflex over a symbol indicates a phasor or complex quantity D: an underline of a symbol indicates a phasor or complex quantity

† denotes symbols not included in the Glossary of Symbols

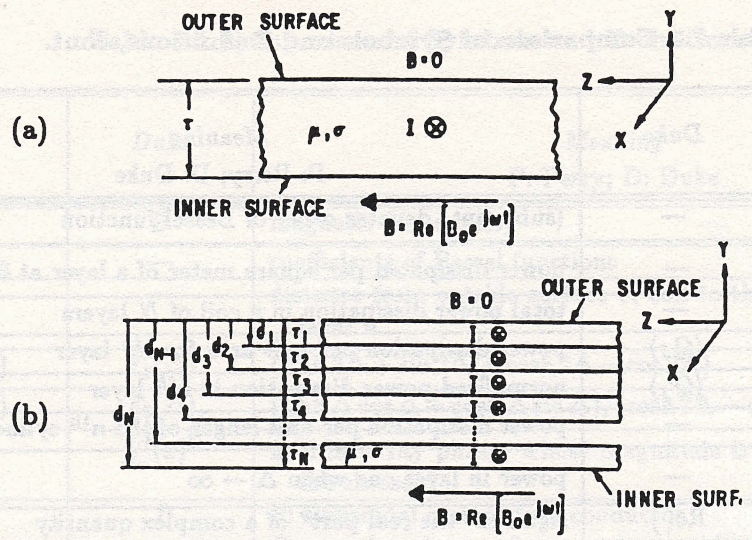


Figure 7.1: (a) Perry's Fig. 2 for the geometry of a single current sheet where the current I is shown by the encircled cross as flowing in the negative x-direction, the thickness of the winding layer is τ in the y direction, and the axial length of the coil is in the z-direction. (b) Perry's Fig. 3 for the cross section of a set of N winding layers each carrying current I.

infinite solenoid, so he does not discuss the frequency-dependent leakage energy stored in the layers and interlayer gaps of the winding. Since he focuses on solenoids rather than transformers, he does not discuss shields or open-circuited layers; however, his methods can be applied to determine the losses in either. Perry is concerned with only sinusoidal excitations and it appears that he uses phasor notation for his current density $\hat{J}_x(y)$, although he does not use the term phasor nor does he specifically define the meaning of the circumflex. Other sinusoidally varying quantities such as the current I' are represented by their peak values. Perry presents no experimental data to verify his results.

7.2 GEOMETRY

In this paper, Perry examines the field solution of the current density and power loss in an infinite solenoid, and addresses this solution using two different approaches. For coils where the curvature can be neglected, he uses a rectangular coordinate system and solves the fields analysis for a current sheet of infinite extent in two directions and τ "thick" in the third. Figure 7.1 shows the geometry that Perry uses to set up the rectangular-coordinate analysis in his paper. Part (a), which is Perry's Fig. 2, shows a cross section of an infinite current sheet with zero magnetic flux density $B = 0$ on the upper surface and a sinusoidally varying flux density $B = \text{Re}\left[B_0 e^{j\omega t}\right]$ tangential to the lower boundary of the sheet. Except for the difference in orientation of the x and y axes, this figure is

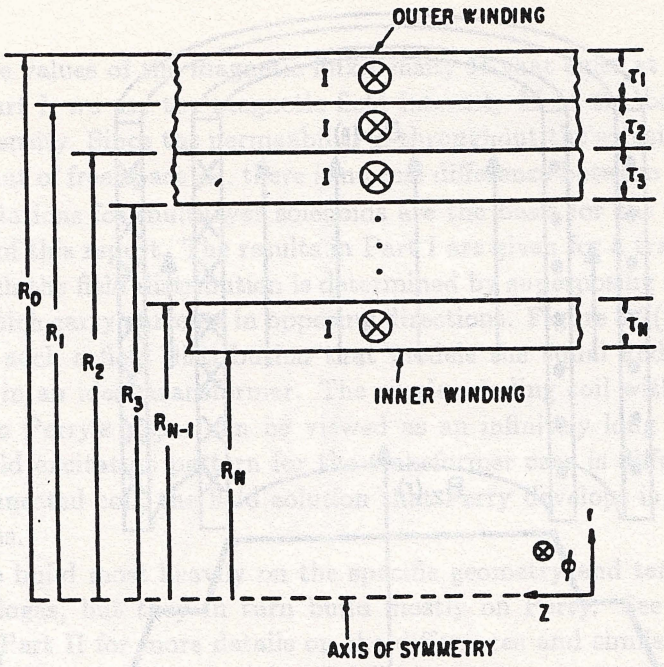


Figure 7.2: Perry's Fig. 7. Dimensions and definition of axis for eddy current calculation in cylindrical coordinates. {Perry's caption}.

similar to Fig. 3.15 in Section 3.3.1 of Part I which shows the layer geometry that we employ in Part I of this report. Perry uses the terms "thickness" for the y-direction shown in the coordinate system of Fig. 7.1(a), and "length" for the z-direction. These correspond to the terms "height" and "breadth" used in Part I.

Figure 7.1(b) is Perry's Fig. 3 and shows a "cross-section of a multilayer current sheet...wound into a solenoid.[1]" As in part (a), each of the current sheets is infinite in two directions and τ_n thick in the third. Using this geometry, Perry's field analysis results in an expression for Q_n, the loss per unit area of the x-z plane defined by Fig. 7.1(b). This directly corresponds to the analysis presented in Chapter 4 of Part I where we solve for the field solution in an infinite current sheet and determine $\langle Q_J \rangle$, the average power dissipation per square meter of current sheet in Duke's y-z plane.

For coils where the curvature of the solenoid cannot be neglected, Perry uses a cylindrical coordinate system to solve for the current density and power loss in a cylindrical current sheet τ_n "thick" and infinite in length. This configuration is shown in Fig. 7.2. The fields analysis in cylindrical coordinates results in an expression for Q'_n, the power dissipation per unit length of the coil, where length is in Perry's z-direction.

The essential aspects of the problem that Perry solves are the same as those in Part I of this report; the key point, that the fields inside an infinite current sheet can be determined directly from the thickness of the layer and the sinusoidal magnetic fields on the layer surfaces, is exactly the same in both documents. For his rectangular-coordinate

[1]Perry's caption for his Fig. 3.

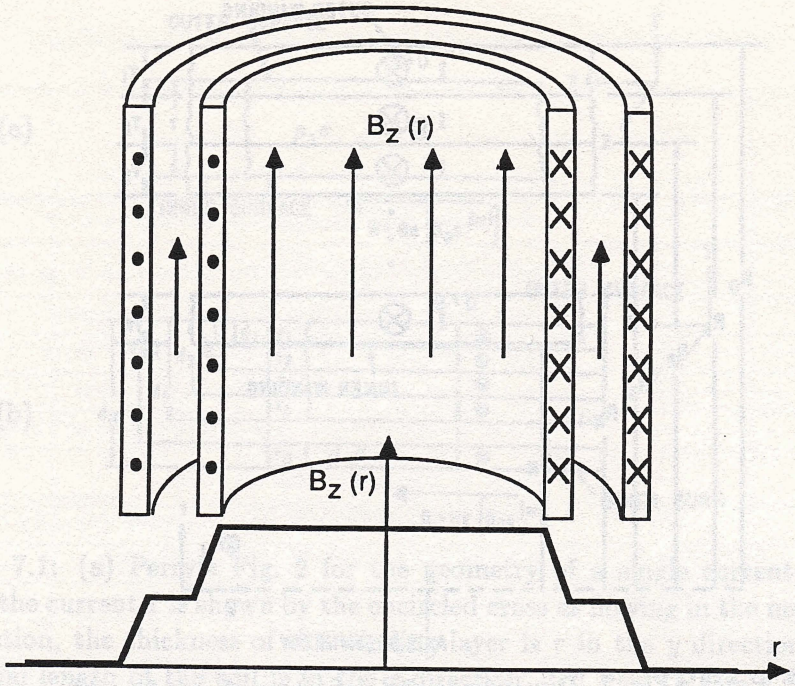


Figure 7.3: Excitation diagram for a section of the infinite solenoid configuration that Perry examines.

solution, however, Perry uses a different coordinate reference frame from the one we use in Part I, and he is somewhat unclear in defining some of his reference directions. Since it is rather tedious to translate the results presented in Part I of this report into the geometry used in Perry's paper, we have not examined in detail the derivation of Perry's equations in his coordinate system. In the discussion that follows, we focus mainly on how to view Perry's approach as equivalent in essence to the detailed discussion of Part I.

7.3 GENERAL COMMENTS ON PERRY'S ANALYSIS

Perry's analysis applies to infinitely long structures or to structures such as the transformers we consider in Part I of this report which approximate infinitely long structures. In this ideal case, the magnetic-field-intensity function is uniform in the interior region of the solenoid structure and is zero outside the coils. In a multilayer solenoid such as Perry analyzes, the total field at any point in the winding structure is the superposition of the contributions of the coil layers of greater radius, each of which carries the same net current per unit length. Figure 7.3 shows an example of the dc or low-frequency excitation pattern for the infinite solenoid geometry that Perry analyzes in his paper. We see that the field distribution in Fig. 7.3 is equivalent to that shown in Fig. 3.7(a) in Section 3.1.2 of Part I.

Perry solves for the current density inside the infinite current sheets of such a struc-

ture based on the values of the magnetic flux density **B** that exist at the boundaries of each layer; in Part I, we use the magnetic field intensity **H** at the boundaries to solve for the current density. Since the permeability μ throughout the solution space is always assumed to be that of free space μ_0, there is no real difference between the two solutions.

Perry's calculations for multilayer solenoids are the basis for the field analysis presented in Part I of this report. The results in Part I are given for a transformer winding structure in which the field distribution is determined by superposing the field contributions of layers which carry currents in opposing directions. Figure 3.7(b) in Section 3.1.2 of Part I shows such a field distribution that models the equal and opposite ampere turns that exist in an ideal transformer. The single-winding coil with series-connected winding layers in Perry's paper can be viewed as an infinitely long air-core inductor. Although the field excitation pattern for the transformer case is different from that in such a series connected coil, the field solution that Perry develops is just as applicable in both situations.

In Part I, we build most heavily on the specific geometry and terminology used by Vandelac and Ziogas, but they in turn build mostly on Perry. See the discussion in Section 8.2.1 of Part II for more details on the differences and similarities between the analysis given by Perry and by Vandelac and Ziogas.

7.4 IMPORTANT RESULTS

7.4.1 Normalized Power Dissipation

Perry computes the normalized power dissipation Q_n/Q_{ref} in the general n^{th} winding layer as a function of the winding height—which he calls the *thickness* τ_n of the n^{th} winding layer—normalized to the skin depth δ of the conductive material at the frequency of excitation. Q_{ref} is defined as the value of loss in the outermost layer when the normalized conductor height approaches infinity, i.e., $Q_{ref} = Q_1(\Delta \rightarrow \infty)$. More is said about Q_{ref} and Q_n/Q_{ref} in Section 7.6.3. In his Fig. 4, which is reproduced here as Fig. 7.4(b), Perry plots the variation of the normalized power dissipation for the first, second, and third layers of a multilayer structure where the first layer is the outermost layer, the second layer is the one just inside that one, etc. In Fig. 7.4(a), we have added a sketch of a three-layer structure and indicate graphically which layer is associated with each of the curves in the plot. By locating the minimum point of each curve, Fig. 7.4(b) can be used to determine the normalized layer height for each layer which minimizes the losses in that particular layer.

Figure 7.5 is a copy of Perry's Fig. 5 in which he plots the minimum relative power dissipation in the n^{th} layer of a structure. In this plot, the loss $Q_n(\Delta_n^c)$ in a layer of optimum height is compared to the loss $Q_n(\infty)$ in the same layer for Δ approaching infinity. By examining Fig. 7.5 we can see that "when $n \geq 2$, the minimum losses are only a small fraction of the losses when the conductor height is large compared to a skin depth." [7, page 120]

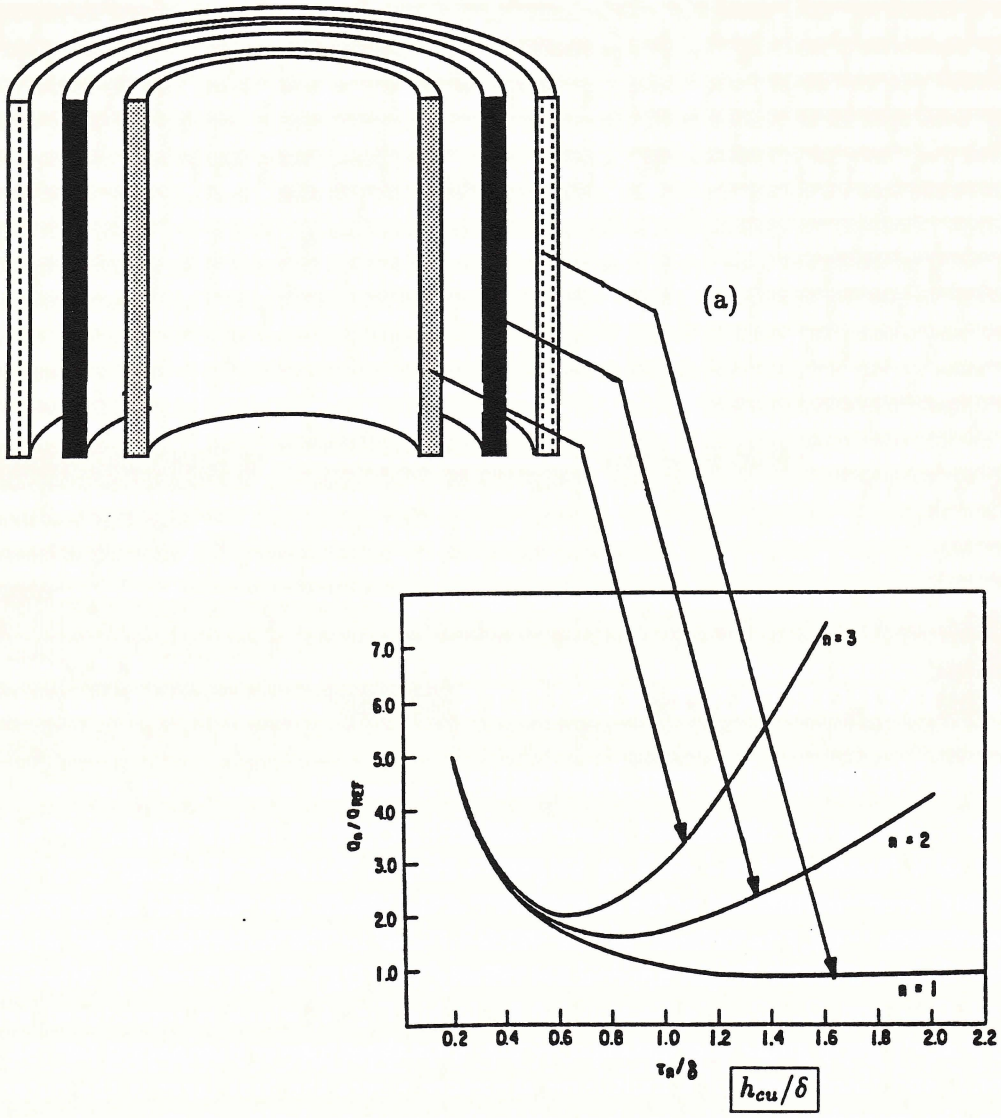


Figure 7.4: (a) Section of a three layer solenoid. (b) Graph from Perry's Fig. 4 which shows the amount of normalized power dissipation in the outer three layers of a solenoid as a function of normalized winding-layer height.

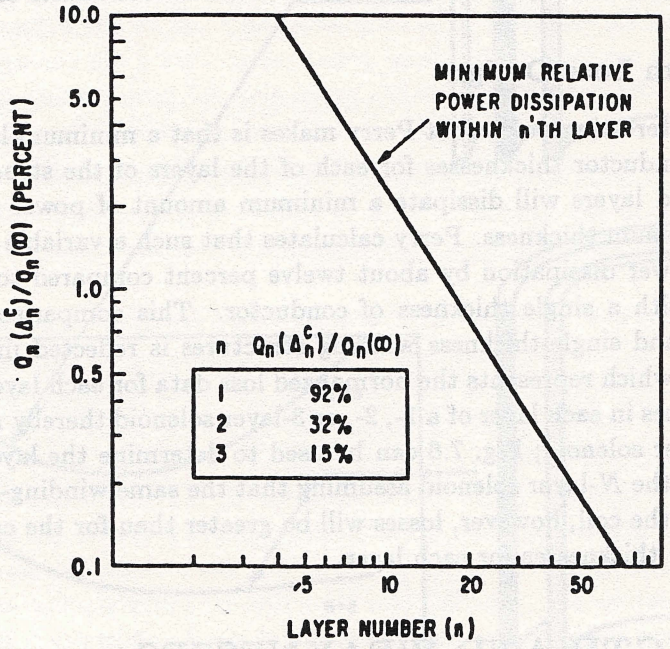


Figure 7.5: Perry's Fig. 5. Minimum possible power dissipation versus layer number (counted from the outside in) expressed as the percentage of the power dissipation if the layer were much thicker than a skin depth. {Perry's caption}

Figure 7.6, which incorporates a copy of Perry's Fig. 6, shows the relative power dissipation for two- and three-layer coils that have the same conductor thickness—or height—for each layer. The plot allows the designer to pick a single conductor size for the multilayer winding which gives the best overall loss performance.

All of the plots and results that Perry presents assume that the excitation frequency is a fixed parameter and that the designer is free to pick the size of the conductors in the winding structure. The same plots can be used just as easily to pick an optimum frequency of excitation for any winding structure where the conductor size is fixed.

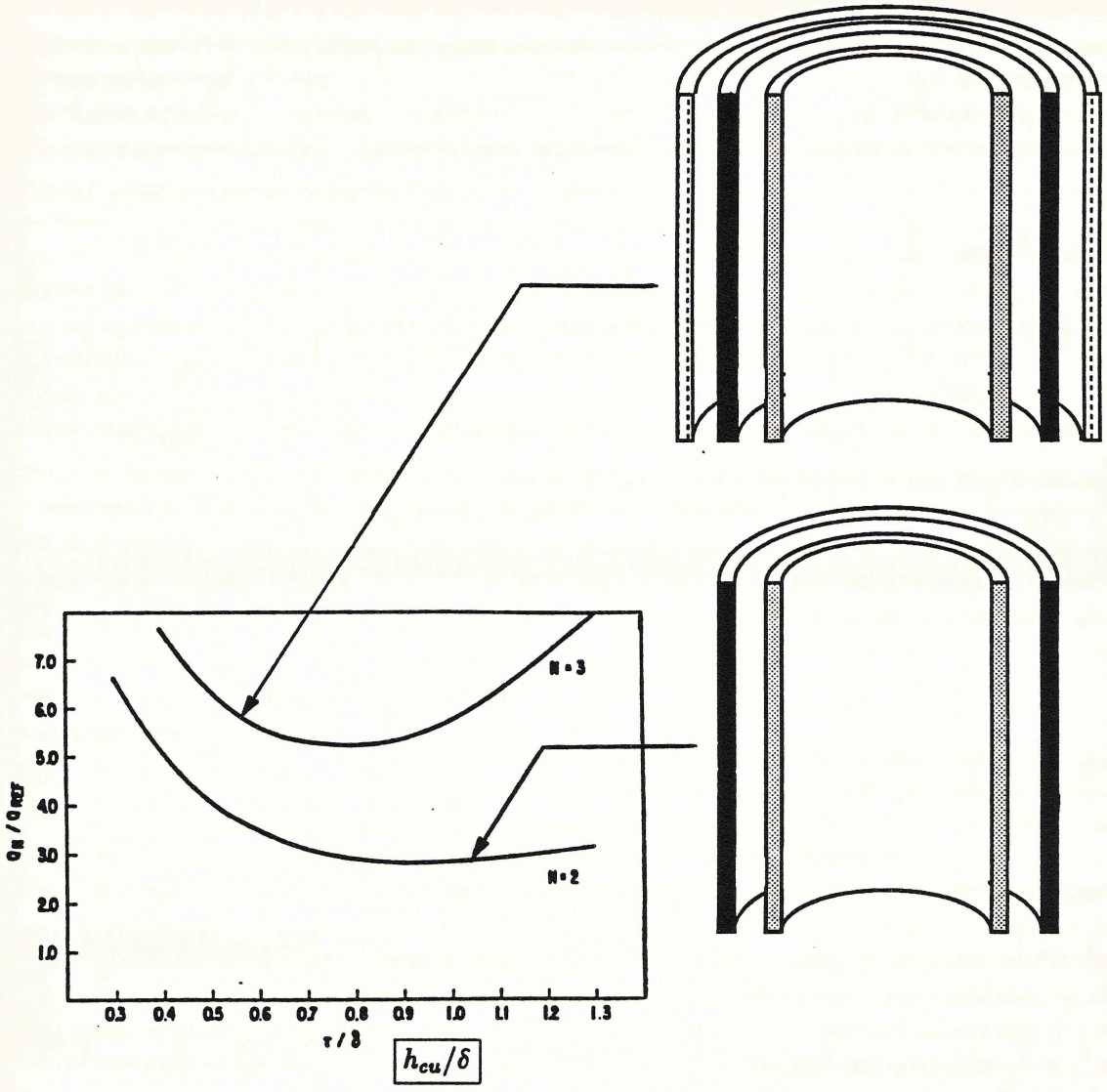
7.4.2 Minimum Loss Design

One particularly interesting point that Perry makes is that a minimum-loss design consists of different conductor thicknesses for each of the layers of the structure. That is, the series connected layers will dissipate a minimum amount of power only if each of the layers is of optimum thickness. Perry calculates that such a variable winding thickness can reduce power dissipation by about twelve percent compared to an equivalent structure wound with a single thickness of conductor. This comparison of losses for variable-thickness and single-thickness winding structures is reflected in Figs. 7.4 and 7.6. Figure 7.4(b), which represents the normalized loss data for each layer, can be used to minimize the losses in each layer of a 1-, 2-, or 3-layer solenoid thereby minimizing the losses in the N-layer solenoid; Fig. 7.6 can be used to determine the layer thickness to minimize losses for the N-layer solenoid assuming that the same winding-layer thickness is used throughout the coil, however, losses will be greater than for the case of different optimum conductor thicknesses for each layer.

7.5 STRENGTH AND WEAKNESSES

The strength of this paper lies in its mathematical basis. The presented field solutions are based on the analysis of an ideal, infinite winding layer; the results that Perry gets from this analysis are general to any other similar fields problem. Perry is the only author reviewed in this report who carries out both a rectangular-coordinate and a cylindrical-coordinate analysis. In so doing, he shows the expected fact that in the cylindrical case the field solutions must be evaluated using Bessel functions. Perry points out that as long as the height of the winding layers is small compared to the diameter of the coil, the curvature of the layer can be neglected. In that case, the solenoid structure can be analyzed in rectangular coordinates which is what we choose to do in Part I of this report.

The greatest problem with Perry's paper is that it is too brief. Since there is not sufficient space to develop the mathematical derivations in detail, the reader must expend considerable effort to gain confidence in Perry's stated results. All results in this paper are stated without derivations; therefore, the reader is forced to either accept the results as given, or to rederive them. In Part I of this report, we present a derivation of the



(a) (b)

Figure 7.6: (a) Graph from Perry's Fig. 6. Relative power dissipation versus thickness within an N-layer coil in which each layer is the same thickness as the other layers. {Perry's caption} (b) Segments of three-layer and two-layer solenoids.

fields solution for an infinite current sheet which parallels most of Perry's rectangular-coordinate analysis, and which includes steps corresponding to many of the key results of Perry's paper with the exception of the cylindrical coordinate analysis. The parts of Perry's analysis that are not treated in Part I are fairly well explained (but not derived) in the text of his paper; the significant points of confusion and many of the important results of Perry's paper are discussed further in Section 7.6.

One problem encountered in reading Perry's paper is that he does not adequately inform the reader that he uses the *peak* value of the current and current density as the phasor magnitude in his solutions. The only effect this has on the form of the solutions that he presents—in comparison to those presented in Part I—is the appearance of an extra factor of 2 in the denominator of his expression for power dissipation. This does not cause too much conceptual difficulty, but the reader should keep it in mind when trying to apply Perry's analysis to an actual transformer design problem.

7.6 NOTABLE EQUATIONS

Many of the equations that Perry gives are specific to the geometry of his analysis and/or are concerned with the field solution in cylindrical coordinates. In this section, we show how some of the most significant of Perry's results relate to the equations presented in Part I of this report. We have not examined the equations relating to the cylindrical analysis in any detail, and we do not discuss them in this section.

Perry is rather unspecific about the orientation of his coordinate system and the assumed direction of positive current density; therefore, it is rather difficult to follow in detail the development of the results he presents. For the present discussion, we assume that that the y-direction or layer-thickness direction in Perry's solution points in the direction of increasing distance from the outside of the coil and in the opposite direction to the x direction or layer-height direction in Part I of this report.

Perry's terminology concerning sinusoidally varying quantities is also inexact. He uses the same symbol to denote both the peak value of a sinusoid and the sinusoid itself. He does not specifically define the circumflex which appears in $\hat{J}_n$, and even defines $\hat{J}_n$ to be the "current density amplitude in the n^{th} layer," [7, page 116] although it is used in his analysis as a phasor. For the discussion below, it is assumed that Perry's circumflex denotes a phasor quantity, and that the current I' is a sinusoid. Since we desire to show only the correspondence between Perry's results and those derived in Part I, and not to rederive fully Perry's analysis, this looseness in terminology is not a major problem. It does, however, produce some inexact correspondences between sinusoidally varying real quantities and phasors in the following discussion.

7.6.1 Current Density

Perry's (8a) for the current density vector at time t is given as,

$$J_x(y,t) = \text{Re}[\hat{J}_n(y)e^{j\omega t}] \qquad \text{for } d_{n-1} \le y \le d_n \tag{7.1}$$

where the phasor $\hat{J}_n(y)$ is given by Perry's (8b) as

$$\hat{J}_n(y) = \frac{kI'[n\cosh k(y - d_{n-1}) - (n-1)\cosh k(y - d_n)]}{\sinh k(d_n - d_{n-1})} \tag{7.2}$$

As previously observed, the precise orientation of the coordinate system in the paper is unclear, however, from the form of this equation it appears that the y-direction in Fig. 7.1 should point down in the direction of increasing d_n rather than up.

Equation (7.2) is essentially the same as (4.39) in Section 4.2 of Part I which is reproduced here as (7.3)

$$\underline{J}_y(x) = \frac{-\underline{k}}{\sinh \underline{k}h_{cu}}\left[\underline{H}_z(h_{cu})\cosh \underline{k}x - \underline{H}_z(0)\cosh \underline{k}(h_{cu} - x)\right] \tag{7.3}$$

By making some simple substitutions and changing the coordinate reference, we can demonstrate the equivalence of (7.2) and (7.3). To denote the relationship between Perry's and Duke's quantities, in the following discussion we adopt the format

$$\text{Perry symbol} \implies \text{Duke symbol}$$

or in more general terms, the left-hand side represents the quantity to be replaced by the quantity on the right-hand side. Using the coordinate system defined in Fig. 3.15 in Section 3.3.1 of Part I, we designate the origin of the new coordinate system to correspond to the point Perry designates $y = d_n$, so

$$y = d_n \implies x = 0 \tag{7.4}$$

$$y = d_{n-1} \implies x = h_{cu} \tag{7.5}$$

From (7.4) and (7.5) we can write

$$y \implies d_n - x \tag{7.6}$$

$$d_n - d_{n-1} \implies h_{cu} \tag{7.7}$$

Substituting (7.6) and (7.7) into (7.2) gives

$$\hat{J}_n(x) = \frac{kI'[n\cosh k(h_{cu} - x) - (n-1)\cosh k(-x)]}{\sinh kh_{cu}} \tag{7.8}$$

$$= \frac{kI'[n\cosh k(h_{cu} - x) - (n-1)\cosh k(x)]}{\sinh kh_{cu}} \tag{7.9}$$

since $\cosh(-x) = \cosh(x)$.

A correspondence must now be found between nI' and $(n-1)I'$ and the values of field intensity at the boundaries of the layer. Recalling (5.4) in Section 5.2.2 of Part I,

$$\underline{H}_z(0) - \underline{H}_z(h_{cu}) = \frac{N_\ell I_\ell}{b_{win}} \tag{7.10}$$

we note that the difference in phasor magnetic-field-intensity boundary conditions for a winding layer is equal to the net ampere turns per meter carried by the layer.[2] Since the magnitudes of the phasor fields of (7.10) are rms values, and Perry's derivations involve peak values, we adopt the notation $\underline{H}'(0)$, $\underline{H}'(h_{cu})$ and $\underline{J}'$ to denote phasors whose magnitudes are peak values. Using this new notation, Perry's currents nI' and $(n-1)I'$ become

$$(n-1)I' \implies \underline{H}'(h_{cu}) \tag{7.11}$$

$$nI' \implies \underline{H}'(0) \tag{7.12}$$

Substituting (7.11) and (7.12) into (7.9) gives

$$J'(x) = \frac{k}{\sinh kh_{cu}} \left[\underline{H}'(0)\cosh k(h_{cu}-x) - \underline{H}'(h_{cu})\cosh k(x)\right] \tag{7.13}$$

$$= \frac{-k}{\sinh kh_{cu}} \left[\underline{H}'(h_{cu})\cosh k(x) - \underline{H}'(0)\cosh k(h_{cu}-x)\right] \tag{7.14}$$

which is the same as (7.3) except that the phasor magnitudes are peak values rather than rms values, the phasor quantities are left unsubscripted, and the complex wave number is Perry's $k = (-1+j)/\delta$ rather than Duke's $\underline{k} = (1+j)/\delta$. It is not clearly understood why Perry chose this form for the complex wave number, or how this form effects his results. However, the correspondence demonstrated in (7.14) between Perry's (8b), given as (7.2), and (4.39) of Part I, given as (7.3), shows the validity of Perry's general discussion, even if some of the specifics such as k and his coordinate system are somewhat fuzzy.

7.6.2 Power Dissipation per Square Meter

Perry's derivation of the power dissipation per unit for the n^{th} layer begins with his (11) reproduced here in his symbols

$$Q_n = \frac{1}{2\sigma}\int_{d_{n-1}}^{d_n} \hat{J}_n(y)\hat{J}_n^*(y)\,dy \tag{7.15}$$

This equation is of the same form as (4.96) in Section 4.5.2 of Part I

$$\langle Q_J \rangle = \frac{1}{\sigma}\int_0^{h_{cu}} \underline{J}_y(X)\,\underline{J}_y^*(X)\,dX \tag{7.16}$$

except for the additional factor of (1/2). This factor is necessary since Perry's (8b) for $\hat{J}_n(y)$ involves peak values whereas Duke's (4.51) in Section 4.2 of Part I for $\underline{J}_y(X)$ involves rms values.

[2] In Duke's nomenclature this is meters in the breadth or y-direction. In Perry's nomenclature this is meters of length in the z-direction.

According to Perry, combining (7.2) and (7.15), results in his (12), reproduced here as it appears in the paper.

$$Q_n = \frac{I'^2}{2\sigma\delta}\left[(2n^2-2n+1)F_1(\Delta_n) - 4n(n-1)F_2(\Delta_n)\right] \tag{7.17}$$

Through a process of equation manipulation and substitution similar to what was done in the Section 7.6.1, it is fairly simple to show the correspondence between this equation and (4.105) in Section 4.5.2 of Part I, given here as (7.18) and (7.19)

$$\langle Q_J\rangle = \frac{|\underline{H}_z(\chi = h_{cu})|^2}{\sigma\delta}\left[(1+\alpha^2+\beta^2)F_1(\Delta) - 4\alpha F_2(\Delta)\right] \tag{7.18}$$

$$= \frac{|\underline{H}_z(\chi = h_{cu})|^2}{\sigma\delta}\langle Q'_J(\alpha,\beta,\Delta)\rangle \tag{7.19}$$

when $\beta = 0$. For an infinite solenoid such as Perry discusses, the boundary conditions of field intensity are always in phase, so β is always zero.

We start the process of equating (7.17) and (7.18) by factoring out an n^2 term from (7.17)

$$Q_n = \frac{n^2 I'^2}{2}\frac{1}{\sigma\delta}\left[\left(\frac{2n^2-2n+1}{n^2}\right)F_1(\Delta_n) - 4\left(\frac{n-1}{n}\right)F_2(\Delta_n)\right]$$

$$= \frac{n^2 I'^2}{2}\frac{1}{\sigma\delta}\left[\left(1+\left(\frac{n-1}{n}\right)^2\right)F_1(\Delta_n) - 4\left(\frac{n-1}{n}\right)F_2(\Delta_n)\right] \tag{7.20}$$

We now have to draw a correspondence between Perry's nI' and $(n-1)I'$ and Duke's $\underline{H}_z(\chi = 0)$ and $\underline{H}_z(\chi = h_{cu})$. According to (4.41) in Section 4.2 of Part I, $|\underline{H}_z(\chi = h_{cu})| \geq |\underline{H}_z(\chi = 0)|$ by definition. Using this information, we make the following transformations which are similar to (7.11) and (7.12)

$$\frac{n^2 I'^2}{2} \Longrightarrow |\underline{H}_z(\chi = h_{cu})|^2 \tag{7.21}$$

$$\frac{(n-1)^2 I'^2}{2} \Longrightarrow |\underline{H}_z(\chi = 0)|^2 \tag{7.22}$$

$$\left(\frac{n-1}{n}\right) \Longrightarrow \alpha \tag{7.23}$$

where α is defined by (4.48) in Section 4.2 of Part I. To make these transformations, it has been assumed that there is no phase difference between the boundary conditions of field intensity for the layer. Substituting (7.21) and (7.23) into (7.20) completes the proof of correspondence between (7.17) and (7.18) for $\beta = 0$.

$$Q_n = \frac{|\underline{H}_z(\chi = h_{cu})|^2}{\sigma\delta}\left[(1+\alpha^2)F_1(\Delta_n) - 4\alpha F_2(\Delta_n)\right]$$

$$= \langle Q_J\rangle\Big|_{\beta=0} \tag{7.24}$$

By inspection it is obvious that Perry's (13a) for $F_1(\Delta_n)$ and (13b) for $F_2(\Delta_n)$ are identical to Duke's equations in Section 4.5.2 of Part I, (4.103) for $F_1(\Delta)$ and (4.104) for $F_2(\Delta)$.

7.6.3 Reference Values

To compare the losses incurred by different winding arrangements, Perry normalized his loss data to two different reference values, $Q_1(\Delta_1 \to \infty)$ and $Q_n(\Delta_n \to \infty)$ which are defined in his (15) and (16) reproduced here using his symbols

$$Q_1(\Delta_1 \to \infty) = Q_{ref} = \frac{I'^2}{2\sigma\delta} \tag{7.25}$$

$$\frac{Q_n(\Delta_n \to \infty)}{Q_{ref}} = n^2 + (n-1)^2 \tag{7.26}$$

These two equations follow directly from (7.17) if one recalls from Fig. 4.27 of Part I that as $\Delta \to \infty$

$$F_1(\Delta \to \infty) \to 1 \tag{7.27}$$

$$F_2(\Delta \to \infty) \to 0 \tag{7.28}$$

Substituting these values into (7.17) gives

$$Q_n(\Delta_n \to \infty) = \frac{I'^2}{2\sigma\delta}\left[\left(2n^2 - 2n - 1\right)\right] \tag{7.29}$$

$$Q_1(\Delta_1 \to \infty) = \frac{I'^2}{2\sigma\delta} \tag{7.30}$$

In the Section 7.6.2 it is shown that (7.17) and (7.18) are equivalent. Using the definition of Q_{ref} given in (7.25), the expression for Q_n given in (7.17), and the transformations reflected in (7.21) to (7.23), we see that Perry's normalized loss factor

$$\frac{Q_n}{Q_{ref}} = \left[(2n^2 - 2n + 1)F_1(\Delta_n) - 4n(n-1)F_2(\Delta_n)\right] \tag{7.31}$$

and Duke's normalized average dissipation in a layer $\langle Q'_J \rangle$ given in (7.19) are similar but not identical quantities. In addition, we see from (7.31) that by normalizing to Q_{ref}, Perry removes from the data presented in Figs. 7.4(b) and 7.6(a) any dependence on current, conductivity, and skin depth. The data are, therefore, dependent only on normalized conductor height and layer number.

In the introduction to his paper, Perry introduces Q_{dc}, the power dissipation in a one-layer coil carrying dc current, and presents (4)

$$Q_{dc} = \frac{I'^2}{2\sigma\tau} \tag{7.32}$$

Comparing (7.25) and (7.32), we see that Q_{ref} is identical to the dc loss for a coil one skin depth in height, or thickness as Perry calls it. Although Perry only defines Q_{dc} for coils of one layer, the dc resistance of any one layer of a multi-layer coil would be of the same form. Therefore, we see that Perry's process of normalizing to Q_{ref} is very similar to Carsten's method of normalizing to the dc resistance of a winding one skin depth in height.

7.7 CONCLUSION

As we demonstrated in Section 7.6, it is quite easy to get bogged-down with translating Perry's results into the forms of the equations in Part I. In general, such translation does not provide any great reward and is not worth the effort it involves. However, it is important to realize—at least from a power electronics perspective—that in Perry's work we find a useful analytical approach that can be applied more thoroughly and directly to specific power electronics applications than can the analysis introduced by Dowell. In the following chapter, we see how Vandelac and Ziogas use Perry's techniques to construct a copper-loss calculation that is broader and more flexible than the analyses examined in previous chapters which rely primarily on Dowell's work.

This page has been left blank intentionally.

Chapter 8

Vandelac & Ziogas

J. P. Vandelac and P. Ziogas, "A Novel Approach for Minimizing High Frequency Transformer Copper Losses," *IEEE Power Electronics Specialist Conference Record*, 1987, pp. 355-367.

8.1 OVERVIEW

The flowchart of literature development in Fig. 1.1 shows that the paper by Vandelac and Ziogas—more than any other paper examined here—brings together the ideas presented in the various earlier papers. Vandelac and Ziogas combine Dowell's result for the frequency-dependent profile of current density across a winding layer, Perry's layer-based approach for calculating winding losses, and Venkatraman's Fourier decomposition of nonsinusoidal excitation waveforms. The result is a method the authors call *field harmonic analysis*, which can be used to predict copper losses in multiwinding transformers in applications where the different windings carry current at different times during the excitation cycle. None of the other papers examined provides this ability, which is necessary for analyzing such common occurrences as flyback- and bridge-converter transformers, and transformers containing electrostatic shields. By carrying out the fast and easy graphical portion of field harmonic analysis, it is possible to determine what sizes of conductors and what arrangement of the winding layers yields the lowest copper losses. If specific loss figures are needed, they can be calculated using equations derived in the appendix of the paper.

To show the relationship between Vandelac and Ziogas's work, that of other authors, and Part I of this report, this discussion is carried out in terms of the common set of symbols found in the Glossary of Symbols, with Vandelac and Ziogas's original symbols translated according to Table 8.1. While Vandelac and Ziogas use boldface variables to distinguish vectors from scalar quantities, they make no such distinction between phasors and instantaneous variables. This ambiguity is removed by noting that phasor variables are intended only for J, $\mathbf{J}$, and H in equations (A-8) through (A-16) in the paper.

Field harmonic analysis is convincingly portrayed as a powerful and fundamentally

Table 8.1: Comparison of Symbols and Definitions

Vandelac & Ziogas	*Duke*	*Meaning* V: Vandelac & Ziogas, D: Duke
—	a_i†	cosine-term coefficient in a Fourier series
b	b_{cu}	breadth of a conductor
—	b_i†	sine-term coefficient in a Fourier series
b_w	b_{win}	V: winding width D: core-window breadth
c_i	—	V: Fourier-series coefficient for the i^{th} harmonic frequency D: unitless base for normalizing Fourier-series coefficients; expresses their functional dependence on the harmonic number i and the duty ratio D
D	—	duty cycle, the fraction of a converter switching period that any main switch is on
$F_1(\phi_i)$	$F_1(\Delta_i)$	$(\sinh 2\Delta_i + \sin 2\Delta_i)/(\cosh 2\Delta_i - \cos 2\Delta_i)$
$F_2(\phi_i)$	$F_2(\Delta_i)$	$(\sinh \Delta_i \cos \Delta_i + \cosh \Delta_i \sin \Delta_i)/(\cosh 2\Delta_i - \cos 2\Delta_i)$
$G_r = P_d/(R_\delta\, i_{rms}^2)$	—	loss normalization factor; ratio of ac losses in a conductor to those produced by the same rms current at low frequency in a conductor with a cross-sectional area of one skin depth squared
g_i	—	"rms factor" for the i^{th} harmonic; $g_0 = 1$ (dc), $g_i = 2$ for $i \geq 1$ (ac)
H_z	$H_{z,PEAK}$	peak value of z-directed magnetic field intensity
H_{zi}	$\sqrt{2}H_{z,i}$	peak value of the i^{th} harmonic component of the z-directed magnetic field intensity
H_n	H_{gn}	instantaneous magnetic field intensity in gap number n
h	h_{cu}	V: thickness of a conductor D: height of a conductor
h/δ'	Δ	conductor height in skin depths; $\Delta = h_{cu}/\delta$
I	I_{PEAK}	peak current
$I' = N_\ell I/b_w$	H_{BASE}	V: peak current density in amperes per meter D: base value for normalizing magnetic field intensity, calculated for the chosen reference layer as $H_{BASE} = N_\ell I_{\ell,PEAK}/b_{win}$

(continued)

† Used only in this chapter.

Table 8.1: Comparison of Symbols and Definitions (continued)

Vandelac & Ziogas	*Duke*	*Meaning* V: Vandelac & Ziogas, D: Duke
i	—	(subscript) harmonic number; 0 = dc, 1 = fundamental
i_{rms}	I_ℓ	net rms winding or layer current
$K_r = (b_w/\delta)G_r$	—	Carsten's normalizing factor
k	$\underline{k}$	complex wave number; $\underline{k} = \sqrt{j\omega\mu_0\eta\sigma_{cu}}$
ℓ_t	ℓ_T	length of turn in a winding layer
mmf()	—	D: magnetic field intensity normalized to both H_{BASE} and c_i
N	—	number of turns in the portion considered for calculating R_δ (correction to the paper's definition)
—	N_c	number of conductors in a layer; $N_c = N_\ell$ in this paper
N_ℓ	N_ℓ	number of turns in a layer
n	n	layer number
P_d	$\langle P_\ell \rangle^\dagger$	time-average power dissipation in a layer
P'_d	$\frac{1}{2}\langle Q'_J \rangle$	normalized power dissipation in a layer
Q_i	$\langle Q_{J,i} \rangle^\dagger$	time-average power dissipation $\langle Q_J \rangle$ per square meter of a winding layer for the i^{th} harmonic component of the current
Q'	$\langle Q_{PLOT} \rangle^\dagger$	time-average power dissipation per square meter of a winding layer, normalized to Q_{BASE}, for a linear current density of 1 A/m in the layer
—	$Q_{BASE}{}^\dagger$	normalization base which is the power dissipation per square meter in a winding layer one skin depth thick carrying dc current at a linear current density of 1 A/m
Q'_i	$\langle Q'_{J,i} \rangle^\dagger$	time-average power dissipation $\langle Q'_J \rangle$ per square meter of a winding layer for the i^{th} harmonic component of the current, normalized to $H^2_{z,i}(\chi{=}h_{cu})/\eta\sigma_{cu}\delta_i$

(continued)

† Used only in this chapter.

Table 8.1: Comparison of Symbols and Definitions (continued)

Vandelac & Ziogas	*Duke*	*Meaning* V: Vandelac & Ziogas, D: Duke
$R_\delta = N\ell_t/\sigma\delta^2$	—	"normalizing resistance" for a conductor; dc resistance of the same length of conductor with a cross-sectional area of one skin depth squared
$r_i = H_{ext,i}/I'$	—	V: relative strength of the external magnetic field D: amplitude of the i^{th} harmonic component of the external magnetic field, normalized to H_{BASE}
$\alpha + j\beta$	$\alpha + j\beta$	V: complex ratio of the phasor magnetic fields at the two surfaces of a winding layer D: complex ratio of the phasor magnetic fields at the two surfaces of a winding layer, with the smaller-magnitude phasor in the numerator
δ_i	δ_i†	V: skin depth for a real conductor at the i^{th} harmonic frequency; D: skin depth for a real conductor ($\eta = 1$) or an equivalent-foil layer ($\eta \leq 1$) at the i^{th} harmonic frequency; $\delta_i = \sqrt{2/i\omega\mu_0\eta\sigma_{cu}}$; no subscript implies $i = 1$
δ_i'		V: equivalent skin depth for spaced conductors at the i^{th} harmonic frequency
η	η	V: conductor spacing factor D: layer porosity; $\eta = N_c b_{cu}/b_{win}$
μ_o	μ_0	permeability of free space, $4\pi \times 10^{-7}$ H/m
ρ	r	radius
σ	σ_{cu}	conductivity of the actual conductor
$\phi_i = h/\delta_i'$	Δ_i	conductor height in skin depths at the i^{th} harmonic frequency; $\Delta_i = h_{cu}/\delta_i$; no subscript implies $i = 1$
ω	ω	angular excitation frequency

† Used only in this chapter.

sound method, but there is little experimental verification provided. In fact, there is only one piece of experimental data in the paper, a ratio of temperature rises for two different transformer designs tested in the same circuit. This piece of data is particularly significant, however, because it confirms a prediction made using field harmonic analysis that contradicts one of the claims made by Jongsma in [6]. Vandelac and Ziogas demonstrate that interleaving the winding layers in the transformer of a flyback converter can reduce copper losses substantially.

Because field harmonic analysis is used to analyze transformers operating under nonsinusoidal-excitation conditions, this method is beyond the scope of Part I of this report. Yet, Part I builds most directly on Vandelac and Ziogas's work because their basic approach to analyzing transformers is the most general of those encountered. Instead of Dowell's winding portion, the authors use the winding layer as the fundamental unit of analysis, which permits calculating ac copper losses for electrostatic shields and open-circuited windings, as well as windings that carry net current. The ability to predict such losses is absolutely necessary for calculating the short-circuit impedances of a transformer having three or more windings, because at least one winding is open-circuited during any short-circuit-impedance test.

Vandelac and Ziogas's method of calculating winding losses is adopted in Part I with few modifications, but leakage inductances are not addressed in their paper. In Part I, where the focus is on short-circuit *impedances*, Vandelac and Ziogas's example is followed to derive equations for magnetic-energy storage and the leakage inductances between pairs of windings. The terminology used in Part I with respect to leakage inductance is intentionally analogous to Vandelac and Ziogas's terminology for power dissipation.

Section 8.2 contains a discussion of the layer-based approach as presented in the paper, including its origin, its merits, and some useful design curves. In Section 8.3, the method of field harmonic analysis is demonstrated using an example more detailed than those in the paper, and the results are mentioned for the sample applications presented in the paper.

8.2 LAYER-BASED APPROACH

Assuming that the magnetic field in the winding space of a shell-wound transformer is tangential to the surfaces of the winding layers and parallel to the center leg of the core, the distribution of magnetic field intensity and current density inside each layer depends only on the thickness of the layer, its conductivity, and the boundary conditions of magnetic field intensity at each of its surfaces. Because these boundary conditions depend only on the net currents in the winding layers and are independent of frequency, they can be determined from easily-drawn low-frequency magnetic-field-intensity profiles. In light of these facts, Vandelac and Ziogas take a layer-based approach to transformer analysis, calculating the copper losses in each winding layer separately.

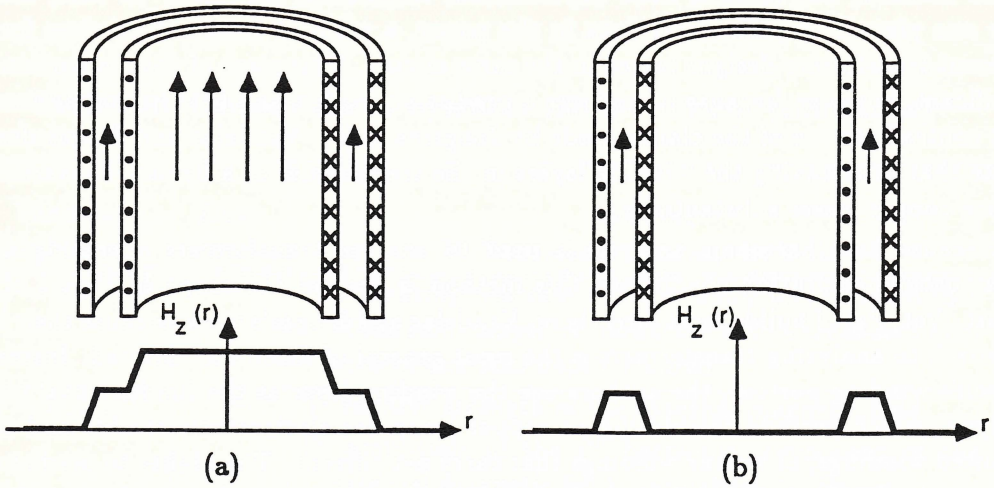


Figure 8.1: (a) Perry's infinite-solenoid model of an inductor, where each layer carries the same current. (b) Vandelac and Ziogas's infinite-solenoid model of a transformer, where the two layers carry equal and opposite ampere-turns.

8.2.1 Comparison to Perry's Analysis

Among the papers examined, Perry is credited with introducing the layer-based approach, and it is clear that Vandelac and Ziogas rely heavily on his work. There are two important differences, however. Perry analyzes multilayer solenoids like the one pictured in Fig. 8.1(a), which have simple, "stairstep" low-frequency field-intensity diagrams. Taking advantage of this regularity, Perry writes an equation for the power dissipation in any layer in terms of a single field intensity and the layer number n. This equation is Perry's (12), reproduced in the previous chapter as (7.17), where the field intensity is disguised as I'. Vandelac and Ziogas analyze similar multilayer structures, shown in Fig. 8.1(b), but different layers carry opposite currents as in a transformer. Because the field-intensity diagrams for multilayer transformers can have many different shapes, Vandelac and Ziogas must use a more general form of the equation for power dissipation in a layer, expressing it as a function of the two boundary conditions of magnetic field intensity for the layer.

8.2.2 Plot of Normalized Power Dissipation

When analyzing sinusoidal-current excitation in a transformer, or when analyzing a single harmonic component of a nonsinusoidal excitation waveform, it is often the case that the boundary conditions of magnetic field intensity for any layer are either in phase or 180 degrees out of phase. Therefore, it is possible to classify winding layers according to the

real-valued boundary-condition ratio α, which is usually a positive or negative ratio of two small integers. Note that Duke's definition of α, given in Table 8.1 and used in this chapter, is more restrictive and always equal to the lower of Vandelac and Ziogas's two values for a layer. Vandelac and Ziogas provide curves of normalized power dissipation for some of the most commonly encountered values of α, repeated in Fig. 8.2(a). These loss curves are essentially the same as the plots of Q_n/Q_{ref} in Perry's paper, shown in Fig. 7.4(b), but Vandelac and Ziogas's plots are more useful because they extend over a much wider range of normalized conductor height Δ.

Three apparent errors, or at least weaknesses, in the paper make it difficult to understand exactly what is plotted in Fig. 8.2(a). First, Vandelac and Ziogas say that all of the curves are for "a sinusoidal magnetic field of one amp/m peak," when a more accurate statement would be that all the curves are for winding layers that have a *difference* of one ampere per meter peak between the magnetic fields on their two surfaces. This characteristic can be expressed more simply: All the curves are for layers carrying a net sinusoidal current with a peak linear current density of one ampere per meter measured in the z-direction. The orientation of the coordinate axes is shown in Fig. 2.2.

The other two errors appear in Vandelac and Ziogas's (1-3), with the corrected version given here in their symbols.

$$Q_i = \frac{(1\ \mathrm{A/m})^2}{2\eta\sigma\delta_i'} Q_{PLOT}(h/\delta_i', \alpha_i) \tag{8.1}$$

The factor $(1\ \mathrm{A/m})^2$ is missing from this equation in the paper, but it is needed to obtain agreement of the units and to accurately represent the base for normalization, which is described in the paper as the dissipation per square meter that would occur in a layer one skin depth thick, when carrying a dc current of linear current density one ampere per meter. In Duke symbols, this base is given by

$$Q_{BASE,i} = \frac{(1\ \mathrm{A/m})^2}{2\eta\sigma_{cu}\delta_i} \tag{8.2}$$

The other error is that the symbol Q', which has been replaced by the new symbol Q_{PLOT} in (8.1), is used in the paper to represent the quantity plotted in Fig. 8.2(a), although this quantity is different from Q_i' in Vandelac and Ziogas's (A-17). It is natural to make the incorrect assumption that Q' and Q_i' represent the same quantity, because the paper implies that (A-17) is the basis of (8.1), and the two equations are quite similar in form. The following derivation is carried out to clarify the difference between these two quantities, to express mathematically the quantity $\langle Q_{PLOT} \rangle$ that is plotted in Fig. 8.2(a), and to show how to calculate losses using this plot.

Equation (A-17) is repeated below in Duke symbols, where Vandelac and Ziogas's Q_i'

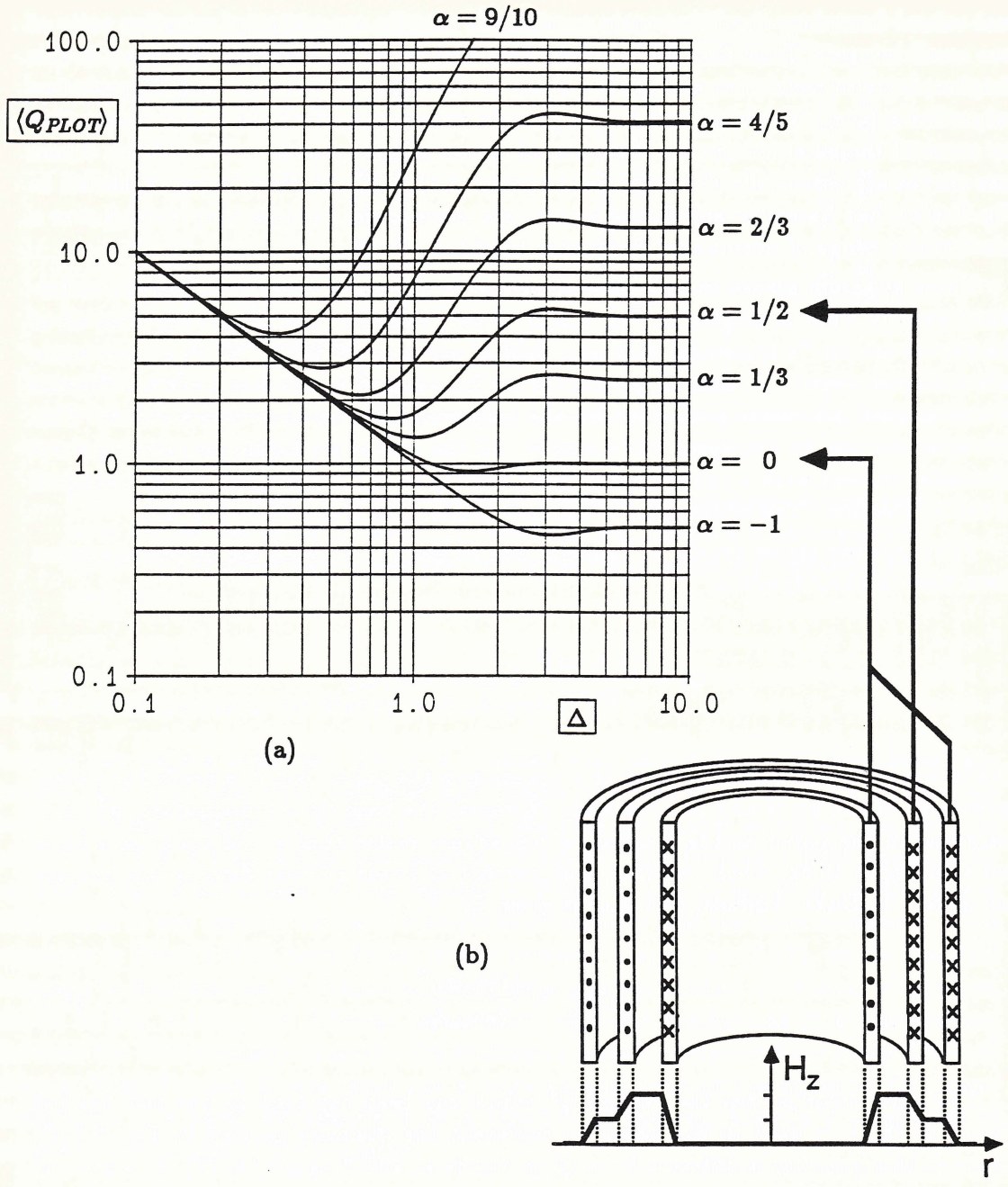


Figure 8.2: (a) Reproduction of the plot in Vandelac and Ziogas's Fig. 1-2, showing curves of normalized power dissipation $\langle Q_{PLOT} \rangle$ versus Δ, the layer height normalized to skin depth, with the ratio α of the magnetic-field-intensity boundary conditions as the parameter. (b) Example of a transformer winding structure where the inner and outer layers have $\alpha = 0$, and the middle layer has $\alpha = 1/2$.

is represented by Duke's $\langle Q'_{J,i} \rangle$.[1]

$$\langle Q_{J,i} \rangle = \frac{H_{z,i}^2(X = h_{cu})}{\eta \sigma_{cu} \delta_i} \left[(1 + \alpha_i^2 + \beta_i^2) F_1(\Delta_i) - 4\alpha_i F_2(\Delta_i) \right] \tag{8.3}$$

$$= \frac{H_{z,i}^2(X = h_{cu})}{\eta \sigma_{cu} \delta_i} \langle Q'_{J,i} \rangle \qquad i = 1, 2, 3, \ldots \tag{8.4}$$

This equation is the same as (4.142) in Part I except that subscript i has been added for the harmonic number. To show how Q_{PLOT} is related to (8.3), it is necessary to first write (8.1) in Duke's symbols.

$$\langle Q_{J,i} \rangle = \frac{(1 \text{ A/m})^2}{2\eta \sigma_{cu} \delta_i} \langle Q_{PLOT} \rangle \tag{8.5}$$

Substituting (8.3) into (8.5) and solving for $\langle Q_{PLOT} \rangle$,

$$\langle Q_{PLOT} \rangle = \frac{2H_{z,i}^2(X = h_{cu})}{(1 \text{ A/m})^2} \left[(1 + \alpha_i^2 + \beta_i^2) F_1(\Delta_i) - 4\alpha_i F_2(\Delta_i) \right] \tag{8.6}$$

As stated earlier, the curves in Fig. 8.2(a) are only for layers with a difference of one ampere per meter peak between the magnetic fields on their two surfaces. This requirement makes $H_{z,i}(X = h_{cu})$ dependent on α as follows.

$$\sqrt{2}\, H_{z,i}(X = h_{cu}) = \frac{1 \text{ A/m}}{1 - \alpha_i} \tag{8.7}$$

Substituting this equation into (8.6) gives the equation used to generate the curves in Fig. 8.2(a).

$$\boxed{\langle Q_{PLOT} \rangle = \frac{1}{(1 - \alpha_i)^2} \left[(1 + \alpha_i^2 + \beta_i^2) F_1(\Delta_i) - 4\alpha_i F_2(\Delta_i) \right]} \tag{8.8}$$

Once again, $\langle Q_{PLOT} \rangle$ is the power dissipation per square meter, normalized to $Q_{BASE,i}$, in a winding layer that carries a net sinusoidal current with a peak linear current density of one ampere per meter.

Although (8.8) and the subsequent plot in Fig. 8.2 have been derived under the assumption that there is a sinusoidal current with a peak linear current density of one ampere per meter in a layer, (8.8) is actually independent of current density. Therefore, the loss in a layer can be calculated for any sinusoidal current density using the loss curves in Fig. 8.2 and the equation derived below.

[1] Vandelac and Ziogas's $g_i = 2$ in the denominator of their right-hand side has been canceled with the 2 obtained in the numerator by expressing their peak-field-intensity variable H_{xi} in terms of Duke's rms variable $H_{z,i}$.

Combining (8.3) and (8.8),

$$\langle Q_{J,i} \rangle = \frac{(1-\alpha)^2 H_{z,i}^2(\chi = h_{cu})}{\eta \sigma_{cu} \delta_i} \langle Q_{PLOT} \rangle \tag{8.9}$$

For a layer with N_ℓ turns, if the i^{th} harmonic component of the winding current has an rms value of $I_{\ell,i}$, it can be shown from Ampere's law that

$$|H_{z,i}(\chi = h_{cu}) - H_{z,i}(\chi = 0)| = |N_\ell I_{\ell,i}/b_{win}| \tag{8.10}$$

$$|(1-\alpha)\, H_{z,i}(\chi = h_{cu})| = |N_\ell I_{\ell,i}/b_{win}| \tag{8.11}$$

$$(1-\alpha)^2 H_{z,i}^2(\chi = h_{cu}) = (N_\ell I_{\ell,i}/b_{win})^2 \tag{8.12}$$

Substituting (8.12) into (8.9), the desired expression is obtained for $\langle Q_{J,i} \rangle$, the power dissipation per square meter of a winding layer for the i^{th} harmonic component of the current.

$$\boxed{\langle Q_{J,i} \rangle = \frac{(N_\ell I_{\ell,i}/b_{win})^2}{\eta \sigma_{cu} \delta_i} \langle Q_{PLOT} \rangle} \tag{8.13}$$

To calculate $\langle Q_{J,i} \rangle$, the value of $\langle Q_{PLOT} \rangle$ is read from Fig. 8.2 for the appropriate values of α and Δ, and the result is multiplied by the fraction in (8.13) which accounts for the geometry of the layer, its material properties, and the current flowing in the layer.

8.2.3 Optimum Layer Height and Arrangement

If the intended use of a transformer is known, and if the transformer is designed with foil or strip conductors whose heights can be varied independently of their breadths, the loss curves of Fig. 8.2(a) can be used to select the arrangement of the layers and the height of each one to minimize copper losses. The winding layers can be interleaved as necessary to obtain the lowest possible values of α, which have the lowest loss curves. If the winding current is sinusoidal with no dc component, the minimum-loss height of each layer corresponds to the minimum point on the appropriate curve of $\langle Q_{PLOT} \rangle$. If the current is nonsinusoidal or has a dc component, the minimum-loss height is a compromise between the best heights for the individual sinusoidal components, as well as the dc component.

If $\alpha \leq 0$ for a layer that carries no dc current, Vandelac and Ziogas point out that it is particularly easy to determine the minimum-loss thickness for the layer. Because the curves of $\langle Q_{PLOT} \rangle$ for these α's are approximately flat to the right of their minima, the thickness that minimizes losses at the fundamental frequency also minimizes the total losses. It is also handy for making comparisons to note that the ratio of the total losses in two such layers that carry the same current is equal to the ratio of their loss-curve minima.

For a winding with the same foil or strip conductor used in all its layers, Vandelac and Ziogas imply that the conductor height for minimum loss corresponds to the minimum value of Carsten's normalized resistance factor K_r, defined in Section 4.1 and (4.18). The K_r factor would typically be plotted against normalized conductor height Δ for a specific winding layout and excitation pattern. For round or square wires, however, Vandelac and Ziogas make the point that K_r is inappropriate because the conductor height cannot be varied independently of its breadth. They introduce a new loss-normalization factor, G_r, that accounts for the simultaneous variation of the height and breadth of round and square conductors. When optimizing the layer height for these conductors, however, a possible complication not addressed in the paper is that an increase in conductor size can reduce the number of turns that fit in a layer.

The ideas that Vandelac and Ziogas present about minimizing winding losses are quite useful, but it is important to recognize that these ideas alone do not produce a minimum-winding-loss design. This is because the authors consider only two design variables, conductor size and winding-layer arrangement. Several other design variables that affect winding losses, as well as core loss, are assumed to be fixed; these include core size, conductor types, number of layers in each winding, and number of turns in each layer. A substantial additional reduction in winding losses might be achieved by changing these aspects of the design as well, although other design considerations such as size and manufacturing cost might impose practical limits.

8.2.4 Losses in Electrostatic Shields

An electrostatic shield in a high-frequency transformer dissipates power just as an open-circuited winding layer does: The time-varying magnetic field surrounding the shield induces eddy currents in it which produce resistive power loss. This loss mechanism is illustrated in Figures 4.22 through 4.26 of Part I. Figure 8.3 of this chapter shows Vandelac and Ziogas's plot of normalized power dissipation $\frac{1}{2}\langle Q'_J \rangle$ in a shield versus Δ, the height of the shield normalized to skin depth, for two waveforms of magnetic field intensity. Note that for Vandelac and Ziogas's definition of the duty cycle D given by Table 8.1 and (8.31), $D = 0.5$ for the quasi-square waveform in the figure, although each transistor switch in an inverter circuit that produces such a waveform would be ON only 25% of the time. The power-dissipation curves show that for both waveforms, thinner shields produce lower losses up to a thickness of about 2.4 skin depths, above which the thickness of the shield has only a small effect on its losses.

The power dissipation in an electrostatic shield is derived below from (8.3) to prove that the "2" in the denominator of Vandelac and Ziogas's (3-1) should not be present, and to show that the plotted quantity P'_d is expressed in Duke symbols as

$$\begin{aligned} P'_d &= \tfrac{1}{2}\langle Q'_J \rangle \\ &= \tfrac{1}{2}\left[(1+\alpha^2+\beta^2)F_1(\Delta) - 4\alpha F_2(\Delta)\right] \end{aligned} \tag{8.14}$$

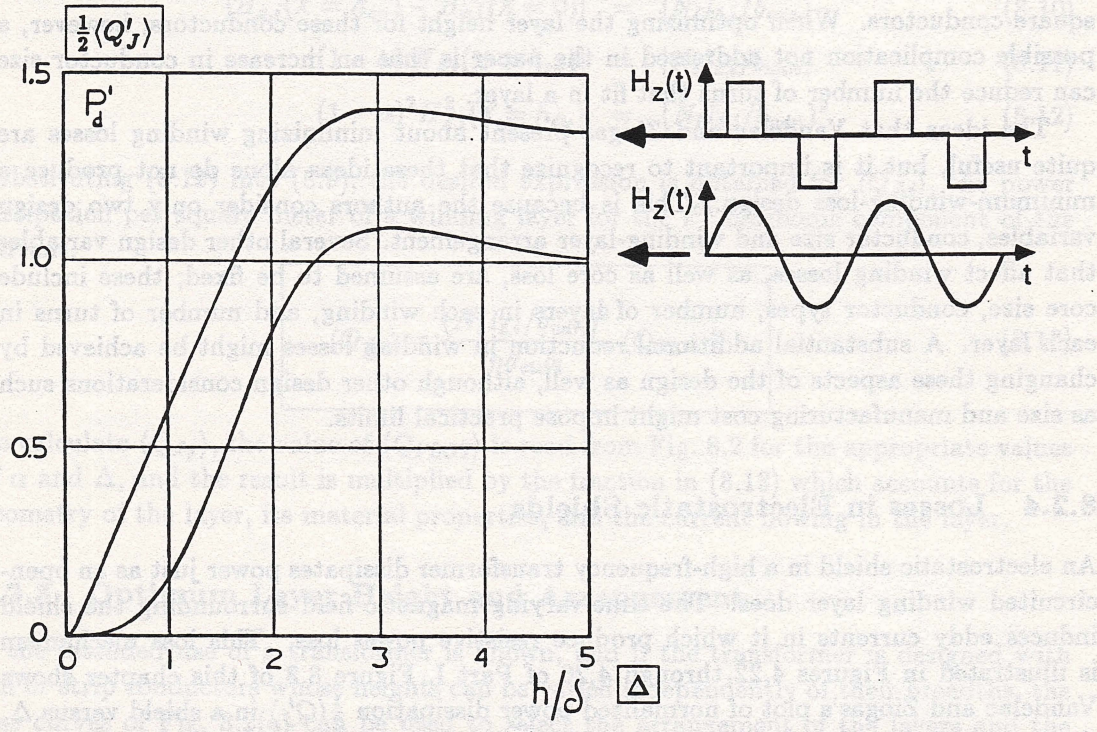


Figure 8.3: Vandelac and Ziogas's Figure 3-1, a plot of normalized power dissipation $\frac{1}{2}\langle Q'_J \rangle$ in an electrostatic shield versus Δ, the shield height normalized to skin depth, for sine-wave and quasi-square-wave excitation. The quasi-square wave is chosen to have a duty cycle $D = 0.5$ as defined in Table 8.1, which permits plotting the losses for the two field-intensity waveforms when the waveforms have equal rms values and equal peak values simultaneously.

For a sinusoidal magnetic field, the time-average power dissipated in a layer may be expressed

$$\langle P_\ell \rangle = b_{win} \ell_T \langle Q_J \rangle \tag{8.15}$$

$\langle Q_J \rangle$ is given by (8.3) without the i subscripts, because only the fundamental frequency is present. Substituting (8.3) into (8.15), where $\alpha = 1$ and $\beta = 0$ for an electrostatic shield, and H_z is the rms value of the surrounding field,

$$\langle P_\ell \rangle = b_{win} \ell_T \left(\frac{H_z^2}{\eta \sigma_{cu} \delta} \right) [2F_1(\Delta) - 4F_2(\Delta)] \tag{8.16}$$

A form similar to (3-1) in the paper is obtained by substituting $H_{z,PEAK}/\sqrt{2}$ for H_z and rearranging.

$$\begin{aligned} \langle P_\ell \rangle &= \left(\frac{b_{win} \ell_T}{\eta \sigma_{cu} \delta} \right) H_{z,PEAK}^2 \left\{ \tfrac{1}{2} [2F_1(\Delta) - 4F_2(\Delta)] \right\} \\ &= \left(\frac{b_{win} \ell_T}{\eta \sigma_{cu} \delta} \right) H_{z,PEAK}^2 \left\{ \tfrac{1}{2} \langle Q'_J \rangle \right\} \end{aligned} \tag{8.17}$$

The quantity in braces { } is equivalent to Vandelac and Ziogas's normalized power dissipation P'_d for sine-wave excitation, plotted in Fig. 8.3.

Equation (8.15) also applies to the quasi-square-wave magnetic field shown in Fig. 8.3, but $\langle Q_J \rangle$ is given instead by the following infinite series.

$$\langle Q_J \rangle = \sum_{i=1}^{\infty} \langle Q_{J,i} \rangle \tag{8.18}$$

$\langle Q_{J,i} \rangle$ is obtained from (8.3) and the following Fourier series of the field-intensity waveform, derived as described in Step 4 of Section 8.3.1.

$$H_z(t') = \sum_{i=1}^{\infty} \left[\frac{2H_{z,PEAK}}{i\pi} \left(\sin \frac{i\pi}{4} + \sin \frac{3i\pi}{4} \right) \right] \cos i\omega t' \tag{8.19}$$

Expressing the rms value of each harmonic component as the coefficient in brackets [] above divided by $\sqrt{2}$, (8.3) may be written

$$\langle Q_{J,i} \rangle = \frac{1}{\eta \sigma_{cu} \delta_i} \left[\frac{2H_{z,PEAK}}{i\pi\sqrt{2}} \left(\sin \frac{i\pi}{4} + \sin \frac{3i\pi}{4} \right) \right]^2 [2F_1(\Delta_i) - 4F_2(\Delta_i)] \tag{8.20}$$

The dependencies of δ_i and Δ_i on the harmonic number i are obtained from the definitions given in Table 8.1.

$$\delta_i = \sqrt{\frac{2}{i\omega\mu_0\eta\sigma_{cu}}} = \frac{\delta_1}{\sqrt{i}} \tag{8.21}$$

$$\Delta_i = \frac{h_{cu}}{\delta_i} = \Delta_1 \sqrt{i} \tag{8.22}$$

Substituting these expressions into (8.20), the result into (8.18), and that result into (8.15), an expression is obtained for the power dissipation in an electrostatic shield for quasi-square-wave excitation.

$$\langle P_\ell \rangle = \left(\frac{b_{win}\ell_T}{\eta\sigma_{cu}\delta_1}\right) H_{z,PEAK}^2 \times \left\{\sum_{i=1}^{\infty}\sqrt{i}\left[\frac{2}{i\pi\sqrt{2}}\left(\sin\frac{i\pi}{4}+\sin\frac{3i\pi}{4}\right)\right]^2\left[2F_1\left(\Delta_1\sqrt{i}\right)-4F_2\left(\Delta_1\sqrt{i}\right)\right]\right\} \quad (8.23)$$

$$= \left(\frac{b_{win}\ell_T}{\eta\sigma_{cu}\delta_1}\right) H_{z,PEAK}^2 \left\{\tfrac{1}{2}\langle Q_J'\rangle\right\} \quad (8.24)$$

The quantity in braces { } here is equivalent to Vandelac and Ziogas's P_d' for quasi-square-wave excitation, plotted in Fig. 8.3.

To calculate copper losses for nonsinusoidal excitation, it is usually necessary to truncate an infinite series like the one in (8.23), which has the effect of underestimating the losses. The number of terms, or harmonics, that must be calculated to obtain a desired accuracy depends on the shape of the excitation waveforms, of course, but a single example can serve as a useful point of comparison. The example given here corresponds to the point on the quasi-square-wave loss curve in Fig. 8.3 where $\Delta_1 = 3.125$, which is near the maximum.

Equation (8.23) is evaluated using from one to 100,000 terms of the infinite series, and the percent error in the result is plotted in Fig. 8.4 versus the number of harmonics included in the calculation. The same loss figures are used to calculate both of the curves, but two different references are used to calculate the error. For the dashed curve, the reference is the loss calculated by (8.23) for 100,000 harmonics, and for the solid curve, it is an estimate of the "true" loss which would be calculated for an infinite number of harmonics. This estimate was refined empirically, based on the observation that the greater the number of harmonics used to calculate the reference value, the straighter the loss curve. It is recognized that the cumulative error in summing such a large number of terms might be significant, but no effort was made to evaluate it.

The solid curve in Fig. 8.4 shows that approximately 30 harmonics are needed to obtain 90% accuracy in the calculated power dissipation, 130 harmonics are needed for 95% accuracy, and 800 harmonics are needed to obtain 98% accuracy. These figures are valid only for a quasi-square waveform with $D = 0.5$, but comparisons can be made based on trends: To obtain the same accuracy, fewer harmonics are needed as the rise and fall times of the waveform are increased from zero, and fewer harmonics are needed as the duty ratio is increased.

8.2.5 Other Winding Geometries

All of the mathematical development in Part I and in Vandelac and Ziogas's paper is carried out for shell-type winding structures, described in Section 2.1.1 of Part I.

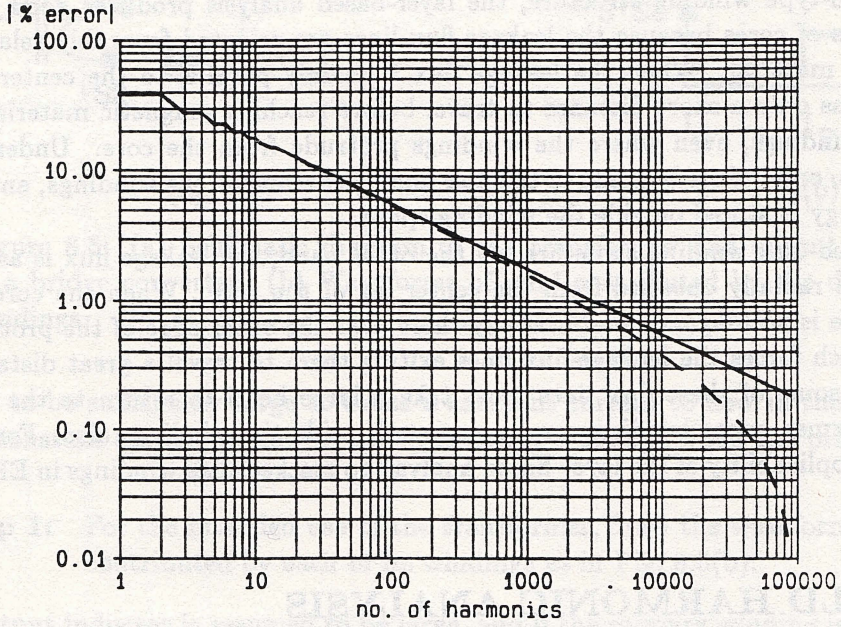


Figure 8.4: For an electrostatic shield of thickness $\Delta_1 = 3.125$, located in a quasi-square-wave magnetic field with $D = 0.5$, these curves give the percent error in the calculated loss versus the number of harmonics included in the calculation. The dashed curve represents the error relative to the loss calculated for 100,000 harmonics, $\frac{1}{2}\langle Q'_J \rangle = 1.43932$, and the solid curve represents the error relative to an estimate of the true loss, $\frac{1}{2}\langle Q'_J \rangle = 1.4418$.

Vandelac and Ziogas point out that their layer-based analysis can be applied to any winding structure where the magnetic field between the winding layers is known and is approximately tangential to the surfaces of the layers. To show that a stacked-disk winding structure like the one pictured in Fig. 9.1 meets these requirements, they include a finite-element plot of the magnetic flux in such a winding structure. In making this claim, the authors make no mention of the shape of the core they are considering. It seems reasonable that a layer-based analysis would be applicable to a stacked-disk winding structure in a pot core, but not an EE core, for the reasons described below.

For a shell-type winding structure, the layer-based analysis produces good results for both types of cores because the leakage-flux lines are oriented favorably relative to the magnetic material. When the leakage flux is mainly parallel to the center leg of the core, it has only a short distance to travel before reaching magnetic material after exiting the windings, even where the windings protrude from the core. Under these circumstances, only minor bending of the flux lines occurs inside the windings, and little magnetic energy is stored outside the winding space.

In a stacked-disk winding structure, on the other hand, the leakage flux is assumed to be directed radially outward from the center leg of the core. When the core is an EE-type, there is no magnetic material anywhere near the outer edge of the protruding windings, which forces the leakage-flux lines exiting there to travel a great distance in air. Because some of these flux lines must take a large bend to return to the center of the transformer, more bending can be expected inside the windings also. For these reasons, the applicability of the layer-based analysis to stacked-disk windings in EE cores is questioned.

8.3 FIELD HARMONIC ANALYSIS

8.3.1 Method

Vandelac and Ziogas's method of field harmonic analysis can be viewed as a five-step procedure, outlined in this section and illustrated with an example. Detailed analyses are carried out in the paper for two example problems, the push-pull primary winding of a transformer and a flyback-converter transformer. To supplement those examples, and to fill in some details omitted in the paper, a third detailed example is presented in this section, an analysis of the center-tapped-secondary transformer of a bridge converter, for which Vandelac and Ziogas give only the results. The circuit is taken from Vandelac and Ziogas's Fig. 3-2(a), and the winding layout is the same as their Fig. 3-4, except that the primary winding of the transformer analyzed here has two layers instead of three. The purpose of this change is only to make the resulting field-intensity plots easier to read. The final product of the analysis carried out below is a "time-harmonic mmf diagram" similar to Fig. 3-4(b) in the paper.

Figure 8.5(a) shows a schematic diagram of the transformer analyzed in this example. The output circuit of the converter is included to show the output inductor that is

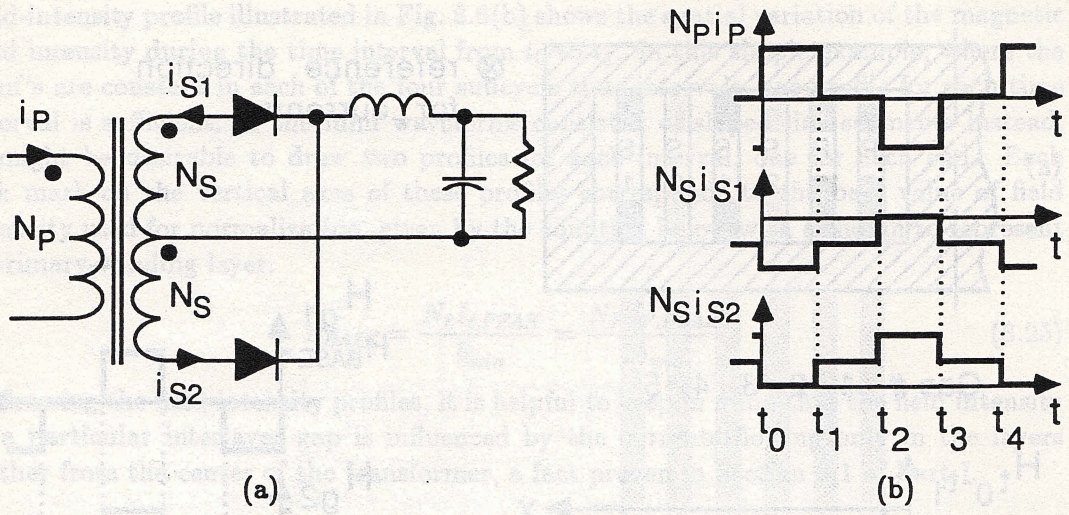


Figure 8.5: (a) Schematic diagram of the transformer and output circuit of a bridge converter. (b) Waveforms of mmf contributed by the different windings.

assumed to be sufficiently large to cause a constant current to flow in the load, and to cause a constant current to flow in both secondary windings when the primary voltage is zero.

Step 1: For the intended use of the transformer, draw the waveform of mmf contributed by each of its windings as in Fig. 8.5(b).

If the output inductor is assumed to be large, and if the primary winding is excited with voltage pulses of alternating polarity, the mmf waveforms for the windings are drawn in Fig. 8.5(b). These waveforms are similar to the ones in Vandelac and Ziogas's Fig. 3-2(b), except that the reference directions for the currents have been changed to always be into the dotted terminals. If this convention is followed, the mmf waveforms must sum to zero at every instant, and in Step 2 below, all the winding layers have the same reference direction for current.

Step 2: Draw a sequence of low-frequency magnetic-field-intensity profiles, arranged vertically, for one cycle of transformer operation as in Fig. 8.6(b).

Following Duke's convention, the right side of the transformer cross section is shown in Fig. 8.6(a), instead of the left side typically shown by Vandelac and Ziogas. Using the mmf waveforms in Fig. 8.5(b), Ampere's law is applied to the cross-sectional diagram as described in Section 3.1.2 of Part I to obtain the field-intensity profiles in Fig. 8.6(b). The time instants represented by the profiles should be chosen to give a representative picture of the field-intensity variation over one excitation cycle. For instance, the first

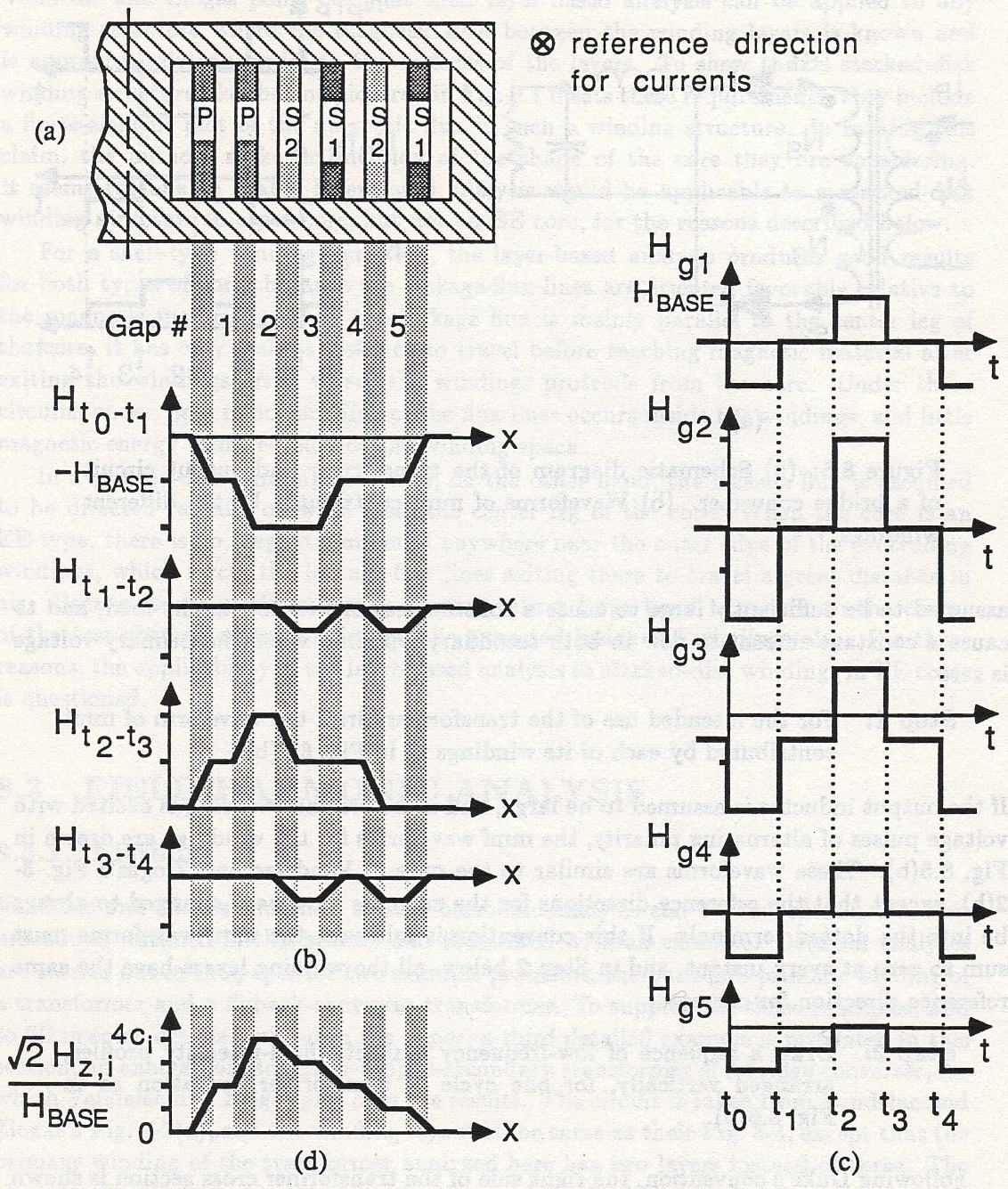


Figure 8.6: (a) Cross section of the right half of the transformer. (b) Profiles of magnetic field intensity across the winding space during different time intervals in one cycle of converter operation. (c) Waveforms of magnetic field intensity in the interlayer gaps. (d) Time-harmonic mmf diagram.

field-intensity profile illustrated in Fig. 8.6(b) shows the spatial variation of the magnetic field intensity during the time interval from t_0 to t_1. In this simple example, where the mmf's are constant in each of the four subcycle time intervals, one profile for each time interval is sufficient. If the mmf waveforms consisted of sloped line segments instead, it might be desirable to draw two profiles for each interval, one for each end. Each tick mark on the vertical axes of these profiles corresponds to the base value of field intensity used for normalization, given by the equation below with ℓ chosen to represent a primary-winding layer.

$$H_{BASE} = \frac{N_\ell I_{\ell,PEAK}}{b_{win}} = \frac{N_P I_{P,PEAK}}{2b_{win}} \tag{8.25}$$

In drawing the field-intensity profiles, it is helpful to keep in mind that the field intensity in a particular interlayer gap is influenced by the currents flowing only in the layers farther from the center of the transformer, a fact proven in Section 3.1 of Part I.

Step 3: Draw the time waveform of magnetic field intensity in each interlayer gap as in Fig. 8.6(c).

Vertical slices through the field-intensity profiles in Fig. 8.6(b) give a time sequence of field-intensity values for each interlayer gap. In Fig. 8.6(c), these values for each gap are plotted along a time axis, and the points are connected in a manner consistent with the mmf waveforms in Fig. 8.5(b). The result shown is the time waveform of the magnetic field intensity in each interlayer gap.

Step 4: Calculate the Fourier-series coefficients for each waveform of field intensity in an interlayer gap.

For a general function f of the angle ωt, the Fourier series is given by

$$f(\omega t) = \frac{a_0}{2} + \sum_{i=1}^{\infty}(a_i \cos i\omega t + b_i \sin i\omega t) \tag{8.26}$$

$$a_i = \frac{1}{\pi}\int_{-\pi}^{\pi} f(\omega t)\cos i\omega t\, d(\omega t) \qquad i = 0,1,2,\ldots \tag{8.27}$$

$$b_i = \frac{1}{\pi}\int_{-\pi}^{\pi} f(\omega t)\sin i\omega t\, d(\omega t) \qquad i = 1,2,3,\ldots \tag{8.28}$$

where i is the harmonic number. For the field-intensity waveforms in Fig. 8.6(c), sine terms can be avoided in this Fourier series by shifting the time axis to make all of the field-intensity waveforms even functions. The new time axis, designated t', is positioned as shown in Fig. 8.7(b) with $t'=0$ at $t=(t_0+t_1)/2$. Then the integral in (8.28), taken with respect to $\omega t'$, is always equal to zero in this example, leaving the cosine-term coefficients given by (8.27). Because $f(\omega t')$ is an even function, (8.27) can be simplified to

$$a_i = \frac{2}{\pi}\int_{0}^{\pi} f(\omega t')\cos i\omega t'\, d(\omega t') \qquad i = 0,1,2,\ldots \tag{8.29}$$

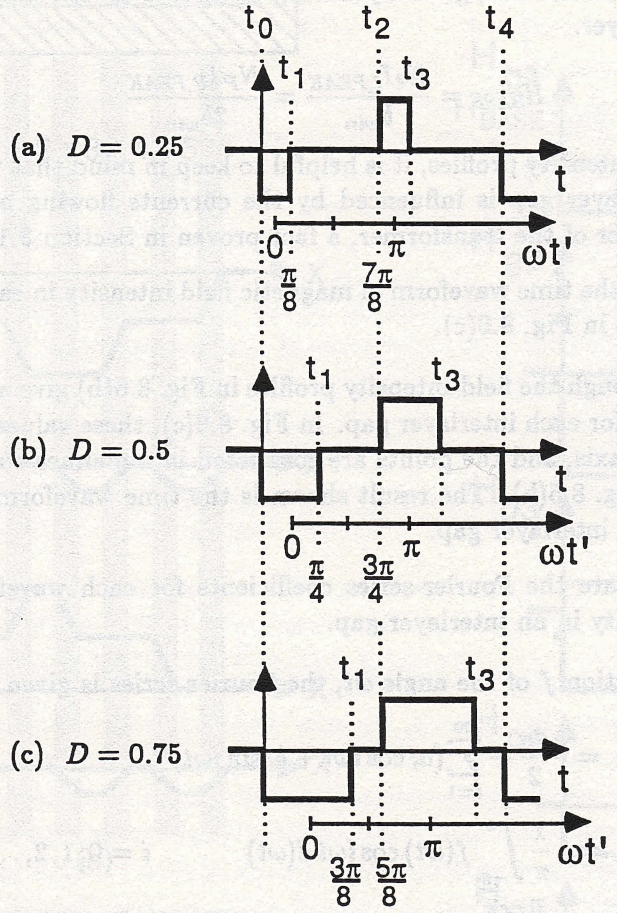


Figure 8.7: The waveform of field intensity H_{g1} in interlayer gap number 1 for three different duty cycles D. The Fourier coefficients are calculated by integrating from 0 to π along the $\omega t'$ axis, which shifts with the duty ratio as shown.

As an example, the Fourier-coefficient expression for H_{g1} in Fig. 8.6(c) is derived below for $i \geq 1$.

$$\begin{aligned} a_{i,g1} &= \frac{2}{\pi}\int_0^{\pi} H_{g1}(\omega t')\cos i\omega t' d(\omega t') \\ &= \frac{2H_{BASE}}{\pi}\left[\int_0^{\frac{\pi}{4}}(-1)\cos i\omega t' d(\omega t') + \int_{\frac{3\pi}{4}}^{\pi}\cos i\omega t' d(\omega t')\right] \\ &= \frac{2H_{BASE}}{i\pi}\left[-\sin i\omega t'\Big|_0^{\frac{\pi}{4}} + \sin i\omega t'\Big|_{\frac{3\pi}{4}}^{\pi}\right] \\ &= \frac{2H_{BASE}}{i\pi}\left[-\sin\frac{i\pi}{4} - \sin\frac{3i\pi}{4}\right] \end{aligned} \tag{8.30}$$

A more useful expression for these coefficients is obtained if Vandelac and Ziogas's duty cycle

$$D = \frac{t_1 - t_0}{t_2 - t_0} \tag{8.31}$$

is left as a variable instead of being fixed, as it is above at 0.5. Note that this definition of duty cycle gives the fraction of time that *any* transistor switch in the primary circuit is ON, although the fraction of time that *each* transistor switch is ON is only half of D. The t' axis shifts with the duty ratio as shown in Fig. 8.7, but the intermediate limits of integration, which are the trailing edge of the first pulse and the leading edge of the second, are always given by

$$\omega t'\big|_{t_1} = \frac{\pi D}{2} \tag{8.32}$$

$$\omega t'\big|_{t_2} = \pi\left(1 - \frac{D}{2}\right) \tag{8.33}$$

Making use of these limits, the integration in (8.30) is repeated below with a variable duty ratio D.

$$\begin{aligned} a_{i,g1} &= \frac{2}{\pi}\int_0^{\pi} H_{g1}(\omega t')\cos i\omega t' d(\omega t') \\ &= \frac{2H_{BASE}}{\pi}\left[\int_0^{\frac{\pi D}{2}}(-1)\cos i\omega t' d(\omega t') + \int_{\pi\left(1-\frac{D}{2}\right)}^{\pi}\cos i\omega t' d(\omega t')\right] \\ &= \frac{2H_{BASE}}{i\pi}\left[-\sin i\omega t'\Big|_0^{\frac{\pi D}{2}} + \sin i\omega t'\Big|_{\pi\left(1-\frac{D}{2}\right)}^{\pi}\right] \\ &= \frac{2H_{BASE}}{i\pi}\left[-\sin\frac{i\pi D}{2} - \sin i\pi\left(1 - \frac{D}{2}\right)\right] \end{aligned} \tag{8.34}$$

The Fourier coefficients for each of the other field-intensity waveforms in Fig. 8.6(c) are calculated similarly, with the following results for $i \geq 1$.

$$a_{i,g2} = \frac{2H_{BASE}}{i\pi}\left[-2\sin\frac{i\pi D}{2} - 2\sin i\pi\left(1-\frac{D}{2}\right)\right] \tag{8.35}$$

$$a_{i,g3} = \frac{2H_{BASE}}{i\pi}\left[-\frac{3}{2}\sin\frac{i\pi D}{2} - \frac{3}{2}\sin i\pi\left(1-\frac{D}{2}\right)\right] \tag{8.36}$$

$$a_{i,g4} = \frac{2H_{BASE}}{i\pi}\left[-\sin\frac{i\pi D}{2} - \sin i\pi\left(1-\frac{D}{2}\right)\right] \tag{8.37}$$

$$a_{i,g5} = \frac{2H_{BASE}}{i\pi}\left[-\frac{1}{2}\sin\frac{i\pi D}{2} - \frac{1}{2}\sin i\pi\left(1-\frac{D}{2}\right)\right] \tag{8.38}$$

Vandelac and Ziogas point out that these Fourier-coefficient expressions can also be obtained without performing Steps 2 and 3 above. First, Fourier series are written directly for the waveforms of mmf in Fig. 8.5(b). The resulting coefficient expressions for $i \geq 1$ are:

$$a_{i,N_P i_P} = \frac{2N_P I_{P,PEAK}}{i\pi}\left[\sin\frac{i\pi D}{2} + \sin i\pi\left(1-\frac{D}{2}\right)\right] \tag{8.39}$$

$$a_{i,N_S i_{S1}} = \frac{2N_S\,|I_{S1,PEAK}|}{i\pi}\left[-\frac{1}{2}\sin\frac{i\pi D}{2} - \frac{1}{2}\sin i\pi\left(1-\frac{D}{2}\right)\right] \tag{8.40}$$

$$a_{i,N_S i_{S2}} = \frac{2N_S I_{S2,PEAK}}{i\pi}\left[-\frac{1}{2}\sin\frac{i\pi D}{2} - \frac{1}{2}\sin i\pi\left(1-\frac{D}{2}\right)\right] \tag{8.41}$$

$I_{S1,PEAK}$ is used here as the most negative point on the waveform. Next, the Fourier-coefficient expressions for the waveforms of magnetic field intensity produced by each winding acting alone are obtained by dividing the above expressions by the breadth b_{win} of the core window. Recognizing that for equal and opposite ampere-turns,

$$N_P I_{P,PEAK} = |N_S I_{S1,PEAK}| = N_S I_{S2,PEAK} \tag{8.42}$$

the results are simplified by substituting H_{BASE} from (8.25).

$$a_{i,H_P} = \frac{4H_{BASE}}{i\pi}\left[\sin\frac{i\pi D}{2} + \sin i\pi\left(1-\frac{D}{2}\right)\right] \tag{8.43}$$

$$a_{i,H_{S1}} = a_{i,H_{S2}} = \frac{4H_{BASE}}{i\pi}\left[-\frac{1}{2}\sin\frac{i\pi D}{2} - \frac{1}{2}\sin i\pi\left(1-\frac{D}{2}\right)\right] \tag{8.44}$$

Finally, the coefficient expressions (8.34) through (8.38) are obtained as linear combinations of (8.43) and (8.44) by applying Ampere's law to the transformer cross section in Fig. 8.6(a).

$$\begin{aligned} a_{i,g1} &= \tfrac{1}{2}a_{i,H_P} + a_{i,H_{S1}} + a_{i,H_{S2}} \\ a_{i,g2} &= a_{i,H_{S1}} + a_{i,H_{S2}} \\ a_{i,g3} &= a_{i,H_{S1}} + \tfrac{1}{2}a_{i,H_{S2}} \\ a_{i,g4} &= \tfrac{1}{2}a_{i,H_{S1}} + \tfrac{1}{2}a_{i,H_{S2}} \\ a_{i,g5} &= \tfrac{1}{2}a_{i,H_{S1}} \end{aligned} \tag{8.45}$$

This method is certainly faster, but as the authors point out, some useful insight might be lost.

Step 5: Draw the time-harmonic mmf diagrams as in Fig. 8.6(d).

A *time-harmonic mmf diagram*, shown in Fig. 8.6(d) for this example, is a profile across the winding space of the peak magnetic field intensity for one harmonic component of the nonsinusoidal magnetic field. By normalizing this profile appropriately, a single time-harmonic mmf diagram can sometimes represent all of the harmonic frequencies, as in this example, or one diagram can represent a set of frequencies such as the even-numbered harmonics. The authors' use of the term *mmf* is not strictly correct here, but to avoid confusion, their name for these diagrams is used throughout this chapter.

The magnetic-field-intensity Fourier-coefficient expressions, given by (8.34) through (8.38) for this example, can always be normalized to H_{BASE} as defined in (8.25), which eliminates the dependence of the remaining quantity on the magnitude of the exciting current. If the Fourier-coefficient expressions are similar in form, they can also be normalized to a second, unitless base, designated c_i, that contains the functional dependence of the field intensity on both the harmonic number i and the duty ratio D. If possible, it is most convenient to choose c_i so that the resulting normalized quantity is an integer. For this example, c_i is taken from the smallest of the Fourier-coefficient expressions, (8.38).

$$c_i = \frac{2}{i\pi}\left[-\frac{1}{2}\sin\frac{i\pi D}{2} - \frac{1}{2}\sin i\pi\left(1-\frac{D}{2}\right)\right] \tag{8.46}$$

The Fourier-coefficient expressions (8.34) through (8.38) can now be expressed in terms of the two normalization bases.

$$\begin{aligned} a_{i,g1} &= 2\,H_{BASE}\,c_i \\ a_{i,g2} &= 4\,H_{BASE}\,c_i \\ a_{i,g3} &= 3\,H_{BASE}\,c_i \\ a_{i,g4} &= 2\,H_{BASE}\,c_i \\ a_{i,g5} &= H_{BASE}\,c_i \end{aligned} \tag{8.47}$$

The time-harmonic mmf diagram is just a plot of a_i/H_{BASE} versus x, with the vertical axis labeled in terms of c_i. To be consistent with the vertical-axis labeling in the paper,

the Fourier coefficient a_i can be written $\sqrt{2}H_{z,i}$ instead, where $H_{z,i}$ is the rms value of the i^{th} harmonic component of the z-directed magnetic field intensity. In this case, a single time-harmonic mmf diagram can be used to represent all harmonics, although further examination of (8.46) reveals that $c_i = 0$ for all even harmonics, independent of D.

In some problems, no common factor c_i can be found for all the Fourier-coefficient expressions. In these cases, it is sometimes possible to find a suitable c_i by considering the odd and even harmonics separately to simplify the Fourier-coefficient expressions. This technique is illustrated below for a different example, the push-pull primary winding in Fig. 2-1 of the paper. For H_{BASE} defined as $N_a I_{a,PEAK}/2b_{win}$, the following Fourier coefficient expressions are obtained for the field-intensity waveforms in Part (e) of their figure.

$$a_{i,g1} = \frac{2H_{BASE}}{i\pi}\left[\sin\frac{i\pi D}{2}\right] \tag{8.48}$$

$$a_{i,g2} = \frac{2H_{BASE}}{i\pi}\left[\sin\frac{i\pi D}{2} + \sin i\pi\left(1-\frac{D}{2}\right)\right] \tag{8.49}$$

$$a_{i,g3} = \frac{2H_{BASE}}{i\pi}\left[2\sin\frac{i\pi D}{2} + \sin i\pi\left(1-\frac{D}{2}\right)\right] \tag{8.50}$$

$$a_{i,g4} = \frac{2H_{BASE}}{i\pi}\left[2\sin\frac{i\pi D}{2} + 2\sin i\pi\left(1-\frac{D}{2}\right)\right] \tag{8.51}$$

There is no common c_i factor for these expressions, but they can be simplified if the odd and even harmonics are considered separately. The following new expressions can be obtained by applying trigonometric identities, or by examining the pattern of coefficient values for various duty ratios at several harmonic frequencies.

$$a_{i,g1} = \frac{2H_{BASE}}{i\pi}\left[\sin\frac{i\pi D}{2}\right] \tag{8.52}$$

$$a_{i,g2} = \begin{cases} \dfrac{2H_{BASE}}{i\pi}\left[2\sin\dfrac{i\pi D}{2}\right] & i = 1,3,5,\ldots \\ 0 & i = 2,4,6,\ldots \end{cases} \tag{8.53}$$

$$a_{i,g3} = \begin{cases} \dfrac{2H_{BASE}}{i\pi}\left[3\sin\dfrac{i\pi D}{2}\right] & i = 1,3,5,\ldots \\ \dfrac{2H_{BASE}}{i\pi}\left[\sin\dfrac{i\pi D}{2}\right] & i = 2,4,6,\ldots \end{cases} \tag{8.54}$$

$$a_{i,g4} = \begin{cases} \dfrac{2H_{BASE}}{i\pi}\left[4\sin\dfrac{i\pi D}{2}\right] & i = 1,3,5,\ldots \\ 0 & i = 2,4,6,\ldots \end{cases} \tag{8.55}$$

From these simplified expressions, the clear choice for c_i is given by (2-1) in the paper.

$$c_i = \frac{2}{i\pi} \sin \frac{i\pi D}{2} \tag{8.56}$$

Then the Fourier coefficients above can be expressed

		odd harmonics	even harmonics
$a_{i,g1}$	=	$H_{BASE}\, c_i$	$H_{BASE}\, c_i$
$a_{i,g2}$	=	$2\, H_{BASE}\, c_i$	0
$a_{i,g3}$	=	$3\, H_{BASE}\, c_i$	$H_{BASE}\, c_i$
$a_{i,g4}$	=	$4\, H_{BASE}\, c_i$	0

(8.57)

The two time-harmonic mmf diagrams in Vandelac and Ziogas's Fig. 2-1 are obtained by plotting these coefficients versus x, except that their even-harmonic diagram is inverted from that obtained here. Although c_i is given in the paper as (8.56), Vandelac and Ziogas's diagrams can be obtained by selecting a different c_i,

$$c_i = \frac{2}{i\pi} \sin i\pi \left(1 - \frac{D}{2}\right) \tag{8.58}$$

and simplifying the Fourier-coefficient expressions (8.48) through (8.51) in terms of this factor instead.

The time-harmonic mmf diagram is used to determine the boundary-condition ratio α for each layer, which might be different for different harmonics. Knowing the α's for the various layers is the key to making the qualitative comparisons and the power-loss calculations described in Section 8.3.2.

It should be recognized that the nature of the specific examples considered in this section permits some simplifications that are not always possible. For one, sine terms are avoided altogether in the Fourier series by shifting the time axis appropriately. In cases where this is not possible, one or more additional time-harmonic mmf diagrams would be generated for the sine terms. The power dissipation represented by the sine terms would simply be added to that of the cosine terms. Another simplification in these examples is that all harmonic components can be represented by one or two time-harmonic mmf diagrams. In other cases, their might be a different diagram for every harmonic frequency, which would severely limit the usefulness of the time-harmonic mmf diagrams. Although these simplifications are not always possible, the method of field harmonic analysis is quite general, and winding losses can always be calculated if the current waveforms are known.

8.3.2 Applications

8.3.2.1 Qualitative Comparisons

Using time-harmonic mmf diagrams, it is possible to make useful qualitative comparisons between different winding-layer arrangements without performing any power-loss calculations. The results from examples given in the paper are briefly mentioned here.

For the bridge transformer used as an example in Section 8.3.1, two other arrangements of the winding layers are considered. If the secondary winding layers shown in Fig. 8.6(a) are not interleaved, the same time-harmonic mmf diagram shown in Fig. 8.6(d) is obtained. From this fact, it is concluded that the interleaving of the secondary windings has no effect on winding losses in this transformer for the assumed winding-current waveforms.

However, it *is* possible to achieve lower winding losses by placing one secondary winding on each side of the primary, although the worst possible magnetic coupling between the secondary windings is obtained with this arrangement. The time-harmonic mmf diagram given in the paper shows most layers to have lower α's, which corresponds lower minimum losses on the curves of Fig. 8.2.

Vandelac and Ziogas argue that it is frequently necessary to consider what Dowell calls "nonoptimal" winding arrangements, those with a zero of mmf inside a winding layer but not at its center. Dowell's loss equations are not applicable in this case, but Vandelac and Ziogas's layer-based approach handles it with ease. The authors' point is well taken, but there appears to be a flaw in their example of a non-optimal winding arrangement in Fig. 3-6 of the paper. When different winding layers are connected in parallel, they cannot be expected to share the net winding current equally. In the example given, the natural tendency toward minimum-energy systems would cause more current to flow in the inner foil layers and less in the outer foil layers of each paralleled set of layers. The effect would be to lower the peaks in the mmf diagram, reducing both winding losses and magnetic-energy storage.

A flyback transformer is the last example given in the paper. For continuous-mmf operation, assuming a very large magnetizing inductance, field harmonic analysis is used to show that a lower-loss design can be achieved if the winding layers are interleaved. Because the waveforms of magnetic field intensity in the interlayer gaps all have the same shape, it is possible to determine the α for each layer by inspection, without calculating any Fourier series and without drawing the time-harmonic mmf diagram. The conclusion that interleaved windings produce lower losses is confirmed experimentally by comparing the temperature rise of two transformers with different winding arrangements.

To show that field harmonic analysis works for current waveshapes other than the rectangular pulses used in most of the examples, the flyback transformer is also analyzed assuming a lower magnetizing inductance, with the converter operating at the boundary between the continuous- and discontinuous-mmf modes. Again, a qualitative comparison of the two winding arrangements can be made by inspection of the interlayer-gap magnetic-field-intensity waveforms, this time because only one waveform changes between the two different designs. Although the α's for the layers cannot be determined by inspection in this example, it it safe to say that for the waveform that changes, the version with the lower amplitude and visibly lower harmonic content corresponds to the lower-loss design.

8.3.2.2 Power-Loss Calculations

For all of the qualitative examples given in the paper, it is possible to calculate specific loss figures using equations derived in the appendix of the paper. The basic equations for power dissipation are equivalent to those derived in Chapter 4 of Part I, except that an extra subscript i is added for the harmonic number, and total losses are the sum of the losses calculated for each harmonic frequency. Additional flexibility is offered in the equations given in the paper by providing for an external magnetic field that is proportional to a winding current.

The nature of the *mmf* function introduced in Vandelac and Ziogas's (A-25) may not be clear at first, in part because it does not actually represent magnetomotive force. Instead, it represents an interlayer-gap magnetic field intensity normalized to both H_{BASE} and c_i. This *mmf* is expressed as a function of the gap number n, which is on the side of layer number n where $x=h_{cu}$. Gap number $(n-1)$ is on the other side of layer number n, where $x=0$. This "mmf" is best understood as the quantity plotted in a time-harmonic mmf diagram. The normalization makes it independent of the magnitudes of the winding currents, which are all assumed to be proportional, and independent of the harmonic number to whatever extent is possible. In the paper, the clearest understanding of the mmf function is given by (A-31).

One of Vandelac and Ziogas's most important contributions is to eliminate the dependence of transformer analysis on Dowell's winding portions, but they say that in many cases, it is convenient to calculate losses for a whole winding at once. Their "winding" is more accurately described as a winding portion. The authors follow Dowell's example in deriving power-loss equations for winding portions with a whole number of layers and a half-layer, but the new equations are more powerful in two respects: Nonsinusoidal currents are handled by summing the losses calculated for each harmonic component, and provision is made for an external magnetic field that is proportional to the winding current. The derivation of these equations has not been verified.

8.3.3 Limitations

Vandelac and Ziogas's method of field harmonic analysis is a powerful tool for choosing the best arrangement of the winding layers and the best thicknesses of the layers to minimize losses for applications with nonsinusoidal winding currents. However, field harmonic analysis is subject to all the limitations reviewed in Section 9.2 of Part I except the first one, which requires sinusoidal excitation. If a transformer analysis problem does not greatly exceed any of these limitations, which are ambiguous by their nature, then the accuracy of the results obtained by field harmonic analysis is probably sufficient.

This page has been left blank intentionally.

Chapter 9

Rosa

Rosa, John, "Calculation of Flux Linkages in Multiwinding Transformers," *PESC Record*, 1986, pp. 639-644.

9.1 OVERVIEW

This paper presents a simplified coupled-coils model for transformers with multiple secondary windings, and details the method to calculate the circuit element values for that model. The equivalent circuit presented in the paper models the inductive interactions between the secondaries of a multiwinding transformer. Calculation of the self- and mutual-inductances is based upon the layout of the transformer winding layers. Rosa examines the flux linkage phenomena in both the shell winding structure shown in Fig. 2.1 of Part I of this report, and the stacked-disk winding structure shown in Fig. 9.1 of the present chapter. The analysis of the leakage flux linkages is given for only low-frequency sinusoidal excitations and the resultant equations predict only inductance values. The paper does not address copper losses.

For shell-wound transformers, Rosa's simplified coupled-coils model is discussed at length in Chapter 8 of Part I, where we show how this equivalent circuit can be applied for high-frequency excitations to model both resistive and inductive effects in multiwinding transformers. It is advised that the reader review Chapter 8 of Part I with particular emphasis on Sections 8.1 and 8.2. Table 9.1 presents a comparison of the symbols and definitions used by Rosa and those used in Part I.

Rosa presents no experimental results in his paper to show how well his modeling technique works for an actual transformer. He uses sinusoidal currents and voltages in his discussion, but it is unclear whether he means peak or rms when he uses a current of 1 ampere. [9, page 641] He does not analyze winding structures which include conductive shields, but it appears that his analysis does include the inductive energy storage of interlayer gaps and open-circuited windings which occur in regions of nonzero magnetic field. Thus, it is believed that Rosa's methods are extendable to winding structures which include shields.

Table 9.1 Comparison of Symbols and Definitions

Rosa	*Duke*	*Meaning* *R: Rosa; D; Duke*
—	A	cross-sectional area
—	B	instantaneous magnetic flux density
b	b_{win}	R: breadth of the core window in *centimeters* D: breadth of the core window in *meters*
c, d	X_{bob}, Y_{bob}	R: dimensions of center leg of the core D: dimensions of center leg of the bobbin
—	$\mathcal{F}$	instantaneous magnetomotive force
$H(x)$	$\underline{H}_z(x)$	R: mmf distribution in the transformer-core window D: phasor of magnetic field intensity in the window
$H_i(x)$	$H_{(jk)}$	R: mmf distribution for short-circuit test where winding i is excited and the n^{th} or primary winding is shorted D: magnetic-field-intensity profile for short-circuit test where winding j is excited and winding k is shorted
—	i	instantaneous current
L_{ii}	L_{jj}	R: self-inductance of the i^{th} secondary D: self-inductance of the j^{th} secondary
L_{ij}	L_{jk}	mutual inductance between windings. Voltage drop (or rise) in winding denoted by first subscript is due to changes in current of winding denoted by second subscript
—	ℓ_m	magnetic path length
m	$(K-1)$	number of secondary windings
N_i	N_j	R: number of turns in winding i D: number of turns in winding j

(Continued on next page)

Table 9.1 Comparison of Symbols and Definitions, cont.

Rosa	*Duke*	*Meaning* *R: Rosa; D; Duke*
n	K	total number of windings in a transformer
—	n	number of turns per meter across the breadth of a winding; layer or interlayer gap number
—	$\mathcal{P}$	permeance.
$Q_i(x)$	—	low-frequency mmf distribution due to the i^{th} winding
S	—	susceptance
—	S	surface
$T_i(x)$	—	normalized turns function for a winding which describes the location of the layers of the winding in the core window.
w	—	height of the core window in *centimeters*
x	x	direction orthogonal to the center post of the transformer core and parallel to the core's yoke
y	z	direction parallel to the center post of the core
Λ	—	mmf, permeance, flux linkage, flux. Under Rosa's one-amp one-turn assumption all are numerically equal
—	Λ	instantaneous flux linkage
Λ_{ij}	—	flux linking winding i due to current in winding j
Λ_m	—	"main" flux (that portion of the flux that exists only in the high permeability core material)
Λ_{mi}	—	the portion of Λ_m that is caused by winding i
$d\Lambda$	—	differential flux linkage. Numerically equal to differential permeance and differential flux due to one amp, one turn assumption
μ_0	μ_0	permeability of free space
—	ϕ	instantaneous magnetic flux

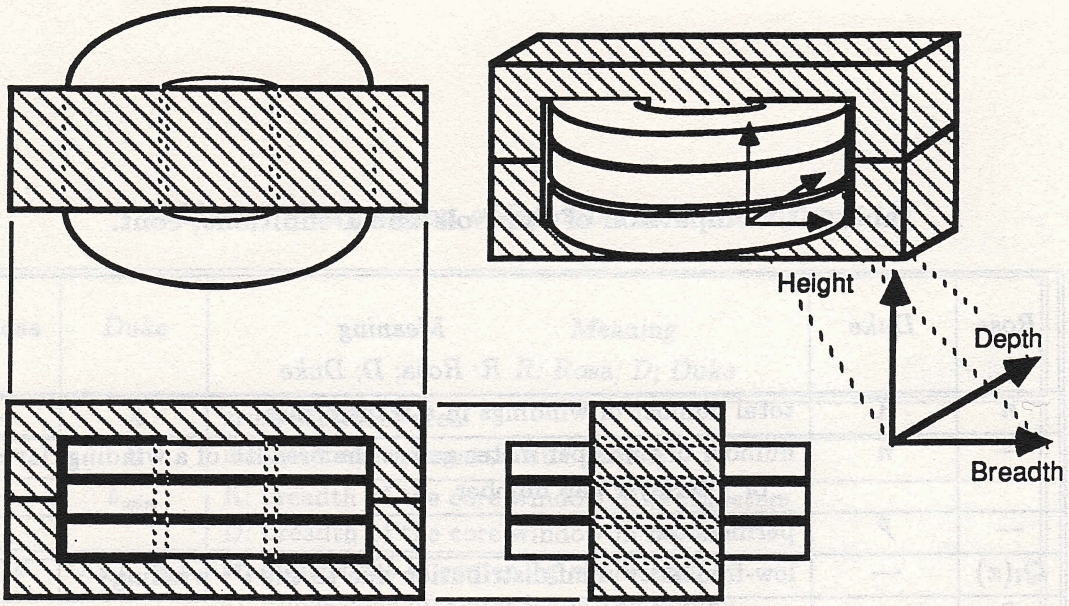


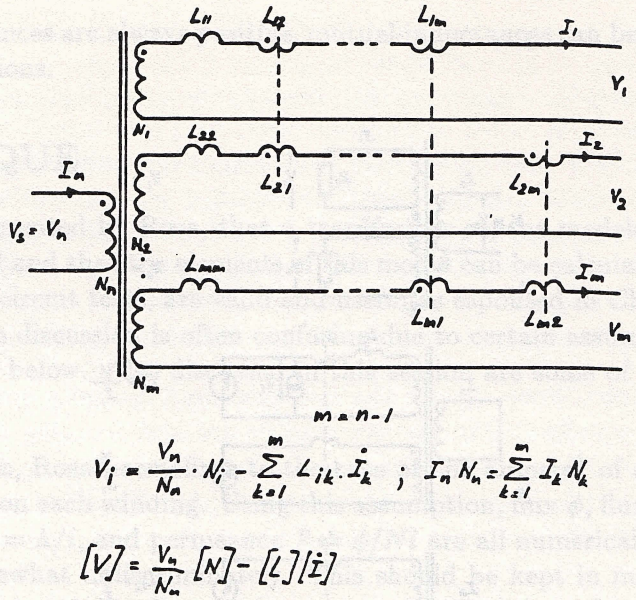
Figure 9.1: E-E core with stacked-disk winding structure.

9.2 SUMMARY

The simplified coupled-coils model that Rosa proposes is reproduced here as Fig. 9.2. We see in this model that each secondary winding of a K-winding transformer contains $(K-1)$ series leakage inductances, one of which is a self-inductance L_{ii} and $(K-2)$ of which are mutual-inductances L_{ij}. Corresponding pairs of mutual-inductances are denoted by dotted lines. Since the primary winding in Fig. 9.2 is represented without any leakage elements, one might erroneously assume that Rosa ignores the leakage of the primary winding. Actually, each of the self-inductances of Fig. 9.2 represents the leakage inductance between the primary and that particular secondary, as is discussed in Section 8.2.1 of Part I.

For an actual transformer, the leakage inductances for the circuit for Fig. 9.2 can be measured through a series of short-circuit tests in which the primary winding is shorted and each of the $(K-1)$ secondaries is excited sequentially, as is pictured in Fig. 9.3. To characterize the $(K-1)$ secondaries, there must be $(K-1)$ short-circuit tests. In each short-circuit test, the primary winding is shorted, and the voltages across the $(K-1)$ secondary windings are measured while a current is injected into one of the secondaries. In these tests, the shorted primary winding is assumed to present a perfect short to the ideal transformer represented by the two parallel lines in Rosa's equivalent circuit of Fig. 9.3. This means the net flux linking the shorted primary winding is assumed to be zero.

To calculate the values of the inductances for the circuit of Fig. 9.2, Rosa performs



$$m = n-1$$

$$V_i = \frac{V_n}{N_n} \cdot N_i - \sum_{k=1}^{m} L_{ik} \cdot \dot{I}_k \quad ; \quad I_n N_n = \sum_{k=1}^{m} I_k N_k$$

$$[V] = \frac{V_n}{N_n} [N] - [L][\dot{I}]$$

Figure 9.2: Rosa's Fig. 2. Equivalent circuit diagram of a K-winding transformer. For a K-winding transformer, the leakage-inductance effects are modeled by including a self-inductance and $(K-2)$ mutual-inductances in each of the $(K-1)$ secondaries.

$(K-1)$ *hypothetical* short-circuit tests. Like the tests in Fig. 9.3, the primary is always shorted and the $(K-1)$ secondaries are excited sequentially. Since these are hypothetical tests, the secondary voltages cannot actually be measured. Instead, Rosa takes the low-frequency field-intensity diagram associated with each hypothetical test and uses it to determine the flux linkage for each winding. From these flux linkages he determines the values of the self- and mutual-inductances for each test.

Rosa determines equations for the leakage inductances using two different winding structures. First, he examines shell winding structures where all the winding layers are of the same breadth. In these structures, all the flux in the transformer window is parallel to the axis of the transformer's center leg. Second, Rosa determines equations for the stacked disk configuration where all the disks are of identical radii. In these structures, all the window flux is perpendicular to the core center leg and parallel to the winding radius.

After these derivations, Rosa discusses what he calls the "general case". This term describes transformers where both axial and radial magnetic field components occur due to either shell windings of differing breadths or stacked-disk windings of differing radii. This "general case" is handled by applying both the shell-winding and disk-winding analyses to the transformer and adding the resultant inductances.

The paper concludes with some discussion on the relative placement of windings within the winding structure, and how placement effects the leakage inductances. Al-

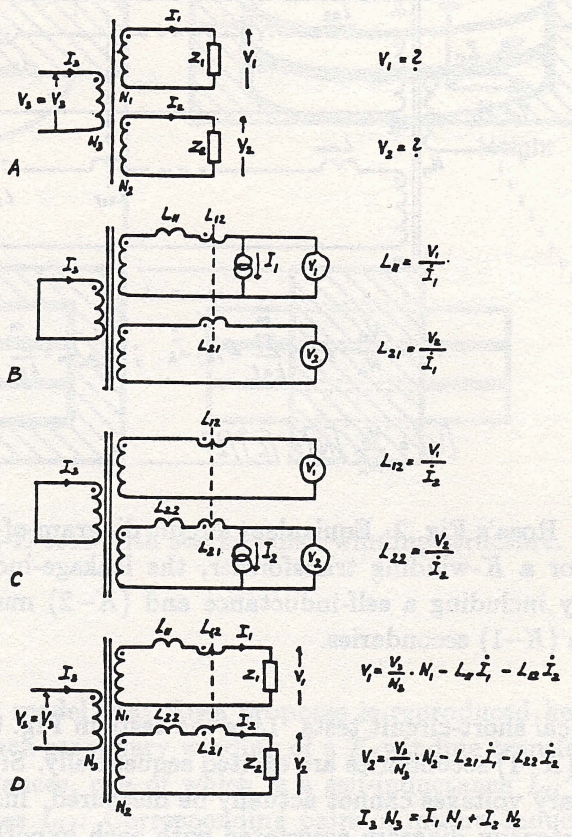


Figure 9.3: Rosa's Fig. 1. Leakage inductances for a K-winding transformer can be measured through a series of $(K-1)$ short-circuit tests. Equations for calculating the leakage impedances are determined through the same series of *hypothetical* short-circuit tests. (a) Three-winding transformer with unknown leakage properties. (b) Inductances L_{11} and L_{21} are determined by shorting the primary, injecting a current into winding 1 and measuring voltages of windings 1 and 2. (c) L_{12} and L_{22} are determined by repeating part (b) with current injected into winding 2. (d) Leakage between the windings is now modeled by self- and mutual-inductances between the secondaries.

though self-inductances are always positive, mutual-inductances can be negative for some winding configurations.

9.3 CRITIQUE

The basic ideas presented by Rosa, that a transformer can be modeled by a simplified coupled-coils model and that the elements of this model can be calculated by performing hypothetical short-circuit tests, are valid and useful as espoused in Chapter 8 of Part I. Nonetheless, Rosa's discussion is often confusing due to certain assumptions and errors which are itemized below. Also discussed in this section are some of the limitations of Rosa's analysis.

- In his analysis, Rosa normalizes to the case of one ampere[1] of excitation current and one turn on each winding. Using this assumption, flux ϕ, flux linkage $\Lambda = N\phi$, inductance $L = \Lambda/i$, and permeance $\mathcal{P} = \phi/Ni$ are all numerically equal and used by Rosa somewhat indiscriminately. This should be kept in mind when reading Rosa's paper since it can be a major source of confusion to the reader.

- The paper contains three typographical errors of note.

  1. On page 643 in the first line of the left column he writes "...the permeance $dS(y)$ of the flux channel". This should read "...the *susceptance* $dS(y)$ of the flux channel".

  2. In Fig. 4 of Rosa's article the final equation is given as

$$Q_j(x) = 1/\text{build} \qquad \text{If } x_{o2}(j) < x \leq w$$

     This should be

$$Q_j(x) = 1 \qquad \text{If } x_{o2}(j) < x \leq w$$

  3. On page 642, in the last line of the fourth paragraph of the right column, he writes "...and Λ_{21} are obtained." To be consistent with his equations, this should be "...and Λ_{12} are obtained," but as $\Lambda_{21} = \Lambda_{12}$ this may have been intentional.

- From Part I of this report, we know that the use of low-frequency field-intensity diagrams does not automatically limit an analysis of transformers to low frequencies. In Rosa's analysis, however, the high-frequency redistribution of field intensity is ignored and no means for determining this distribution is provided. In other words, Rosa's analysis is equivalent to a magnetostatic solution which does not involve the general field solution techniques developed by Dowell and Perry. Thus, Rosa's analysis and equations are limited to excitation conditions in which the distribution

[1] Rosa is not specific as to whether this is peak or RMS.

of current in the transformer windings due to the skin and proximity effects is negligible. By using (8.67) and (8.68) from Part I, the reader can determine the self- and mutual-impedances for the shell winding structure without this restriction.

- The model which Rosa presents in his paper ignores resistive losses due to both ac and dc excitation. Since resistive winding losses increase monotonically with frequency, this is a fairly severe shortcoming if one is interested in modeling high-frequency transformers. Again, (8.67) and (8.68) of Part I can be used to calculate for a shell winding structure both inductive and resistive circuit elements for the modified version of Rosa's circuit model proposed in Fig. 8.3 of Part I.

- In his equations, Rosa ignores the fact that field intensity is a phasor and thus a complex quantity. Since his calculations are tied to using low-frequency mmf diagrams and at dc phasors reduce to real functions, this does not adversely affect his results. Also because of this restriction to low frequencies, his multiplication of mmf distributions as real functions rather than as phasors is believed to be legitimate.

- Although he uses the term *build* in several of his expressions, he defines it only with an equation buried in his Fig. 4 and not with a word definition. From examining the equations in Rosa's Fig. 4, it appears that he considers build to be equal to the total height of a winding. It also appears that Rosa's build excludes the height of any insulation outside the outermost layer of the winding or inside the innermost layer, whereas in Part I of this report, build includes the height of any insulation in those positions.

- Lastly, Rosa's use of susceptance as the reciprocal of permeance is highly suspect. In his paper Rosa does not define what he means by the terms susceptance and permeance, but according to the IEEE Dictionary susceptance is "the imaginary part of admittance." [15, page 970] For conditions of zero resistance, susceptance[2] S is equal to the *negative reciprocal* of reactance X. In other words, $S = -1/X$. When there is no capacitance, the reactance equals the angular frequency times inductance, i.e., $X = \omega L$, so $S = -1/\omega L$. Since Rosa's one-ampere one-turn assumption allows us to to equate inductance and permeance, $S = -1/\omega \mathcal{P}$. Thus we see that as defined by the IEEE Dictionary, susceptance can not be equal to the reciprocal of permeance. This is not a major problem, however, since the equations[3] Rosa gives for the differential permeance are easily reconstructed using

$$\mathcal{P} = \frac{\phi}{\mathcal{F}} = \frac{BA}{H\ell} = \mu_0 \frac{A}{\ell_m} \tag{9.1}$$

where the symbols in (9.1) are defined in Table 9.1.

[2] In general, the symbol B is used for susceptance, however, to avoid confusion with flux density, we have chosen to use Rosa's symbol S for susceptance.

[3] Equation (2) in both of his Tables 1 and 2

9.4 NOTABLE EQUATIONS

Most of the equations in Rosa's paper are easy to understand so a recapitulation is considered unnecessary. Those that pose some difficulty to the reader due to typographical errors or unclear terminology are discussed in Section 9.3. Nevertheless, the problems discussed in Section 9.3 are deeply entwined in Rosa's analysis, so the reader interested in modeling a shell-winding transformer using Rosa's proposed equivalent circuit is advised to use the analysis presented in Chapter 8 of Part I.

This page has been left blank intentionally.

Chapter 10

Transformer Equivalent Circuits

M.I.T. Staff, *Magnetic Circuits and Transformers*, John Wiley & Sons, Inc., New York, 1943, pp. 622–642.

Starr, F. M., "Equivalent Circuits," *Transactions of the American Institute of Electrical Engineers*, Vol. 51, No. 2, June 1932, pp. 287–298.

Blume, L. F. , et al., *Transformer Engineering*, John Wiley & Sons, Inc., New York, 1938 & 1951, pp. 94–97, 117–127.

10.1 INTRODUCTION

The admittance-link equivalent circuit presented in Chapter 7 of Part I was developed many years ago as a tool for analyzing 60-Hz distribution systems containing multiwinding transformers. A thorough analysis of the equivalent circuit was completed then and published in references such as those listed above. Although the frequencies of switching power converters are now rising into the megahertz range, it is believed that the same admittance-link model might be a valuable tool for analyzing certain characteristics of high-frequency transformers as well.

This chapter is different from the others in Part II of this report because it does not summarize the relevant parts of the background references listed above. Instead, its primary purpose is to show the relationships between the symbols used in Chapter 7 of Part I, hereafter called *the admittance-link chapter*, and those used in each of the three references. If the analyses by different authors are compared in terms of a common set of symbols, it can be seen that the admittance-link chapter and each of the three background references are consistent with one another and exhibit a fair amount of overlap. The equivalence between the symbols used by the different authors is listed in Table 10.1, which is arranged in the approximate order that the Duke symbols are introduced in the admittance-link chapter. The Duke symbols may also be found in the Glossary of Symbols, but the Table 10.1 listing is more detailed.

Table 10.1: Comparison of Symbols and Definitions

Duke	*M.I.T.*	*Starr*	*Blume*	*Meaning* *D: Duke, M: M.I.T., S: Starr, B: Blume*
Actual Transformer or K-Port Network $(j,k = 1,2,\ldots,K)$				
K	n	n	n	number of windings in the transformer
$\underline{V}_j$	V_j	V_j	—	phasor voltage across winding or port j
$\underline{I}_k$	I_k	I_k	—	D & M: phasor current in winding or port k with a reference direction into the positive terminal S: current flowing into the circuit at point k
—	$I_{j(k)}$	—	—	M: the current produced in circuit j by voltage V_k applied to circuit k with all circuits but k short-circuited
$\underline{Z}_{jk}$	Z_{jk}	A_{jk}	—	D & M: mutual impedance of the transformer; $\underline{V}_j/\underline{I}_k$ with all currents except $\underline{I}_j$ and $\underline{I}_k$ equal to zero S: characteristic impedance coefficient
$\underline{Z}_{jj}$	Z_{jj}			D & M: self-impedance of the transformer
$\underline{Z}_{(jk)}$	—	—	—	short-circuit impedance seen at winding j with winding k short-circuited and all other windings open-circuited; $-\underline{V}_j/(\frac{N_k}{N_j}\,\underline{I}_k)$
$\underline{Y}_{jk}$	y_{jk} Y_{jk}	B_{jk}	—	D: admittance of the transformer; $\underline{I}_k/\underline{V}_j$ with all other winding voltages equal to zero M: short-circuit transfer admittance; mutual admittance of nodes j and k S: characteristic admittance coefficient
	y_{jj} Y_{jj}			M: short-circuit driving point admittance; self-admittance of node j
Transformer Circuits Referred to a Common Winding $(j,k = 1,2,\ldots,K)$				
$\underline{V}'_j$	V_j	—	e_j	D & M: phasor voltage across winding or port j B: voltage of terminal j relative to the common return
$\underline{I}'_k$	I_k	—	i_k	D & M: phasor current in winding or port k with a reference direction into the positive terminal B: current into the positive terminal of a port

(continued)

Table 10.1: Comparison of Symbols and Definitions (continued)

Duke	*M.I.T.*	*Starr*	*Blume*	*Meaning* *D: Duke, M: M.I.T., S: Starr, B: Blume*
Transformer Circuits Referred to a Common Winding (continued) $(j,k = 1,2,\ldots,K)$				
—	$I_{j(k)}$	—	—	M: the current produced in circuit j by voltage V_k applied to circuit k with all circuits but k short-circuited
$\underline{Z}'_{jk}$	Z_{jk}	—	—	D & M: mutual impedance, $\underline{V}'_j/\underline{I}'_k$ with all currents except $\underline{I}'_j$ and $\underline{I}'_k$ equal to zero
$\underline{Z}'_{jj}$	Z_{jj}	—	—	D & M: self-impedance, $\underline{V}'_j/\underline{I}'_j$ with all currents except $\underline{I}'_j$ equal to zero
$\underline{Y}'_{jk}$	Y_{jk}	—	—	D: admittance $\underline{I}'_k/\underline{V}'_j$ with all winding voltages except $\underline{V}'_j$ equal to zero M: mutual admittance of nodes j and k; short-circuit transfer admittance
	Y_{jj}			M: self-admittance of node j; short-circuit driving point admittance
$(K-1)$-**Port Network** $[j,k = 1,2,\ldots,(K-1)]$				
K	—	0	K	winding or node number chosen as a reference
$(K-1)$	—	m	—	S: one less than the number of points of entry of a general network
$\underline{V}_{jK}$	—	V_{j0}	$(\mathrm{e}_j - \mathrm{e}_K)$	D: phasor differential voltage between nodes j and reference node K S: voltage impressed from point j to ground B: vector voltage difference (voltage regulation)
$\underline{I}'_k$	I_k	I_k	i_k	D & M: phasor current in port k, or or the phasor current in winding k referred to winding K S: current flowing into the circuit at point k, except I_0 is directed out of the circuit (this is *not* the same as I_k for the K-port network) B: current flowing into terminal k

(continued)

Table 10.1: Comparison of Symbols and Definitions (continued)

Duke	*M.I.T.*	*Starr*	*Blume*	*Meaning* *D: Duke, M: M.I.T., S: Starr, B: Blume*
$(K-1)$-Port Network (continued) $[j,k=1,2,\ldots,(K-1)]$				
$\underline{Z}_{r,jk}$	—	C_{jk}	$\mathbf{Z}_{K(jk)}$	D: impedance $\underline{V}_{jK}/\underline{I}'_k$ with all other port currents equal to zero S: characteristic impedance coefficient B: individual three-circuit impedance of circuit K with respect to circuits j and k
			$\mathbf{Z}_{K(jj)}$	B: leakage reactance between circuits K and j
$-1/\underline{Y}_{r,jk}$	—	Z_{jk}	—	S: transfer impedance; the exciting voltage divided by the current at one of the grounded terminals during a short-circuit-admittance test
$(\frac{N_K}{N_j})^2\underline{Z}_{(jk)}$	$Z_{(jk)}$	Z_{j-k}	$\mathbf{Z}_{jk}$	M: equivalent impedance of windings j and k S: through impedance between terminals j and k B: leakage impedance between circuits j and k
$\underline{Y}_{r,jk}$	Y_{jk}	D_{jk}	$\mathbf{Y}_{jk}$	D: admittance $\underline{I}'_k/\underline{V}_{jK}$ with all other port voltages equal to zero M: mutual admittance of nodes j and k; short-circuit transfer admittance S: D coefficient B: transfer admittance
			$\mathbf{Y}_{jK}$	B: $\sum_{k=1}^{n-1}-\mathbf{Y}_{jk}$ (negative sign is missing from Blume)
	Y_{jj}		$\mathbf{Y}_{jj}$	M: self-admittance of node j; short-circuit driving point admittance B: driving-point admittance
K-Terminal Equivalent Circuit $(j,k=1,2,\ldots,K)$				
$\underline{y}_{jk}$	$Y_{\overline{jk}}$	—	$\mathbf{y}_{jk}$	D & M: admittance of the link connected between nodes j and k B: admittance link; transfer admittance (uses same symbol, but says signs are opposite)
—	—	—	$\mathbf{y}_{jj}$	B: $\sum_{k\neq j}\mathbf{y}_{jk}$
$\underline{y}_{jk}^{-1}$	—	$Z_{\overline{jk}}$	—	S: impedance of the link connected between nodes j and k

All the three of the background references share some common features. All voltages and currents are measured "vectorially," i.e., expressed as phasors, and both resistive and inductive effects are analyzed. Although electrostatic shields between windings are not specifically addressed, their effects are automatically included in the admittance-link equivalent circuit because the model parameters are calculated from short-circuit impedances which reflect both the losses and the leakage inductances associated with any shields that may be present. Only theoretical results are given, but they have been successfully applied to 60-Hz power systems for many years.

A couple of terms introduced in the admittance-link chapter and used throughout this discussion are reviewed here. A *short-circuit impedance test*, called just a *short-circuit test* in most of Part I, is performed by exciting one winding of a transformer, short-circuiting another, and leaving all the remaining windings open-circuited. With winding j excited and winding k short-circuited, the excitation voltage divided by the excitation current, both expressed as phasors, is the short-circuit impedance $\underline{Z}_{(jk)}$. The corresponding conditions for the admittance-link equivalent circuit are illustrated in Fig. 7.13 of Part I, where terminal j is excited relative to terminal k and the remaining terminals are unconnected.

Another important term is *short-circuit-admittance test*, performed by exciting one winding of the transformer and shorting all the other windings simultaneously. This test is not discussed in Part I of this report, but it could be used to obtain measured values for the admittance matrix $[\underline{Y}]$ associated with the K-port model of the transformer, introduced in Section 7.1 of Part I. The phasor current in one of the shorted windings j divided by the phasor voltage in the excited winding k is the admittance $\underline{Y}_{jk}$. The corresponding conditions for the admittance-link model are illustrated in Fig. 7.10 of Part I, where all the terminals are shorted together except one, which is excited relative to the others.

Essentially the same equations derived in the admittance-link chapter can be found in the references listed above, but in those references, the equations are typically buried in derivations which solve for quantities not directly relevant to the current research, e.g., fault currents and load division in 60-Hz distribution systems. The admittance-link chapter, on the other hand, applies the same concepts to a different problem, namely, calculating the parameters of the admittance-link model from the short-circuit impedances of a transformer.

The next three sections discuss the three background references in a logical order of consideration for someone unfamiliar with them. First is a section of the M.I.T. book, which provides the best overview of the subject and is the easiest to follow. Second is Starr's article, which extends M.I.T.'s analysis to what most closely matches that found in the admittance-link chapter, although Starr actually published before M.I.T. And third is a section of Blume's book, which presents an analysis that is closely related to the others and is essentially correct, but it adds nothing to the first two references and it is the most difficult to follow.

For each of the three background references, some general comments are made about

the approach taken, some potentially confusing aspects of the analysis are explained, and the relationship between each analysis and the others is made clear. No details of the derivations are included here because the admittance-link model is derived completely in Part I, and that derivation is consistent with each of the three background references.

10.2 M.I.T.

The M.I.T. presentation of equivalent circuits for multiwinding transformers is a good starting point because it provides an overview of the subject, referencing both of the other publications discussed in this chapter. Furthermore, it is an exceptional piece of technical writing—clear definition of symbols and thorough explanation of concepts makes it relatively easy reading. M.I.T. also includes the most complete discussion of the expected signs of numerical results, which is used in the admittance-link chapter to check whether the calculated results are reasonable.

The discussion in Section 7.2 of the admittance-link chapter closely follows the M.I.T. book. The big difference occurs after the exciting current of the magnetic core is neglected: M.I.T. continues the analysis in terms of an $(K \times K)$ system of equations, but the admittance-link chapter shifts to a reduced-order $[(K-1) \times (K-1)]$ system. Because one of the K winding currents in the M.I.T. equations is not independent of the others, the M.I.T. admittance matrix is singular, of rank $(K-1)$. By using a system of equations larger than is needed, M.I.T. simplifies the algebra but incurs a penalty of having to carry redundant information through the analysis. In addition, it is implied that an extra, redundant test is needed to generate the redundant information.

One example of the simplification brought about by using a higher-order system of equations is M.I.T.'s (35), which encompasses both equations (7.96) and (7.97) in the admittance-link chapter. Those key Duke equations give the admittance-link values $\underline{y}_{jk}$ as functions of the reduced-order-matrix admittances $\underline{Y}_{r,jk}$. M.I.T.'s (35) looks similar to (7.96), but an M.I.T. counterpart to (7.97) is unnecessary because the subscripts in (35) range from 1 to K, while the subscripts in (7.96) range only from 1 to $(K-1)$. Duke needs a special equation, (7.97), to handle the admittance links connected to node K, because Duke uses the reduced-order system of equations instead of M.I.T.'s $(K \times K)$ system containing redundant information. Note, however, that a counterpart to (7.97) is easily derived from M.I.T.'s (35) and (36).

The M.I.T. analysis is carried out in terms of short-circuit admittance tests, but the authors state that short-circuit *impedance* tests should be the basis of the analysis instead when the admittance-link values are to be calculated without performing any measurements. The reason is that the short-circuit impedances can be calculated readily from the geometry of the transformer, but the short-circuit admittances cannot. Since an analysis in terms of short-circuit impedances is not actually carried out, there are no M.I.T. equations which correspond to the other key equations in the admittance-link chapter, (7.94) and (7.95). M.I.T. does suggests one approach for such an analysis, but a different, simpler one is taken in the admittance-link chapter.

In Table 10.1, the *M.I.T.* column contains the same group of symbols listed twice, in reference to both the actual transformer and the transformer circuits referred to a common winding. This particular subset of symbols is initially defined in Article 1 of the M.I.T. analysis in terms of the currents and voltages of the actual transformer, but in the rest of the analysis, the same symbols are used under the assumption that all transformer circuits are referred to a common winding. While the derivation is clear, the use of the same symbol to represent two different quantities might cause some confusion when applying M.I.T.'s results to a real problem.

In addition to the two places mentioned above, the transfer admittance Y_{jk} appears in a third place in the table, in reference to the $(K-1)$-port network. There, it is given as equivalent to Duke's $\underline{Y}_{r,jk}$, although M.I.T. never considers an $(K-1)$-port network or a reduced-order system of equations anywhere in its analysis. This apparent paradox can be understood if the short-circuit-admittance tests described on p. 634 of the M.I.T. book are compared with those in Section 7.2.5 of the admittance-link chapter. By correlating symbols, it can be seen that Duke's matrix $[\underline{Y}_r]$, with elements $\underline{Y}_{r,jk}$, is equal to the first $(K-1)$ rows and columns of Duke's $[\underline{Y}]$, with elements $\underline{Y}_{jk}$. Therefore, each matrix element $\underline{Y}_{r,jk}$ is in fact equal to $\underline{Y}_{jk}$ for $j,k < K$, and both admittances are labeled Y_{jk} by M.I.T.

There is no Duke symbol which corresponds to M.I.T.'s $Z_{(jk)}$, given as the equivalent impedance of windings j and k. Because every other author does have a symbol for this quantity, and because the equivalent Duke expression is not immediately apparent, the equivalent Duke expression given in Table 10.1 is derived here.

M.I.T.'s Fig. 5 shows that $Z_{(12)}$ is the impedance between terminals 1 and 2 of the admittance-link equivalent circuit with no external connections made to terminals 3 and 4. Comparing this figure with Fig. 7.15 of Part I, which is a different representation of the same circuit, it is clear that M.I.T.'s impedance $Z_{(jk)}$ is equal to $\underline{V}_{12}/\underline{I}'_1$ in Duke symbols. Therefore, (7.68) in the admittance-link chapter gives the equivalent Duke expression.

$$\frac{\underline{V}_{12}}{\underline{I}'_1} = \left(\frac{N_4}{N_1}\right)^2 \underline{Z}_{(12)} \tag{10.1}$$

For the case where $j = 4$ or $k = 4$, a similar argument can be made using other equations in the admittance-link chapter. For example,

$$\frac{\underline{V}_{14}}{\underline{I}'_1} = \left(\frac{N_4}{N_1}\right)^2 \underline{Z}_{(14)} \tag{10.2}$$

can be shown from Duke's Fig. 7.10, (7.56), and (7.58). These results are generalized to obtain the following expression in Duke symbols which is equivalent to M.I.T.'s $Z_{(jk)}$:

$$\left(\frac{N_4}{N_j}\right)^2 \underline{Z}_{(jk)}$$

10.3 STARR

In a paper written for the purpose of predicting fault currents in 60-Hz distribution systems, Starr presents a thorough discussion of transformer equivalent circuits. His most general equivalent circuit, derived in his Appendix A, is more complex than what is needed in this report to develop the admittance-link model; however, his Appendix B contains most of the key equations derived in the admittance-link chapter, and of the three background references, Starr's article contains the only discussion of short-circuit-impedance tests, which are the subject of Chapter 6 in Part I.

Starr's symbols that appear in Table 10.1 under the heading *(K–1)-Port Network* are from his Appendix B, while his symbols under the heading *Actual Transformer or K-Port Network* are from his Appendix A, included only for completeness. Note that Starr's own list of symbols and definitions is found in his Appendix E.

In Starr's Appendix B, an equivalent circuit is derived which contains the minimum number of immittances, either impedances or admittances, needed to produce the same terminal characteristics as another arbitrary circuit. For the derivation, that arbitrary circuit must be described by equations that relate its terminal currents to its terminal voltages relative to a chosen reference terminal. Starr's minimum-immittance circuit corresponds to the admittance-link equivalent circuit of Fig. 7.9(b) in Part I, and Starr's arbitrary circuit corresponds to the 3-port-network circuit of Fig. 7.9(a), described by (7.20) in Part I.

The key equations in the admittance-link chapter have counterparts in Starr's appendix as follows: Equations (7.94) and (7.95) in Part I, which give the elements $\underline{Z}_{r,jk}$ of the reduced-order impedance matrix $[\underline{Z}_r]$ as functions of the short-circuit impedances $\underline{Z}_{(jk)}$, correspond to Starr's (13b) and (15b) respectively. The obvious difference, besides Duke's use of node 4 as the reference instead of Starr's node 0, is that turn ratios are present only in Duke's equations. The reason is that Starr's equations are written in terms of his *through-impedances*, which pertain to the transformer equivalent circuit after referral to a common winding, while the equations of Part I are written in terms of the short-circuit impedances of the actual transformer. The simple relationship between Duke's short-circuit impedances and Starr's through-impedances is given in Table 10.1, under the symbol Z_{j-k} in the *Starr* column.

A term central to Starr's derivation but absent from the others is *transfer impedance*, the quantity Z_{jk} which is obtained from a short-circuit-admittance test. In such a test, one terminal of the circuit is excited relative to a "ground" node, to which all the other terminals are connected, and a transfer impedance is the exciting voltage divided by the current flowing at one of the grounded terminals, both expressed as phasors. Starr argues that each impedance link in a minimum-immittance equivalent circuit is equal to a transfer impedance of the arbitrary circuit. To avoid confusion, note that the *driving-point impedance* in Starr's paper applies only to the multiport circuits analyzed in his Appendix A; there is no such quantity for the arbitrary circuit discussed in his Appendix B.

The other key equations in the admittance-link chapter, (7.96) and (7.97), give the admittance-link values $\underline{y}_{jk}$ in terms of the elements $\underline{Y}_{r,jk}$ of the reduced-order admittance matrix $[\underline{Y}_r]$. These equations correspond to the inverted forms of Starr's (6b) and (7b), respectively.

10.4 BLUME

Considering only what is relevant to the current research, Blume presents a subset of what is found in Starr's article, and he presents it in a more obscure manner. Most of the difficulty arises from a confusing use of symbols and a lack of equations to accompany some of the discussion. Nevertheless, it can be seen from the relationships in Table 10.1 that Blume's analysis is consistent with the others.

Beginning on p. 117, Blume introduces the admittance-link equivalent circuit with little justification, arguing only that it accurately represents an K-winding transformer because it has $K(K-1)/2$ independent elements. Relationships equivalent to the admittance-link chapter's (7.96) and (7.97) are then derived, the first one expressed in words in the paragraph following Blume's (63), the second one as his (70) combined with the sentence preceding it. Blume does not directly derive equations equivalent to (7.94) and (7.95) of the admittance-link chapter, but in his calculation example, he recalls (73) from an earlier discussion of three-winding transformers on p. 95, an equation equivalent to (7.95) in Part I. This equivalence is demonstrated by replacing X in Blume's (73) by $\omega\mathbf{Z}_{jk}$, dividing the result by ω, and replacing Blume's $\mathbf{Z}_{jk}$ by the equivalent Duke expression from Table 10.1, $(N_K/N_j)^2\underline{Z}_{(jk)}$.

The following is simply a collection of helpful hints for someone attempting to relate Blume's work to that of the other authors, with the hints arranged in their approximate order of intended use.

It is apparent that the symbols in Blume's Fig. 17 do not match those in the associated text and equations. The admittance values y_{jk} in the figure do correspond to the $\mathbf{y}_{jk}$'s in the text, but the directions indicated in the figure for the currents I_k are *not* the same as the reference directions for the corresponding currents $\mathbf{i}_k$ appearing in the text and equations. The correct reference directions are described in the paragraph preceding Blume's (57).

In most of the analysis, Blume uses the symbol $\mathbf{y}_{jk}$ to represent the value of an admittance link. In his (63), however, he uses the same symbol to represent a different quantity, transfer admittance, which has the same magnitude but differs in sign. It would be much clearer if the symbol $\mathbf{Y}_{jk}$ were used in (63) instead, the symbol introduced later as this very transfer admittance. Note that Blume uses the term *transfer admittance* to mean the inverse of Starr's transfer *impedance* Z_{jk}, except for a sign change.

There is a lengthy discussion following Blume's (63) regarding the sign of admittances. The point is that for the chosen reference directions of voltage and current, the transfer admittances are typically negative, making the admittance-link values typically positive.

Immediately after his (64), Blume defines $\mathbf{Z}_{4(jk)}$ as "the individual three-circuit impedance of circuit 4 with respect to circuits j and k." A clear explanation of this quantity may be found on pp. 96–97, although it is not called by the same name there. Briefly, the impedance $\mathbf{Z}_{4(jk)}$ may be obtained by performing a standard short-circuit-impedance test but measuring the voltages of open-circuited windings. Specifically, with winding k excited, winding 4 short-circuited, and all other windings open-circuited, $\mathbf{Z}_{4(jk)}$ is the voltage across open-circuited winding j divided by the current in winding k, both referred to a common winding. The same impedance value is obtained by exchanging the roles of windings j and k.

For convenience, Blume introduces two new symbols which are not found in the other analyses, $\mathbf{y}_{jj}$ and $\mathbf{Y}_{j4}$, both defined in Table 10.1. Because $\mathbf{y}_{jj}$ looks like an admittance-link value but is not, and because $\mathbf{Y}_{j4}$ looks like an element of the $\mathbf{Y}$ matrix but is not, it could be argued that they confuse the presentation rather than clarify it. The use of $\mathbf{Y}_{j4}$ is even more confusing because the right-hand sides of all the equations in Blume's (70) should be negated, effectively changing Blume's definition of $\mathbf{Y}_{j4}$. An alternative form of (70) that is much easier to understand can be obtained by simply replacing all of the $\mathbf{Y}_{j4}$'s with $\mathbf{y}_{j4}$'s.

Chapter 11

Conclusion

The design of transformers for high-frequency switch-mode applications is quite challenging, and the literature on the subject is both complex and diverse. An in-depth study of the literature on this subject was carried out as a starting point for developing the analysis method presented in Part I of this report. Part II is intended to convey to others the understanding that the Duke researchers have gained from studying the eight papers listed in Table 1.1. This part is meant to serve both as background for Part I, and as an aid for someone attempting to understand one of the reviewed articles.

As background for Part I, each chapter of Part II makes clear how the ideas of a paper relate to the ideas presented in Part I, and whether the results of each paper are applicable to the analysis in Part I. To better show the relationships among the articles and Part I, the major results of each paper are repeated in Part II in terms of the common set of symbols listed in the Glossary of Symbols.

The transformer modeling techniques and the field analysis described in Chapters 2, 3, and 4 of Part I are based in large part on the methods presented in the papers reviewed in Part II. However, Part I has a different goal than most of the papers. Part I is concerned with predicting the terminal characteristics of a transformer, i.e., its leakage impedances, while most of the papers attempt to predict and minimize copper losses. As a consequence, the form of the results in Part I is distinct from that in most of the papers.

In addition to serving as background for Part I, Part II is written to aid someone interested in understanding one of the reviewed articles. To this end, the major results of each article are analyzed, with special emphasis placed on material applicable to Part I. For someone faced with a particular high-frequency-transformer design problem, Fig. 1.1 and Table 1.2 are provided to help in selecting the most useful articles. By reading the corresponding chapter of Part II along with an article, in most cases the reader should be able to understand the article more quickly, and immediately gain additional confidence in its results. The chapters of Part II should not be used as substitutes for the original papers, however, because only the major results and those directly relevant to Part I are presented in this report. It is hoped that with the help of this literature review, a

design engineer can make more effective use of the literature on high-frequency effects in transformer windings.

APPENDIX A

Characterizing High-Frequency Effects in Transformer Windings—A Guide to Several Significant Articles

IEEE Applied Power Electronics Conference

Record, 89CH2719-3, March 1989

This page has been left blank intentionally.

CHARACTERIZING HIGH-FREQUENCY EFFECTS IN TRANSFORMER WINDINGS—A GUIDE TO SEVERAL SIGNIFICANT ARTICLES

Audrey M. Urling Van A. Niemela Glenn R. Skutt† Thomas G. Wilson

Department of Electrical Engineering
Duke University, Durham, NC 27706

Abstract

Several articles pertaining to the design and modeling of high-frequency transformer windings are reviewed. Each paper is summarized, stressing its significant contributions and its relationship to the others. The emphases and relative merits of each are discussed, and the understandability and applicability are evaluated.

1 INTRODUCTION

A key element in many power-processing systems is the transformer. This is particularly true in high-frequency multiple-output dc-to-dc converters where the transformer must deliver the voltage waveform of the primary winding to several outputs through the appropriate turn ratios. Generally, the current and voltage waveforms seen by the transformer windings are highly nonsinusoidal.

Because the temperature rise of the windings is a primary design constraint, it has been common practice in the past to design the windings of this key circuit element using the dc resistance of the winding wires or by using formulae or tables for calculating the ac resistance for simple one- or two-wire configurations from data presented in resources such as [10]. Since winding losses increase dramatically with frequency due to eddy currents, and since the configuration of wires in a transformer winding is considerably more complex than those described in [10], this method is not sufficient. Considering the high-frequency harmonic content of the nonsinusoidal waveforms in switch-mode converters, and the trend toward higher operating frequencies in such converters, the design engineer has an imperative and growing need to understand high-frequency effects which have a great impact on transformer performance and design.

This work was supported in part by a research contract with Digital Equipment Corp. Maynard, MA.

†Now with Digital Equipment Corp., Northboro, MA.

In the past few years, several articles on the analysis and design of high-frequency transformer windings have been published [1-9]. These nine articles, which are the focus of this paper, cover a wide range of interests, for example, predicting high-frequency losses for sinusoidal and nonsinusoidal current waveforms, and designing minimum-loss transformer windings in an algorithmic fashion. Yet, for a number of reasons, it is debatable how much help has actually been provided to the design engineer. Much of the literature is difficult to read because it is based in electromagnetic field theory and because of the necessary brevity of journal articles. Also, articles which build upon earlier papers often do not fully apprise the reader of the assumptions made in the earlier works. Frequently the engineer is found little-the-wiser after the first reading of an article, and a full comprehension of the relevant articles entails a larger time commitment than he or she is able or willing to make.

In this paper, our objective is to allay some of these difficulties by summarizing the principal results of several articles of interest, and to provide a context in which the design engineer can assimilate the information more effectively and efficiently. Highlighted are the major focus and the significant contributions of each paper, as well as the assumptions in each author's method, and how the various methods relate to one another. Most of the discussion herein is kept general to allow anyone familiar with the design of low-frequency transformers to follow. However, to derive full benefit from the discussion and the comparisons made, the reader should refer directly to the original articles. Because the principal results in the papers are typically presented in the form of numerous graphs and equations, often with specially defined symbols, it is not feasible to present even samples of the key results in this overview. The goals of this presentation are to clarify what useful results are available in the literature, to stimulate the reader to seek out the original papers, and to assist him or her in understanding them.

Section 2 introduces the reader to some of the ter-

CH2719-3/89/0000-0373 $1.00 © 1989 IEEE

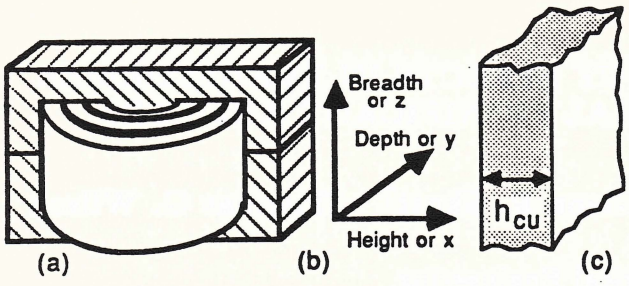


Figure 1: (a) EE-core transformer with shell windings. (b) Coordinate system adopted for this paper. (c) Current sheet obtained by unwrapping one transformer winding layer.

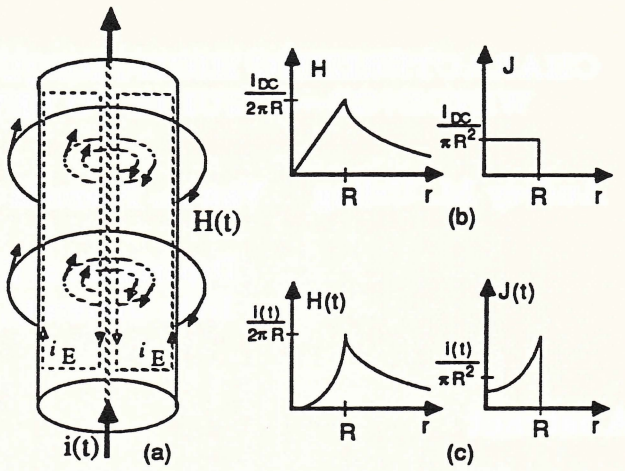


Figure 2: (a) Skin effect in an isolated conductor carrying an alternating current $i(t)$. At the instant shown, the current $i(t)$ is assumed to be increasing in the direction indicated. (b) Radial distribution of H and J for a dc current. (c) Radial distribution of $H(t)$ and $J(t)$ at some time instant for an ac current.

minology and background concepts used in the papers under review. Section 3 contains the summaries of the papers, and Section 4 draws conclusions and compares the authors' different approaches to several common topics.

2 BACKGROUND

Before discussing the specifics of the nine principal articles reviewed, background information pertinent to most of them is presented. Since the articles under review cover a wide range of topics, not all the information discussed in this section is contained in all of the articles or is assumed by each author. The common items discussed in this section include skin and proximity effects and their influence on transformer windings, the modeling of transformer layers as current sheets, and the use of low-frequency field-intensity diagrams.

2.1 Transformer Analyzed

For the discussion of transformer windings presented in this paper, the coordinate system of Fig. 1 is adopted for the current sheet obtained by unwrapping and smoothing out the conductors of one layer of windings. Shown in Fig. 1(b) is a three-dimensional right-hand Cartesian system where the x-direction corresponds to the radial "height" of the winding, the y-direction corresponds to the "depth" along one turn of the winding, and the z-direction, parallel to the center leg of the core, corresponds to the winding "breadth." This coordinate system is not adopted by all the papers, but it is common to several of them.

In general, the papers assume that the transformer being analyzed is wound on a pot core or an EE core. The core material is assumed to have high permeability, and energy storage is not a requirement of the transformer, therefore the magnetizing current is assumed to be negligible. In this paper, only transformers with "shell" windings as shown in Fig. 1(a) are discussed because it is this configuration which most often appears in the reviewed papers. Two papers also discuss flat or stacked-disk windings [7,8]. Since the authors are generally interested in only eddy-current effects in the transformer *windings*, all papers but [9] ignore core loss.

2.2 Eddy-Current Effects

An isolated cylindrical conductor carrying alternating current $i(t)$ generates a time-varying circular magnetic field $H(t)$ which exists both inside and outside the conductor and depends on the instantaneous current, the time rate of change of the current, and the radial distance r from the center of the conductor. Such a conductor and its associated field are shown in Fig. 2. The field $H(t)$ is shown as solid-line circles outside the conductor and as dotted-line circles inside the conductor. For a constant current I_{DC} flowing in the wire, Fig. 2(b) shows that inside the conductor, the current-density distribution J is uniform and the magnetic field intensity H increases linearly with radial distance r. Outside the conductor, H decreases inversely with r. For an alternating current $i(t)$ flowing in the wire, the alternating magnetic field inside the conductor induces eddy currents i_E in the conductor which produce a field that tends to cancel the field produced by $i(t)$. These induced eddy currents as pictorialized in Fig. 2(a) are

directed so that they add to the main current on the surface of the conductor and subtract from it in the interior region. The result is time-varying nonlinear magnetic-field and current-density distributions within the conductor, illustrated in Fig. 2(c). The net instantaneous current $i(t)$ in the conductor is unchanged by the eddy currents; it is the radial distribution of the current over the cross-section of the conductor that changes. The intensity of the induced eddy currents is directly proportional to the rate of change of the main current; therefore, the nonuniform distribution of the current in a conductor is more pronounced for higher excitation frequencies. This change in the current-density function in the wire is usually referred to as *skin effect*. It is important to note that the magnetic field intensity outside of the conductor depends only on the net current $i(t)$ and is unchanged by the redistribution of current inside the wire due to skin effect.

In the discussion above, the redistribution of current due to skin effect depends solely on the magnetic field induced by the alternating current in the conductor itself. Another type of frequency-dependent eddy-current phenomenon occurs in any conductor that is placed in a region of space containing an externally-generated time-varying magnetic field with a component that is normal to the axis of the conductor. Whenever this situation occurs, there are eddy currents induced in the conductor which act to oppose the penetration of this external field. Since this external field can be caused by the alternating current in some other nearby wire, this eddy-current phenomenon is often referred to as the *proximity effect*.

Figure 3(a) shows a conductor with circular cross-section that is positioned in a uniform time-varying magnetic field. The conductor is isolated in space and carries no net current. For this discussion, the uniform external field $H_{ext}(t)$ in Fig. 3 is assumed to be increasing in magnitude in the indicated direction. The time-varying field lines which pass through the conductor induce eddy currents in the conductor, and these eddy currents induce a field which opposes the external magnetic field. In Fig. 3(b), the eddy currents are shown as circular currents which surround each of the crosses that represent the downwardly directed external field $H_{ext}(t)$.

The cross-sectional view of the conductor in Fig. 3(c) shows that the net effect of the induced eddy currents is to generate a circulating current that flows into the right side of the cross-section and out of the left side. This circulating current produces losses in the conductor even though it carries no net current. The upwardly directed arrows in Fig. 3(c) represent the opposing magnetic field generated by the eddy currents. The superposition of this reaction field and the external field that induces it results in a reduction in the net

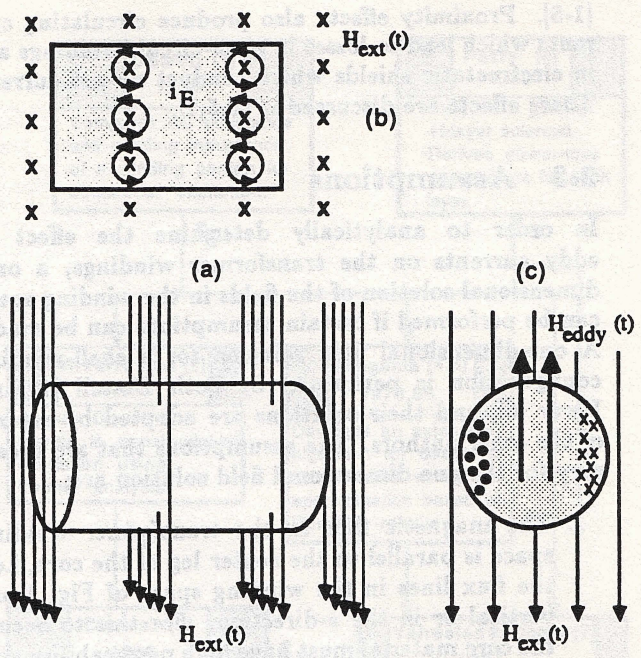


Figure 3: Illustration of proximity effect. (a) Perspective view of a conductor in a uniform time-varying magnetic field. (b) Top view of the conductor indicating that the field lines that pass through the conductor induce eddy currents i_E which can be thought of as circulating around each field line. (c) Cross-sectional view showing the opposing field $H_{eddy}(t)$ generated by the eddy currents.

amount of magnetic flux that penetrates the conductor. Since the energy stored in the magnetic field in any region of space is directly related to the magnetic field intensity in that region, the reduction of the amount of magnetic flux that penetrates a conductor decreases the magnetic energy that is stored in the conductor.

The two eddy-current effects discussed above, the skin and proximity effects, occur simultaneously in a conductor that carries an alternating current and is positioned in an external alternating field. This is exactly the situation that exists for the conductors in the layers of a transformer winding. The essence of the combination of these effects is that the current in each conductor produces a skin effect in itself and a proximity effect in other conductors that are close to it. The circulating eddy currents due to skin and proximity effects cause the power losses in the transformer windings to increase dramatically with frequency. It is not uncommon for the winding loss at 1 MHz to be one hundred times that at dc. Determining the increase in the apparent winding resistance with frequency is the principal subject of many of the reviewed papers

[1-5]. Proximity effects also produce circulating currents which lead to losses in open-circuit windings and in electrostatic shields which conduct no net current. These effects are discussed in [3,5,7].

2.3 Assumptions

In order to analytically determine the effect of eddy currents on the transformer windings, a one-dimensional solution of the fields in the winding space can be performed if certain assumptions can be made. A one-dimensional field solution for a shell-winding configuration is performed by both Dowell [1] and Perry [6], and their solutions are adopted by several of the other authors. The assumptions that are necessary for the one-dimensional field solution are:

1. The magnetic flux in the transformer winding space is parallel to the center leg of the core, i.e., the flux lines in the winding space of Fig. 1 are vertical or in the z-direction. For this to occur, the core material must have high permeability and there can be no gaps in the core. Also, the wires composing a winding layer should fill the entire breadth of the bobbin.

2. The layers of conductors can be modeled as equivalent foil conductors which fill the full core-window breadth. This is discussed further in Section 2.4.

3. The curvature of the transformer windings can be neglected when calculating the radial field distribution across a winding layer. Therefore, the equivalent foil conductors which represent winding layers can be effectively "unwrapped" and modeled as pieces of infinite current sheets. These current sheets have the same height as the equivalent foil conductors but extend to infinity in the directions of depth and breadth.

4. Capacitive effects in the windings can be ignored.

5. The magnetic field generated by any winding layer is negligible outside that layer, i.e., at a radius greater than the layer [7, p. 365].

2.4 Creating Equivalent Foil Conductors

The method by which round-wire windings are transformed into foil windings is a key step in converting the various actual windings into their equivalent foil conductors for analysis. This transformation is introduced in [1] and is used extensively in other works. The steps in deriving an equivalent foil conductor from a layer of round-wire conductors are shown in Fig. 4.

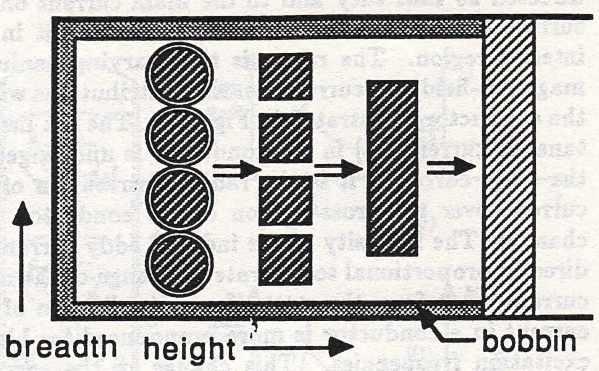


Figure 4: Steps in transforming a layer of round wires on a bobbin into a foil layer.

In the modeling process, the round wires are first replaced by square conductors of equal copper cross-sectional area. These square conductors are then brought together to form an equivalent foil winding with a height equal to that of the square-wire height and a breadth equal to the number of conductors in the layer times the breadth of the equivalent square conductors. This foil winding of copper, which does not extend the entire breadth of the core window, is then in effect "stretched" in the breadth direction to become a foil of equal height that does extend across the entire window breadth. This stretching increases the cross-sectional area of the foil layer, which is compensated by a "layer porosity" factor discussed below. Rectangular-conductor windings and actual copper-foil windings can be transformed similarly into equivalent "stretched-foil" conductors.

In order for this transformation to be valid, there must be some factor introduced which compensates for the increased cross-sectional area and insures that the dc resistance of the model winding is the same as the dc resistance of the original winding that it represents. This compensation factor is referred to by several names such as layer porosity [11], conductor spacing factor [7] and layer copper factor [4,5,12], and it is equal to the ratio of the breadth of the equivalent foil conductor before "stretching" to the breadth of the core window. Mathematically, the introduction of layer porosity has the effect of reducing the conductivity of the equivalent foil conductors.

Although the concept of layer porosity is generally accepted in the literature [1,2,4,5,7], the reader should be aware that the indiscriminate use of layer porosity can lead to erroneous results. As pointed out by Snelling, the analysis performed in [1] is "reliable" only for values of layer porosity which are not "too small" [12, pp. 322, 323]. Although it is unclear from the literature which values of layer porosity are "too small," when such a value occurs the assumption that the mag-

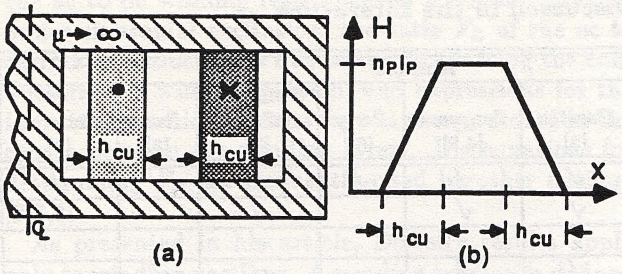


Figure 5: (a) A simple two-winding two-layer transformer. (b) The related low-frequency field-intensity diagram.

netic flux is parallel to the winding layers may not be valid.

2.5 Low-Frequency MMF Diagrams

Another convention generally adopted by the articles under review is the use of low-frequency field-intensity diagrams or profiles. In the literature, these are also called "mmf (magnetomotive force) diagrams" and "leakage-flux diagrams." In the winding space of a transformer, the mmf, the magnetic field intensity, and the magnetic flux are linearly related, which allows any of these terms to be used.

Figure 5 shows the right-hand side of a simple two-winding transformer and its associated field-intensity diagram. The outer winding conducts a current of I_P amperes and is composed of one layer of n_P turns per vertical meter, therefore it contributes a total field intensity of $n_P I_P$ ampere-turns/meter. The inner winding contributes $n_P I_P$ ampere-turns/meter in the opposite direction. Assuming uniform current distribution throughout each winding, the field intensity increases linearly as the outer-winding layer is traversed from right to left. In the space between the windings, the field intensity remains constant, then it decreases linearly as the inner winding is traversed. The field intensity in the interlayer space is dictated by the *total* field intensity generated by the outer winding; therefore, it is unaffected by any redistribution of current within that winding due to skin and proximity effects.

Since these field-intensity diagrams are derived assuming uniform current density across the height of the winding layers, the resulting field-intensity distribution inside the conducting layers is accurate for low frequencies only. However, the field-intensity values in the interlayer spaces are invariant with frequency, and for the one-dimensional field analysis, they become the boundary conditions of the magnetic field intensity at the two surfaces of each infinite current sheet. Also, qualitative information on the relative energy storage

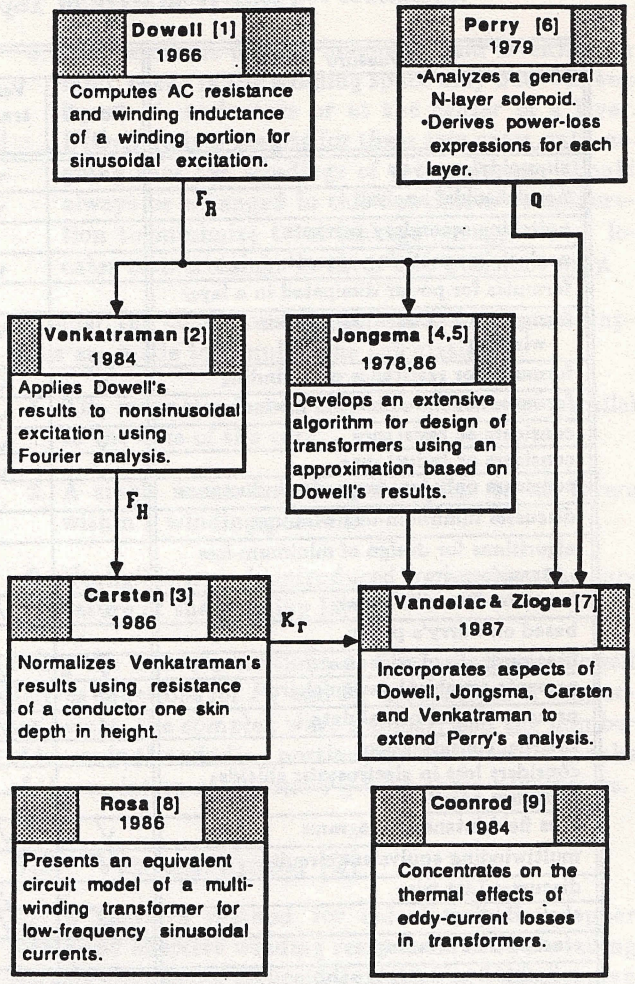


Figure 6: Literature Flowchart

and power dissipation of different winding layouts may be obtained by comparing the general shape and relative peak values of low-frequency diagrams belonging to the layouts. Thus, low-frequency field-intensity diagrams are a useful tool for high-frequency transformer design.

3 ARTICLE SUMMARIES

In the previous section, we present some of the background ideas that are required in order to understand the papers discussed in this review. We now summarize the individual articles, focusing on each author's significant contributions and assumptions, the interrelationships between the articles, and the general flavor of each.

A primary contribution of each author and the relationships between the papers under review are in-

Table 1: Matrix of Topics Discussed in the Literature

Feature	*Authors*							
	Dowell [1]	*Venka-traman* [2]	*Carsten* [3]	*Jongsma* [4,5]	*Perry* [6]	*Vandelac & Ziogas* [7]	*Rosa* [8]	*Coonrod* [9]
sinusoidal analysis	√	√	√	√	√	√	√	√
nonsinusoidal analysis		√	√	√		√		
switching secondary currents						√		
neglects magnetizing current	√	√	√	√		√	√	
formulas for power dissipated in a layer					√	√		
formulas for power dissipated in a winding		√	√			√		√
formulas for resistance of a winding	√	√	√	√				√
formulas for inductance of a winding	√	√						
considers ac resistance	√	√	√	√				√
considers ac inductance	√	√						
considers only low-frequency inductance							√	
discusses minimum-loss windings			√	√	√	√		
algorithms for design of minimum-loss transformers				√				√
based on Dowell's paper	√	√	√	√				
based on Perry's paper					√	√		
uses normalized wire size	√	√	√	√	√	√		
presents graphical design charts	√	√	√	√	√	√		√
presents experimental data		√						√
thermal considerations								√
considers loss in electrostatic shields			√	√		√		
considers core loss								√
uses field-intensity diagrams	√	√		√		√	√	
multiwinding equivalent circuits							√	
discusses Litz wire		√	√	√				
shell windings	√	√	√	√	√	√	√	
stacked-disk windings						√	√	
cylindrical-coordinate solution					√			

dicated in Fig. 6. Although the earliest work in this diagram was published by Dowell in 1966, over half of the papers first appeared in the last five years. The key analysis is done in [1] and [6]; the rest of the papers shown are primarily applications of the basic ideas developed in there. Figure 6 shows that most of the articles discussed are based upon Dowell's work, therefore, the summary of Dowell's article presented below is more detailed than the others. Figure 6 also shows that two articles [8,9] bear no direct relation to the others, therefore, these two are summarized below but are not generally analyzed further in Section 4. The four coefficients shown in the figure—F_R, F_H, K_r, and Q—represent important results of the authors' derivations and, in some cases, these coefficients are used by subsequent authors. The definitions of these coefficients are given in the individual summaries below.

Table 1 is a detailed comparison of the papers. Several topics of significance are listed, and check marks indicate which authors address each topic. Although not all of these topics are discussed in detail in this paper, they are included for completeness. By examining Table 1, we see that out of eight authors, only two provide measurement data to substantiate their results. We also see that virtually all of the authors focus on the changes in ac resistance with frequency but that they do not address the corresponding changes in the leakage inductances associated with the windings. In addition, only one author discusses an equivalent circuit to model the behavior of a multiwinding transformer in a circuit. The individual summaries given below lay the groundwork for the comparisons which follow in Section 4.

3.1 Dowell [1]

For a two-winding transformer under sinusoidal excitation, Dowell shows how to calculate the ac winding resistance and ac leakage inductance associated with each winding from the geometry of the transformer.

In his paper, he derives expressions for the ratio F_R of the ac to dc winding resistances of a winding portion under sinusoidal excitation, the ratio F_L of the ac to dc leakage inductances due to the flux cutting the conductors of a winding portion, and expressions for the inductances which account for the energy stored in the spaces between the winding layers. His equations for determining F_R are frequently cited by other authors [2,3,4].

As presented in his article, Dowell's results apply only to winding portions. A winding portion is defined as a part of a transformer winding which, when examining the low-frequency magnetic-field-intensity diagram, extends in either direction along the axis of winding height from a position of zero field intensity to the first positive or negative peak of magnetic field intensity. Leakage inductance and winding resistance are calculated for each winding portion, one at a time, then summed over each winding or the whole transformer.

Unfortunately, this approach is not suitable for analyzing transformers with three or more windings. Associating the stored energy in the interlayer spaces with particular windings is not as straightforward in multiple-output transformers as it is for the two-winding case. Also, the positions of the zero-crossings in the magnetic-field-intensity profile can move as the relative loads on such transformers change. The zero-crossings may occur at any position across the height of a winding layer, but Dowell's equations apply only for two positions, namely, between two layers of conductors and exactly at the center of a layer.

As for experimental verification, Dowell only mentions that he obtained good agreement between calculated and measured values for leakage inductance and resistance in tests over the frequency range from dc to 10 MHz on a transformer with single-layer windings. No details are given.

Dowell's results apply only under the following conditions:

1. The transformer has two windings.
2. Voltages and currents in both windings are sinusoidal.
3. There are no conducting shields or open-circuit windings present in which eddy-current losses would occur.
4. The transformer is wound with circular conductors where each layer fills the breadth of the winding space. Although he does not actually do it, Dowell's results are easily extended to windings using paralleled wires, and to square, strip, and foil conductors, but not to twisted-wire bundles or Litz wire. The effect of a partial layer, one which spans substantially less than the core-window breadth, is not considered.
5. The positions of zero magnetic field intensity, or mmf, occur in the winding space only between two layers of conductors or at the center of a layer. Dowell derives results for these two cases only, arguing that the windings of a transformer should always be arranged in this "optimum" configuration to minimize total leakage energy, which locates zero-crossings in these two positions only.

Under the conditions above, the following assumptions are made to simplify the calculations:

1. The magnetic flux in the core window is parallel to the axis of the core.
2. A single mean turn length applies to all layers within a winding portion.
3. Negligible error is introduced by ignoring the curvature of the winding layer.

Using the above conditions and assumptions, Dowell derives equations for F_R and F_L as functions of conductor height, the complex wave number, and the number of layers in the winding portion, and he presents graphs of the variation of F_R and F_L with these parameters.

3.2 Venkatraman [2]

Given Dowell's method for calculating the copper losses and effective winding resistances of two-winding transformers under sinusoidal excitation, Venkatraman uses Fourier analysis to extend those results to the nonsinusoidal excitation commonly found in switch-mode power converters. Specifically, he considers unipolar pulse-current excitation having a rectangular or trapezoidal waveform. Venkatraman determines the harmonic content of the nonsinusoidal waveform through Fourier analysis, then applies Dowell's results repeatedly to determine the winding resistance at each harmonic. These data are used to determine winding losses for the nonsinusoidal waveform.

Under conditions of nonsinusoidal excitation, the effective winding resistances are shown to vary greatly with the duty ratio and the rise and fall times of the exciting-current waveform, as well as with the frequency of excitation and the winding geometry. Venkatraman introduces the quantity F_H, the ratio of rectangular-wave losses to sine-wave losses, which may be precalculated and used in conjunction with Dowell's ac-to-dc resistance ratio F_R to easily compute the effective winding resistances for nonsinusoidal excitation. Experimental data are provided which validate the approach.

Because Venkatraman uses Dowell's results directly, most of Dowell's restrictions and assumptions apply. Most importantly, only two-winding transformers with no conducting shields or open-circuit windings are considered, and only Dowell's "optimum" winding arrangements can be analyzed with the existing equations. While Dowell discusses windings of only single, round conductors, Venkatraman demonstrates that the analysis performed by both authors applies to windings of multiple, electrically-paralleled, round conductors, as well as strip conductors and foil. For Litz wire, Venkatraman shows that the calculated F_H is accurate, but F_R calculated according to Dowell is not.

Venkatraman's paper is all the more commendable for including experimental verification of the results, an element which is absent from most of the other papers considered in this report. Furthermore, an important conclusion not mentioned in the paper can be drawn from those results. That is, the approach taken by both Dowell and Venkatraman works very well for EE cores, where it is not intuitively clear that a one-dimensional analysis of the fields present in the winding space is adequate. Recall that a key assumption in Dowell's method is that the magnetic flux in the winding space is parallel to the center leg of the core, an assumption expected to be good for pot cores but questionable for EE cores.

3.3 Carsten [3]

Carsten's paper focuses on the calculation and minimization of losses due to skin and proximity effects in transformer windings carrying arbitrary current waveforms. Carsten's Fourier-series method for determining these losses is similar to Venkatraman's, but the two author's methods are distinguished by the specific form of their results.

The effective winding resistance, which accounts for power losses due to all the harmonics, is used in the paper to calculate what Carsten calls K_r, the normalized effective resistance factor. K_r is defined as the ratio of the effective resistance of the winding for the specific nonsinusoidal current waveform of interest to the dc resistance of a similar winding having a conductor height of one skin depth at the fundamental frequency. This makes Carsten's results more convenient to use than Venkatraman's because no recalculation of dc resistance is necessary to compare the losses for wires of different sizes. Values of K_r for various nonsinusoidal current waveforms are presented graphically and are used to determine both the optimum winding height for minimum losses, and the variation of K_r with parameters such as waveform rise and fall time and number of winding layers.

Carsten's paper has some weaknesses that the reader should keep in mind. Although Carsten builds upon Dowell's work, he differs somewhat from Dowell in terminology. Dowell's equations are all derived for winding portions which may or may not contain a half-layer. Carsten uses only Dowell's equations for portions with integral numbers of layers (no half layers) and refers to such groups of layers as *windings* instead of *portions*. In addition, Carsten does not as adequately as might be desired apprise the reader of the assumptions and conditions inherent in Dowell's analysis.

The paper discusses additional topics of interest. A comparison is made of the predicted losses in transformers conducting bipolar square-wave currents versus those conducting unipolar-pulse currents. Carsten briefly discusses the reduction of leakage inductance with increasing frequency, but he dismisses this as a minor effect and analyzes only the case of resistive loss. The use of Litz wire to reduce losses is also covered in the article; Carsten's analysis of Litz wire is discussed in Section 4.3 below. The appendix to Carsten's paper contains a comprehensible derivation of the expressions for the real parts of Dowell's complex variables M and D. His resultant equations (20) and (21) are more useful than Dowell's equations for M and D which contain hyperbolic functions of complex variables. Unfortunately, during the course of this derivation, Carsten inserts an erroneous "j" in the trigonometric terms of his expressions, a "j" which should be deleted from his equations (16) through (21).

3.4 Jongsma [4,5]

If a designer is primarily interested in minimum-loss transformer windings, Jongsma provides an easy-to-follow, almost mechanical method of achieving this. The primary focus of Jongsma's articles is to adapt Dowell's analysis to the algorithmic design of minimum-loss transformer windings. Neither of Jongsma's papers contains evidence of experimental verification, which makes it difficult to predict the accuracy of the loss calculations or judge whether the designs resulting from the algorithm are truly minimum-loss.

The analysis presented in [4] is applicable to sinusoidal excitations only and focuses primarily on round-wire windings, although many winding types are discussed. The methods are applicable only for two-winding transformers and they assume Dowell's "optimum" configurations. Part 1 of the paper is a theoretical development of the necessary equations and a discussion of several issues related to the design of minimum-loss transformers. Part 2 includes several design charts and provides an algorithm to use these charts to design the lowest-loss combination of windings which fit into the available winding height.

On the other hand, the analysis presented in [5] is applicable to both sinusoidal and nonsinusoidal cur-

rents. The latter are accommodated by determining an effective sinusoidal frequency for the nonsinusoidal current. As in [4], many winding types are discussed, but more emphasis is placed on strip windings. Since Dowell's equations apply to only two-winding transformers, Jongsma provides equations in [5] to determine the losses in additional conducting windings which do not fit the definition of a winding portion, such as occur in multiple-output transformers. Additional losses due to open-circuit windings or electrostatic shields are discussed qualitatively, but cannot be determined quantitatively with the equations provided. The design algorithm presented in [5] relies for the most part on equations and tabular data which are provided in the paper, not design charts as does [4]. The first third of the paper is primarily a verbal flowchart detailing the design algorithm with appropriate equations and tables; the rest of the paper explains the theory behind the first part, including some of the assumptions made.

3.5 Perry [6]

Perry solves for the current-density distribution in the coils of a single-winding, multilayer, series-connected, infinite solenoid. His analysis is based on general field solutions for the distribution of current density in the layers of an infinitely long, cylindrical current sheet. He presents this analysis in both rectangular and cylindrical coordinates.

Perry's paper is primarily analysis, and it is important because it represents a significant break from Dowell's approach. Whereas Dowell's primary unit of interest is the winding *portion*, Perry's analysis is based on a single winding *layer*. Consequently, although Perry is interested only in multilayer solenoids (air-core inductors), his method is applicable to multiwinding transformers as well. Vandelac and Ziogas demonstrate this applicability by extending Perry's analysis to determine the losses in multiwinding transformers conducting nonsinusoidal currents [7]. Skutt extends Perry's work in a different direction to calculate the magnetic energy stored by the winding structure of a multiwinding transformer [11].

Perry uses the results he obtains for the current density in the layers to calculate, for the solenoid, the power dissipation per unit area of the y-z plane of Fig. 1. He then examines these power-dissipation predictions to determine the optimum height for each of the layers of the multilayer solenoid. His expressions for high-frequency power dissipation in the winding layers are written as functions of normalized layer height and are normalized to a convenient value of power for comparison. The symbol Q shown in Fig. 6 represents the amount of power dissipated per unit area of the winding layer based on its height, the frequency, and the magnetic-field boundary conditions for the layer.

3.6 Vandelac and Ziogas [7]

Figure 6 shows that the paper by Vandelac and Ziogas—more than any other paper examined here—brings together the ideas presented by the other authors. In many ways, this paper takes the essential points from both Dowell and Perry and combines them into a single, unified analysis. The paper also incorporates Venkatraman's use of Fourier analysis and Carsten's normalization to the dc resistance of a conductor one skin depth in height. Vandelac and Ziogas apply the layer-based field analysis that Perry develops for single-winding inductors to transformer problems similar to those examined by Dowell, Venkatraman, Carsten and Jongsma. Vandelac and Ziogas show that the field distribution in a transformer, which Dowell describes using the idea of winding portions, can be viewed as a combination of the layer-by-layer field solutions developed by Perry.

A key advantage of Vandelac and Ziogas's analysis technique is that it is not based on Dowell's formulas for ac resistance, therefore it is not limited to excitation conditions that give rise to what Dowell calls "optimum" field distributions. Vandelac and Ziogas base their work on Perry's infinite-current-sheet analysis, which permits the transformer designer to calculate copper losses for a wide variety of winding arrangements, including those with open-circuit windings and electrostatic shields. Only the excitation conditions in the transformer windings and the geometry of the winding structure are needed. The generality of this approach is a very valuable contribution to the analysis of high-frequency transformer windings.

Two ideas presented in this paper make it particularly interesting for power electronics applications. First, Vandelac and Ziogas use Venkatraman's Fourier-decomposition approach to extend Perry's sinusoidal analysis to situations where the excitation current is nonsinusoidal. This method of nonsinusoidal analysis is again quite general, and it is useful for a variety of excitation conditions. The second significant contribution Vandelac and Ziogas make is what they call a "field harmonic" analysis. This technique considers the field-intensity diagrams for each of the different conduction periods of a switched-load circuit in order to arrive at a periodic, nonsinusoidal waveform of magnetic field for each space between winding layers. The method of field harmonic analysis is described further in Section 4.2.

3.7 Rosa [8]

Rosa's paper presents a method to calculate values for the circuit elements of a simplified coupled-coils model for transformers with multiple secondary windings. The analysis is given only for low-frequency excitations and considers only inductance values; the paper does not address losses at all.

This paper is the only one under review that presents an equivalent circuit for multiwinding transformers. In order to include the leakage impedances of the transformer windings in a SPICE-like simulation of a circuit employing a multiwinding transformer, such an equivalent circuit is necessary. Dowell's analysis is insufficient to determine the leakage impedances in a multiwinding transformer because it assumes only two windings. The layer-based analysis presented by Vandelac and Ziogas can be applied to multiwinding transformers, but their results are presented in terms of transformer losses rather than equivalent resistances and so cannot be applied directly to an equivalent circuit.

In the simplified coupled-coils model that Rosa proposes, each secondary winding of an n-winding transformer contains $(n-1)$ series leakage inductances, one of which is a self inductance and $(n-2)$ of which are mutual inductances. The values of the inductances are determined by performing hypothetical short-circuit tests which involve shorting the primary winding and sequentially exciting each of the $(n-1)$ secondaries. In order to characterize the $(n-1)$ secondaries, there must be $(n-1)$ of these hypothetical short-circuit tests. Each short-circuit test sets up a different field-intensity distribution in the window of the transformer. These field distributions are then used to calculate the various winding-inductance values.

For the case of no interlayer spaces, Rosa presents equations for the self and mutual inductances for two different winding structures. The first of these structures is the shell winding structure shown in Fig. 1 where the leakage flux is parallel to the center leg of the core. He also examines the stacked-disk winding structure where flat, washer-shaped windings are stacked as rings encircling the core center leg, and the resulting leakage flux is perpendicular to the center leg.

Rosa also discusses what he calls the "general case." This is a transformer where both axial and radial magnetic-field components occur due to either shell windings of differing breadths or stacked-disk windings of differing radii. This "general case" is handled by applying both analyses to the core and adding the resultant inductance. Rosa is the only author who analyzes shell windings with incomplete layers.

In his analysis, Rosa normalizes to one ampere of excitation current and one turn on each winding. Using this assumption, flux, flux linkage, inductance, and permeance are all numerically equal and used by Rosa somewhat interchangeably. This normalization should be kept in mind when reading Rosa's paper since it may be a source of confusion.

3.8 Coonrod [9]

Coonrod presents a computer algorithm for designing the smallest transformer for an intended application, to operate under conditions of high-frequency excitation where core loss is a limiting factor in the design. Only two-winding transformers wound on toroidal ferrite cores are considered. Such transformers have none of the losses associated with open-circuit windings and electrostatic shields. It is stated in the paper that the algorithm is applicable to pulse-width-modulated voltage or current excitation, but only sinusoidal excitation is represented in the test data. Among the papers reviewed, this is the only one which discusses core loss.

For a transformer designed by conventional methods, achieving a peak flux density near saturation would normally be accompanied by excessively high core loss at high frequencies. Coonrod's alternative design approach starts from thermal considerations and has the effect of automatically limiting the flux density to a lower, "best" value.

Coonrod's approach is to first calculate the maximum power which a transformer of a given size can dissipate without exceeding an allowed temperature rise above ambient. Then that maximum power is allocated according to the optimum ratio of core loss to copper loss, which Coonrod derives by minimizing the total loss. Choosing numbers of turns and wire sizes to achieve that ratio, different core sizes and different wire "bundles" are systematically considered until the smallest windable design is found. A wire bundle contains from one to seven strands of wire twisted together.

The equations used to calculate core loss and maximum power dissipation are derived empirically from results displayed in the paper that are obtained from numerous laboratory tests, but there are no data presented to support the assertion that the final design is optimum. Another weakness is that the ac winding resistances are calculated from skin effect alone, then multiplied by an empirically-determined factor of 1.5 to account for proximity effects. Coonrod admits that this factor is only a crude approximation.

The empirical nature of some of Coonrod's equations prevents widespread application of his results to other types of transformers, but his thorough treatment of the thermal aspects of transformer design provides good insight, as well as an approach which can be applied to other transformer-design problems.

Table 2: Equivalent Symbols for Normalized Layer Height

Author		*Symbol*
Dowell	[1]	$\sqrt{\lvert\alpha^2 h^2\rvert/2}$
Venkatraman	[2]	A
Carsten	[3]	X or h/δ
Jongsma	[4,5]	φ
Perry	[6]	Δ_n
Vandelac & Ziogas	[7]	h/δ or h/δ'

4 COMPARISONS

In the previous section, brief summaries of each of the articles under review are presented. We now wish to pull together some of the common threads which appear in the various articles. This discussion clarifies some of the commonalities among the articles and contrasts the different authors' approaches and conclusions on several topics common to the papers.

4.1 Comparable Symbols and Normalization

When looking at Venkatraman's plot of F_R versus "A," the reader may note that it has the same shape as Dowell's plot of F_R versus $|\alpha^2 h^2|$ and of Jongsma's F_R versus φ. This is because $|\alpha^2 h^2| = 2A^2$ and $A = \varphi$. This is an example of the variation in symbols used by the different authors which helps mask the commonalities among these papers. Virtually all of the authors use the height of the winding layer in skin depths, called "A" by Venkatraman. Table 2 contains a summary of these equivalences. The calculation of loss is made easier by normalizing the layer or conductor height to skin depth because all of the dependence on wire size and frequency is thereby included in the plots.

Individual authors normalize other quantities, choosing convenient base values as needed. Generally, these are well explained in the papers, but the variety of normalized quantities and base values makes it difficult to compare directly the different authors' results. One notable exception is the relationship between Venkatraman's F_H, the ratio of rectangular-wave to sine-wave losses, and Carsten's K_r, the normalized effective resistance factor. Carsten groups F_H, F_R, and the size-dependence of the dc resistance into a single term, his K_r. Thus, only one precalculated factor changes when comparing conductors of different sizes, whereas three factors change in Venkatraman's equations. Other symbols which represent essentially the same quantities are K_r and Jongsma's F_R/φ^2 for round-wire windings [4], K_r and Jongsma's F_R/φ for strip conductors [5], and Carsten's R_{w*} and Vandelac and Ziogas's R_δ. For this last example, R_{w*} is the dc resistance of a winding when the conductor height is one skin depth and R_δ is the dc resistance of a winding when the cross-sectional area of the conductor is one skin depth squared.

4.2 Nonsinusoidal Winding Excitation

Another point of comparison is the authors' different approaches to nonsinusoidal excitation of the transformer windings. Three separate methods are proposed in the articles under review.

Jongsma proposes an effective frequency to account for the high-frequency content of the nonsinusoidal waveform [5]. Since he provides no laboratory verification, it is hard to judge the validity of this method.

Venkatraman, Carsten, and Vandelac and Ziogas all employ Fourier-analysis techniques to determine winding losses due to nonsinusoidal excitations. In each case, the nonsinusoidal current is decomposed into its constituent harmonics, and the losses at the harmonic frequencies are calculated separately and totalled to yield the loss for the original waveform of current.

Vandelac and Ziogas propose a third possible approach to determining losses due to nonsinusoidal winding currents, as well as switched-load currents. In their method, called field harmonic analysis, the low-frequency mmf diagrams for each interval of the switching cycle are drawn. From these diagrams, waveforms of mmf $\mathcal{F}$ versus time for each *interlayer space* can be drawn. These waveforms of $\mathcal{F}(t)$ are then decomposed through Fourier analysis to determine an mmf diagram for each harmonic of the switching frequency. Although somewhat more complicated conceptually than Venkatraman's method, field harmonic analysis does incorporate losses in open-circuit windings and shields, and is applicable to winding arrangements that are not "optimum" as defined by Dowell.

4.3 Litz Wire and Paralleled Wires

The possibility of reducing winding losses by using paralleled wires or twisted, bunched wire is discussed by four of the authors. Paralleled wires are multiple wire strands which are collinear in a winding layer and have been wound simultaneously and then electrically paralleled. Bunched wires are multiple wire strands which are twisted or woven together to form a wire bundle, then wound onto the transformer as a bundle. Litz wire is a specific type of bunched wire where particular care is taken to insure that all the strands of the bundle occupy each position within the bundle for an equal

distance. This insures equal current sharing among the strands.

In both of his papers, Jongsma accepts the common belief that Litz wire always reduces total losses by virtually eliminating eddy-current losses, and that its major drawback is poor winding-space utilization. Jongsma also provides charts showing that, under certain conditions, paralleling two wires can reduce ac resistance by as much as 20% and paralleling three wires can reduce it by as much as 30% over comparable single-wire designs.

Venkatraman shows results from two test cores wound with Litz wire. He concludes that for Litz wire, Dowell's F_R is not accurate, but that calculations of F_H are accurate if they are made from measured values of resistance at the harmonics of the fundamental frequency. He also tested a transformer wound with Litz wire against a similar transformer wound with round wire. Tests were conducted under both sinusoidal and nonsinusoidal conditions. A significant conclusion drawn from this test is that Litz wire is not as effective in reducing losses for rectangular waveforms as it is for sinusoidal waveforms. It is noted that the moderate gain in efficiency with Litz wire may not offset its higher cost. Venkatraman also includes designs employing paralleled wires, but does not compare their losses against comparable single-wire designs.

Carsten analyzes the losses in Litz-wire windings by breaking a layer of regular conductors into several layers of conductors of less height. He calls this technique "vertical sectionalizing." He distinguishes real Litz wire from twisted, bunched wires which he claims do not adequately share current among the strands. If the heights of both windings are chosen to produce minimum losses, a Litz-wire winding will have lower losses than the comparable solid-wire winding for both pulse and square-wave currents. If the winding height of the Litz wire exceeds that which produces the minimum loss, Litz wire can actually have a detrimental effect and produce higher losses than the comparable solid-wire winding.

A fourth author, Coonrod, compares twisted wire bundles with different numbers of strands and different sizes of wire such that the ac resistance of the bundle is larger than a calculated minimum. He effectively chooses an "optimum" degree of stranding, with strands small enough that skin effect is not too pronounced, but large enough that insulation does not occupy too much of the available core window.

Although the specifics of the arguments differ, one thing is clear from both Carsten's and Venkatraman's papers: Litz wire is not a universal solution for winding-loss problems in transformers that conduct nonsinusoidal currents. From these papers, it also appears that more work needs to be done in the area of predicting losses in Litz-wire windings and in verifying the authors' claims experimentally.

4.4 Tapered Windings

Tapered windings are multilayer windings where the height of each layer is individually chosen to minimize losses in that layer. For engineers used to conventional multilayer round-wire windings, tapered windings may seem a mere mathematical abstraction. Yet, it is possible to construct such a winding, if the improvement in winding losses is sufficient to justify the additional complication and expense of manufacture. Perry and Carsten discuss tapered windings in their papers.

Perry analyzes a tapered-winding design for an air-core inductor with sinusoidal excitation. When the normalized loss data for the tapered-winding design are compared to the loss data for a minimum-loss design employing a constant height for all the layers, an improvement of 12% is noted for windings of three or more layers.

Carsten analyzes a tapered winding design for a 50%-duty-cycle pulse of current with rise and fall times of 0.1% of the duty cycle. When loss data for both winding types are compared, Carsten reports a 10% improvement using tapered windings for two layers and a 16% improvement with ten layers.

Although both authors predict improvements in the same range, they draw opposite conclusions about tapered windings. Carsten deems the results "quite disappointing" and "generally not...worth the effort involved."[3, p. 170] Perry, on the other hand, reports that "substantial energy savings can be realized" [6, p. 118] and suggests tapered windings as a possible alternative transformer winding design [6, p. 122].

4.5 Minimum-Loss Designs

Most of the papers under review discuss, to some degree, the minimization of loss through proper winding design. Articles [2-7] all contain plots displaying some indicator of winding or layer loss as a function of normalized winding height. These are generally accompanied by some discussion on minimizing loss through the judicious choice of conductor height. Although these designs are generally called minimum- or lowest-loss, none of the authors performs an exhaustive search of core sizes and winding configurations to determine the design with the absolute lowest losses, so what they mean by "minimum loss" is actually "minimum loss, given certain conditions." This should be kept in mind when reading these articles, particularly those whose major focus is minimum-loss design [5,9].

As an example, Jongsma's algorithm in [5] initially assumes that there are certain "boundary conditions," such as operating frequency and core size, that are

only re-evaluated if the lowest-loss winding structure for those boundary conditions has losses which exceed the specified maximum for the transformer windings. Likewise, the goal of Coonrod's algorithm is to produce the smallest transformer with an acceptable temperature rise, but this is achieved by choosing a core size and then analyzing the temperature rise produced by the lowest-loss design given that core size.

5 CONCLUSION

The design of transformer windings for high-frequency switch-mode applications is complicated, and is made more so by the diversity and complexity of the available literature. The goal of this paper is to make these articles more understandable and useful to the design engineer. To this end we provide assistance in several forms. Figure 6 shows the relationship between the reviewed articles and gives a major contribution of each. Table 1 highlights several key issues covered by the articles, and Sections 3 and 4 discuss the authors' approaches to several common issues. Thus, the design engineer is guided toward the article most useful for a specific application, and to a clearer understanding of the assumptions, significant contributions, and shortcomings of each article. The end result should be a greater understanding of high-frequency effects in transformer and reactor windings.

References

[1] P. L. Dowell, "Effects of Eddy Currents in Transformer Windings," *Proceedings of the IEE*, Vol. 113, No. 8, August 1966, pp. 1387–1394.

[2] P. S. Venkatraman, "Winding Eddy Current Losses in Switch Mode Power Transformers Due to Rectangular Wave Currents," *Proceedings of Powercon 11*, Power Concepts Inc., Ventura, California, 1984, Section A-1, pp. 1–11.

[3] Bruce Carsten, "High Frequency Conductor Losses in Switchmode Magnetics," *High-Frequency Power Converter Conference Record*, May 1986, pp. 155–176.

[4] J. Jongsma, "Minimum-Loss Transformer Windings for Ultrasonic Frequencies, Part 1: Background and Theory," *Philips Electronics Application Bulletin*, E.A.B. 35, No. 3, Philips, The Netherlands, 1978, pp. 146–163. "Part 2: Design Methods and Aids," *Philips Electronics Application Bulletin*, E.A.B. 35, No. 4, Philips, The Netherlands, 1978, pp. 211–226.

[5] ———, "High-Frequency Ferrite Power Transformer and Choke Design, Part 3: Transformer Winding Design," *Philips Electronic Components and Materials Technical Publication*, No. 207, Philips, The Netherlands, 1986.

[6] M. P. Perry, "Multiple Layer Series Connected Winding Design for Minimum Losses," *IEEE Transactions on Power Apparatus and Systems*, Vol. PAS-98, No. 1, Jan./Feb. 1979, pp. 116–123.

[7] J. P. Vandelac, and P. Ziogas, "A Novel Approach for Minimizing High Frequency Transformer Copper Losses," *IEEE Power Electronics Specialists Conference Record*, 87CH2459-6, 1987, pp. 355–367.

[8] John Rosa, "Calculation of Flux Linkages in Multiwinding Transformers," *IEEE Power Electronics Specialists Conference Record*, 86CH2310-1, 1986, pp. 639-644.

[9] N. R. Coonrod, "Transformer Computer Design Aid For Higher Frequency Switching Power Supplies," *IEEE Power Electronics Specialists Conference Record*, 84CH2000-8, 1984, pp. 257–267.

[10] Frederick Terman, *Radio Engineers' Handbook*, 1st ed., (New York: McGraw-Hill Book Co., Inc., 1943), pp. 28-37.

[11] Glenn R. Skutt, *Modeling Multiwinding Transformers for High-Frequency Applications*, M.S. Thesis, Duke University, April 24, 1988.

[12] E. C. Snelling, *Soft Ferrites—Properties and Applications*, (London: Iliffe Books Ltd., 1969).

This page has been left blank intentionally.

Bibliography

[1] Dowell, P.L., "Effects of Eddy Currents in Transformer Windings," *Proceedings of the IEE*, Vol. 113, No. 8, August 1966, pp. 1387–1394.

[2] Venkatraman, P.S., "Winding Eddy Current Losses in Switch Mode Power Transformers Due to Rectangular Wave Currents," *Proceedings of Powercon 11*, Power Concepts Inc., Ventura, California, 1984, Section A-1, pp. 1–11.

[3] Carsten, Bruce, "High Frequency Conductor Losses in Switchmode Magnetics," *High-Frequency Power Converter Conference Record*, May 1986, pp. 155–176.

[4] Jongsma, J., "Minimum-Loss Transformer Windings for Ultrasonic Frequencies, Part 1: Background and Theory," *Philips Electronics Application Bulletin*, E.A.B. 35, No. 3, Philips, The Netherlands, 1978, pp. 146–163.

[5] ———, "Minimum-Loss Transformer Windings for Ultrasonic Frequencies, Part 2: Design Methods and Aids," *Philips Electronics Application Bulletin*, E.A.B. 35, No. 4, Philips, The Netherlands, 1978, pp. 211–226.

[6] ———, "High-Frequency Ferrite Power Transformer and Choke Design, Part 3: Transformer Winding Design," *Philips Electronic Components and Materials Technical Publication*, No. 207, Philips, The Netherlands, 1986.

[7] Perry, M.P., "Multiple Layer Series Connected Winding Design for Minimum Losses," *IEEE Transactions on Power Apparatus and Systems*, Vol. PAS-98, No. 1, Jan./Feb. 1979, pp. 116–123.

[8] Vandelac, J.P., and Ziogas, P., "A Novel Approach for Minimizing High Frequency Transformer Copper Losses," *IEEE Power Electronics Specialists Conference Record*, 87CH2459-6, 1987, pp. 355–367.

[9] Rosa, John, "Calculation of Flux Linkages in Multiwinding Transformers," *IEEE Power Electronics Specialists Conference Record*, 86CH2310-1, 1986, pp. 639–644.

[10] M.I.T. Staff, *Magnetic Circuits and Transformers*, John Wiley & Sons, Inc., New York, 1943, pp. 622–642.

[11] Starr, F.M., "Equivalent Circuits," *Transactions of the American Institute of Electrical Engineers*, Vol. 51, No. 2, June 1932, pp. 287–298.

[12] Blume, L.F., et al., *Transformer Engineering*, John Wiley & Sons, Inc., New York, 1951, pp. 96–97, 117–126.

[13] Weast, Robert C., *Handbook of Chemistry and Physics*, 59th ed., CRC Press, Boca Raton, Florida, 1985.

[14] Snelling, E.C., *Soft Ferrites—Properties and Applications*, Iliffe Books Ltd., London, 1969.

[15] Jay, Frank, ed., *IEEE Standard Dictionary of Electrical and Electronics Terms*, 4th ed., The Institute of Electrical and Electronics Engineers, Inc., New York, 1988.